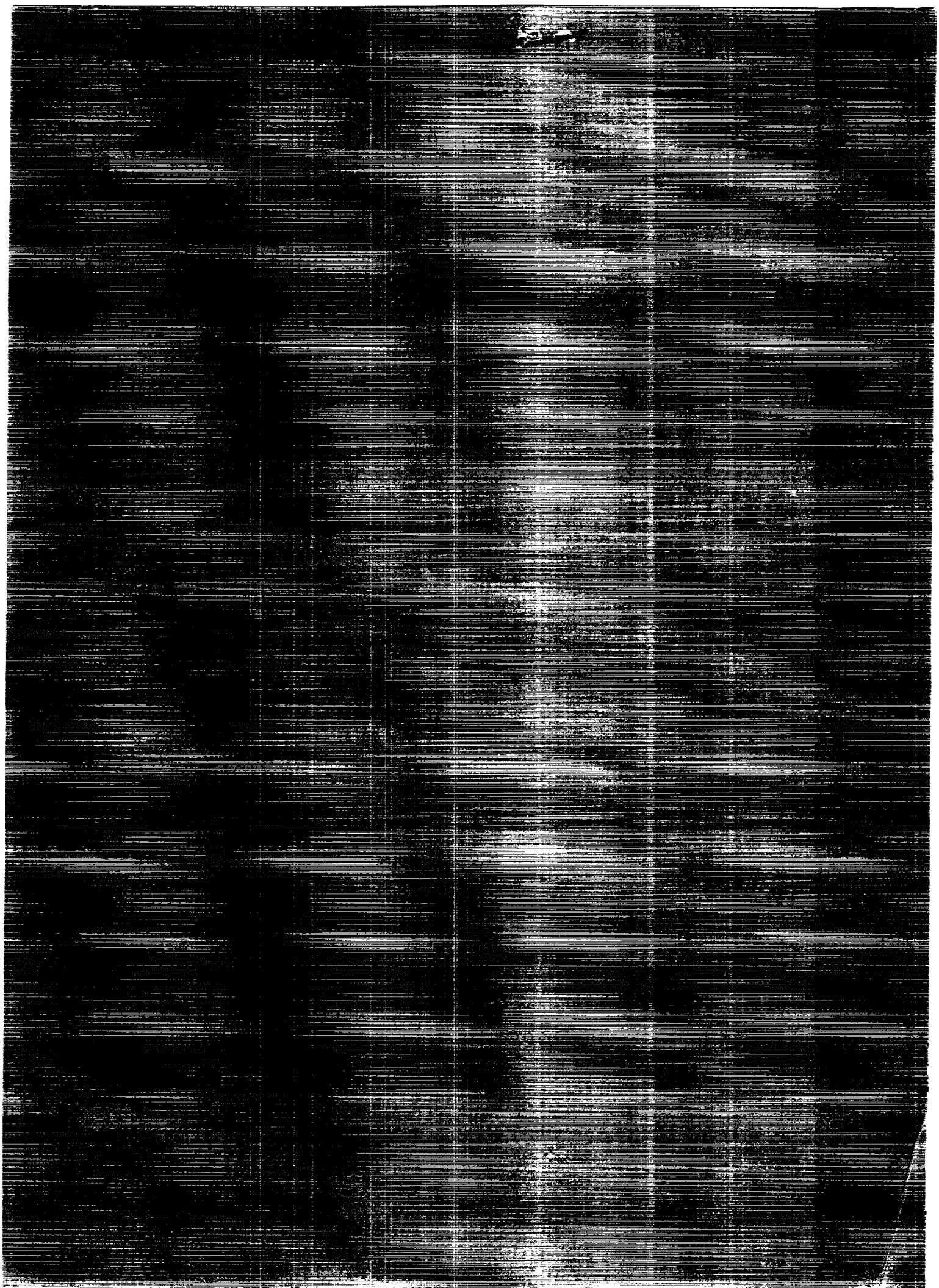

NASA Contractor Report 4370

Atlas of the Global Distribution of Atmospheric Heating During the Global Weather Experiment

December 1978—November 1979

Todd K. Schaack and Donald R. Johnson
University of Wisconsin
Madison, Wisconsin

Prepared for
Goddard Space Flight Center
under Grant NAG5-81

National Aeronautics and
Space Administration
Office of Management
Scientific and Technical
Information Program
1991

Table of Contents

List of Figures

1. Introduction

An understanding of the structure and evolution of atmospheric circulation is ultimately linked with knowledge of atmospheric heat sources and sinks. Prior to the Global Weather Experiment (GWE), from December 1978 through November 1979, detailed global analyses of heating were lacking due to the paucity of data over much of the earth. The enhanced observational system of the GWE in combination with global data assimilation models developed for the GWE has provided unprecedented global data sets for the study of the planetary circulation (National Research Council, 1985). A determination of the global distribution of heating during the annual cycle of the GWE is now feasible.

The large-scale distributions of heating have been estimated by several methods. In one method, net heating is determined from independent estimates of the individual components associated with radiation, condensation and sensible heating (e.g., Budyko, 1963; Newell et al., 1969, 1974; Otto-Bliesner and Johnson, 1982; Zillman and Johnson, 1985). Net heating has also been obtained from analysis of the energy balance required by the First Law of Thermodynamics (e.g., Hantel and Baader, 1978; Geller and Avery, 1978; Lau, 1979) and from the quasi-geostrophic balance of vorticity and energy (e.g., Wiin-Nielsen and Brown, 1962; Brown, 1964).

Numerous investigations have estimated global heating distributions with data from the GWE. Kasahara and Mizzi (1985), Masuda (1984), Sardeshmukh (1984), Holopainen and Fortelius (1986), Chen and Baker (1986) and Kasahara, Mizzi and Mohanty (1987) employed the First Law of Thermodynamics. Boer (1986) and Johnson (1985) estimated vertically integrated heating from total energy balance. Wei, Johnson and Townsend (1983), Johnson and Wei (1985), Johnson, Yanai and Schaack (1987) and Schaack, Johnson and Wei (1990) computed heating through vertical integration of the isentropic equation of mass continuity. Although exact comparisons of heating distributions from the above investigations have not been carried out, overall agreement is apparent in the general features of the distributions calculated from GWE data sets.

The purpose of this atlas is to provide estimates of the global distribution of atmospheric heating throughout the annual cycle of the Global Weather Experiment. Heating rates are calculated through integration of the isentropic mass continuity equation (Wei et al., 1983; Schaack et al., 1990) utilizing the European Centre for Medium-range Weather Forecasts (ECMWF) Level IIIb data set. Distributions of monthly, seasonally and annually averaged heating are presented for isentropic and isobaric layers within the troposphere and for the troposphere as a whole. The horizontal distributions of heating identify planetary heat sources and sinks and their temporal evolution. A systematic vertical variation of heating that is linked with the distribution of continents and oceans is also evident (Schaack et al., 1990). Meridional cross sections of temporally and zonally averaged heating are also presented.

2. Data

The data used in the preparation of this atlas are from the ECMWF GWE Main Level IIIb data set for the period December 1978 through November 1979. Here "Main" denotes the original analysis of the GWE data. ECMWF has subsequently produced a reanalyzed data set for a portion of the GWE. The Level IIIb data, resulting from assimilation, represent a combination of observed and model generated information. The characteristics of the ECMWF data assimilation system utilized in processing the GWE data are discussed by Bengtsson et al. (1982) and Bengtsson (1983). The characteristics of the various assimilation systems employed in the preparation of GWE Level III data sets are summarized in tabular form by Daley et al. (1985) and Daley (1987).

Global distributions of zonal and meridional wind components, temperature and geopotential height were available for 0000, 0600, 1200 and 1800 GMT of each day of the GWE year on a 1.875° latitude-longitude grid for 15 mandatory pressure levels between 1000 and 10 mb. From these data, global isentropic analyses were generated on a 3.75° latitude-longitude grid for 0000 and 1200 GMT of each day of the GWE year through linear interpolation of the relevant meteorological variables with the R over c_p power of pressure (R is the gas constant for dry air and c_p the specific heat of dry air at constant pressure). In employing the Lorenz convention (Dutton and Johnson, 1967) on underground isentropes (i.e., $\theta < \theta_s$; θ_s is the surface potential temperature), the pressure and wind components were set equal to their respective surface values.

Information at the earth's surface was not provided in the ECMWF Main Level IIIb analyses. Therefore, surface values of pressure, temperature and zonal and meridional wind components were estimated from GWE Level III isobaric data. Surface pressure was interpolated by assuming that geopotential varies quadratically with the logarithm of pressure, ln(p) (Gerrity, 1977). Surface temperature and horizontal wind components were assumed to vary linearly with ln(p) except when surface pressure was greater than 1000 mb, in which case temperature was extrapolated downward from 1000 mb using the standard atmosphere lapse rate of 6.5 K km^{-1}.

The fields of zonal and meridional wind components and geopotential height in the ECMWF GWE Main Level IIIb data set were archived before initialization, while the temperature fields were archived after initialization (Bengtsson, 1983). Because of a preference to use only uninitialized information in the analyses, temperature was computed from thickness and layer mean relative humidity. Due to the possibility of errors in the height fields at 150 mb (Julian, 1983), the height information at this level was not utilized in creation of the isentropic data set.

A varying vertical resolution in the isentropic domain was adopted; 10 K between 220 K and 380 K, 20 K between 380 K and 500 K followed by 550 K and 650 K. After a preliminary study of the heating distributions for the months of January and July 1979, the 400 K isentropic level was designated as the top level (θ_T) for the analysis of heating. The global distributions of heating for July calculated using 400 K and 650 K as the top of the isentropic data are very similar. However, the inclusion of the data above 400 K appeared to have a negative impact on the global distribution for January.

Distributions of heating in layers above 400 K in January (not shown), which for the most part are located in the stratosphere, appear to contain unrealistic features in some regions, particularly over eastern Asia. This results from large values of divergence in stratospheric isentropic layers in some regions which are thought to be unrepresentative (National Research Council, 1985; Johnson, 1986). Several changes affecting stratospheric analyses were made in the assimilation system at ECMWF during the analysis of December and January of the GWE year which likely impacted the results for isentropic layers above 400 K. The time-averaged pressure of the 400 K isentropic level is less than 160 mb over the globe in each month of the GWE year. In January the time-averaged pressure of the 400 K isentrope slopes from near 85 mb in the tropics to 150 mb in extratropical latitudes.

3. Description of Analyses

The analyses of the annually, seasonally and monthly averaged heating and pressure for the GWE year presented in this atlas consist of the following:

1. Global analyses of vertically averaged heating for the surface to 400 K isentropic layer.

2. Global analyses of isobaric layer-averaged heating;

   (A) surface to 800 mb
   (B) 800 to 600 mb
   (C) 600 to 400 mb
   (D) 400 to 200 mb

3. Global analyses of isentropic layer-averaged heating;

   (A) surface to 290 K
   (B) 290 to 310 K
   (C) 310 to 330 K
   (D) 330 to 400 K

4. Meridional cross sections of isentropically and isobarically zonally averaged heating; meridional profile of zonally and vertically averaged heating.

5. Global analyses of surface pressure and the pressure difference between the earth's surface and the 400-K isentropic surface.

6. Global analyses of the pressure difference between the upper and lower surfaces of the isentropic layers in (3).

The following points concerning the analyses are noted:

1. The heating distributions were calculated from time-averaged data through vertical integration of the isentropic mass continuity equation. See Appendix A for a detailed discussion of the method of calculation and the following subsection for the definition of the mass-weighted averages.

2. The relation between the heating rate as presented in this atlas by θ and the rate of specific heat addition, Q, is given by

$$\dot{\theta} = Q / \pi \qquad (1)$$

where π, the Exner function, is equal to $c_p(p/p_{00})^{\kappa}$ with $\kappa=R/c_p$.

3. All horizontal heating distributions have been filtered to emphasize wavelengths greater than 4000 km. Details of the filtering employed are discussed in a subsequent subsection along with smoothing of the zonally averaged heating distributions.

4. In the analyses, contours are omitted where the atmospheric layer does not exist (i.e., there is zero mass in the layer). The quasi-horizontal line at the bottom of the analyses in the zonally averaged isentropic cross sections represents the coldest surface potential temperature occurring along the latitude circle during the time period considered.

Since the heating was calculated by integration of the isentropic mass continuity equation, the most direct method to display the vertical distribution from these results is in isentropic coordinates. However, for utilization of the results in studies employing isobaric coordinates, vertically averaged estimates are also presented for four isobaric layers. These distributions were obtained by interpolating the time-averaged isentropic profiles of heating to isobaric levels at 50-mb increments between 200 mb and the earth's surface assuming a linear variation with respect to the R over c_p power of the temporally averaged pressure. These interpolated values were subsequently mass-weighted vertically averaged over the four isobaric layers: surface-800 mb, 800-600 mb, 600-400 mb and 400-200 mb. The global distributions are expressed as heating per unit mass in order to properly account for the condition that the earth's surface bounds the lowest layer, and also occasionally bounds the second lowest layer in regions of elevated orography.

Along with the distributions of heating, several additional fields are provided. These are the time-averaged surface pressure, the time-averaged pressure difference between the surface and the 400-K isentropic surface and the time-averaged pressure difference between the upper and lower surfaces of the four isentropic layers. These analyses indicate the time-averaged mass distribution within the various layers for which heating is estimated. The time-averaged pressure of an isentropic surface bounding any of the layers may be determined from the analyses by subtracting the sum of the pressure differences of the individual isentropic layers up to the level of interest from the time-averaged surface pressure.

3.1. Definition of Mass-weighted Averages

With the hydrostatic assumption, the mass within an isentropic layer is determined by the pressure difference between the upper and lower isentropic levels through integration of the hydrostatic relation

$$\rho J_\theta = -g^{-1}\, \partial p/\partial\theta, \tag{2}$$

where ρ is density, $J_\theta = |\partial z/\partial\theta|$, p is pressure, θ is potential temperature, z is geopotential height and g is the acceleration due to gravity. The mass-weighted temporally and vertically averaged heating is defined by

$$\hat{\dot{\theta}}^{\theta,t} = \int_{\theta_L}^{\theta_U}\int_{t_1}^{t_2} \rho J_\theta \dot{\theta}\, dt d\theta \;/\; \int_{\theta_L}^{\theta_U}\int_{t_1}^{t_2} \rho J_\theta\, dt d\theta \;. \tag{3}$$

The upper and lower isentropic surfaces bounding the isentropic layer are θ_U and θ_L, while the ending and beginning of the time averaging period are t_2 and t_1, respectively. In the vertical average over the entire extent of the isentropic analyses, $\theta_U = \theta_T = 400$ K and $\theta_L = \theta_s$ in (3).

The mass-weighted temporally and zonally averaged heating is defined by

$$\hat{\dot{\theta}}^{\lambda,t} = \int_{0}^{2\pi}\int_{t_1}^{t_2} \rho J_\theta \dot{\theta}\, dt d\lambda \;/\; \int_{0}^{2\pi}\int_{t_1}^{t_2} \rho J_\theta\, dt d\lambda \;, \tag{4}$$

while the temporally, zonally and vertically averaged heating is defined by

$$\hat{\dot{\theta}}^{\theta,\lambda,t} = \int_{\theta_s}^{\theta_T}\int_{0}^{2\pi}\int_{t_1}^{t_2} \rho J_\theta \dot{\theta}\, dt d\lambda d\theta \;/\; \int_{\theta_s}^{\theta_T}\int_{0}^{2\pi}\int_{t_1}^{t_2} \rho J_\theta\, dt d\lambda d\theta \;. \tag{5}$$

The contribution to the above integrals from underground isentropic layers (i.e., where $\theta < \theta_s$) is identically zero due to the hydrostatic assumption and the use of the Lorenz convention (Dutton and Johnson, 1967).

3.2. Filtering of Heating Distributions

All horizontal distributions of heating presented in this atlas have been filtered in order to isolate large-scale features and suppress noise. First, zonal harmonics with wavelengths less than 4000 km are removed through truncation of one dimensional Fourier transforms (Wei et al., 1983). Meridional smoothing is then applied through a combination of four passes of a low pass (2,3,2) filter and one pass of an inverse (-1,5,-1) filter. The frequency response of the meridional smoothing for selected wavelengths is given in Table 1.

Table 1

Frequency Response of Meridional Filtering[1]

Wavelength (km)	% of original amplitude retained
12,000	96
10,000	95
8,000	92
6,000	85
4,000	69
3,000	49
2,000	16

[1]Meridional spatial filter composed of four passes of a low pass (2,3,2) filter and one pass of an inverse (-1,5,-1) filter.

The same meridional smoothing has been applied to the zonally averaged distributions with the following exception. Mass-weighted zonal averaging acts to smooth data in proportion to the meridional distribution of mass which tends to vary proportionally to the cosine of latitude. Recognizing this inherent smoothing, the application of the meridional smoothing was made proportional to the absolute value of the sine of latitude thereby complimenting the smoothing inherent in the mass-weighted average. The weighting by the sine of latitude results in an increase of smoothing with latitude, from zero at the equator to a maximum at the poles.

4. Uncertainties in Estimation of Heating

The accuracy of the heating estimates for the year of the GWE presented in this atlas depends on many factors. The ECMWF Level III data are prepared through use of an assimilation model. Therefore, the accuracy of the heating distributions, being determined from a combination of observations and model generated information, depends on the quality of the observations, the assimilation model and the diagnostic method utilized. Since a detailed analysis of the errors was not feasible, the following discussion is of a general nature that aims simply to direct attention to potential sources of errors in the analyses.

In estimating the four-dimensional distribution of heating within isentropic coordinates, the interpolation of the Level III data to form an isentropic data set and the creation of the surface data introduces uncertainty. The lack of information concerning the diabatic mass flux at the upper level of the analyses and the uncertainty regarding the adjustment employed to remove the bias and insure mass balance are also potential sources of errors in the computations.

In estimating the isobaric heating distributions in this atlas, the interpolation of heating from isentropic to isobaric coordinates using time-averaged data may not truly reflect the time-averaged isobaric profile of heating in some regions due to the transient variation of pressure on isentropic surfaces. In transient baroclinic disturbances, latent heating

likely occurs at higher pressure (i.e., warmer temperatures) than indicated by the time-averaged pressure (i.e., a "mean" temperature) for the isentropic level to which it is assigned.

If the primary objective was to determine the structure of heating relative to isobaric coordinates, optimum estimation suggests that the interpolation of the distribution of heating from isentropic to isobaric coordinates be carried out for each observational time (as in the more limited study in time by Schaack et al. (1990)) rather than interpolating the time-averaged isentropic distribution of heating to isobaric coordinates employing the time-averaged pressure distribution (as in this atlas). Since the primary focus of our research has been to determine the heating distribution relative to isentropic coordinates no attempt was made to interpolate from isentropic to isobaric coordinates for each time period of the GWE year; a step which would have required an extensive reprocessing of the entire GWE data set.

The differences between results employing interpolation of heating from isentropic to isobaric coordinates for each time period (Schaack et al., 1990) versus interpolation of time-averaged structure lie within the realm of uncertainty. Schaack et al. show results for corresponding isobaric layers for January, April, July and October 1979. The most notable differences between estimates occur in January over the oceanic storm tracks of the Northern Hemisphere. These regions are characterized by the combination of sharp temperature gradients associated with land-ocean contrasts and the passage of baroclinic disturbances. In these regions, the results of Schaack et al. (1990) generally show stronger heating in the lower and middle troposphere while the present results are generally stronger in the upper troposphere.

Johnson et al. (1987) presented layer-averaged results for January and July 1979 and zonally averaged results for January, April, July and October 1979 computed from the ECMWF GWE data set. In the free troposphere the methods used in Johnson et al. and the present study are the same. However, the present study uses a different method to estimate ρJ_θ (an inverse static stability measure as shown in (2)) near the earth's surface. The effect of this difference is confined to the low troposphere primarily in highly baroclinic regions. The estimates of ρJ_θ in these regions in the present study tend to be larger than those of Johnson et al. (1987), thereby reducing the magnitude of heating (see Eqs. 3 and 4). Comparison of corresponding distributions shows the only notable differences between estimates in global isobaric layers occur in the surface-to-800 mb layer of January over the western North Atlantic where the results of Johnson et al. (1987) show stronger heating. The largest differences between the two studies are in the zonally averaged heating distributions where the results of Johnson et al. have stronger low-level heating in middle latitudes, particularly in the Northern Hemisphere in January.

While a number of uncertainties are involved, the apparent spatial and temporal continuity of the analyses and their consistency with known features of the large-scale circulation suggests that a realistic four-dimensional structure of the global distribution of heating during the GWE emerges.

5. Acknowledgements

This research was supported by the National Science Foundation under Grant ATM-8517273 and by the National Aeronautics and Space Administration under Grant NAG5-81. Preparation of the figures by Christine Johnson, Kim Koepsel and Cynthia Karls and typing of the manuscript by Judy Mohr is greatly appreciated.

Appendix A: Estimation of Heating

The time-averaged isentropic mass continuity equation is (Johnson, 1980)

$$\overline{\frac{\partial}{\partial t_\theta}(\rho J_\theta)} + \nabla_\theta \cdot \overline{(\rho J_\theta \underset{\sim}{U})} + \overline{\frac{\partial}{\partial \theta}(\rho J_\theta \dot{\theta})} = 0 \ . \tag{A1}$$

With the hydrostatic relation

$$\rho J_\theta = -g^{-1} \, \partial p / \partial \theta \ , \tag{A2}$$

the mass distribution is determined by the pressure distribution.

The time-averaged diabatic mass flux through an isentropic surface obtained by indefinite vertical integration of (A1) is

$$\overline{\rho J_\theta \dot{\theta}} = \int_\theta^{\theta_T} \left[\overline{\frac{\partial}{\partial t_\theta}(\rho J_\theta)} + \nabla_\theta \cdot \overline{(\rho J_\theta \underset{\sim}{U})} \right] d\theta \ , \tag{A3}$$

where the diabatic mass flux has been assumed to vanish at the top isentropic level, θ_T. The boundary value for diabatic mass flux at the earth's surface, obtained from a definite integration of (A1) from the earth's surface at θ_s to the upper surface θ_T, is given by

$$\overline{\rho J_\theta \dot{\theta}}\Big|_{\theta_s} = \int_{\theta_s}^{\theta_T} \left[\overline{\frac{\partial}{\partial t_\theta}(\rho J_\theta)} + \nabla \cdot \overline{(\rho J_\theta \underset{\sim}{U})} \right] d\theta \ . \tag{A4}$$

The mass-weighted time-averaged heating is obtained from the diabatic mass flux according to

$$\hat{\dot{\theta}}^t = \overline{\rho J_\theta \dot{\theta}} \ / \ \overline{\rho J_\theta} \ . \tag{A5}$$

The estimates of heating at lower levels calculated in this manner from the assimilated data are unrealistic at some locations. This results primarily from biases in the estimation of horizontal mass divergence from the assimilated data. In analyses of fields, whether by subjective or objective means, bias errors are readily introduced in estimation of divergence (Schmidt and Johnson, 1972). These errors stem primarily from discrete irregularly

spaced observations which are sparse in relation to the horizontal variation of the velocity and the mass ρJ_θ. While a bias error may only be a minor fraction of the true horizontal divergence within a particular layer, such errors are prevalent in the assimilated data and accumulate in vertical integration. Consequently the integrated bias should be removed. For this step, a mass-weighted adjustment is applied to the mass tendency and divergence subject to the constraint that the sum of the vertically integrated mass tendency and mass divergence must be equal to a particular boundary value for diabatic mass flux at the earth's surface. This particular boundary value must be defined in order to allow the vertical movement of isentropic surfaces relative to the earth's surface in accord with changes of potential temperature at the earth's surface.

An independent estimate of the boundary value of diabatic mass flux is given by the temporal variation of surface potential temperature, $\theta_s(\lambda,\phi,t)$ [equal to $\theta(\lambda,\phi,z_s,t)$], from the chain rule

$$\rho J_\theta \dot{\theta}_s(\lambda,\phi,t) = \rho J_\theta \left[\frac{\partial \theta_s}{\partial t_\theta} + \underset{\sim}{U}_s \cdot \nabla_\theta \theta_s\right] \quad , \tag{A6}$$

where λ is longitude, ϕ is latitude and the subscript s denotes values at the earth's surface. The accuracy of this estimate is dependent on the accuracy of estimates of the tendency and advection of $\theta_s(\lambda,\phi,t)$ at the earth's surface. Biases will stem primarily from inadequate resolution of information at the earth's surface. The largest biases will be found during winter primarily in the regions of strong surface winds and gradients of θ_s, such as over the Kuroshio Current and the Gulf Stream just off the east coasts of Asia and North America, respectively. Analysis of estimates from this method, however, establish that the global patterns of the surface distribution of heating are much more realistic than those from (A4).

With the assumption that the lower boundary value of diabatic mass flux by (A6) is an unbiased estimate of the "true" value

$$\overline{\rho J_\theta \dot{\theta}|^*_{\theta_s}} = \overline{\rho J_\theta \dot{\theta}_s(\lambda,\phi,t)} \quad , \tag{A7}$$

an estimate of the vertically integrated bias error (δ) from the difference between (A4) and (A7) is given by

$$\delta(\lambda,\phi,t) = \overline{\rho J_\theta \dot{\theta}|_{\theta_s}} - \overline{\rho J_\theta \dot{\theta}|^*_{\theta_s}} \quad . \tag{A8}$$

The error per unit mass within the atmospheric column is then defined by

$$\hat{\delta} = \delta \Big/ \int_{\theta_s}^{\theta_T} \overline{\rho J_\theta}\, d\theta \quad ,$$

$$= -g\delta \Big/ \left[\overline{p(\theta_T)} - \overline{p(\theta_s)}\right] \quad . \tag{A9}$$

Through subtraction of the bias error, the adjusted time-averaged diabatic mass flux through an isentropic surface is expressed by

$$\overline{(\rho J_\theta \dot{\theta})}' = \int_\theta^{\theta_T} \left[\frac{\partial}{\partial t_\theta}\overline{(\rho J_\theta)} + \nabla\cdot\overline{(\rho J_\theta \underset{\sim}{U})} \right] - \overline{\rho J_\theta \hat{\delta}}\, d\theta ,$$

$$= \overline{\rho J_\theta \dot{\theta}} + \hat{\delta}\left[\overline{p(\theta_T)} - \overline{p(\theta)}\right] , \qquad \text{(A10)}$$

where the bias error is removed in proportion to the mass within an isentropic layer.

References

Bengtsson, L., M. Kanamitsu, P. Kallberg and S. Uppla, 1982: FGGE 4-dimensional data assimilation at ECMWF. Bull. Amer. Meteor. Soc., 63, 29-43.

Bengtsson, L., 1983: The ECMWF Level III-B data set. U.S. Committee for GARP, Global Weather Experiment Newsletter, No. 1, 1-7.

Boer, G. J., 1986: A comparison of mass and energy budgets from two FGGE datasets and a GCM. Mon. Wea. Rev., 114, 885-902.

Brown, J. A., 1964: A diagnostic study of the tropospheric diabatic heating and the generation of available potential energy. Tellus, 16, 371-388.

Budyko, M. I., 1963: Atlas of the heat balance of the earth. Moscow, Gidrometeoizdast, 69 pp.

Chen, T.-C., and W. E. Baker, 1986: Global diabatic heating during FGGE SOP-1 and SOP-2. Mon. Wea. Rev., 114, 2578-2589.

Daley, R., 1987: Data assimilation techniques used for FGGE IIIb analyses - 1987 update. National Research Council FGGE Workshop, April 27-30, 1987, Airlie House, Virginia, 113-124.

Daley, R., A. Hollingsworth, J. Ploshay, K. Miyakada, W. Baker, E. Kalnay, C. Dey, T. Krishnamurti and E. Barker, 1985: Objective analysis and assimilation techniques for the production of FGGE IIIb analyses. Bull. Amer. Meteor. Soc., 66, 532-538.

Dutton, J. A., and D. R. Johnson, 1967: The theory of available potential energy and a variational approach to atmospheric energetics. Advances in Geophysics, Vol. 12, Academic Press, 333-436.

Geller, M. A., and S. K. Avery, 1978: Northern Hemisphere distributions of diabatic heating in the troposphere derived from general circulation data. Mon. Wea. Rev., 106, 629-636.

Gerrity, J. P., 1977: The LFM model-1976: a documentation. NOAA Technical Memorandum, NWS NMC 60, 68 pp.

Hantel, M., and H.-R. Baader, 1978: Diabatic heating climatology of the zonal atmosphere. J. Atmos. Sci., 35, 1180-1189.

Holopainen E., and C. Fortelius, 1986: Accuracy of estimates of atmospheric large-scale energy flux divergence. Mon. Wea. Rev., 114, 1910-1921.

Johnson, D. R., 1980: A generalized transport equation for use with meteorological coordinate systems. Mon. Wea. Rev., 108, 733-745.

Johnson, D. R., 1985: The global circulation during the FGGE year: On the balance of mass, energy, and angular momentum within isentropic and isobaric coordinates as revealed by different FGGE data sets. WMO Proceedings of the Global Weather Experiment Scientific Seminar, Helsinki, 29-31 August, 1984, Finland. GARP Special Report No. 42, II 28-40.

Johnson, D. R., 1986: Summary of the Proceedings of the First National Workshop on the Global Weather Experiment, Bull. Amer. Meteor. Soc., 67, 1135-1143.

Johnson, D. R., and M.-Y. Wei, 1985: The planetary distribution of heat sources and sinks during FGGE. Proceedings of the First National Workshop on the Global Weather Experiment: Current Achievements and Future Directions. National Academy Press, Washington, D. C. Vol. 2, Part I, 299-316.

Johnson, D. R., M. Yanai and T. K. Schaack, 1987: Global and regional distributions of atmospheric heat sources and sinks during the GWE. Monsoon Meteorology, Eds., C.-P. Chang and T. N. Krishnamurti, Oxford University Press, New York, 271-297.

Julian, P. R., 1983: Comments on the ECMWF IIIb analysis data set. U.S. Committee for GARP, Global Weather Experiment Newsletter, No. 1, 15-17.

Kasahara, A., and A. P. Mizzi, 1985: Preliminary evaluation of diabatic heating distribution from FGGE Level IIIb analysis data. Proceedings of the First National Workshop on the Global Weather Experiment: Current Achievements and Future Directions. National Academy Press, Washington, D.C., Vol. 2, Part I, 317-329.

Kasahara, A., A. P. Mizzi and U. C. Mohanty, 1987: Comparison of global diabatic heating rates from FGGE Level IIIb analyses with satellite radiation imagery data. Mon. Wea. Rev., 115, 2904-2935.

Lau, N.-C., 1979: The observed structure of tropospheric stationary waves and the local balances of vorticity and heat. J. Atmos. Sci., 36, 996-1016.

Masuda, K., 1984: Diabatic heating during the FGGE: A Preliminary Report. J. Meteor. Soc. Japan, 62, 702-708.

National Research Council, 1985: Proceedings of the First National Workshop on the Global Weather Experiment, Vol. I and II, Board on Atmospheric Sciences and Climate, National Academy Press, Washington, D.C., Vol. I, 75 pp., Vol. II, 809 pp.

Newell, R. E., D. G. Vincent, T. G. Dopplick, D. Ferruzza and J. W. Kidson, 1969: The energy balance of the global atmosphere. In: "The global circulation of the atmosphere", G. A. Corby (ed.), Roy. Meteor. Soc., 42-90.

Newell, R. E., J. W. Kidson, D. G. Vincent and G. J. Boer, 1974: The general circulation of the tropical atmosphere and interactions with extratropical latitudes, Vol. 2. The MIT Press, 371 pp.

Otto-Bliesner, B. L., and D. R. Johnson, 1982: Thermally-forced mean mass circulations in the Northern Hemisphere. Mon. Wea. Rev., 110, 916-932.

Sardeshmukh, P. D., 1984: The global circulation of the atmosphere during January-November 1979 based upon ECMWF analyses. Department of Meteorology, University of Reading, Reading, England, 144 pp.

Schaack T. K., D. R. Johnson and M.-Y. Wei, 1990: The three-dimensional distribution of atmospheric heating during the GWE. Tellus, 42A:3, 305-327.

Schmidt, P. J., and D. R. Johnson, 1972: Use of approximating polynomials to estimate profiles of wind, divergence and vertical motion. Mon. Wea. Rev., 100, 345-353.

Wei, M.-Y., D. R. Johnson and R. D. Townsend, 1983: Seasonal distributions of diabatic heating during the First GARP Global Experiment. Tellus, 35A, 241-255.

Wiin-Nielsen, A., and J. A. Brown, Jr., 1962: On diagnostic computations of atmospheric heat sources and sinks and the generation of available potential energy. Proc. of the Int. Symp. on Numerical Weather Prediction, Meteor. Soc. of Japan, Tokyo, November, 519-613.

Zillman, J. W., and D. R. Johnson, 1985: Thermally-forced mean mass circulations in the Southern Hemisphere. Tellus, 37A, 56-76.

December - November

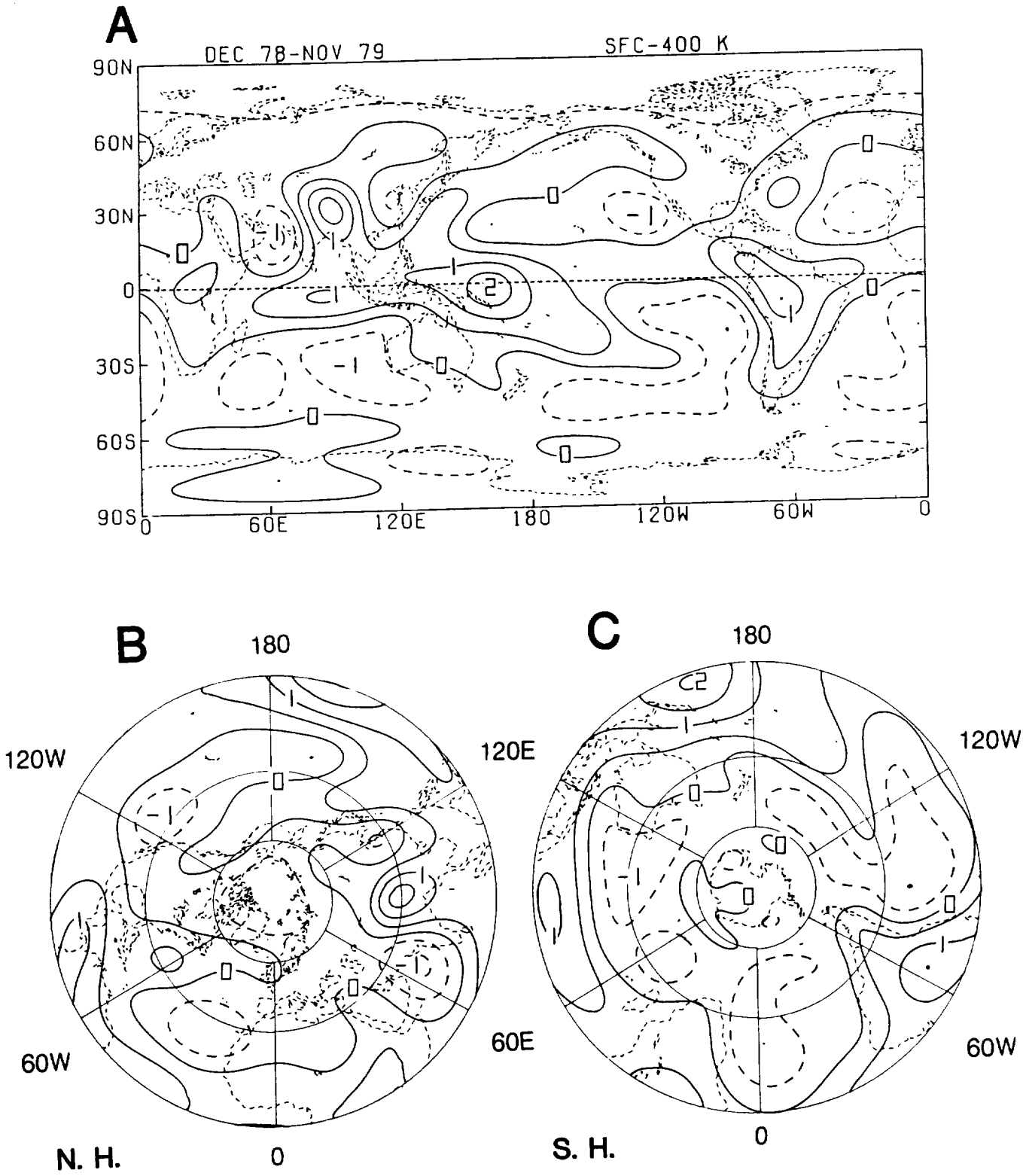

Fig. 1: Annual vertical-averaged heating (K day^{-1}) for December 1978 to November 1979; (A) global, (B) Northern Hemisphere and (C) Southern Hemisphere. Contour interval is 0.5 K day^{-1}.

December - November

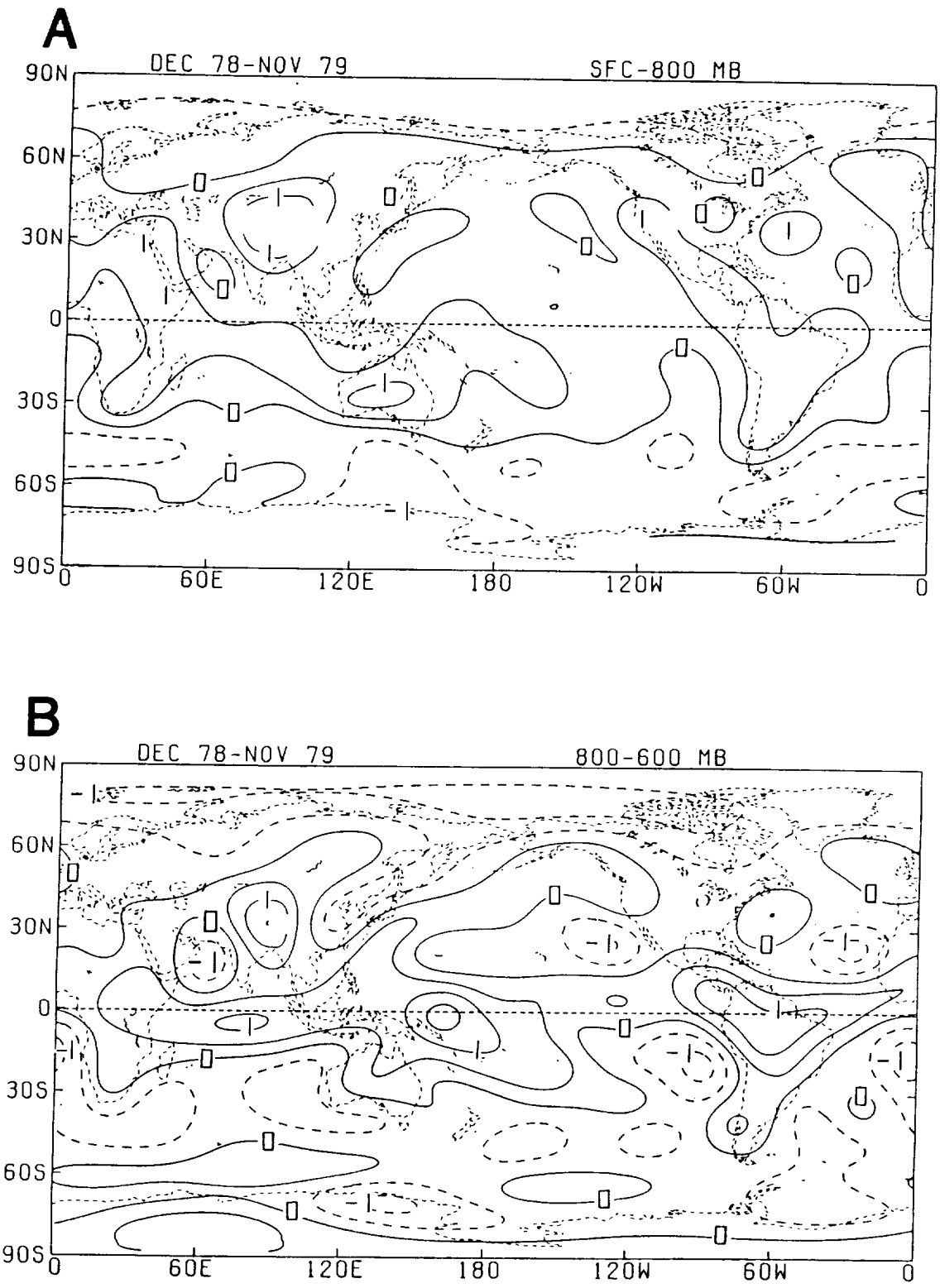

Fig. 2: Annual layer-averaged heating (K day^{-1}) for the (A) surface-800 mb, (B) 800-600 mb, (C) 600-400 mb and (D) 400-200 mb isobaric layers for December 1978 to November 1979. Contour interval is 0.5 K day^{-1}.

December – November

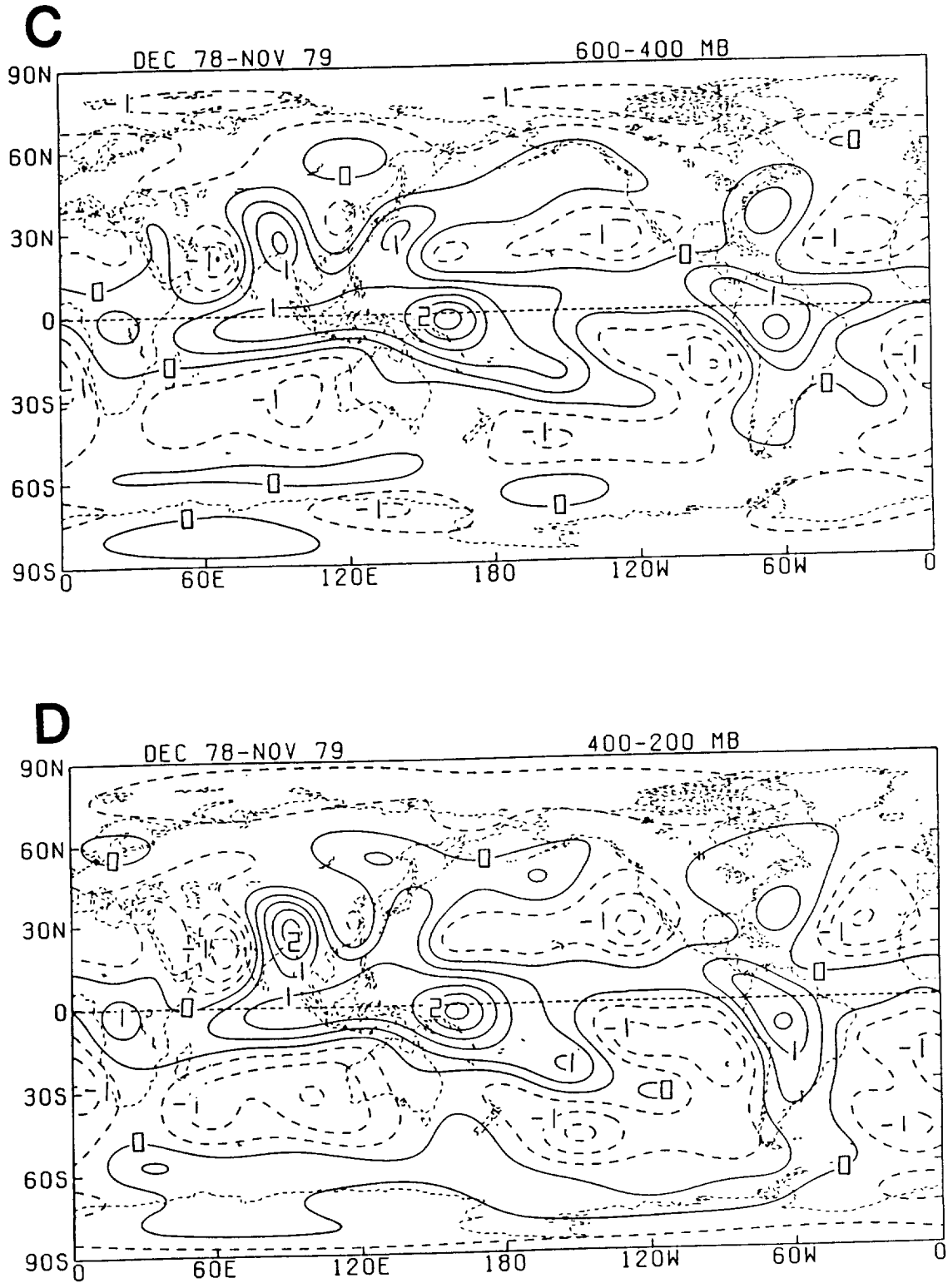

Fig. 2: (Continued).

December - November

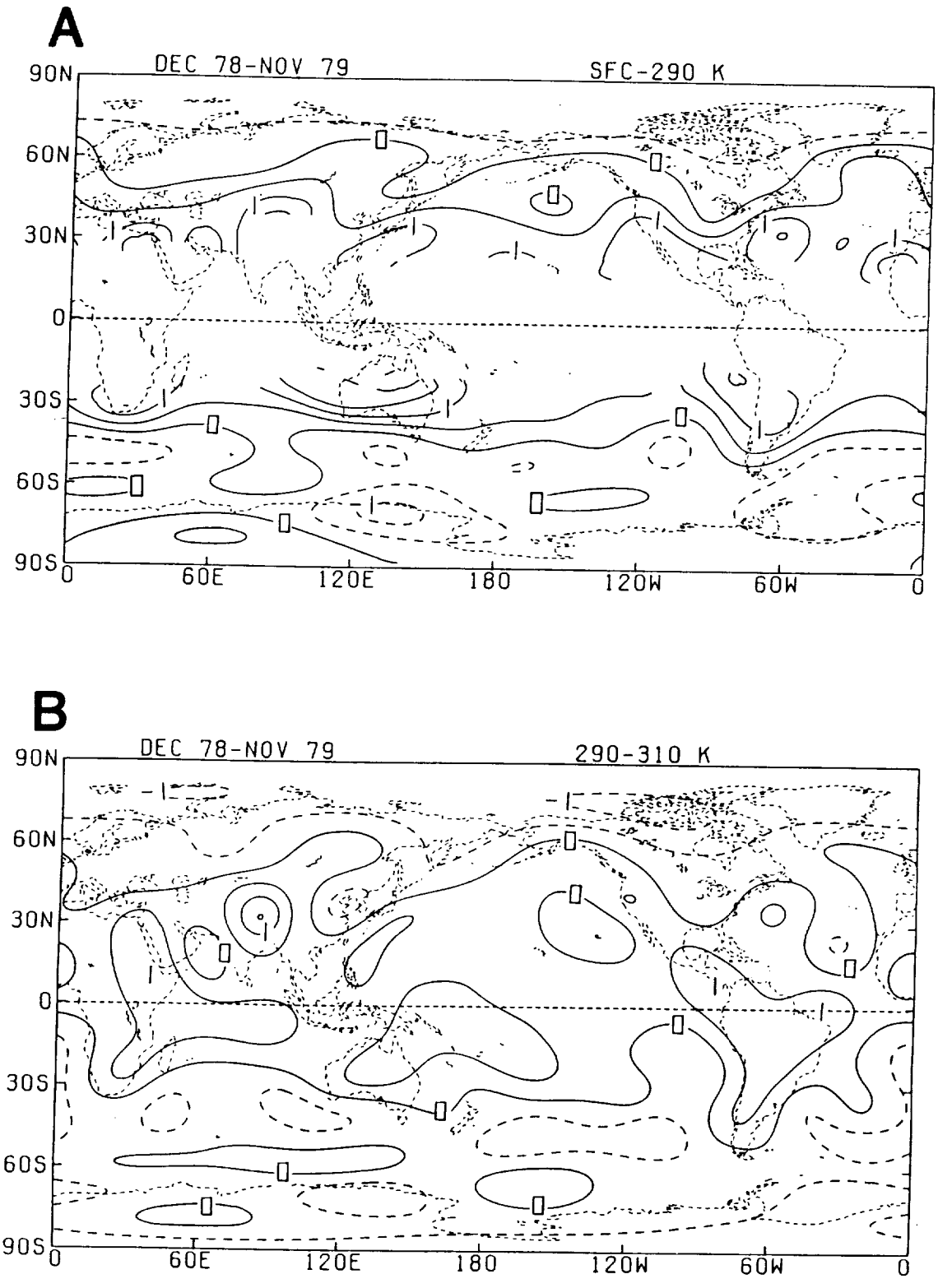

Fig. 3: Annual layer-averaged heating (K day^{-1}) for the (A) surface-290 K, (B) 290-310 K, (C) 310-330 K and (D) 330-400 K isentropic layers for December 1978 to November 1979. Contour interval is 0.5 K day^{-1}.

December – November

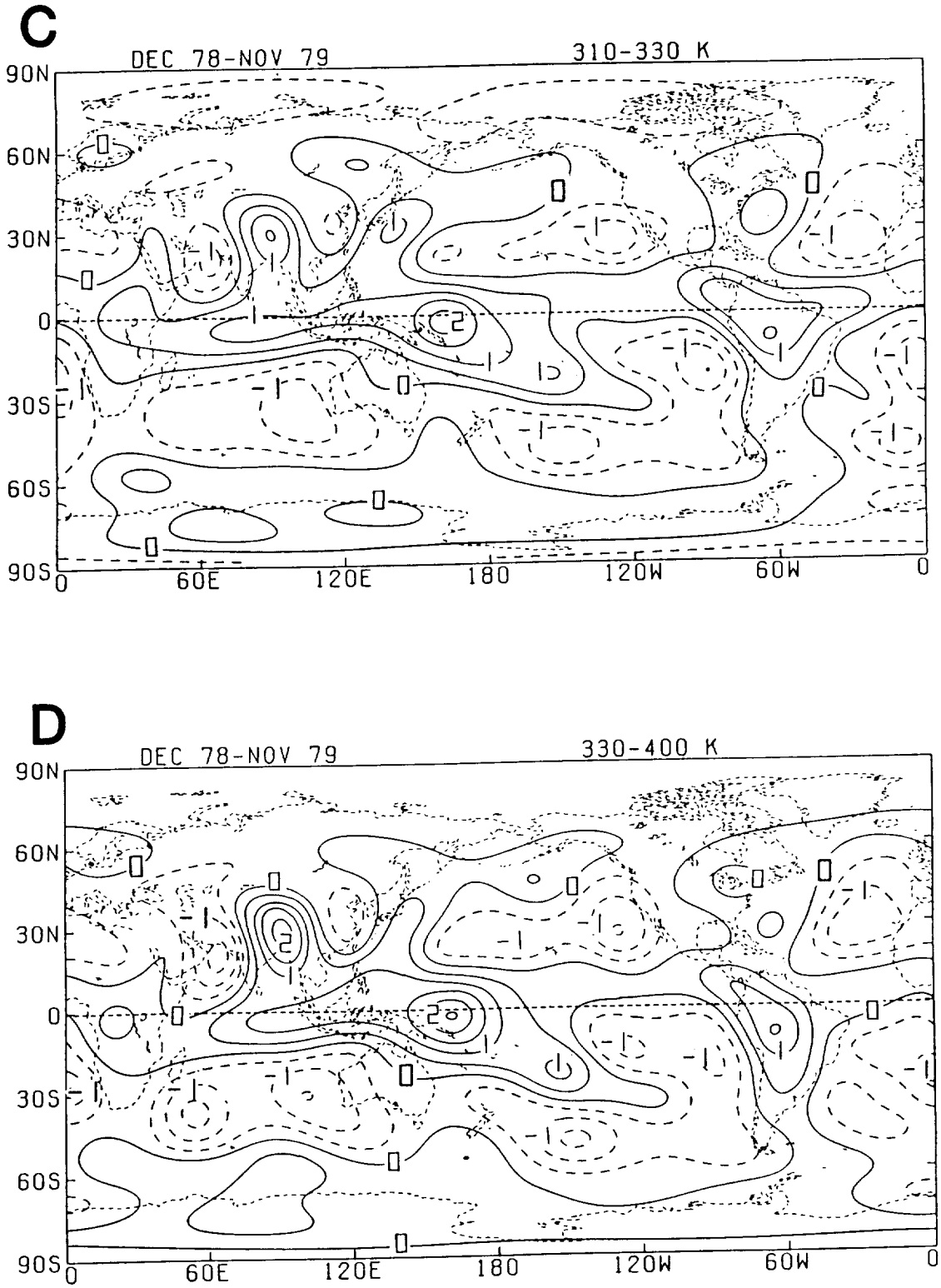

Fig. 3: (Continued).

December - November

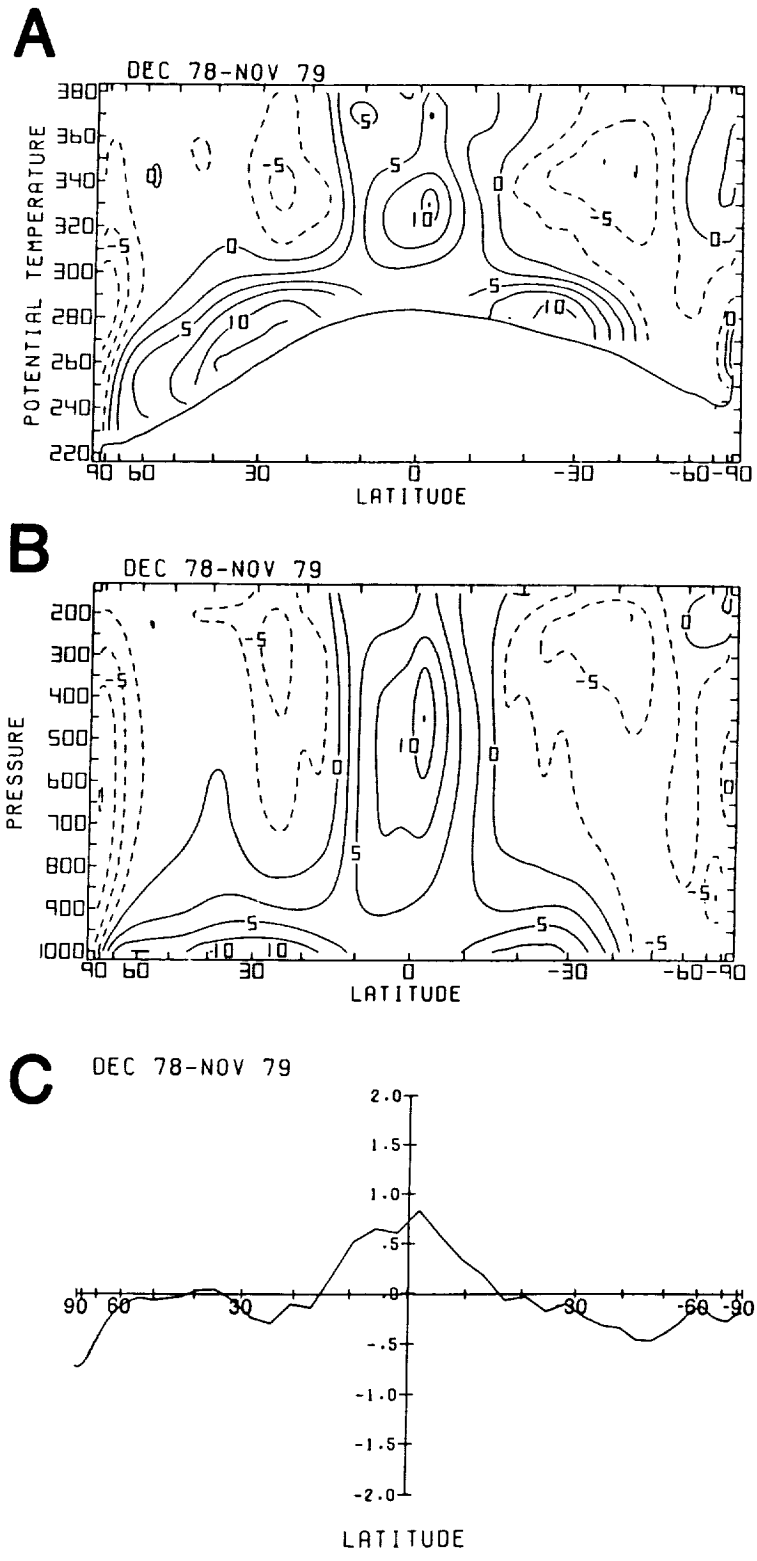

Fig. 4: Meridional cross sections of annual (A) isentropically and (B) isobarically zonally averaged heating (10^{-1} K day^{-1}), and (C) meridional profile of zonally-vertically averaged heating for December 1978 to November 1979 (K day^{-1}). Contour interval in (A) and (B) is 0.25 K day^{-1}.

December – November

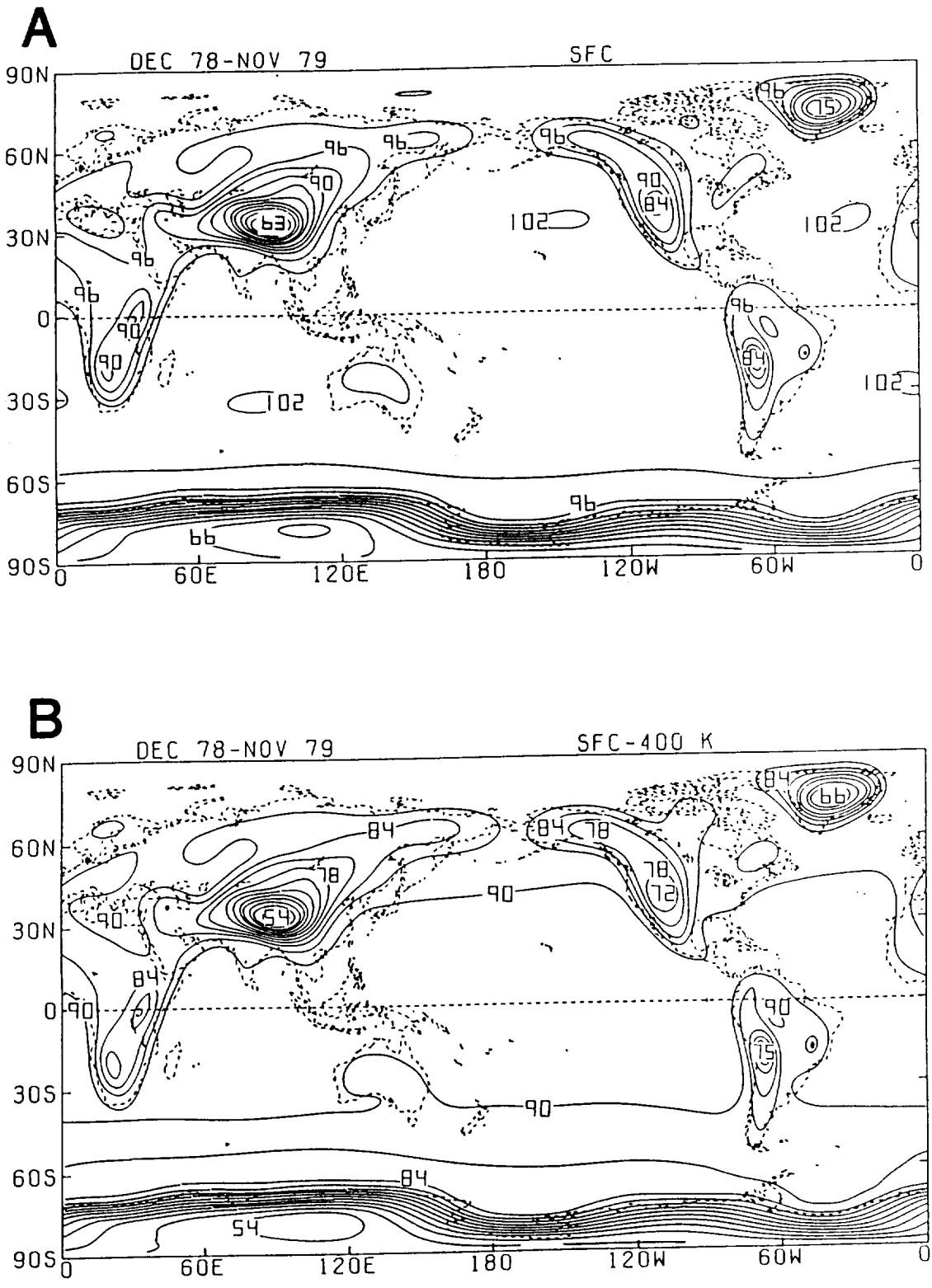

Fig. 5: Global distributions of annual-averaged (A) surface pressure (10^1 mb) and (B) pressure difference (10^1 mb) between the surface and the 400 K isentropic level for December 1978 to November 1979. Contour interval is 30 mb.

December – November

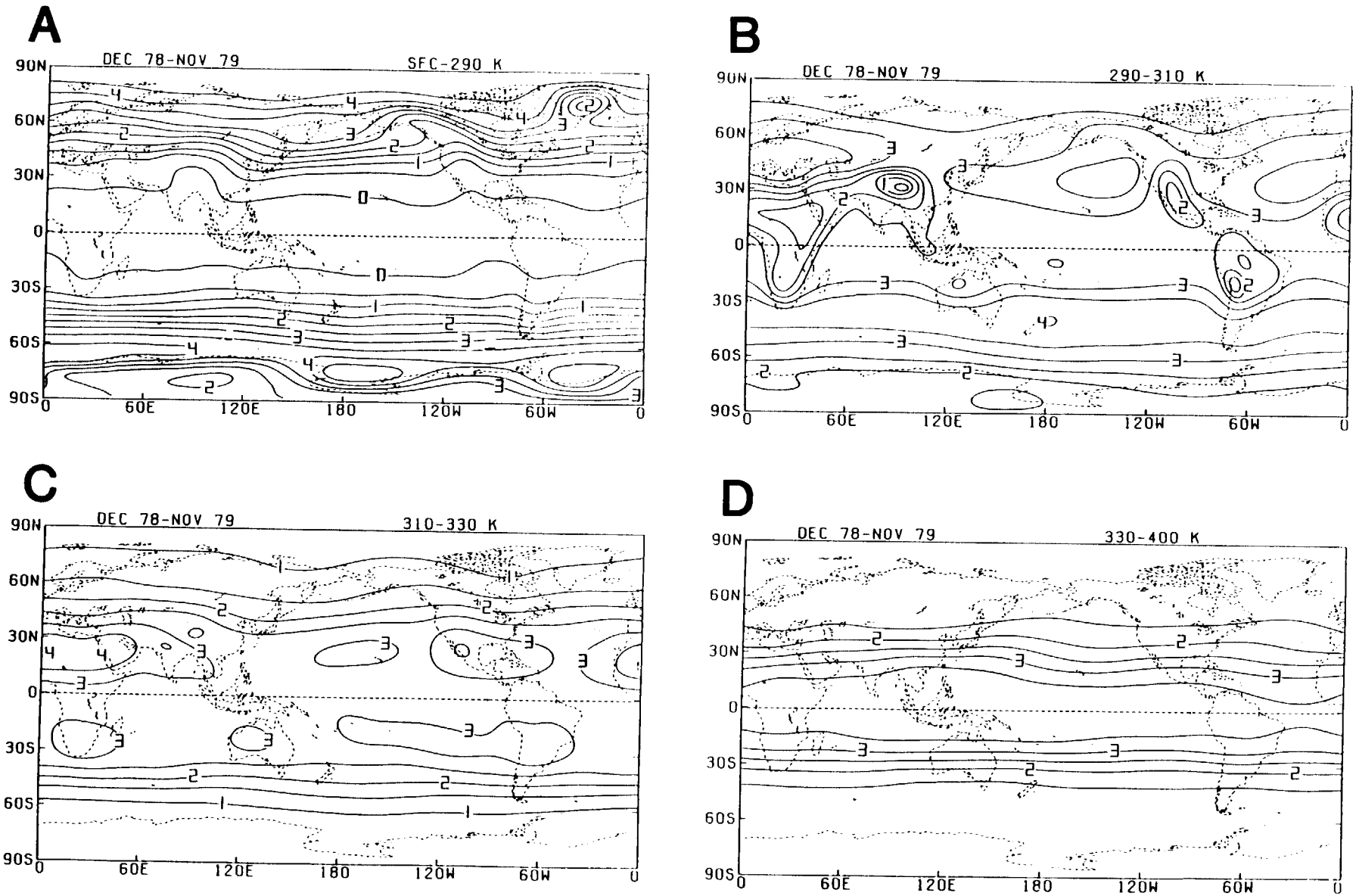

Fig. 6: Annual-averaged pressure difference (10^2 mb) between the upper and lower isentropic levels of the (A) surface-290 K, (B) 290-310 K, (C) 310-330 K and (D) 330-400 K isentropic layers for December 1978 to November 1979. Contour interval is 50 mb.

December - February

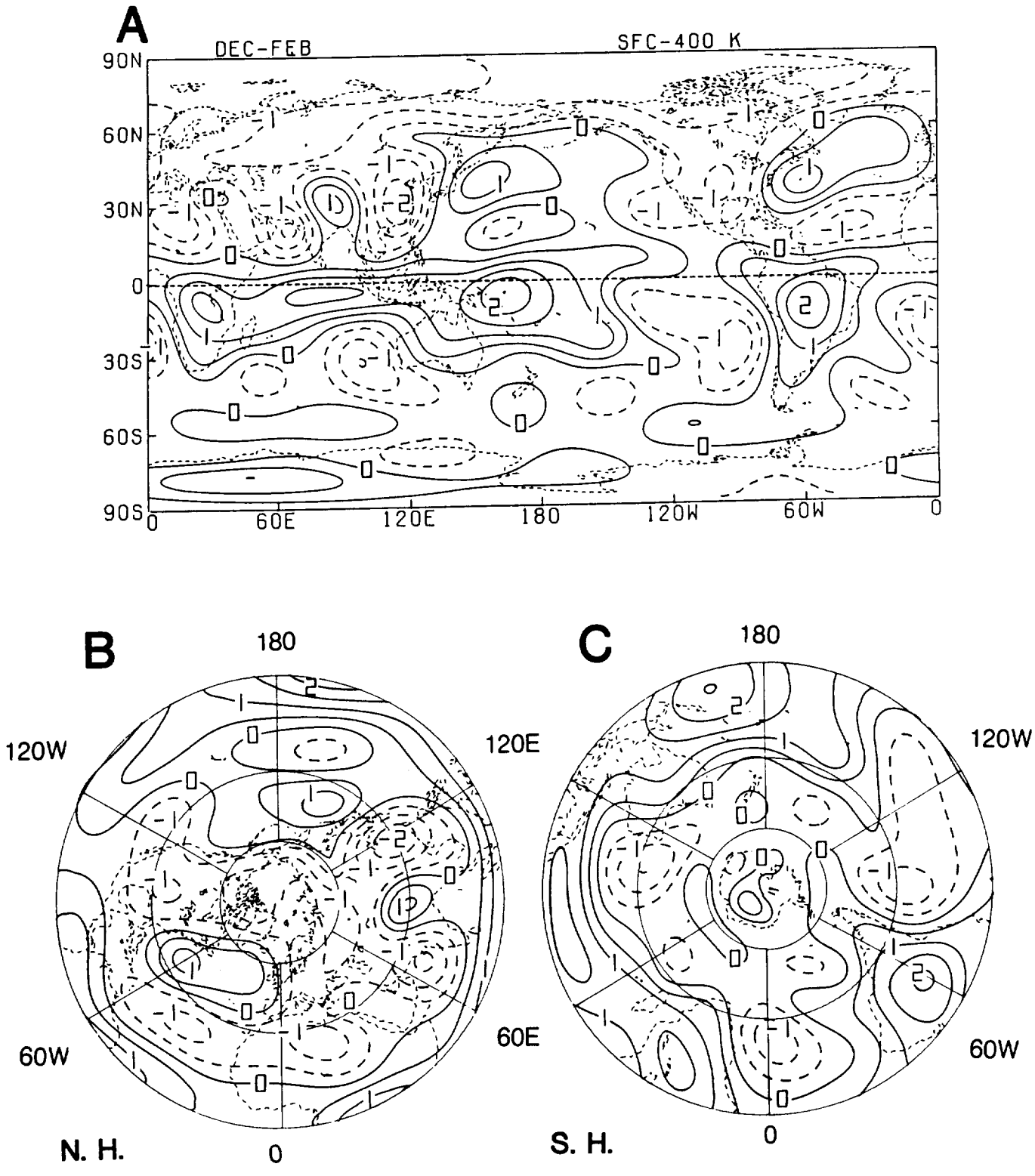

Fig. 7: Seasonal vertical-averaged heating (K day^{-1}) for December 1978 to February 1979; (A) global, (B) Northern and (C) Southern Hemisphere. Contour interval is 0.5 K day^{-1}.

December - February

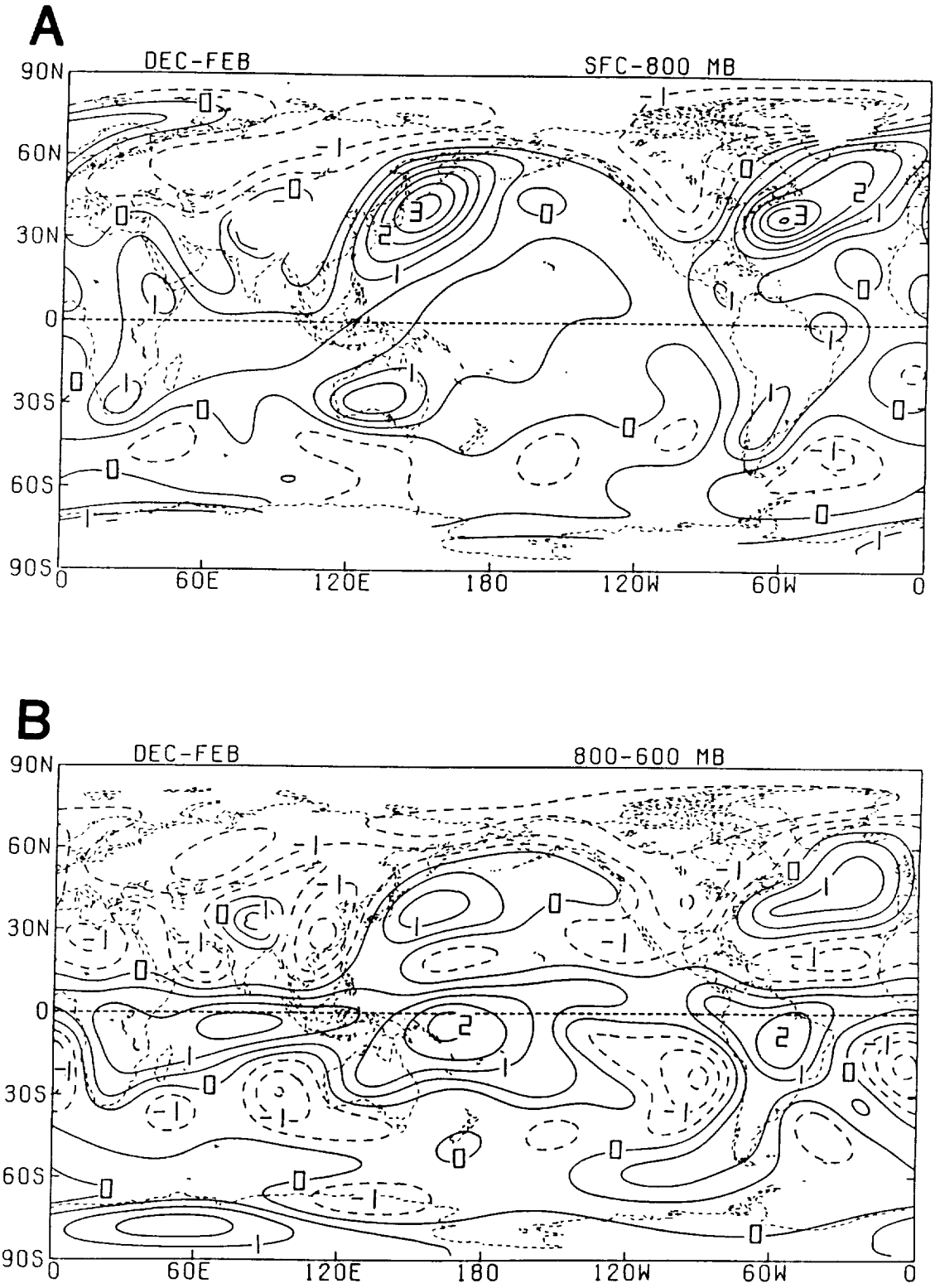

Fig. 8: Seasonal layer-averaged heating (K day^{-1}) for the (A) surface-800 mb, (B) 800-600 mb, (C) 600-400 mb and (D) 400-200 mb isobaric layers for December 1978 to February 1979. Contour interval is 0.5 K day^{-1}.

December - February

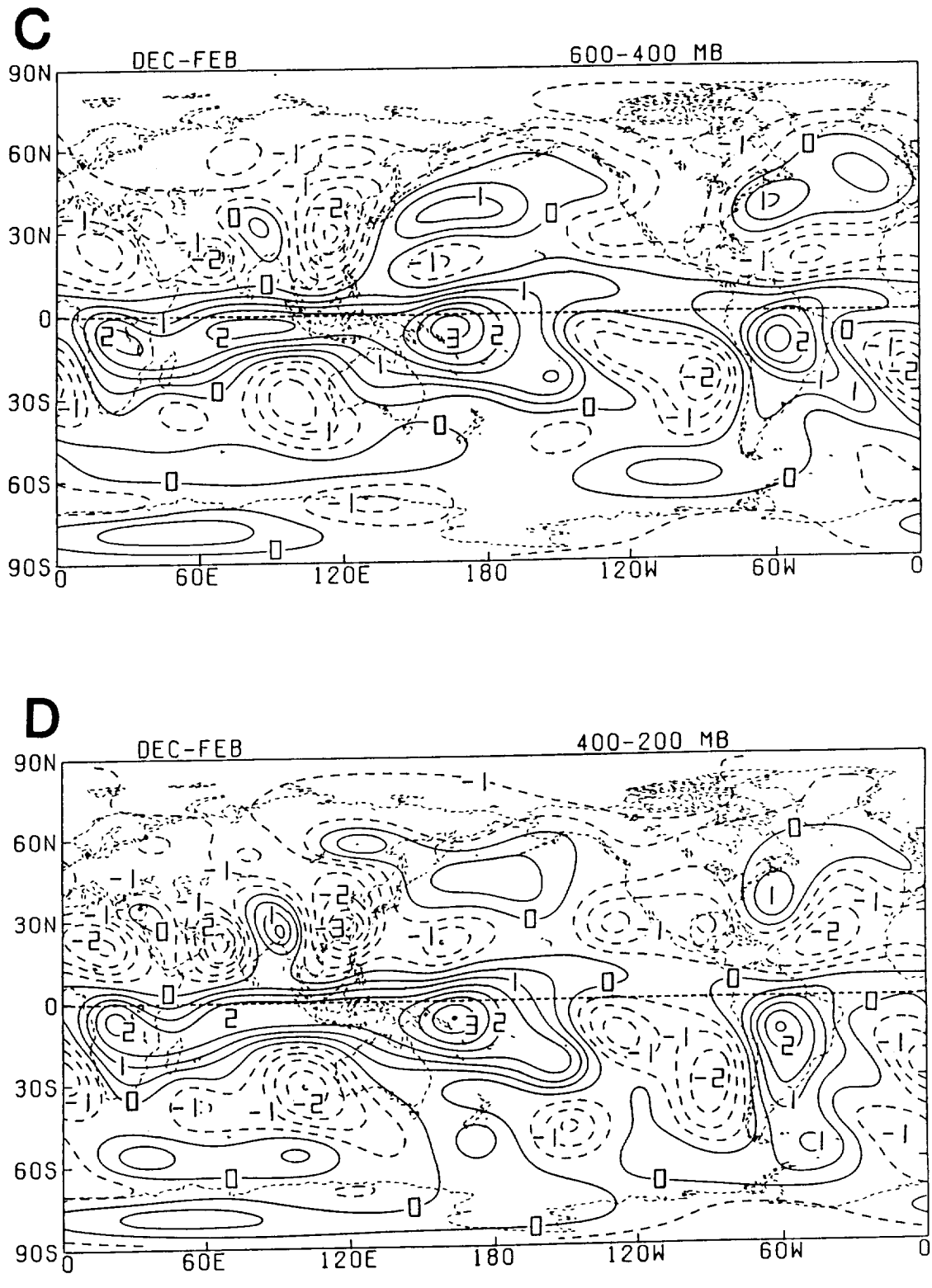

Fig. 8: (Continued).

December - February

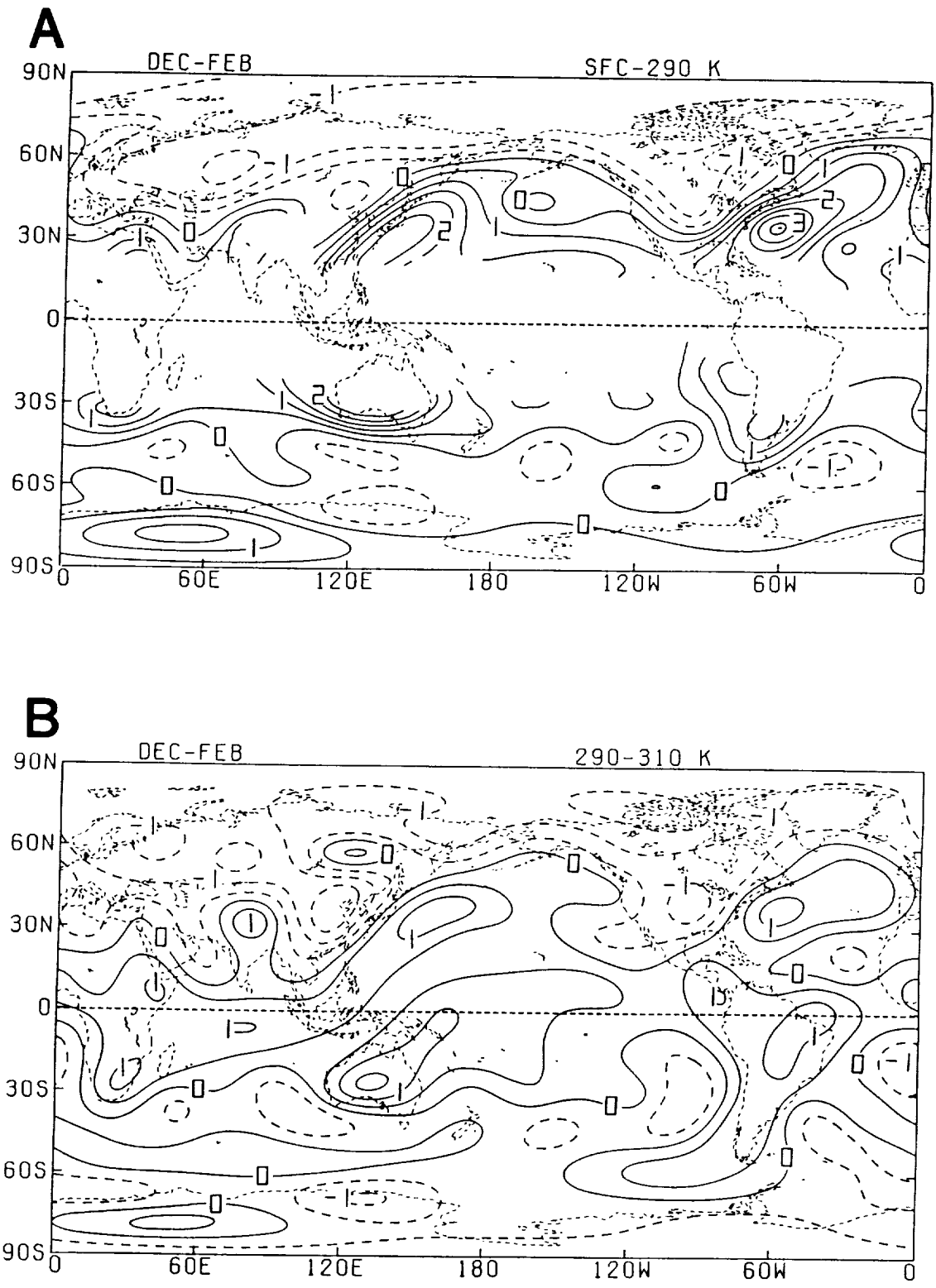

Fig. 9: Seasonal layer-averaged heating (K day^{-1}) for the (A) surface-290 K, (B) 290-310 K, (C) 310-330 K and (D) 330-400 K isentropic layers for December 1978 to February 1979. Contour interval is 0.5 K day^{-1}.

December - February

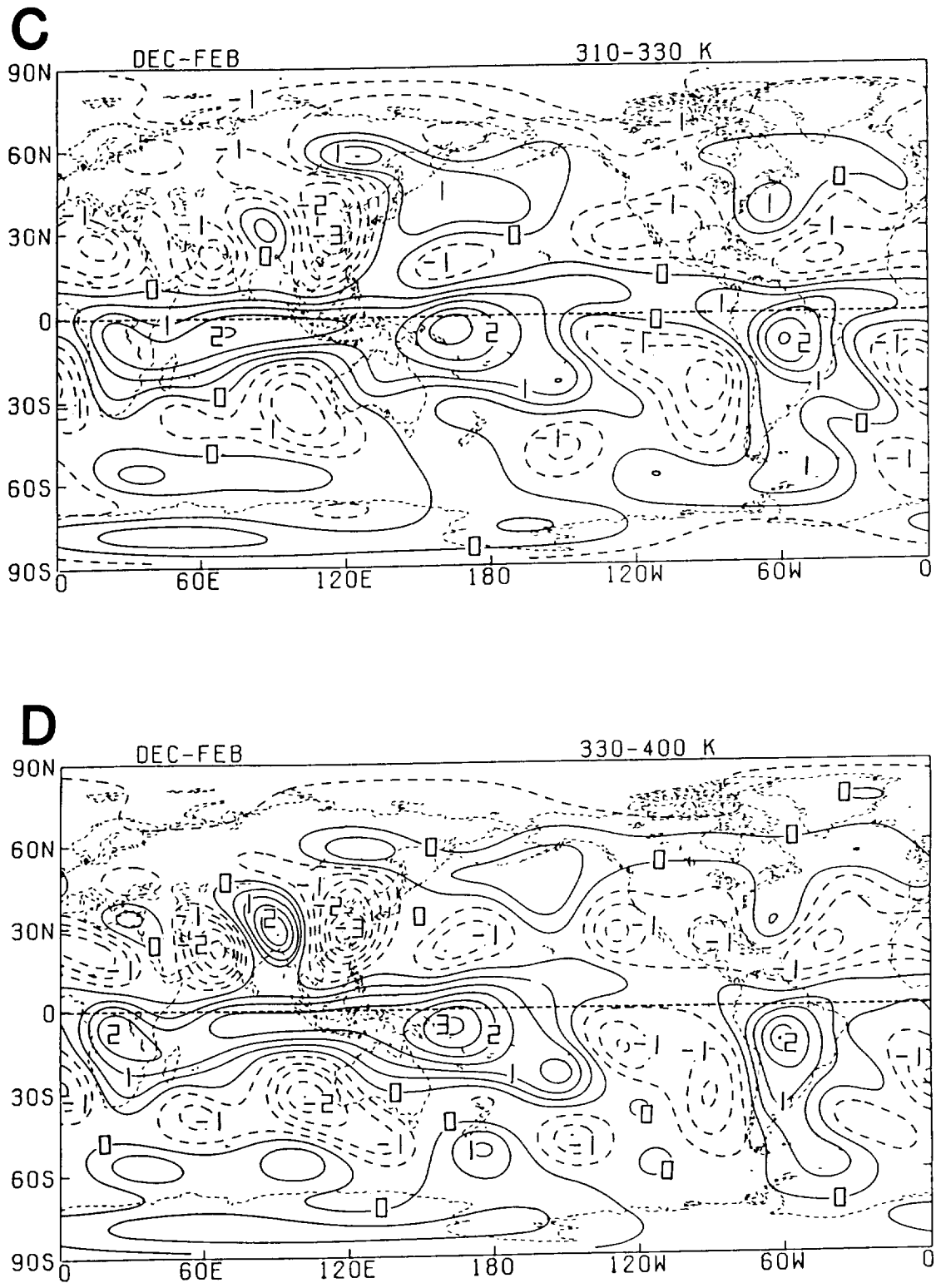

Fig. 9: (Continued).

December - February

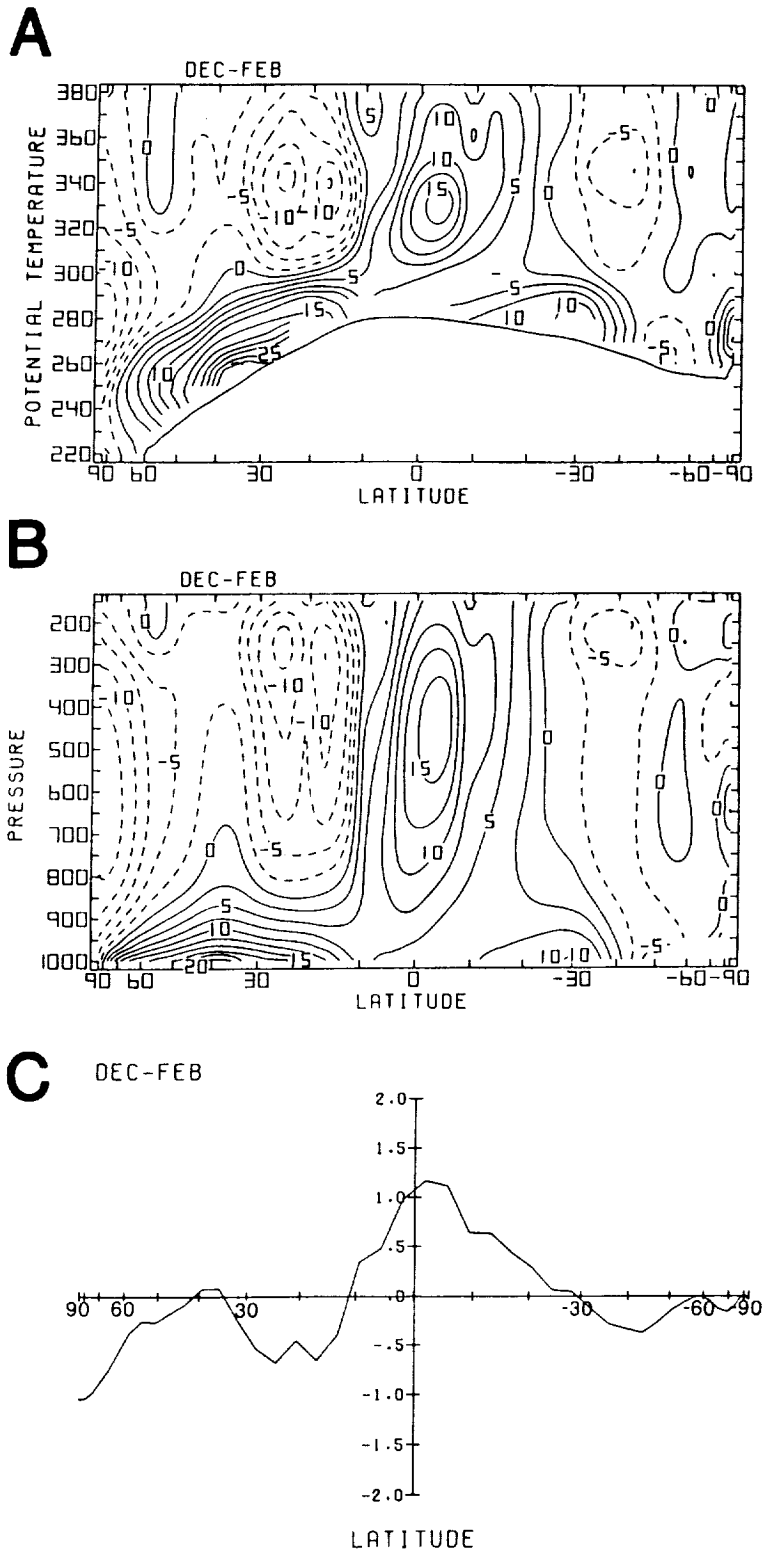

Fig. 10: Meridional cross sections of seasonal (A) isentropically and (B) isobarically zonally averaged heating (10^{-1} K day^{-1}), and (C) meridional profile of zonally-vertically averaged heating for December 1978 to February 1979 (K day^{-1}). Contour interval in (A) and (B) is 0.25 K day^{-1}.

December - February

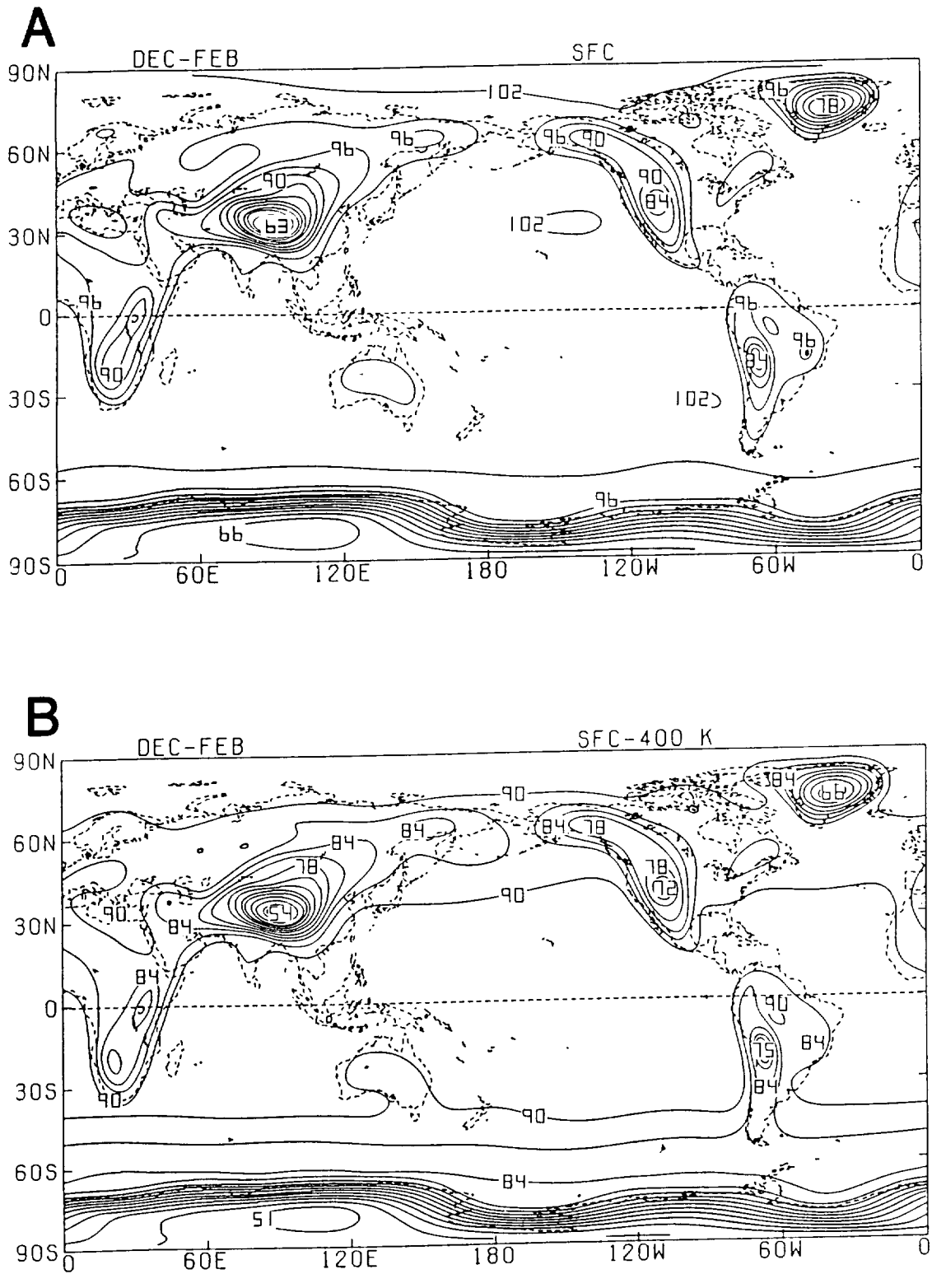

Fig. 11: Global distributions of seasonal-averaged (A) surface pressure (10^1 mb) and (B) pressure difference (10^1 mb) between the surface and the 400 K isentropic level for December 1978 to February 1979. Contour interval is 30 mb.

December – February

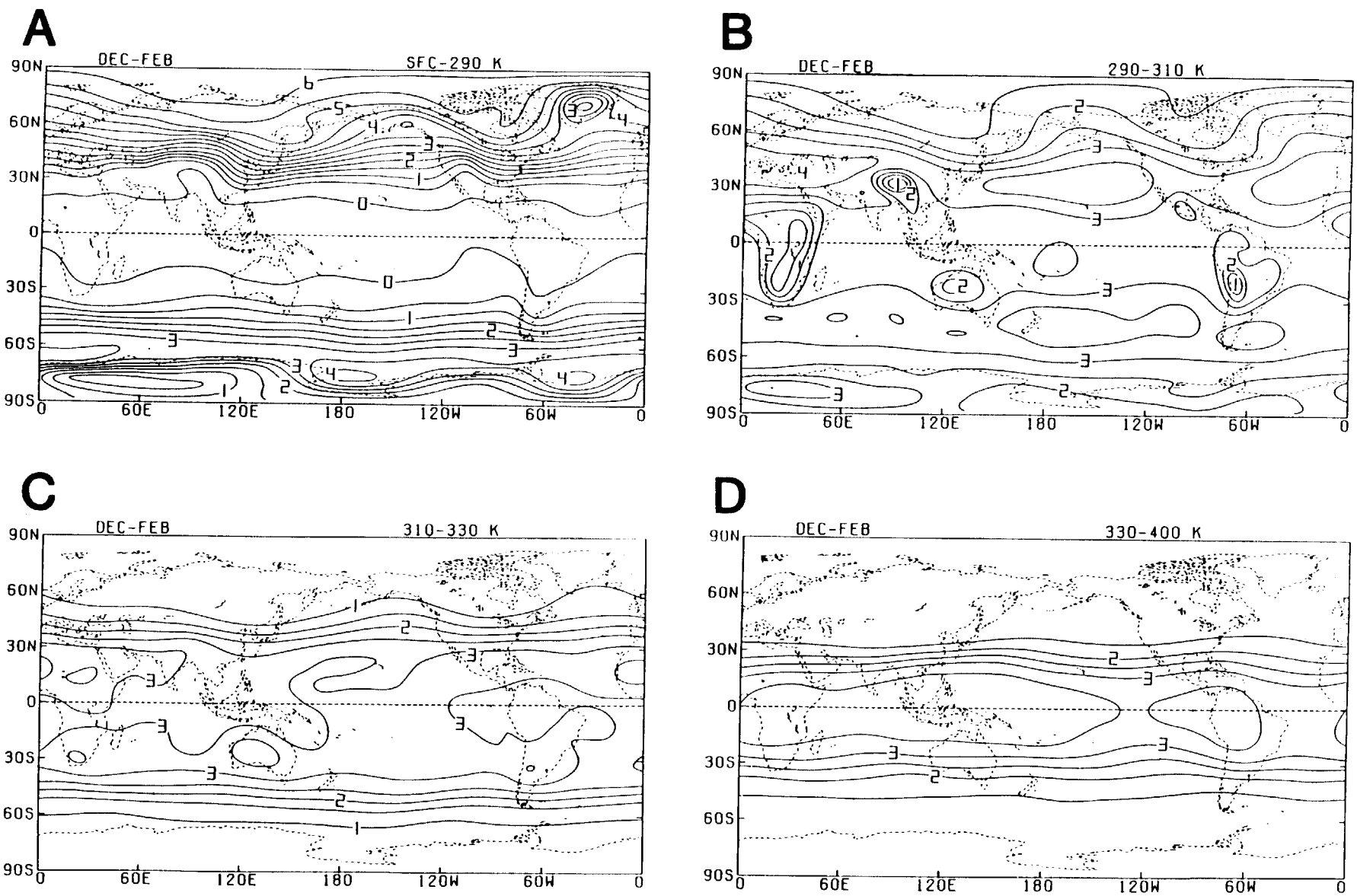

Fig. 12: Seasonal-averaged pressure difference (10^2 mb) between the upper and lower isentropic levels of the (A) surface-290 K, (B) 290-310 K, (C) 310-330 K and (D) 330-400 K isentropic layers for December 1978 to February 1979. Contour interval is 50 mb.

March - May

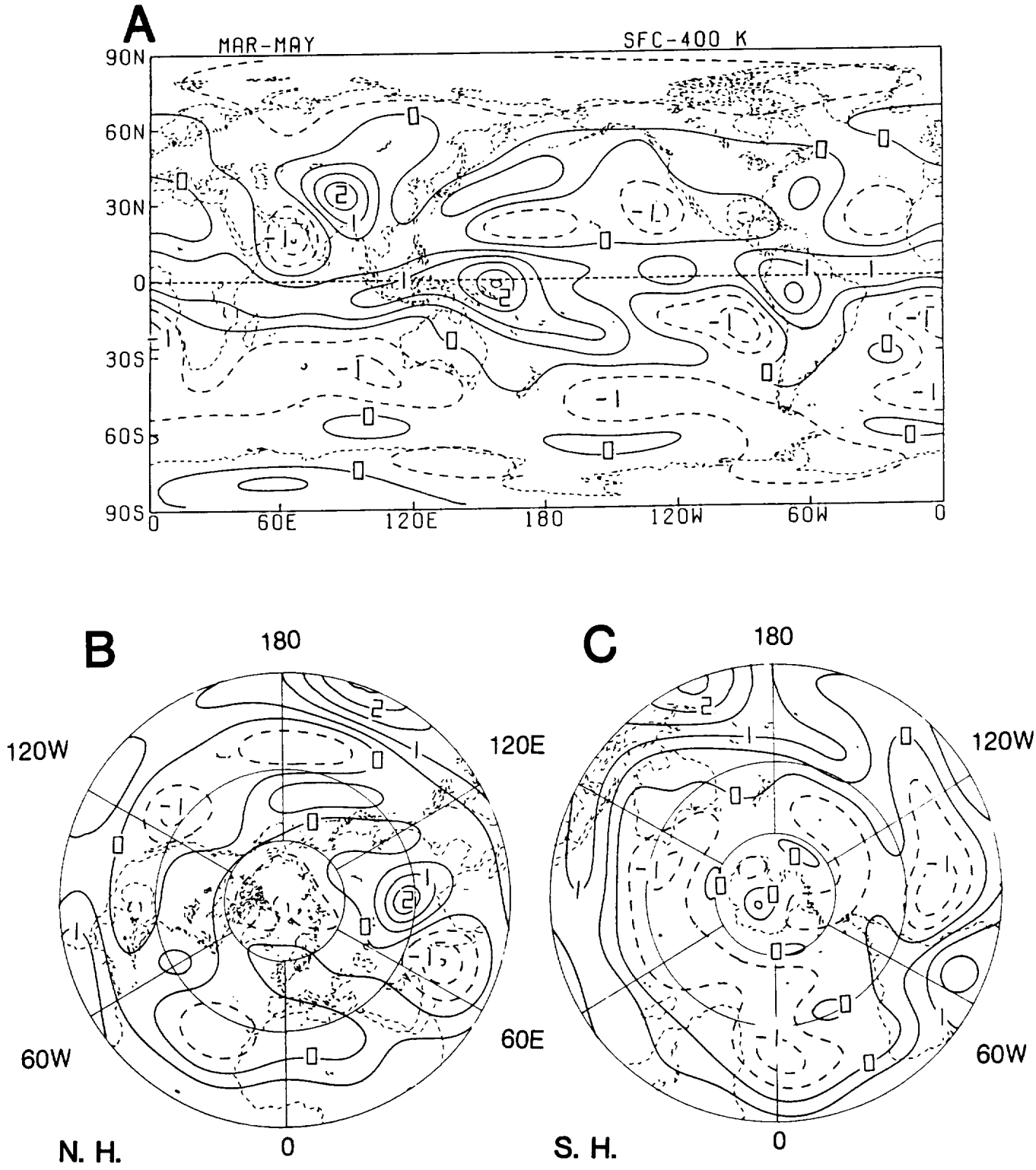

Fig. 13: Seasonal vertical-averaged heating (K day^{-1}) for March 1979 to May 1979; (A) global, (B) Northern and (C) Southern Hemisphere. Contour interval is 0.5 K day^{-1}.

March - May

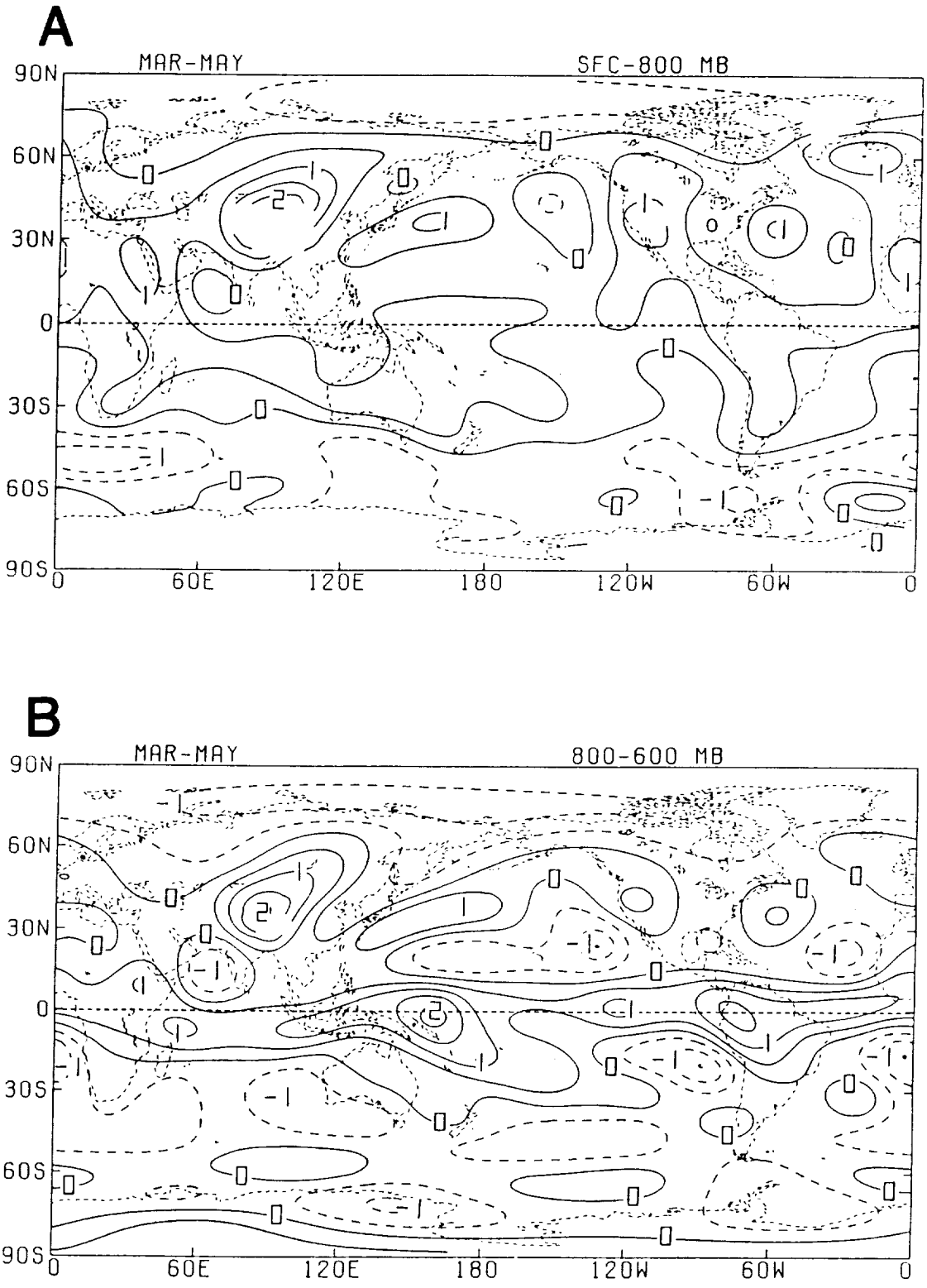

Fig. 14: Seasonal layer-averaged heating (K day^{-1}) for the (A) surface-800 mb, (B) 800-600 mb, (C) 600-400 mb and (D) 400-200 mb isobaric layers for March 1979 to May 1979. Contour interval is 0.5 day^{-1}.

March - May

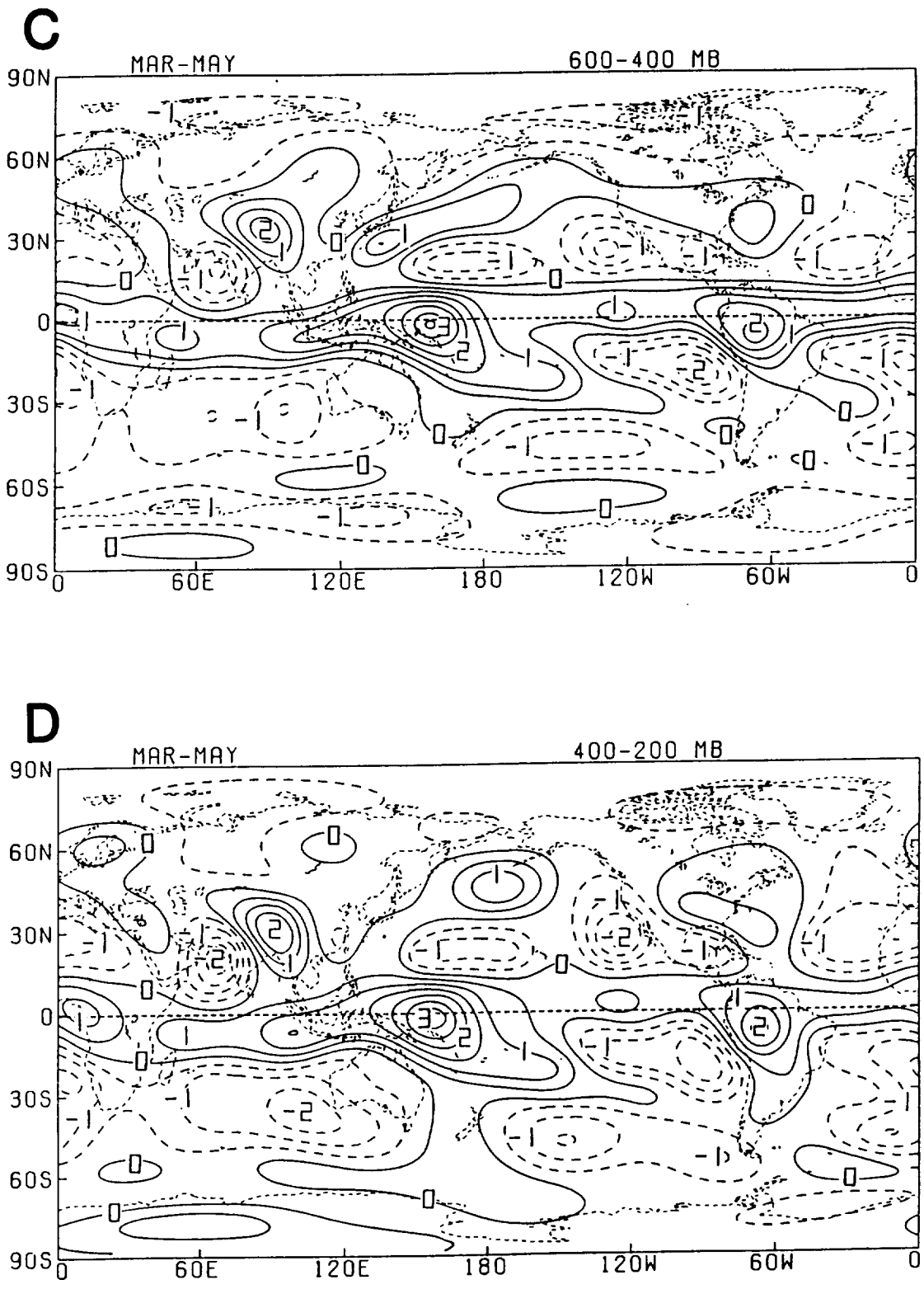

Fig. 14: (Continued).

March - May

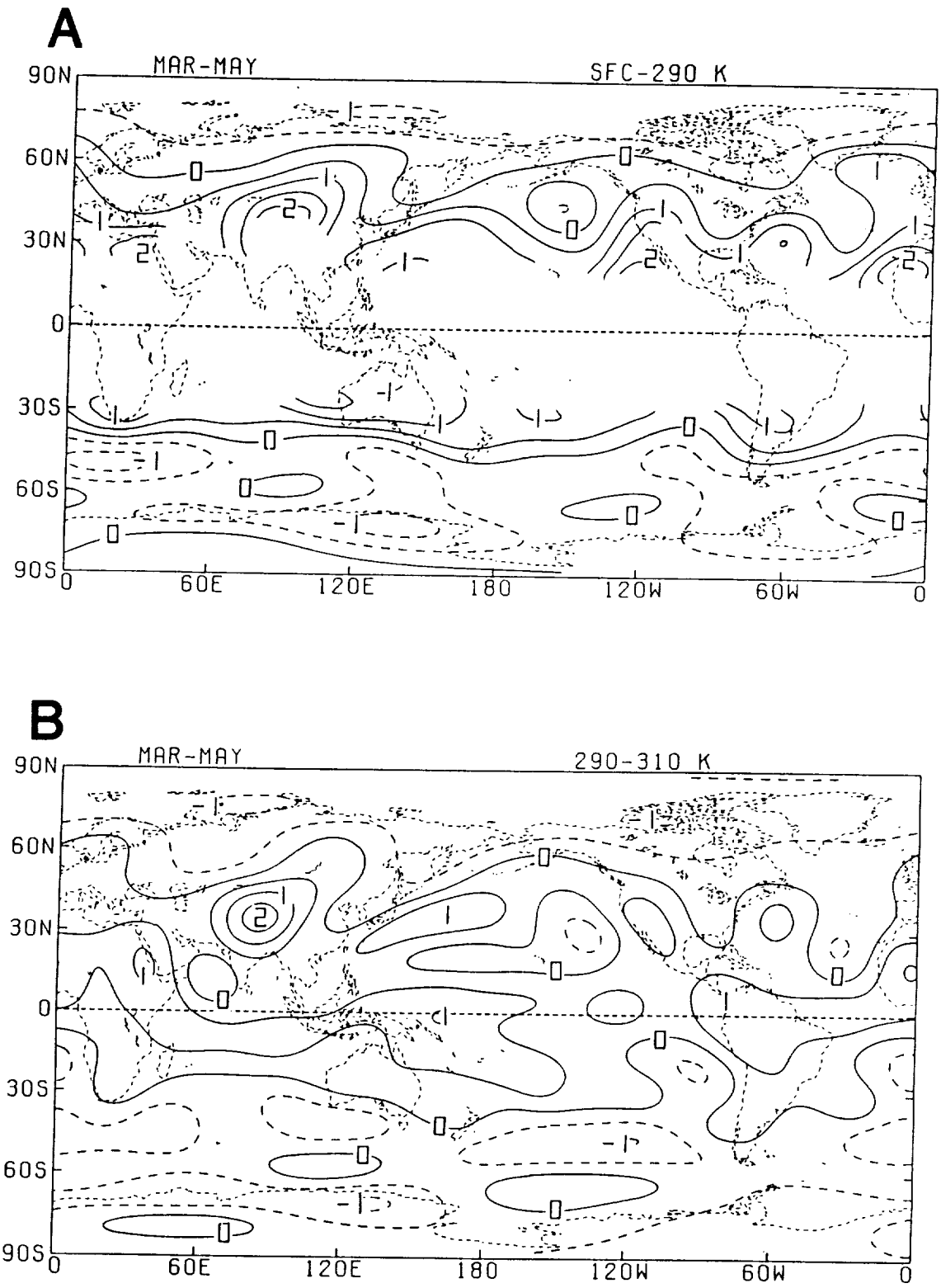

Fig. 15: Seasonal layer-averaged heating (K day^{-1}) for the (A) surface-290 K, (B) 290-310 K, (C) 310-330 K and (D) 330-400 K isentropic layers for March 1979 to May 1979. Contour interval is 0.5 K day^{-1}.

March - May

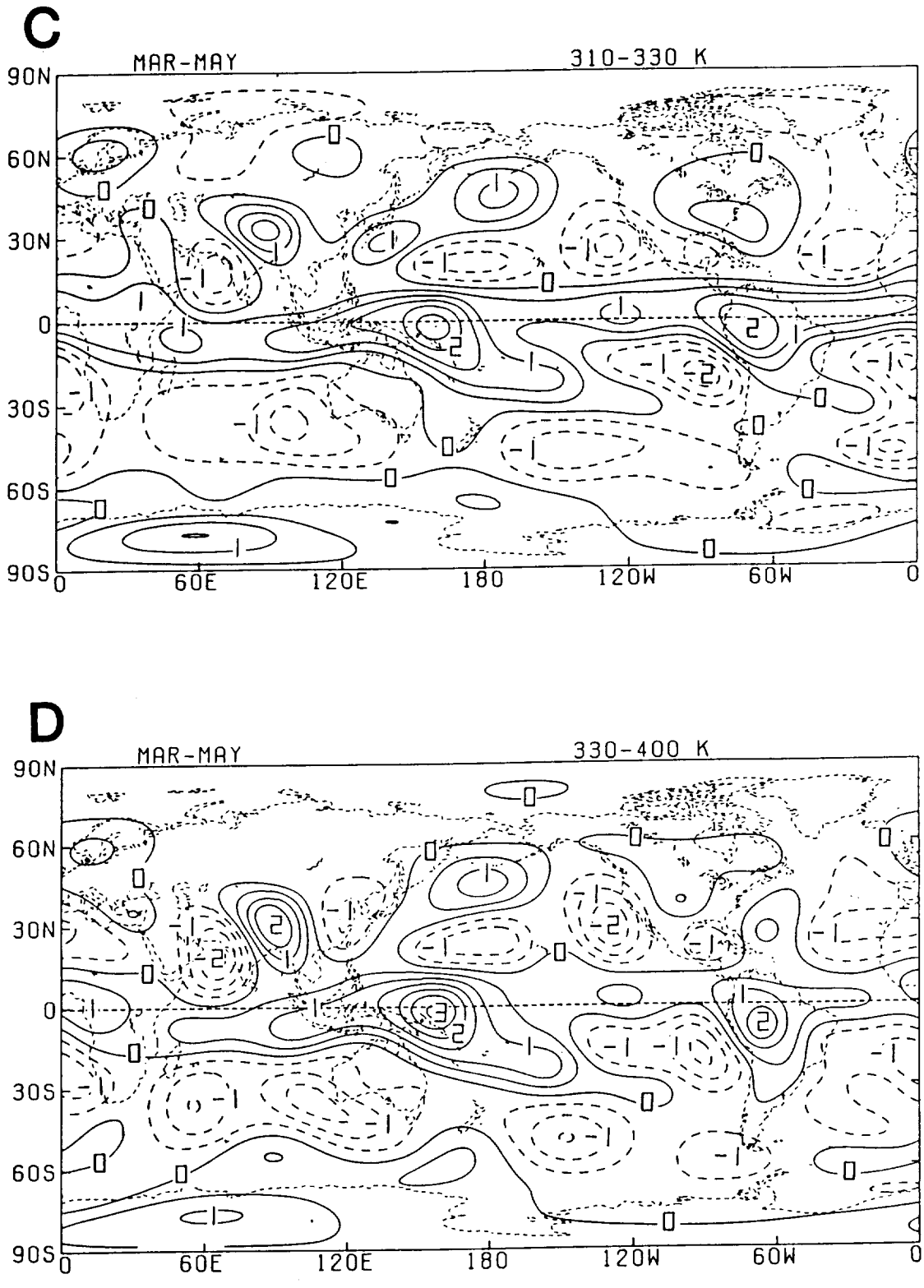

Fig. 15: (Continued).

March - May

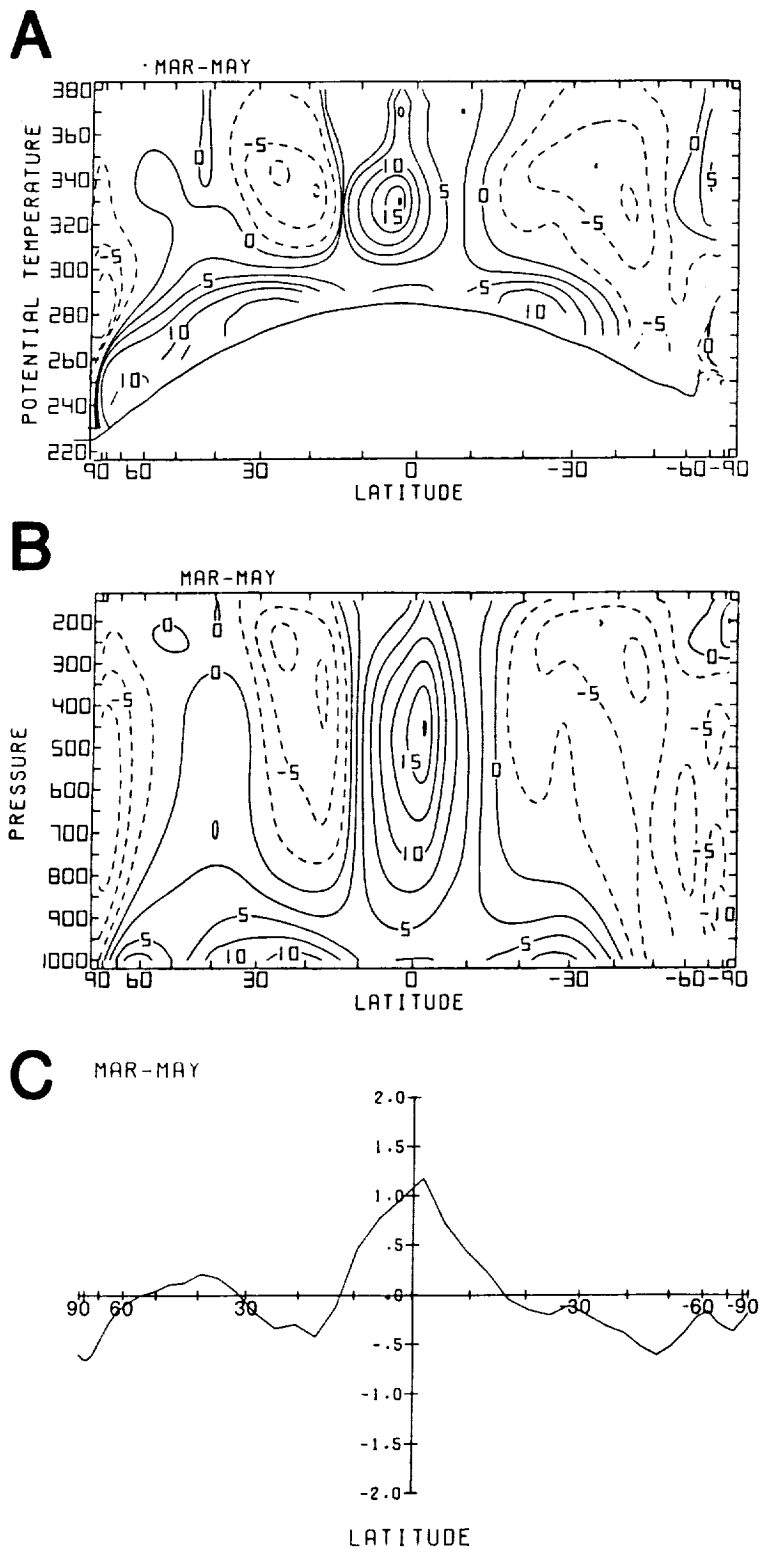

Fig. 16: Meridional cross sections of seasonal (A) isentropically and (B) isobarically zonally averaged heating (10^{-1} K day^{-1}), and (C) meridional profile of zonally-vertically averaged heating for March 1979 to May 1979 (K day^{-1}). Contour interval in (A) and (B) is 0.25 K day^{-1}.

March - May

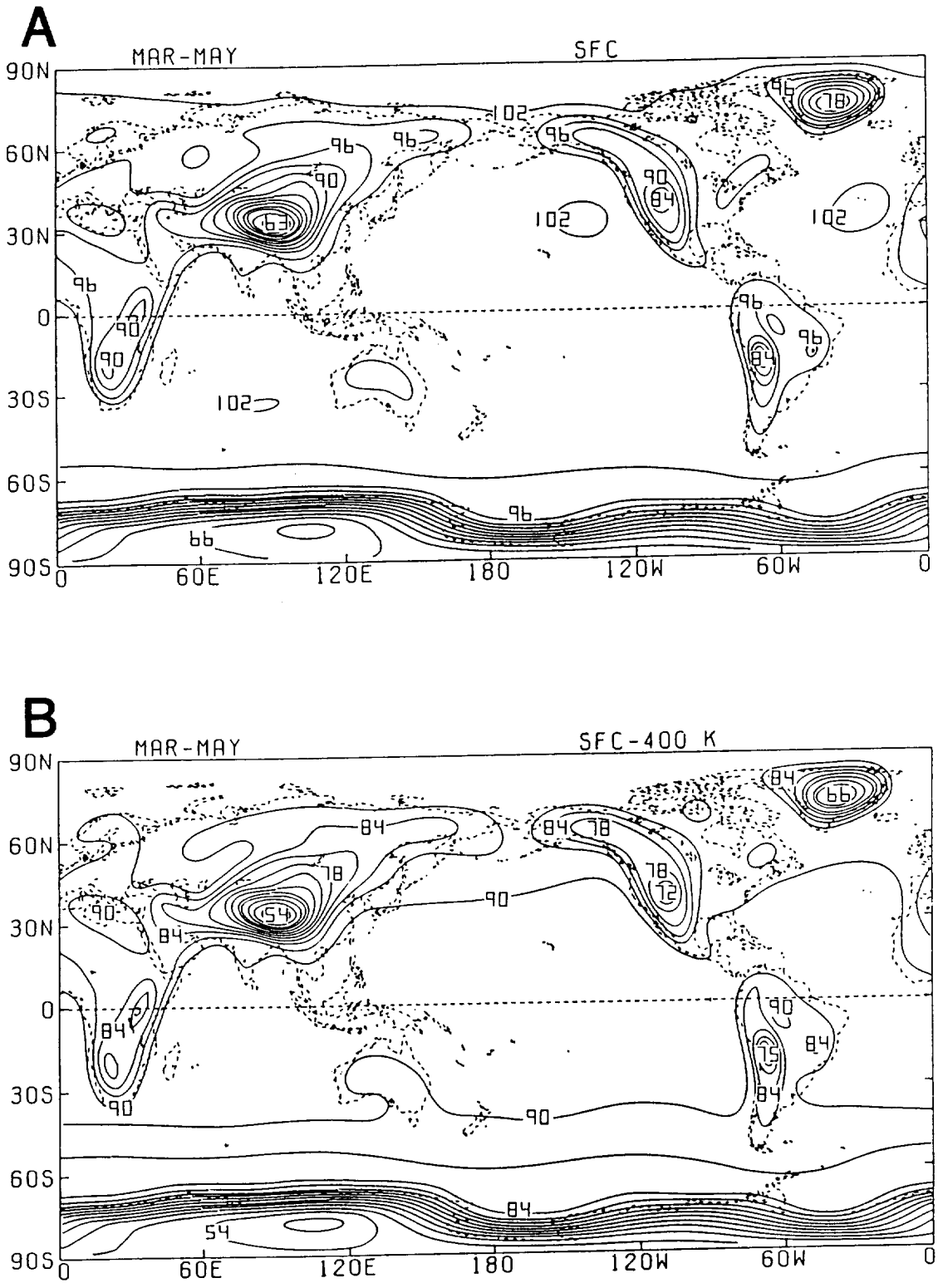

Fig. 17: Global distributions of seasonal-averaged (A) surface pressure (10^1 mb) and (B) pressure difference (10^1 mb) between the surface and the 400 K isentropic level for March 1979 to May 1979. Contour interval is 30 mb.

March – May

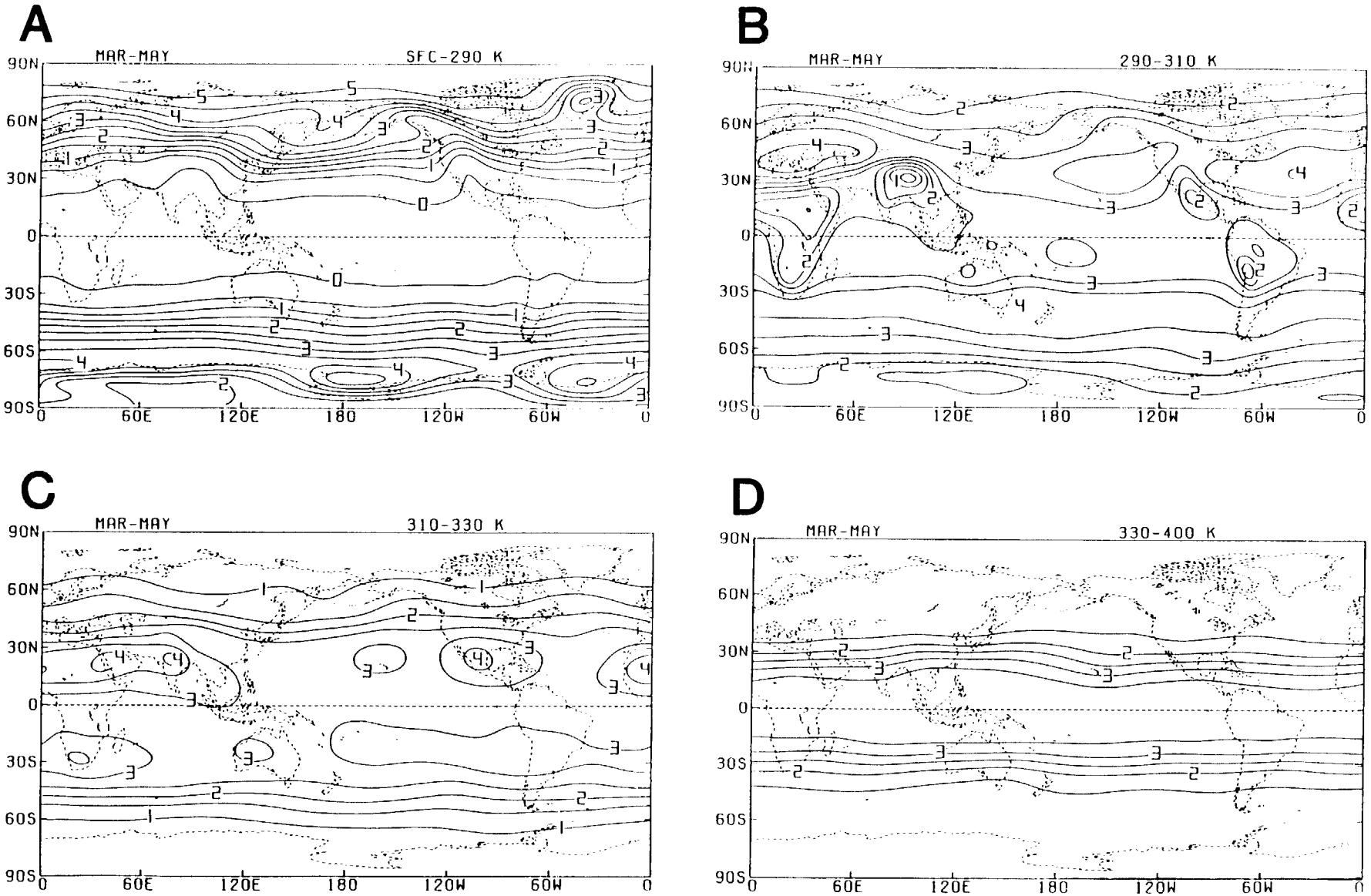

Fig. 18: Seasonal-averaged pressure difference (10^2 mb) between the upper and lower isentropic levels of the (A) surface-290 K, (B) 290-310 K, (C) 310-330 K and (D) 330-400 K isentropic layers for March 1979 to May 1979. Contour interval is 50 mb.

June - August

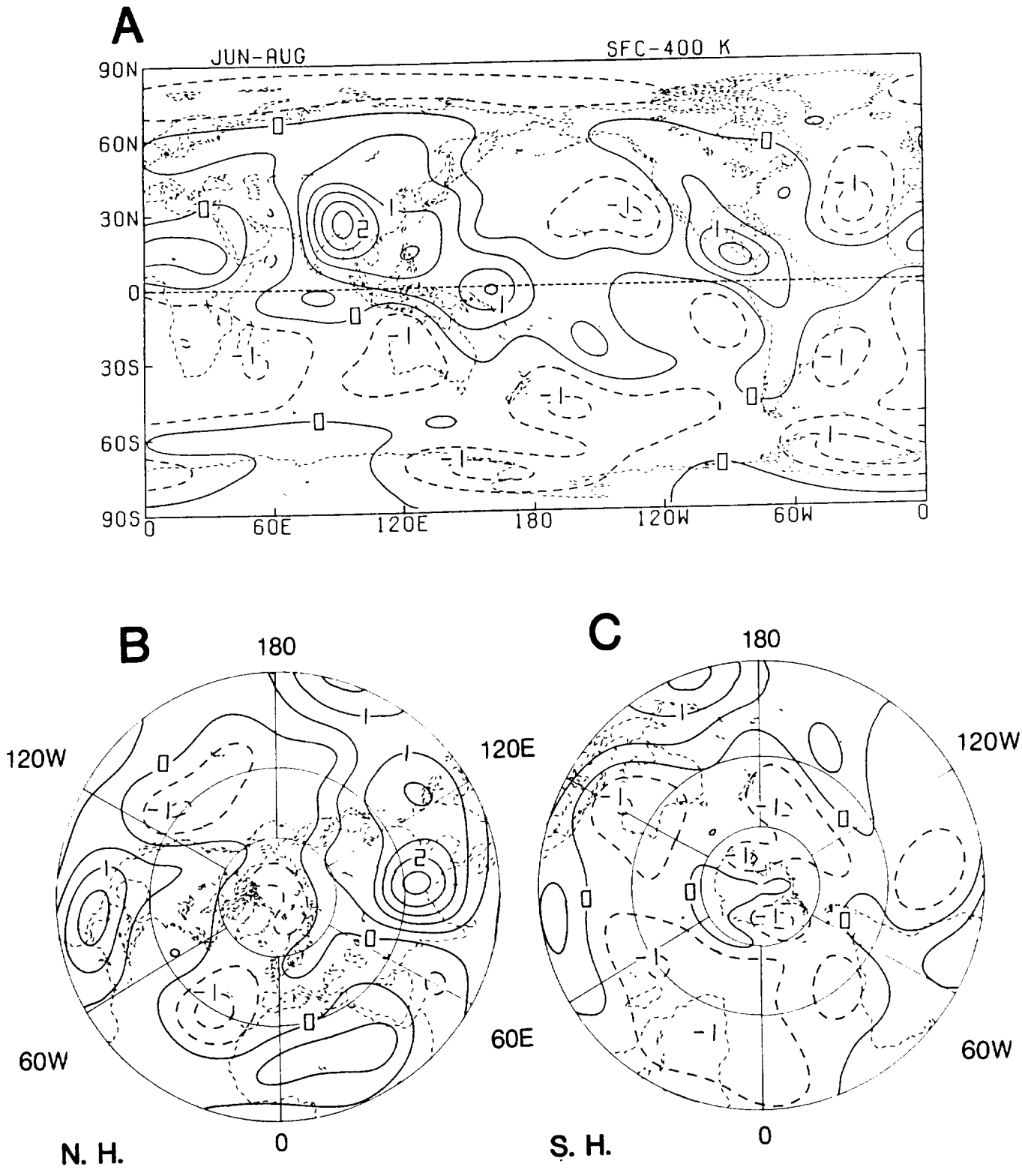

Fig. 19: Seasonal vertical-averaged heating (K day^{-1}) for June 1979 to August 1979; (A) global, (B) Northern and (C) Southern Hemisphere. Contour interval is 0.5 K day^{-1}.

June - August

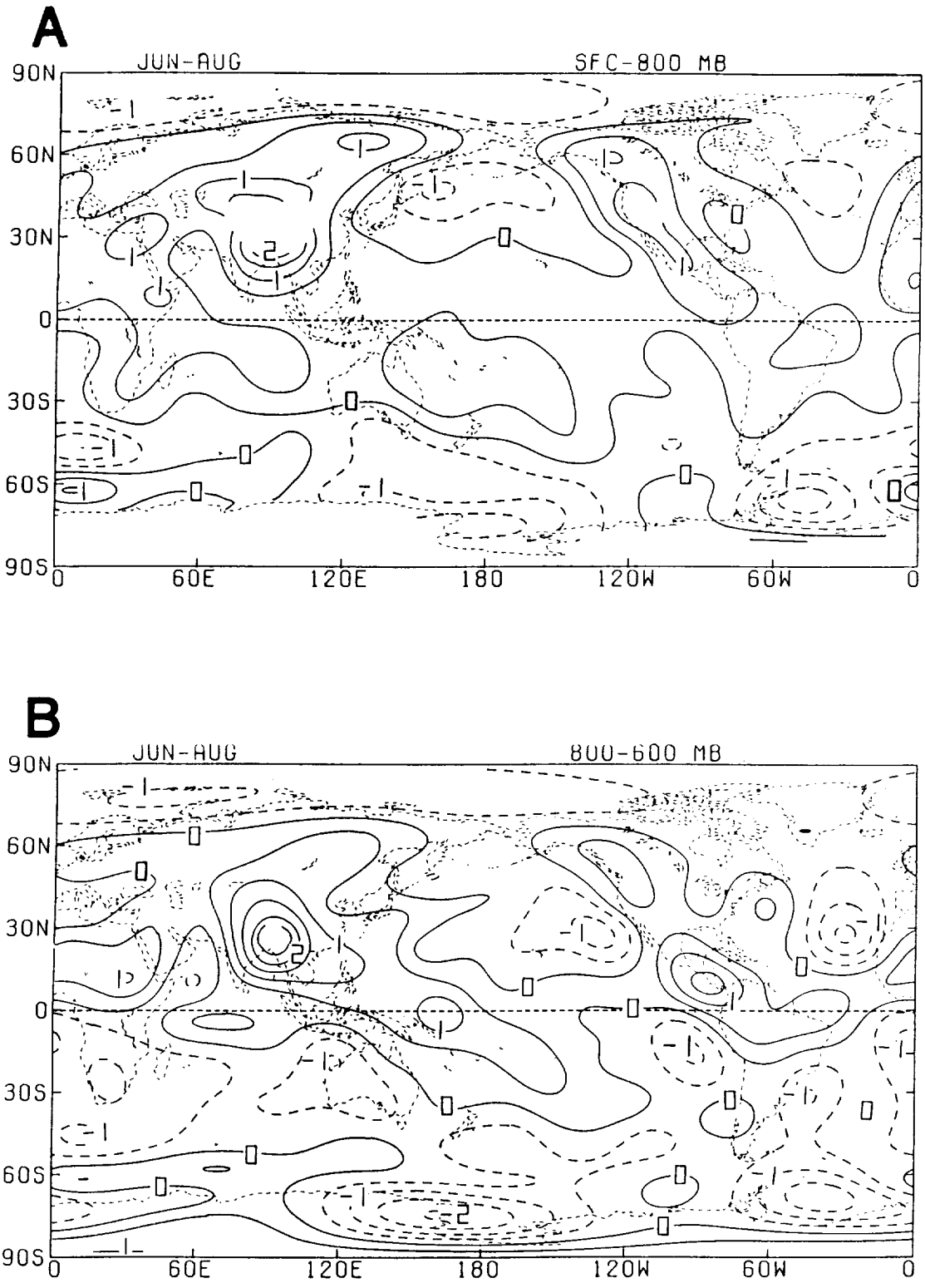

Fig. 20: Seasonal layer-averaged heating (K day^{-1}) for the (A) surface-800 mb, (B) 800-600 mb, (C) 600-400 mb and (D) 400-200 mb isobaric layers for June 1979 to August 1979. Contour interval is 0.5 K day^{-1}.

June – August

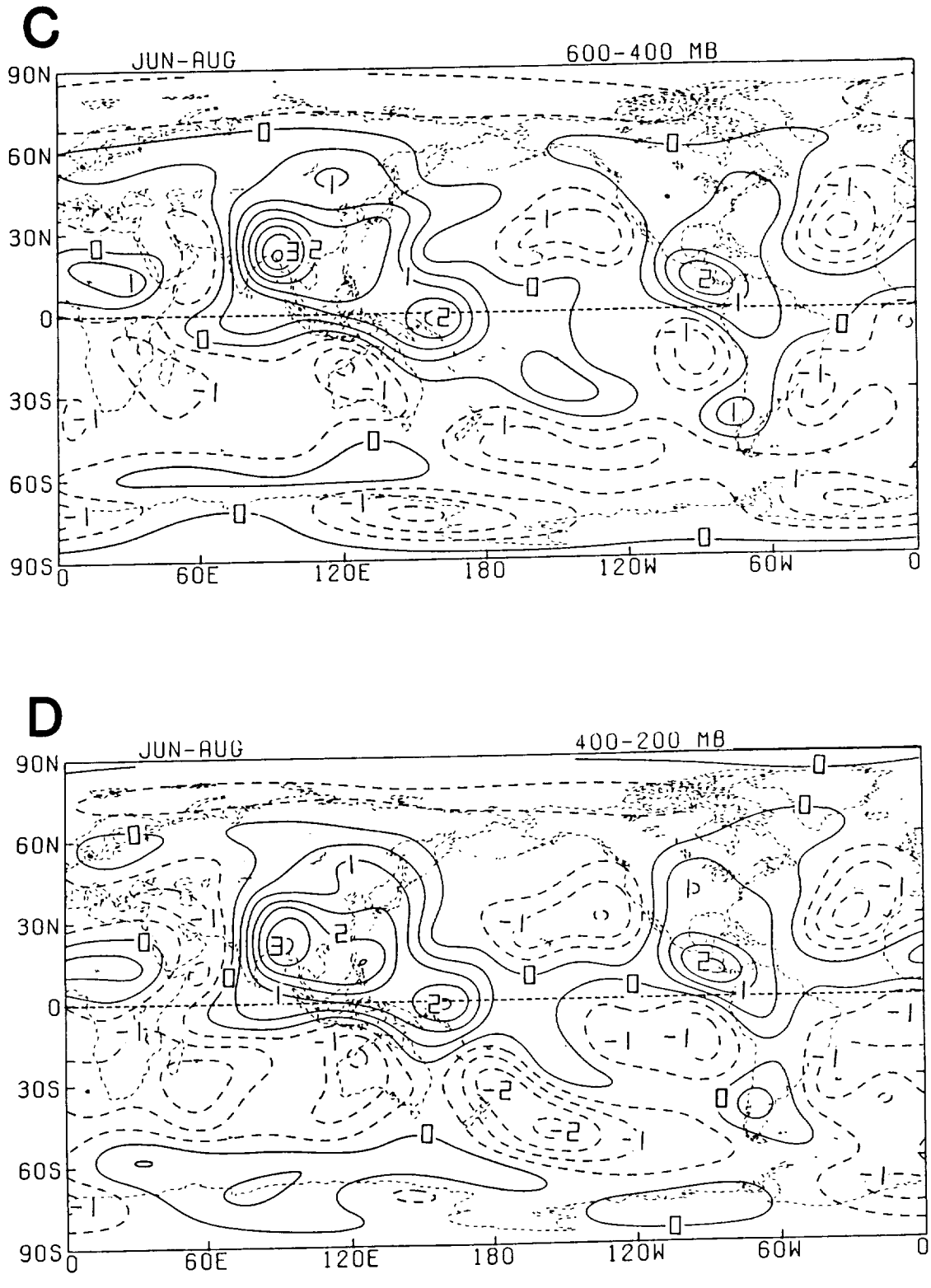

Fig. 20: (Continued).

June - August

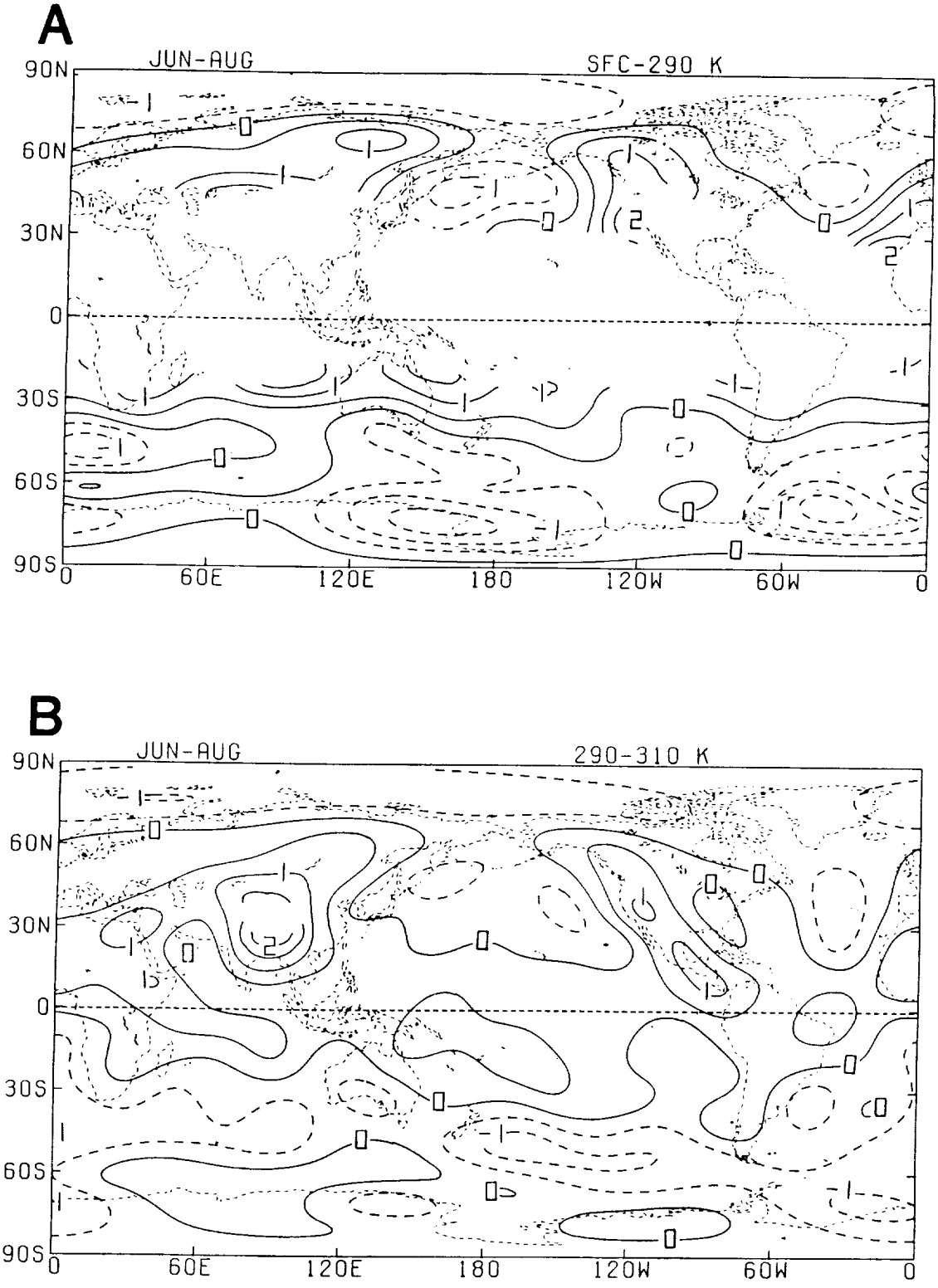

Fig. 21: Seasonal layer-averaged heating (K day^{-1}) for the (A) surface-290 K, (B) 290-310 K, (C) 310-330 K and (D) 330-400 K isentropic layers for June 1979 to August 1979. Contour interval is 0.5 K day^{-1}.

June - August

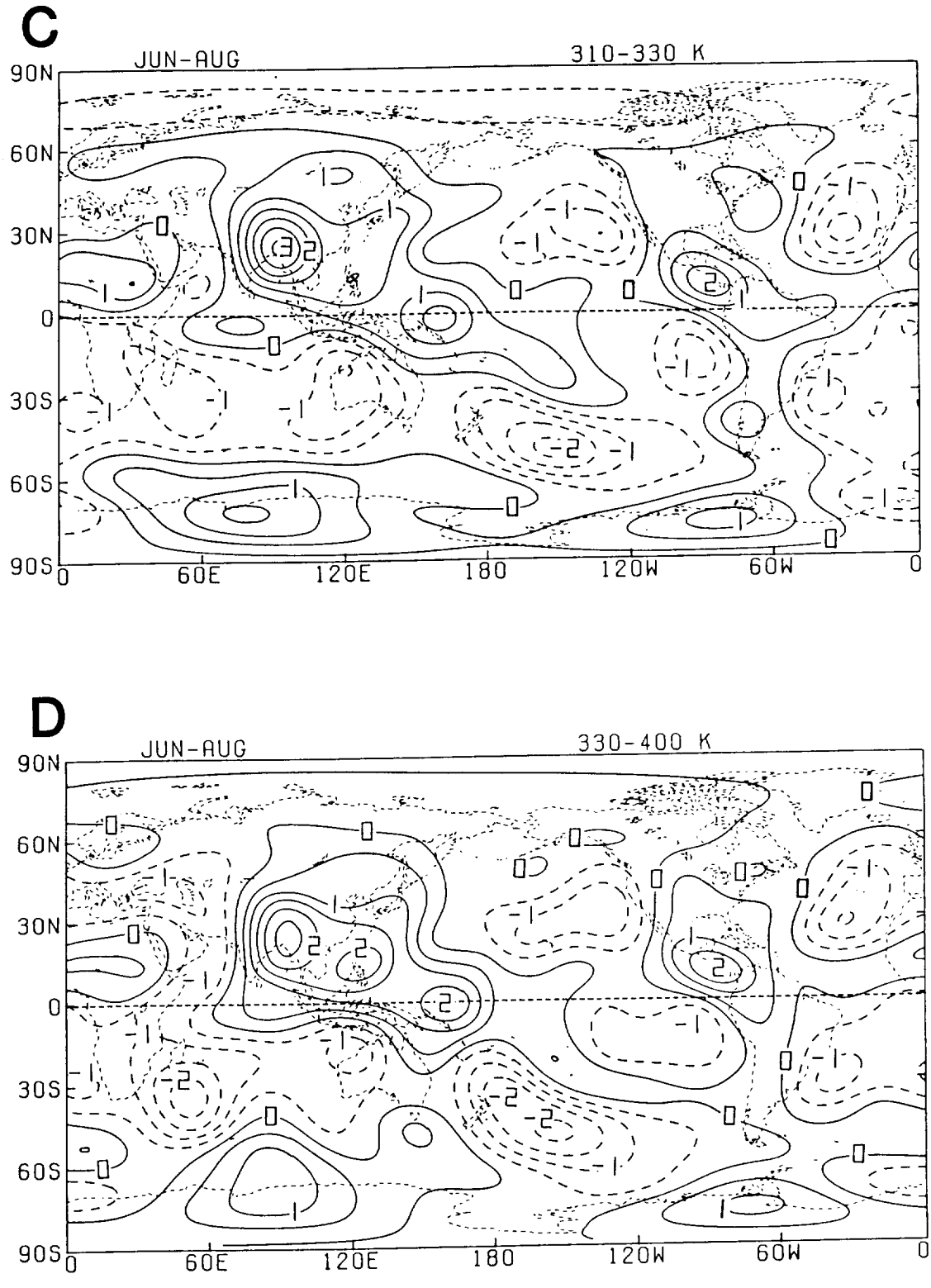

Fig. 21: (Continued).

June - August

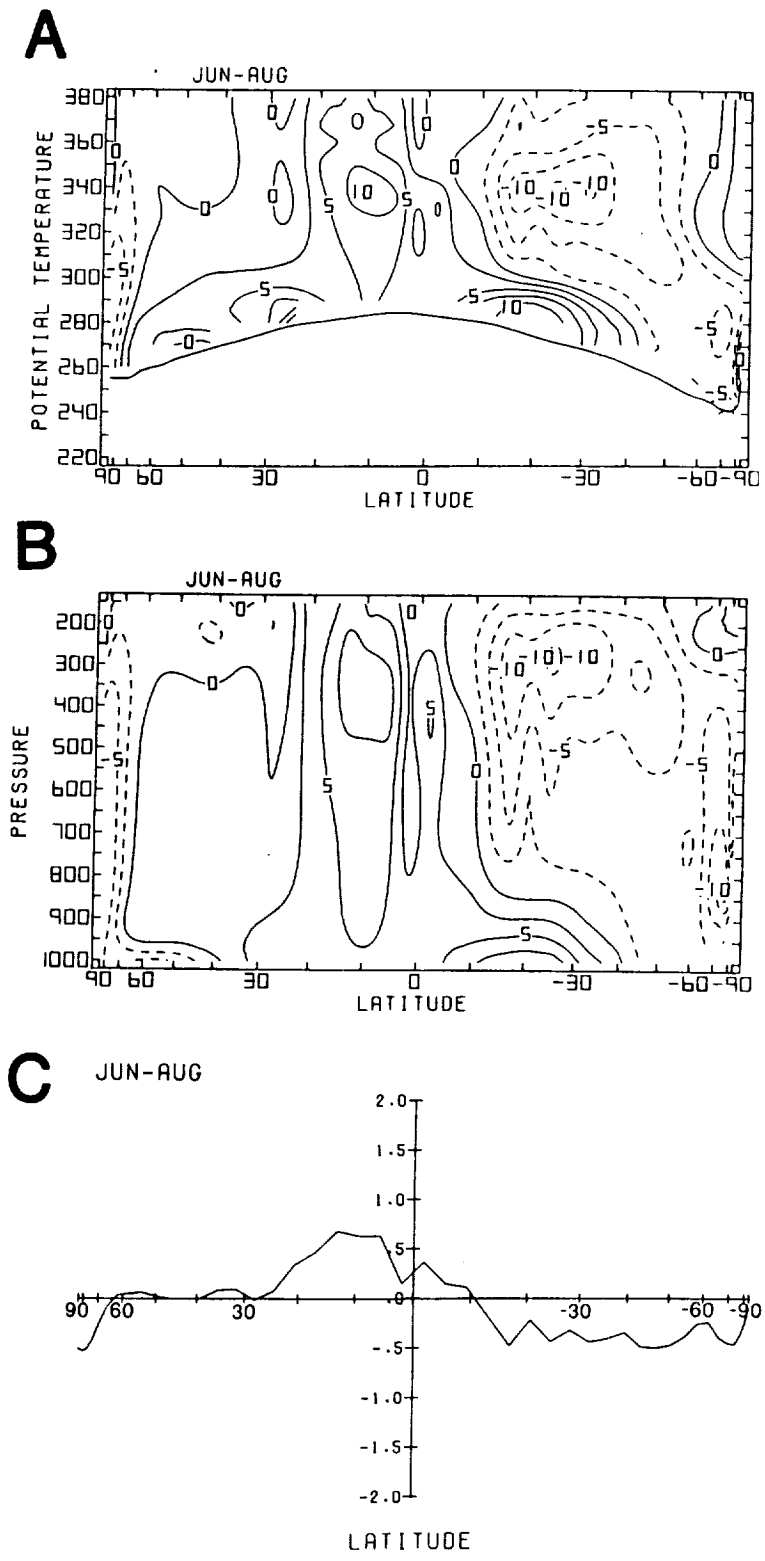

Fig. 22: Meridional cross sections of seasonal (A) isentropically and (B) isobarically zonally averaged heating (10^{-1} K day^{-1}), and (C) meridional profile of zonally-vertically averaged heating for June 1979 to August 1979 (K day^{-1}). Contour interval in (A) and (B) is 0.25 K day^{-1}.

June - August

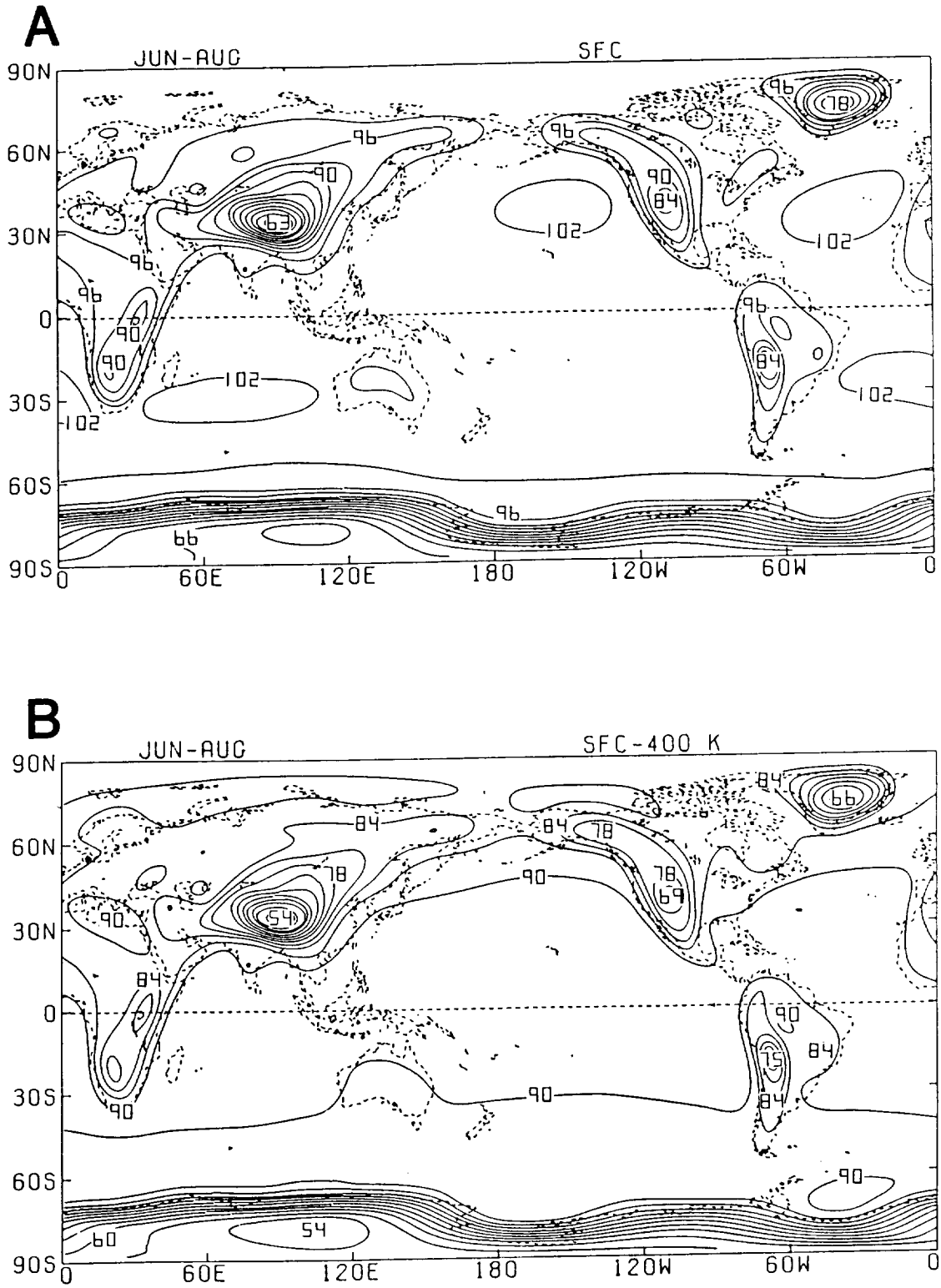

Fig. 23: Global distributions of seasonal-averaged (A) surface pressure (10^1 mb) and (B) pressure difference (10^1 mb) between the surface and the 400 K isentropic level for June 1979 to August 1979. Contour interval is 30 mb.

June – August

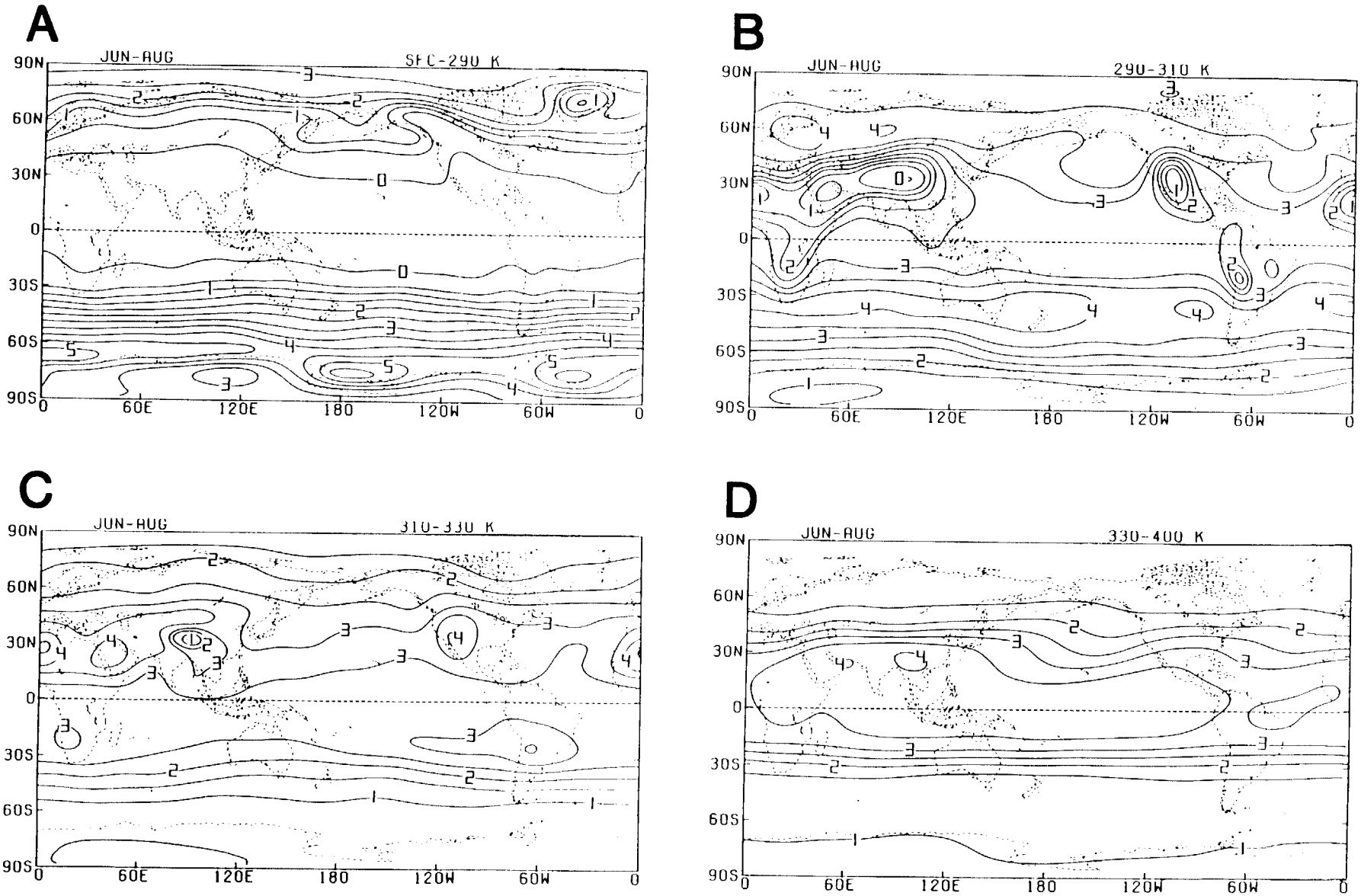

Fig. 24: Seasonal-averaged pressure difference (10^2 mb) between the upper and lower isentropic levels of the (A) surface-290 K, (B) 290-310 K, (C) 310-330 K and (D) 330-400 K isentroipc layers for June 1979 to August 1979. Contour interval is 50 mb.

September - November

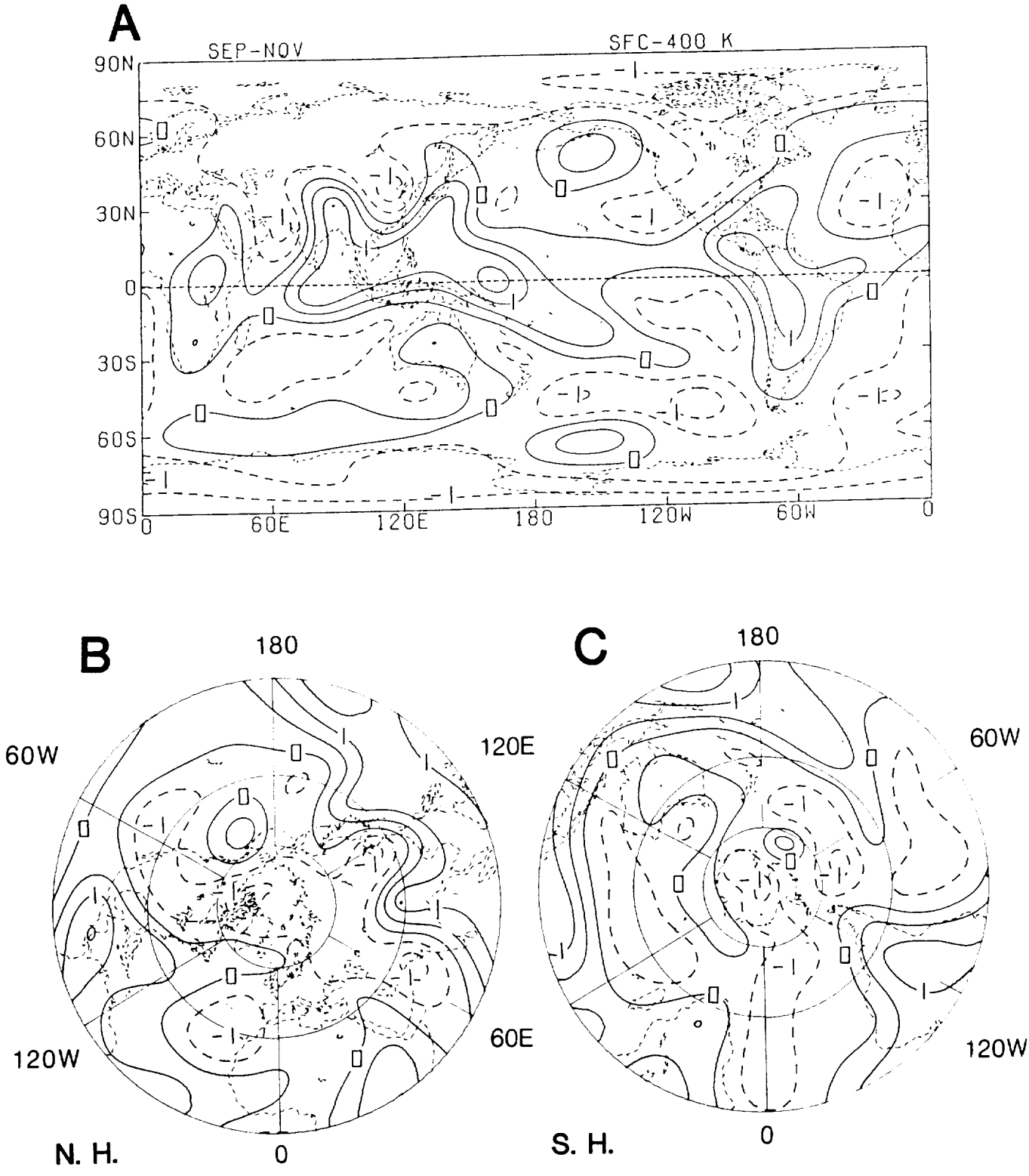

Fig. 25: Seasonal vertical-averaged heating (K day^{-1}) for September 1979 to November 1979; (A) global, (B) Northern and (C) Southern Hemisphere. Contour interval is 0.5 K day^{-1}.

September - November

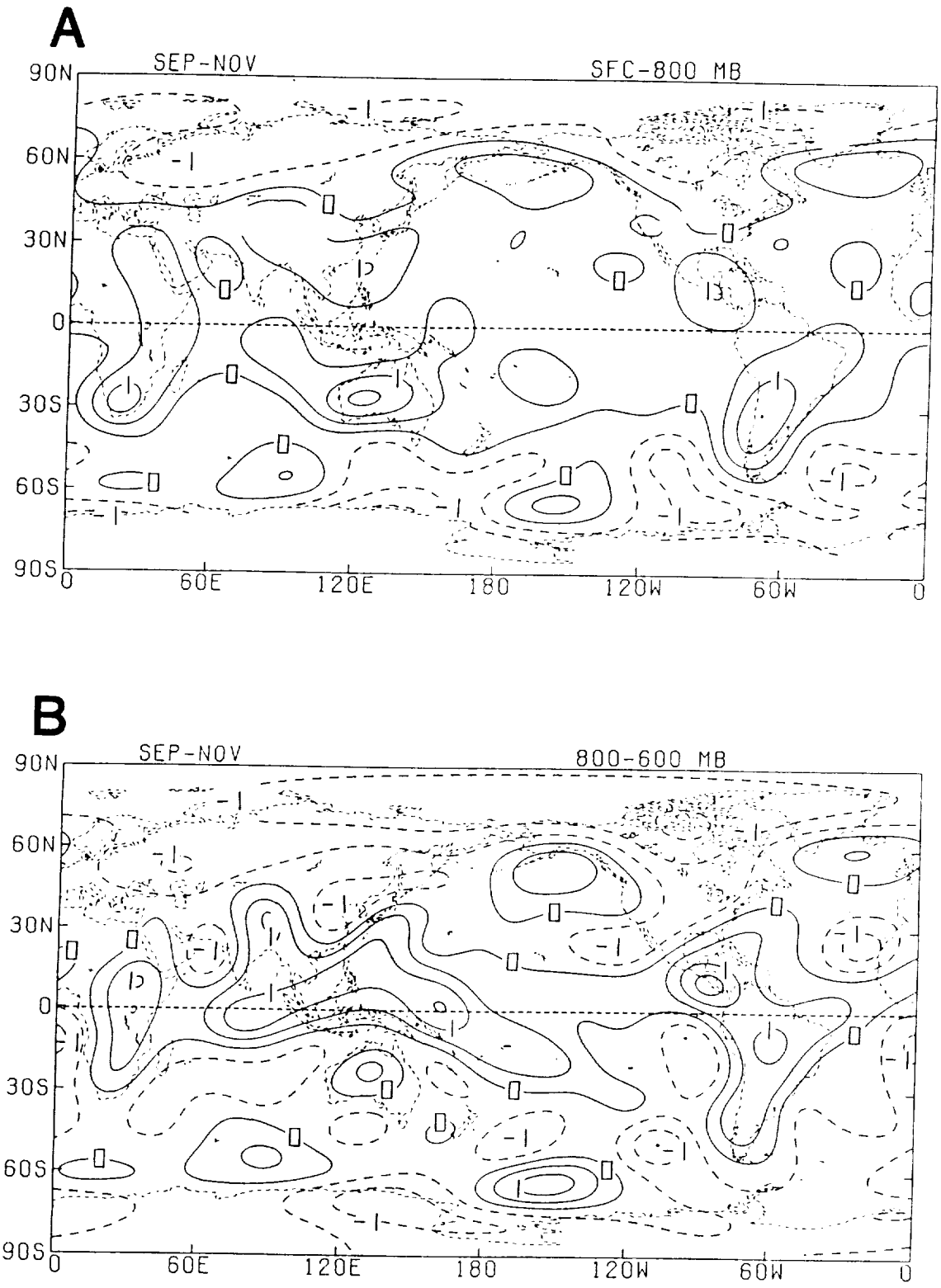

Fig. 26: Seasonal layer-averaged heating (K day^{-1}) for the (A) surface-800 mb, (B) 800-600 mb, (C) 600-400 mb and (D) 400-200 mb isobaric layers for September 1979 to November 1979. Contour interval is 0.5 K day^{-1}.

September - November

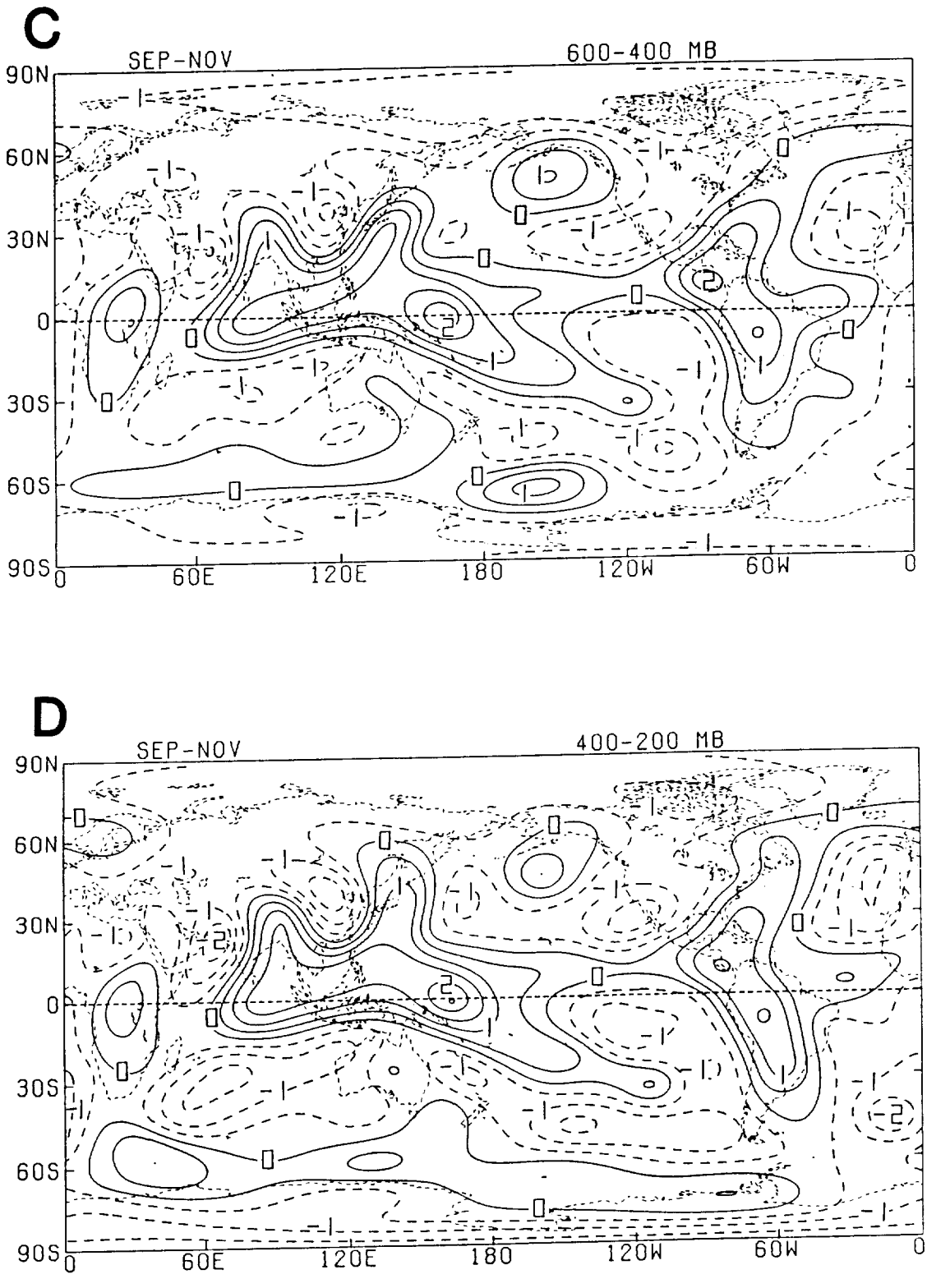

Fig. 26: (Continued).

September - November

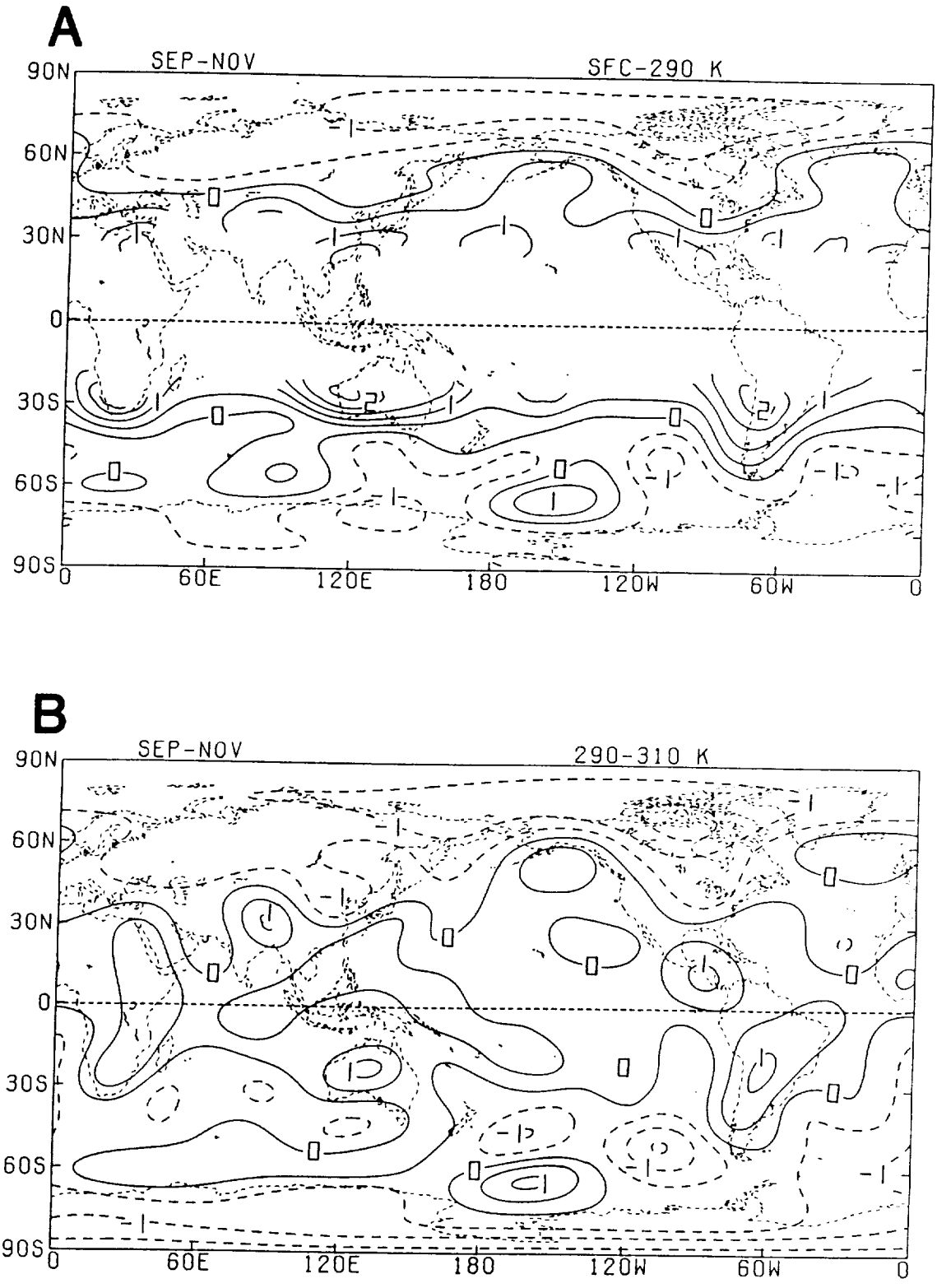

Fig. 27: Seasonal layer-averaged heating (K day^{-1}) for the (A) surface-290 K, (B) 290-310 K, (C) 310-330 K and (D) 330-400 K isentropic layers for September 1979 to November 1979. Contour interval is 0.5 K day^{-1}.

September - November

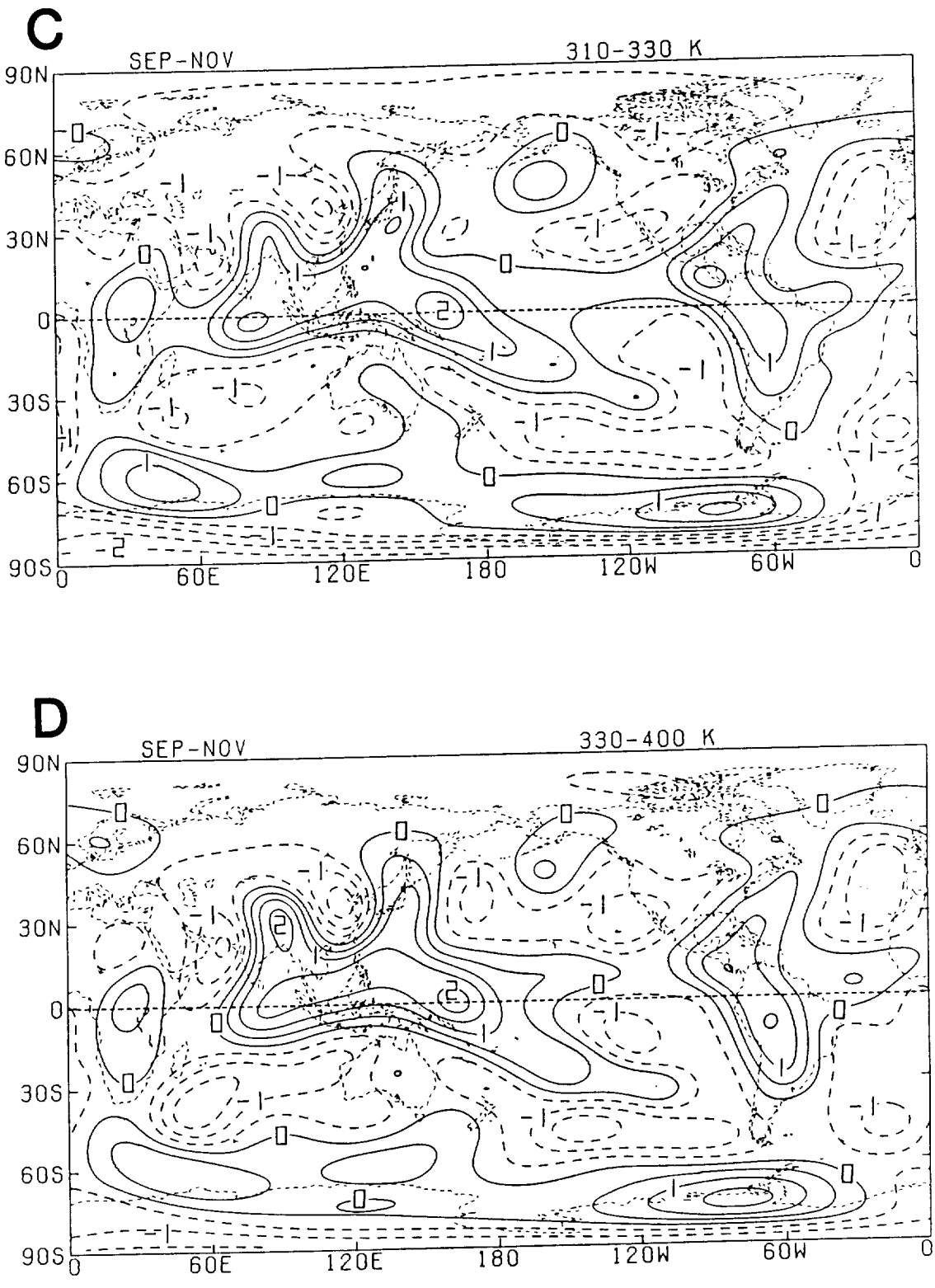

Fig. 27: (Continued).

September - November

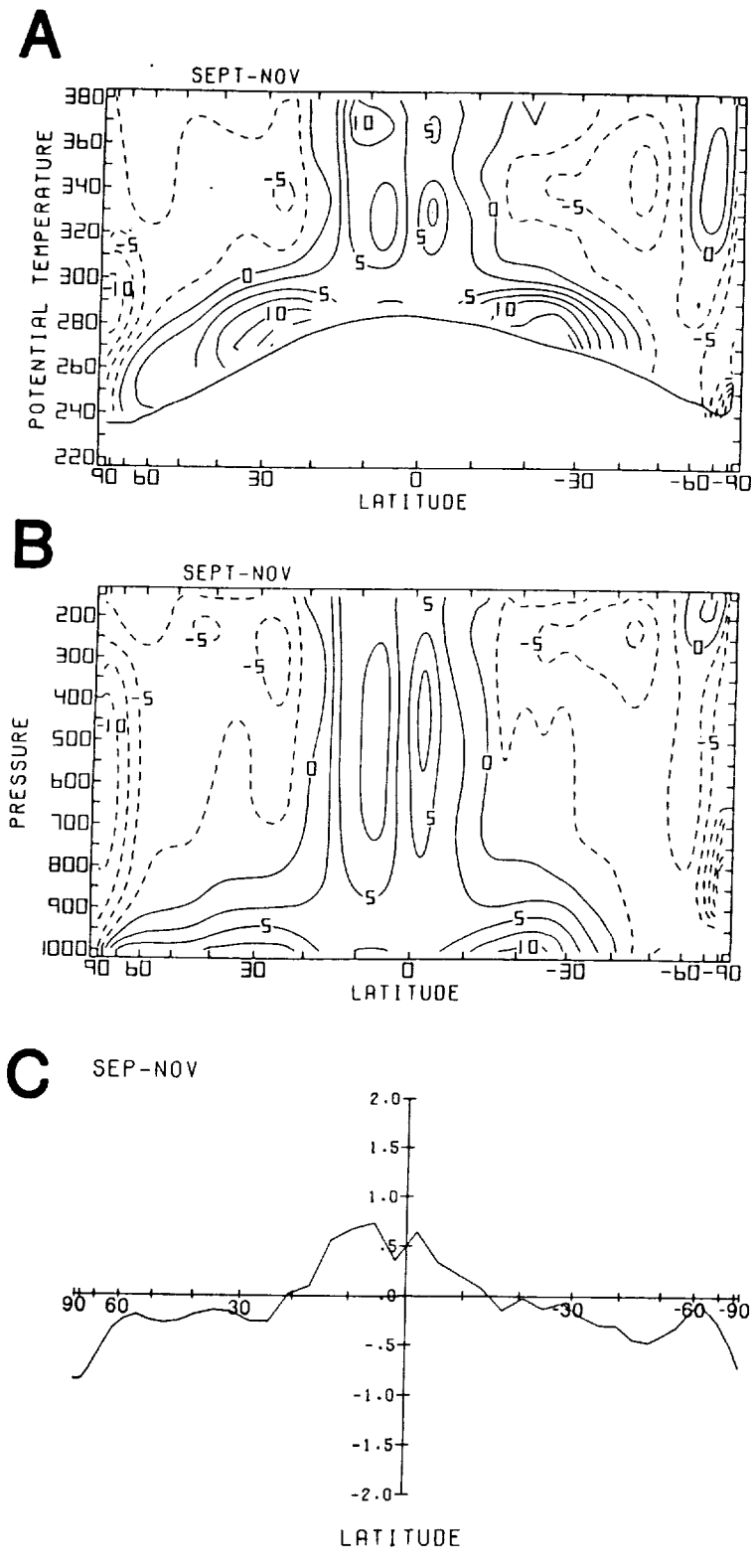

Fig. 28: Meridional cross sections of seasonal (A) isentropically and (B) isobarically zonally averaged heating (10^{-1} K day^{-1}), and (C) meridional profile of zonally-vertically averaged heating for September 1979 to November 1979 (K day^{-1}). Contour interval in (A) and (B) is 0.25 K day^{-1}.

September - November

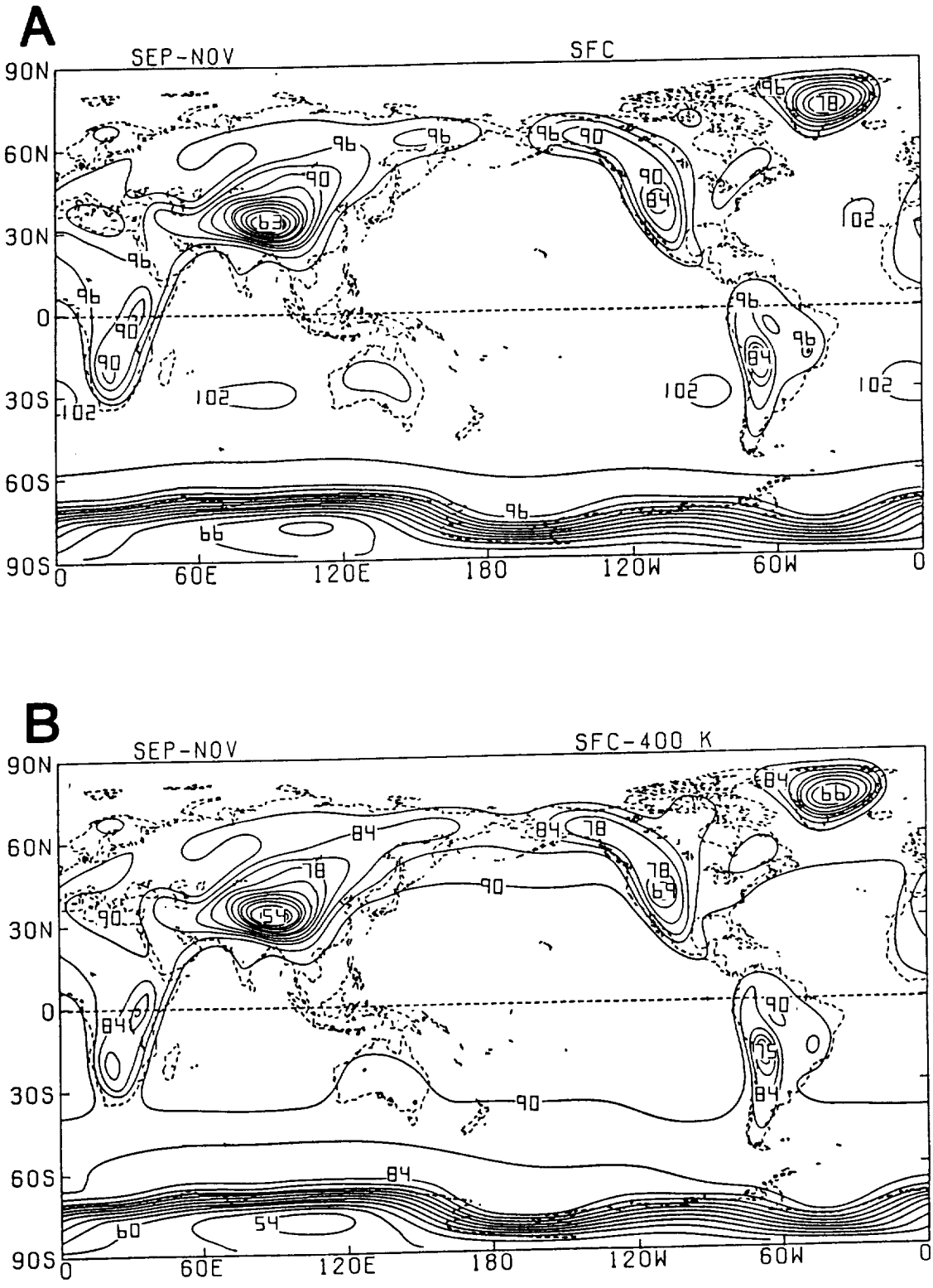

Fig. 29: Global distributions of seasonal-averaged (A) surface pressure (10^1 mb) and (B) pressure difference (10^1 mb) between the surface and the 400 K isentropic level for September 1979 to November 1979. Contour interval is 30 mb.

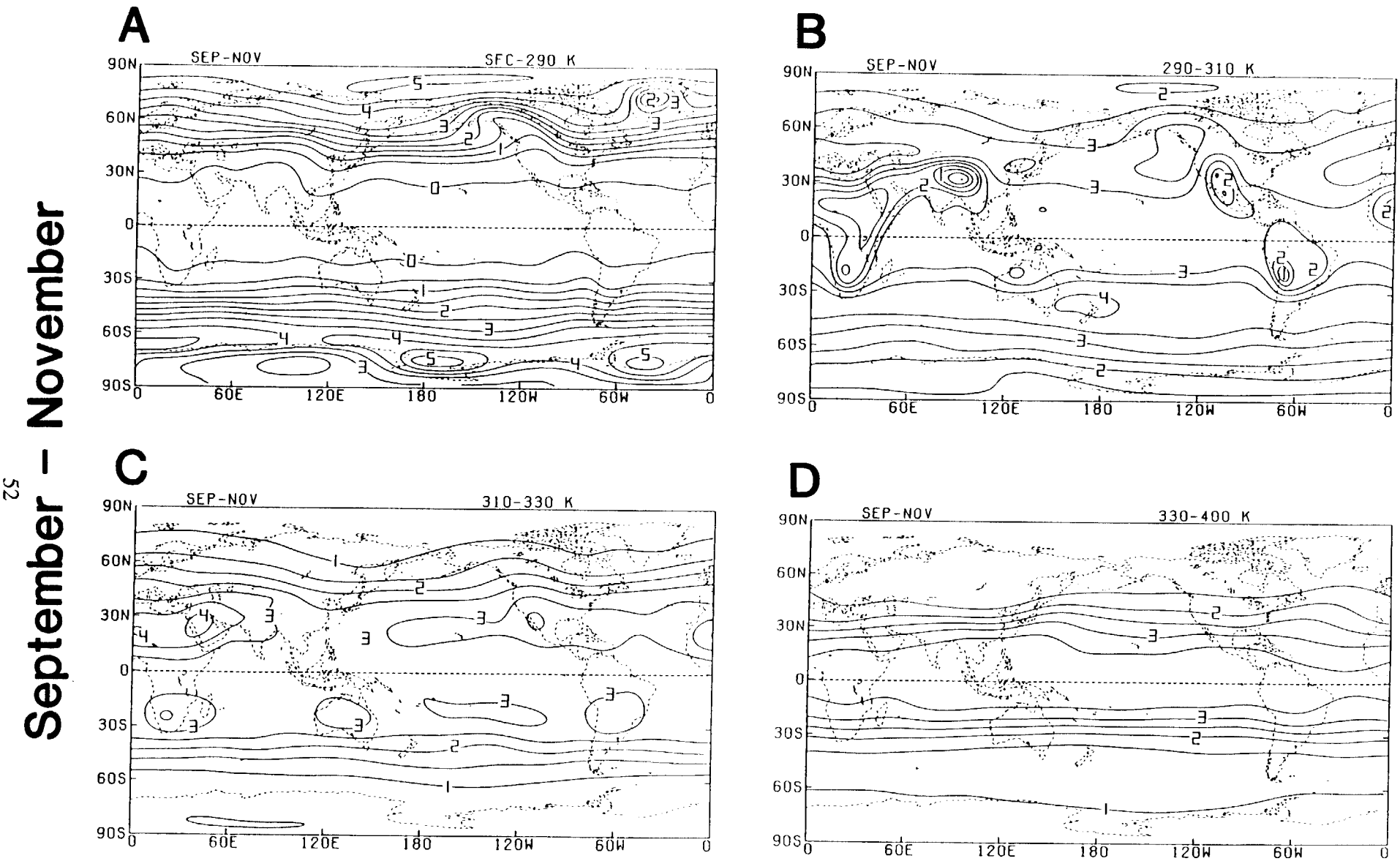

Fig. 30: Seasonal-averaged pressure difference (10^2 mb) between the upper and lower isentropic levels of the (A) surface-290 K, (B) 290-310 K, (C) 310-330 K and (D) 330-400 K isentropic layers for September 1979 to November 1979. Contour interval is 50 mb.

December

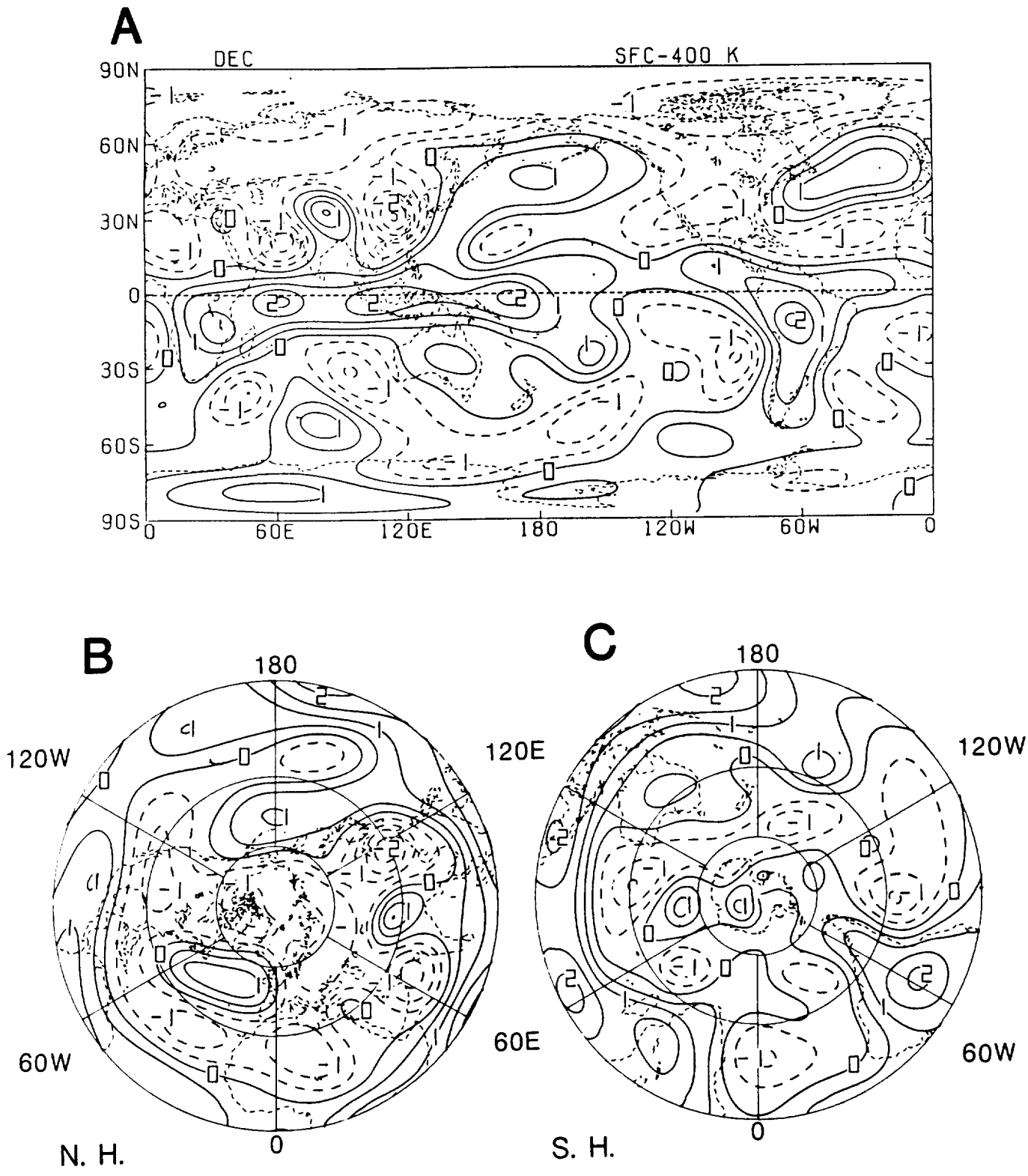

Fig. 31: Monthly vertical-averaged heating (K day^{-1}) for December 1978; (A) global, (B) Northern and (C) Southern Hemisphere. Contour interval is 0.5 K day^{-1}.

December

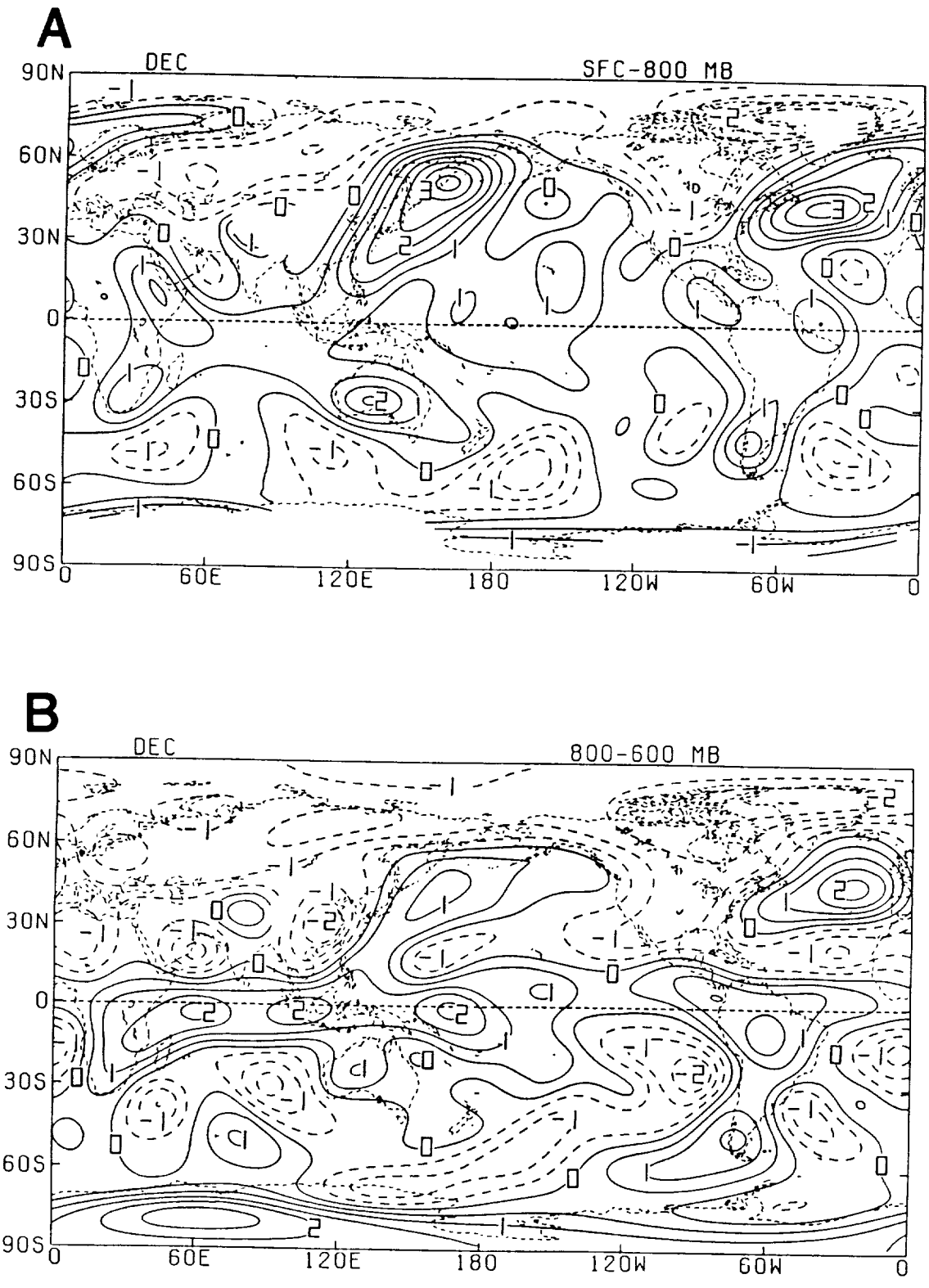

Fig. 32: Monthly layer-averaged heating (K day^{-1}) for the (A) surface-800 mb, (B) 800-600 mb, (C) 600-400 mb and (D) 400-200 mb isobaric layers for December 1978. Contour interval is 0.5 K day^{-1}.

December

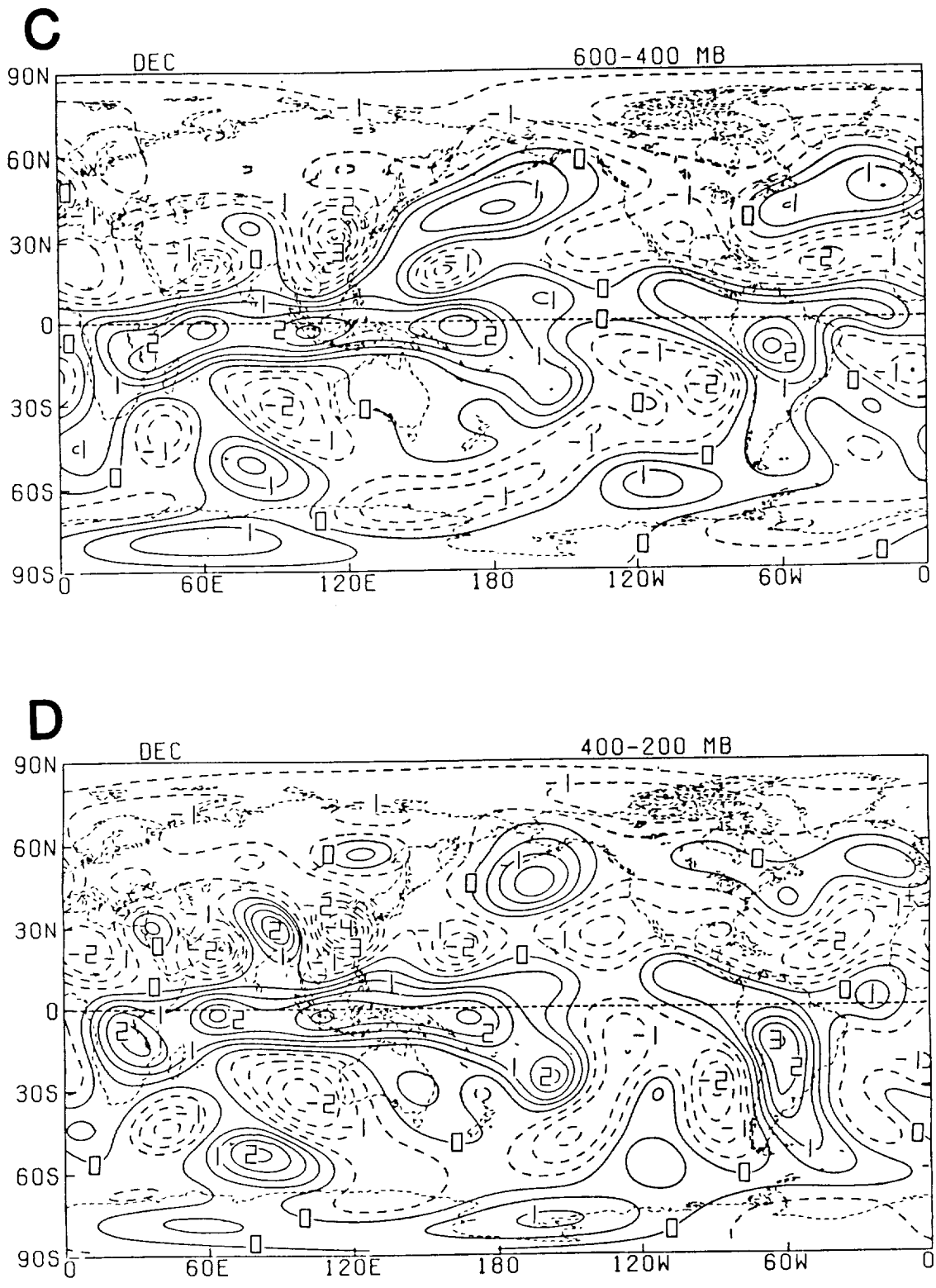

Fig. 32: (Continued).

December

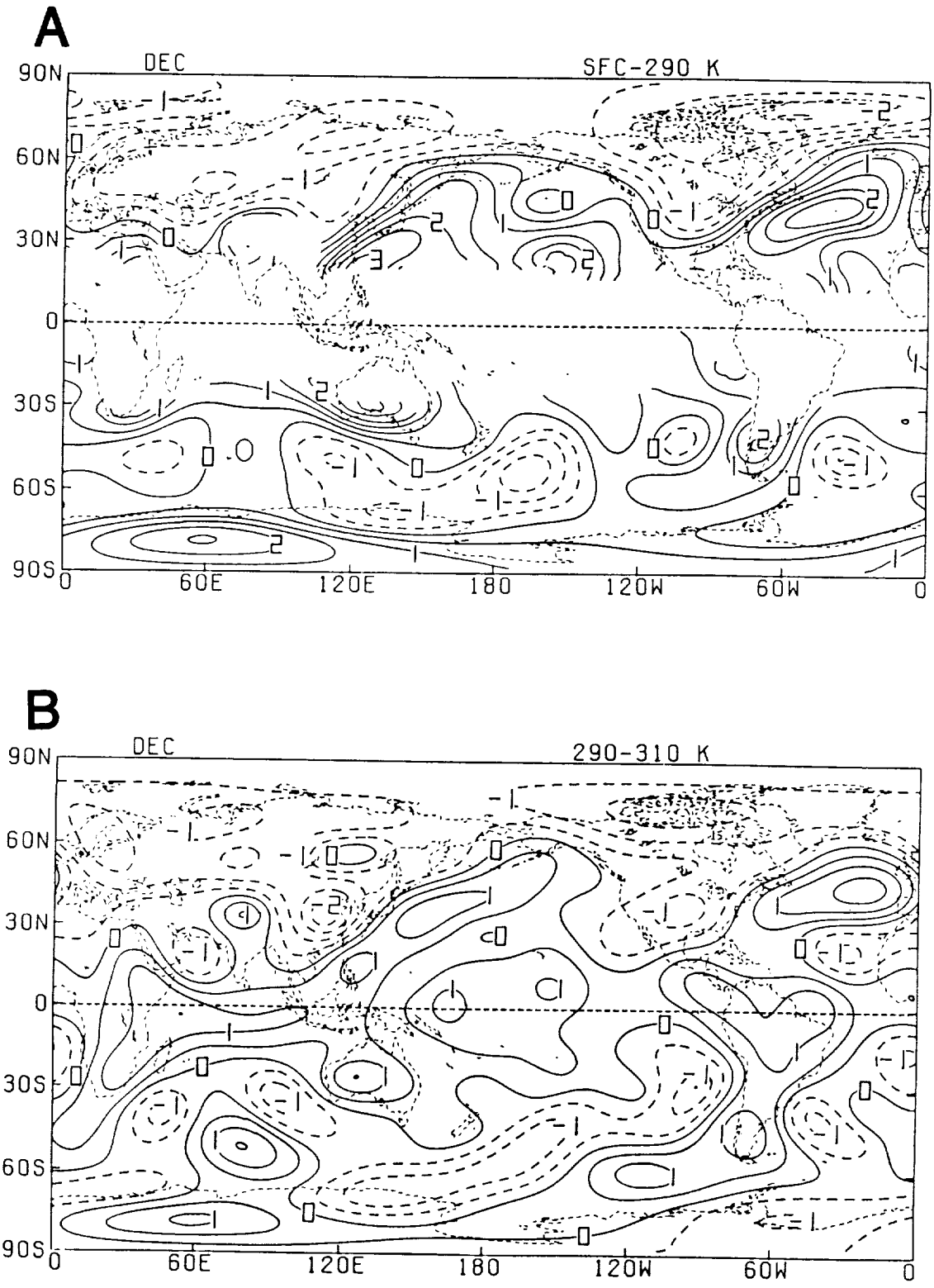

Fig. 33: Monthly layer-averaged heating (K day^{-1}) for the (A) surface-290 K, (B) 290-310 K, (C) 310-330 K and (D) 330-400 K isentropic layers for December 1978. Contour interval is 0.5 K day^{-1}.

December

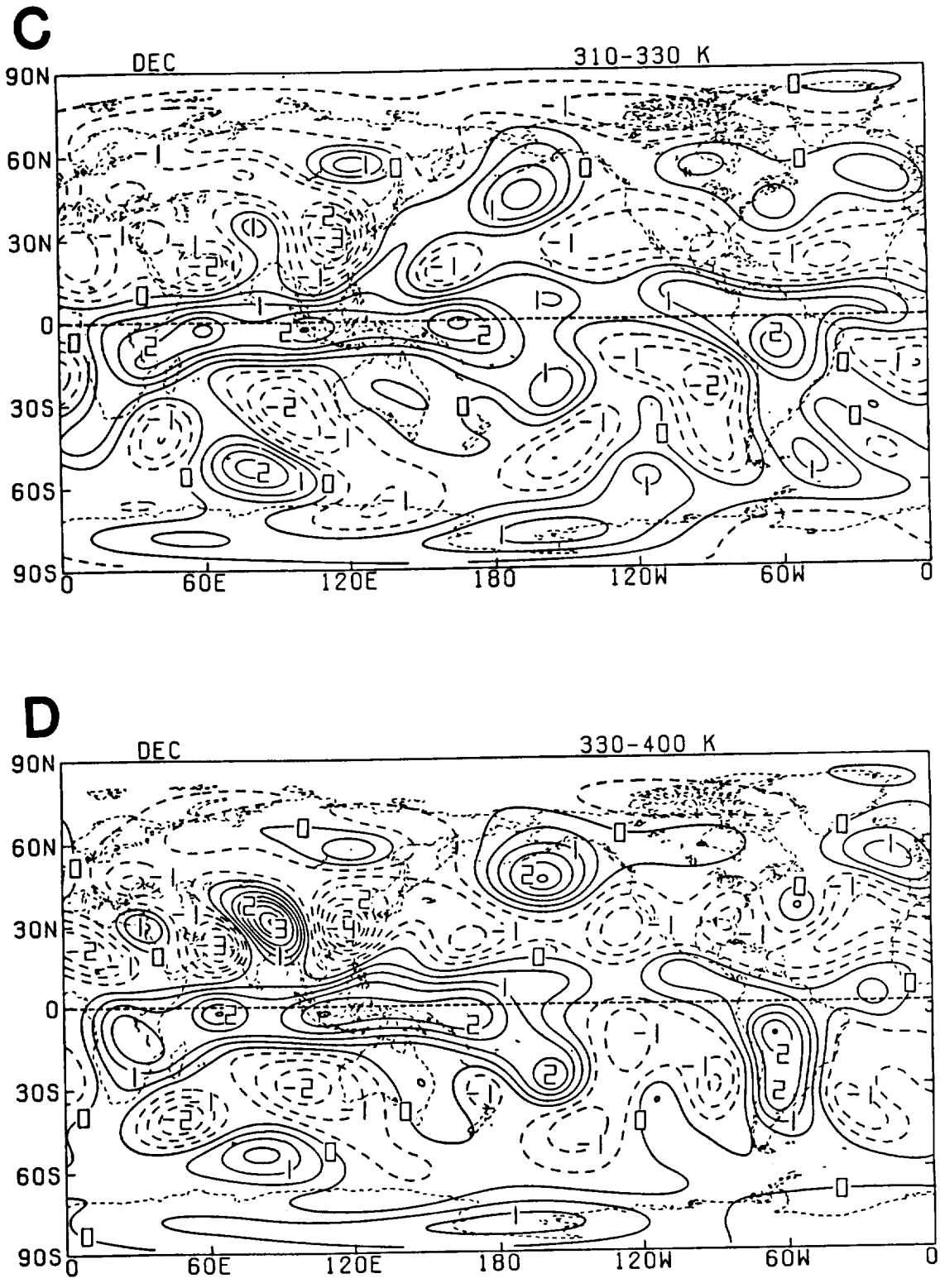

Fig. 33: (Continued).

December

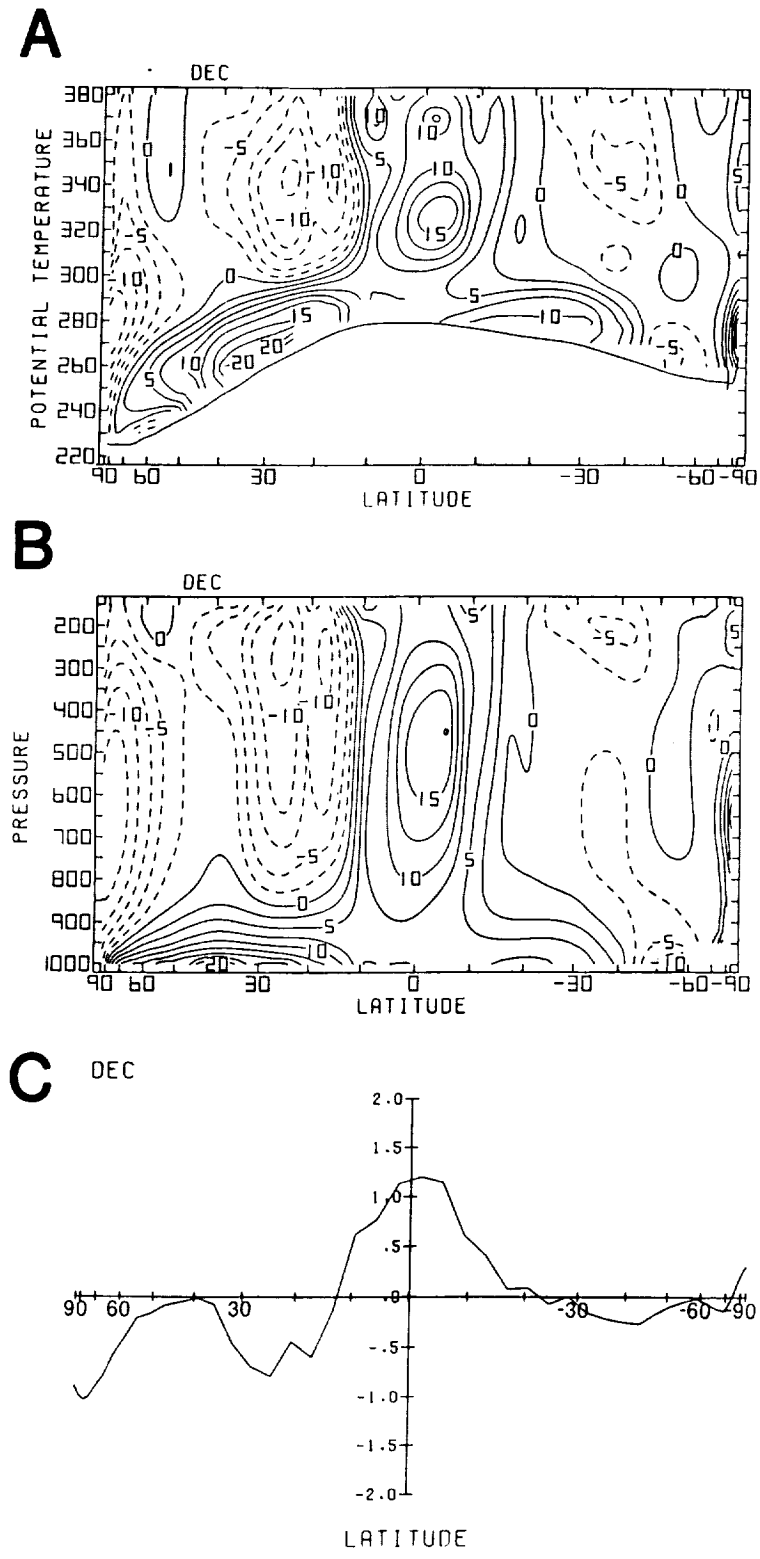

Fig. 34: Meridional cross sections of monthly (A) isentropically and (B) isobarically zonally averaged heating (10^{-1} K day^{-1}), and (C) meridional profile of zonally-vertically averaged heating for December 1978 (K day^{-1}). Contour interval in (A) and (B) is 0.25 K day^{-1}.

December

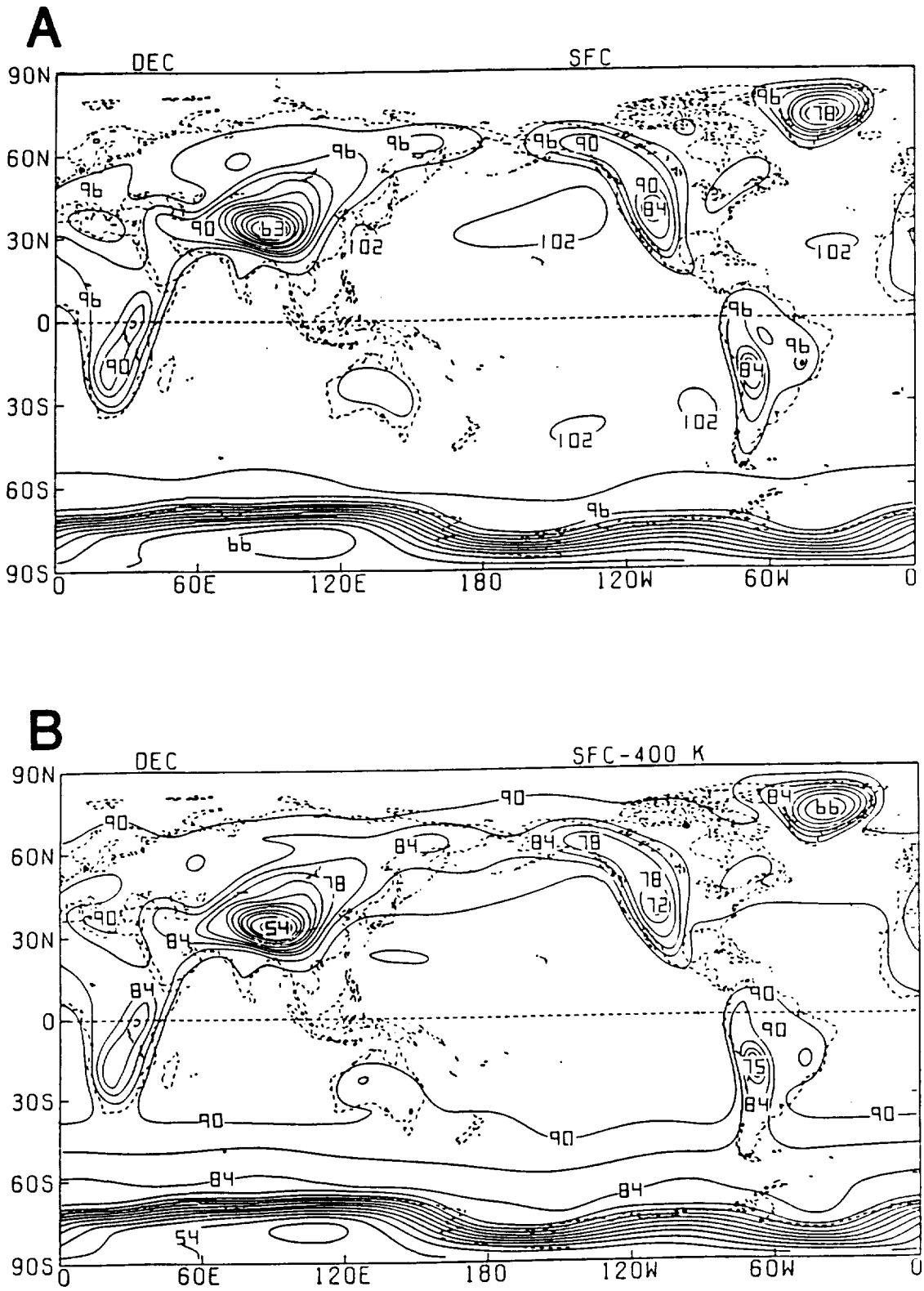

Fig. 35: Global distributions of monthly averaged (A) surface pressure (10^1 mb) and (B) pressure difference (10^1 mb) between the surface and the 400 K isentropic level for December 1978. Contour interval is 30 mb.

December

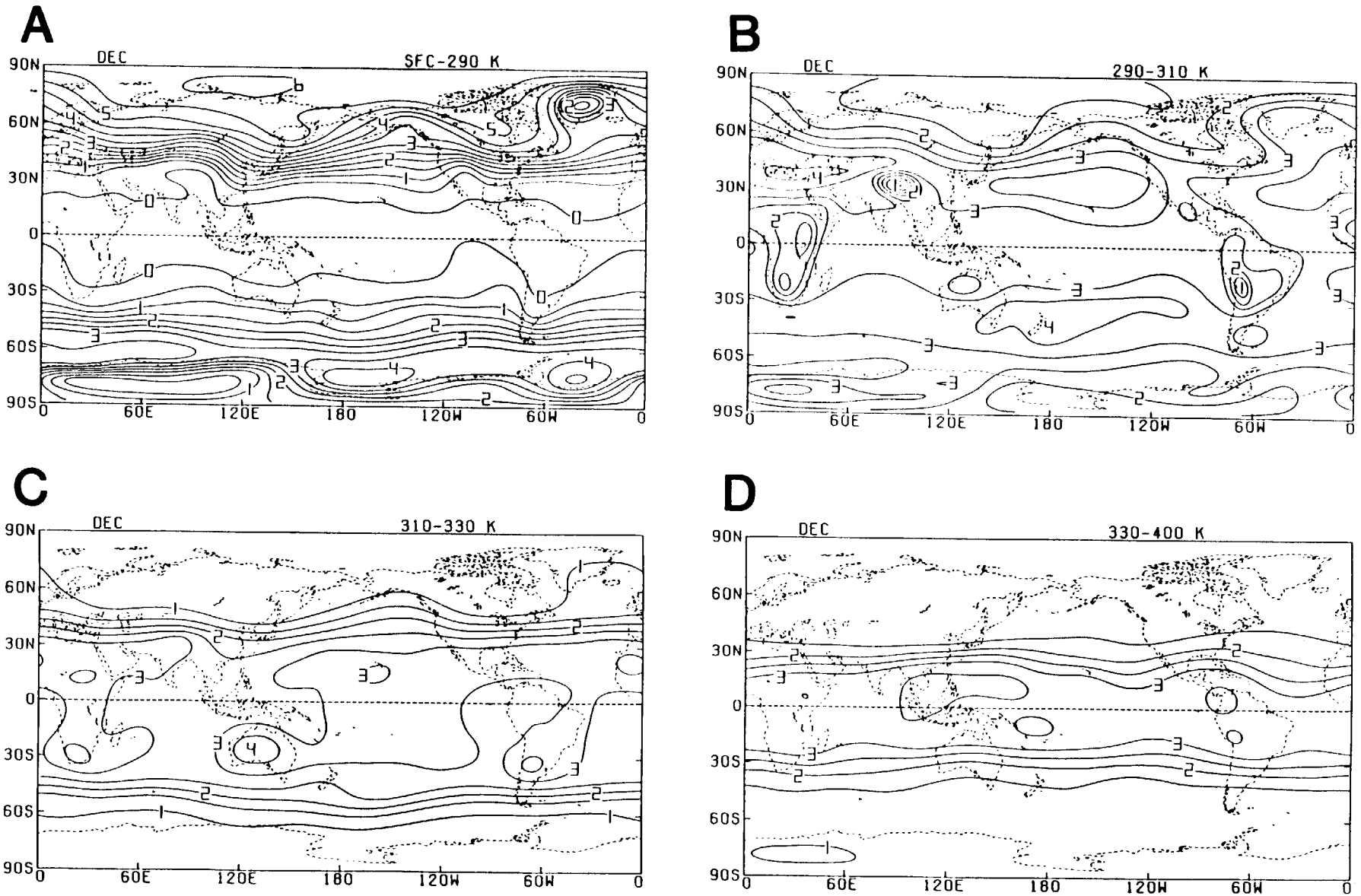

Fig. 36: Monthly averaged pressure difference (10^2 mb) between the upper and lower isentropic levels of the (A) surface-290 K, (B) 290-310 K, (C) 310-330 K and (D) 330-400 K isentropic layers for December 1978. Contour interval is 50 mb.

January

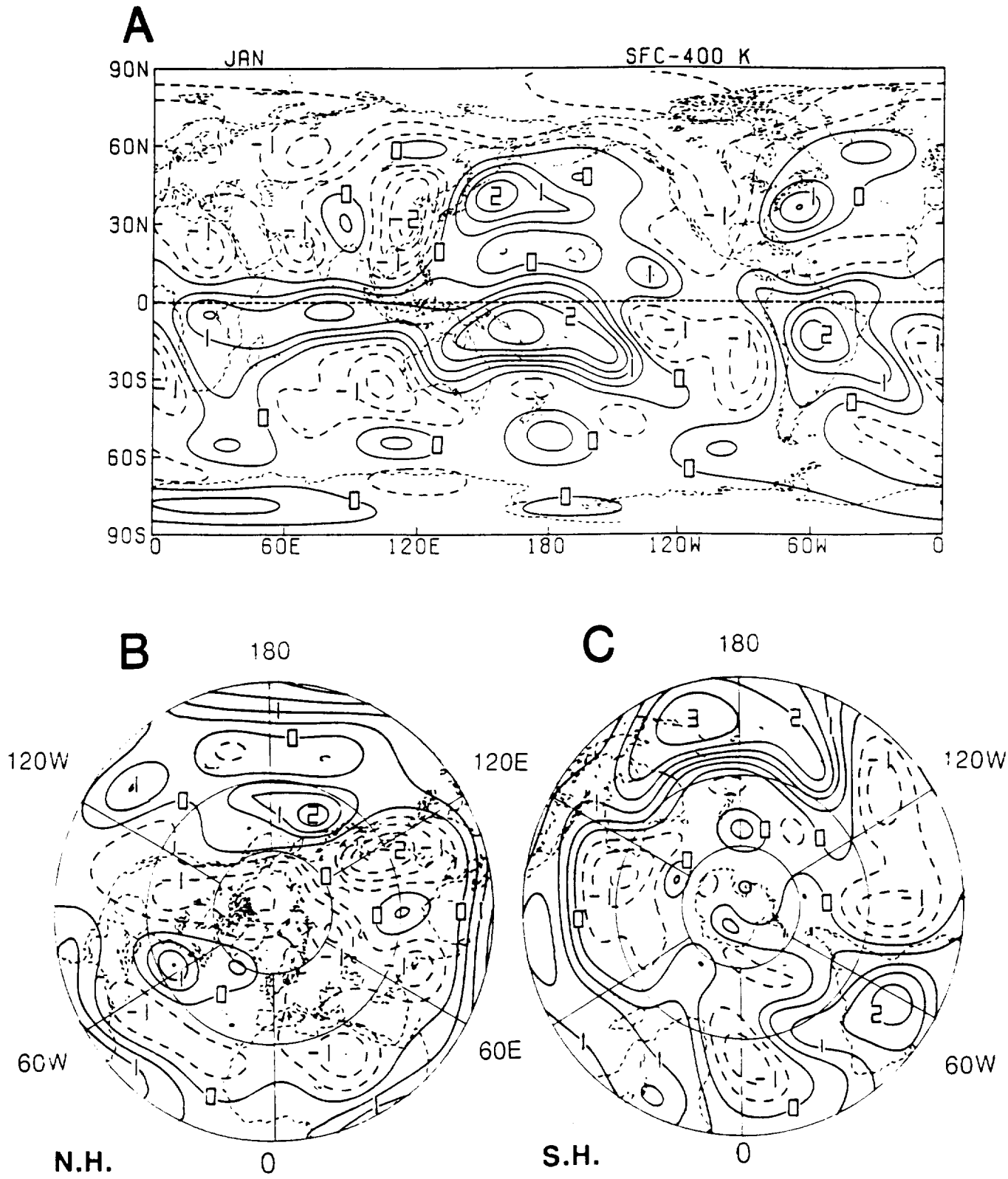

Fig. 37: Monthly vertical-averaged heating (K day^{-1}) for January 1979; (A) global, (B) Northern and (C) Southern Hemisphere. Contour interval is 0.5 K day^{-1}.

January

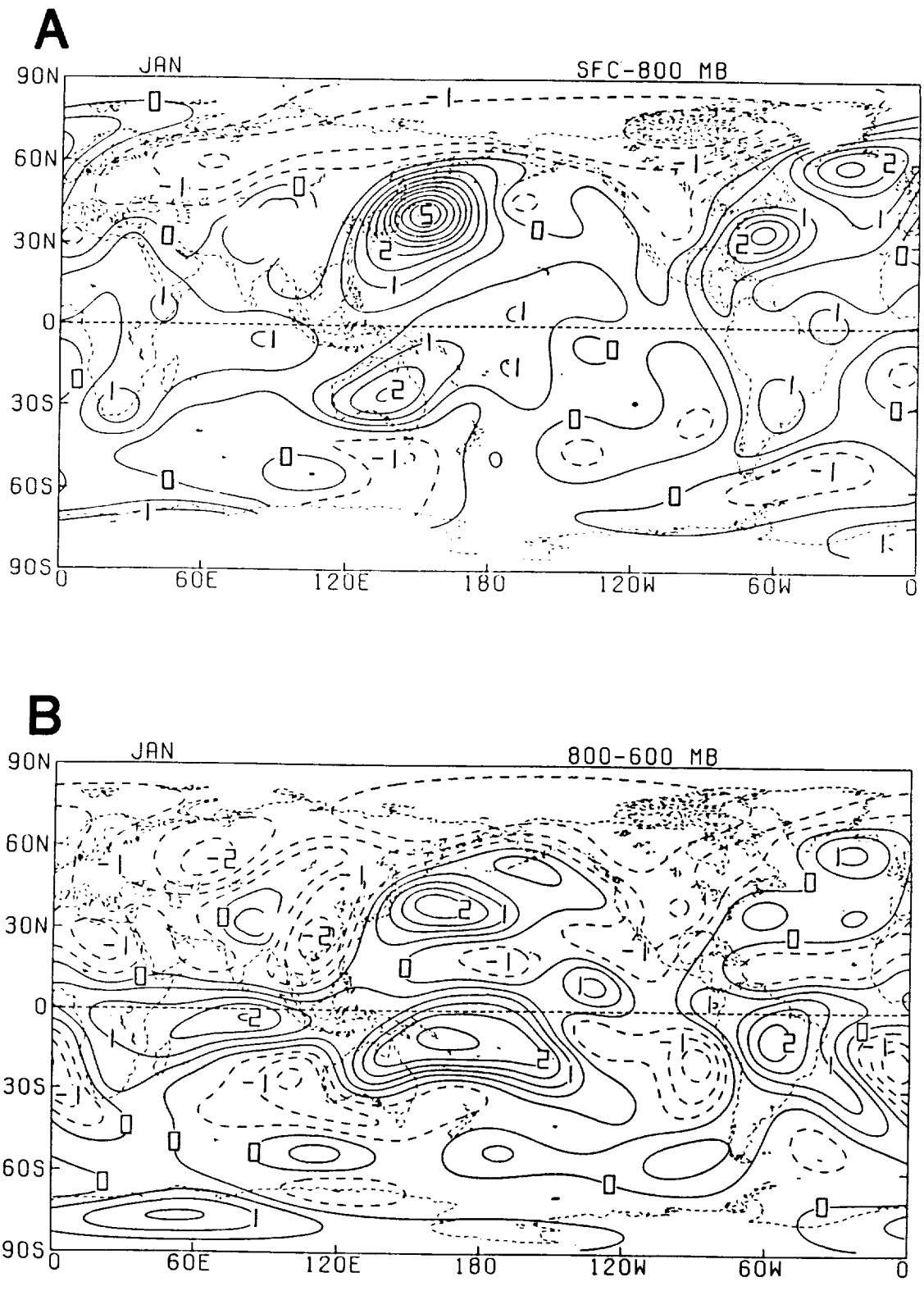

Fig. 38: Monthly layer-averaged heating (K day^{-1}) for the (A) surface-800 mb, (B) 800-600 mb, (C) 600-400 mb and (D) 400-200 mb isobaric layers for January 1979. Contour interval is 0.5 K day^{-1}.

January

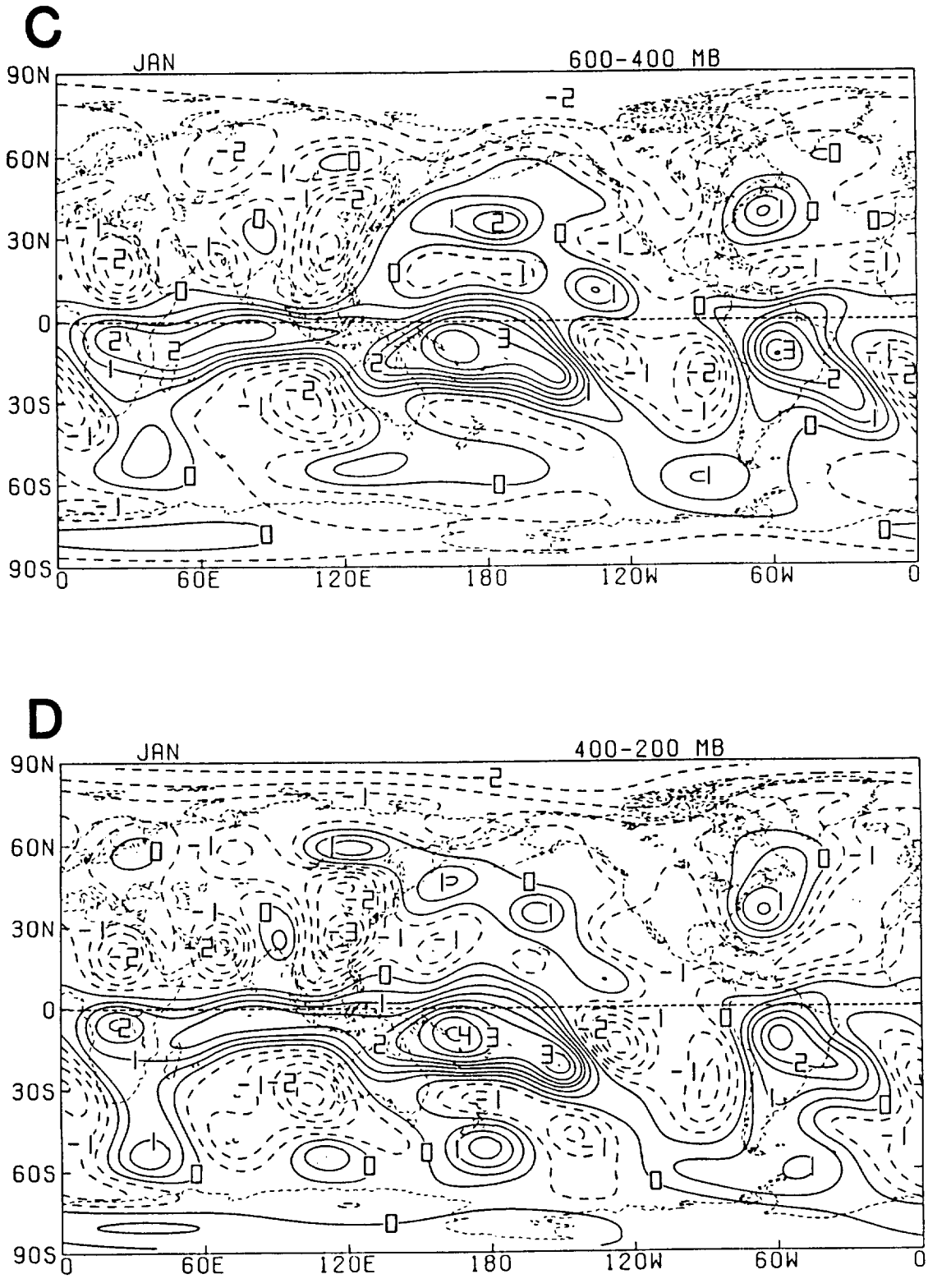

Fig. 38: (Continued).

January

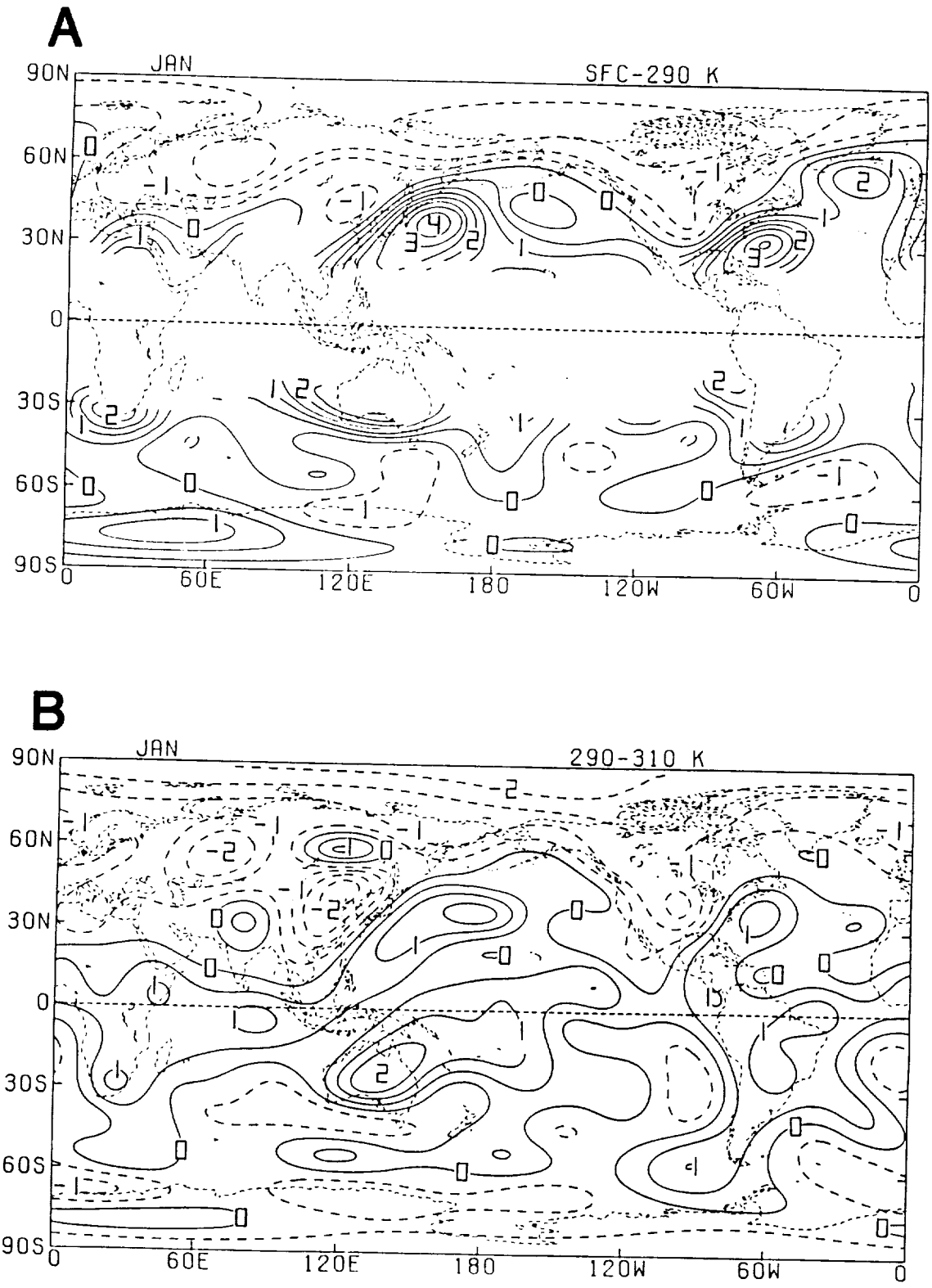

Fig. 39: Monthly layer-averaged heating (K day^{-1}) for the (A) surface-290 K, (B) 290-310 K, (C) 310-330 K and (D) 330-400 K isentropic layers for January 1979. Contour interval is 0.5 K day^{-1}.

January

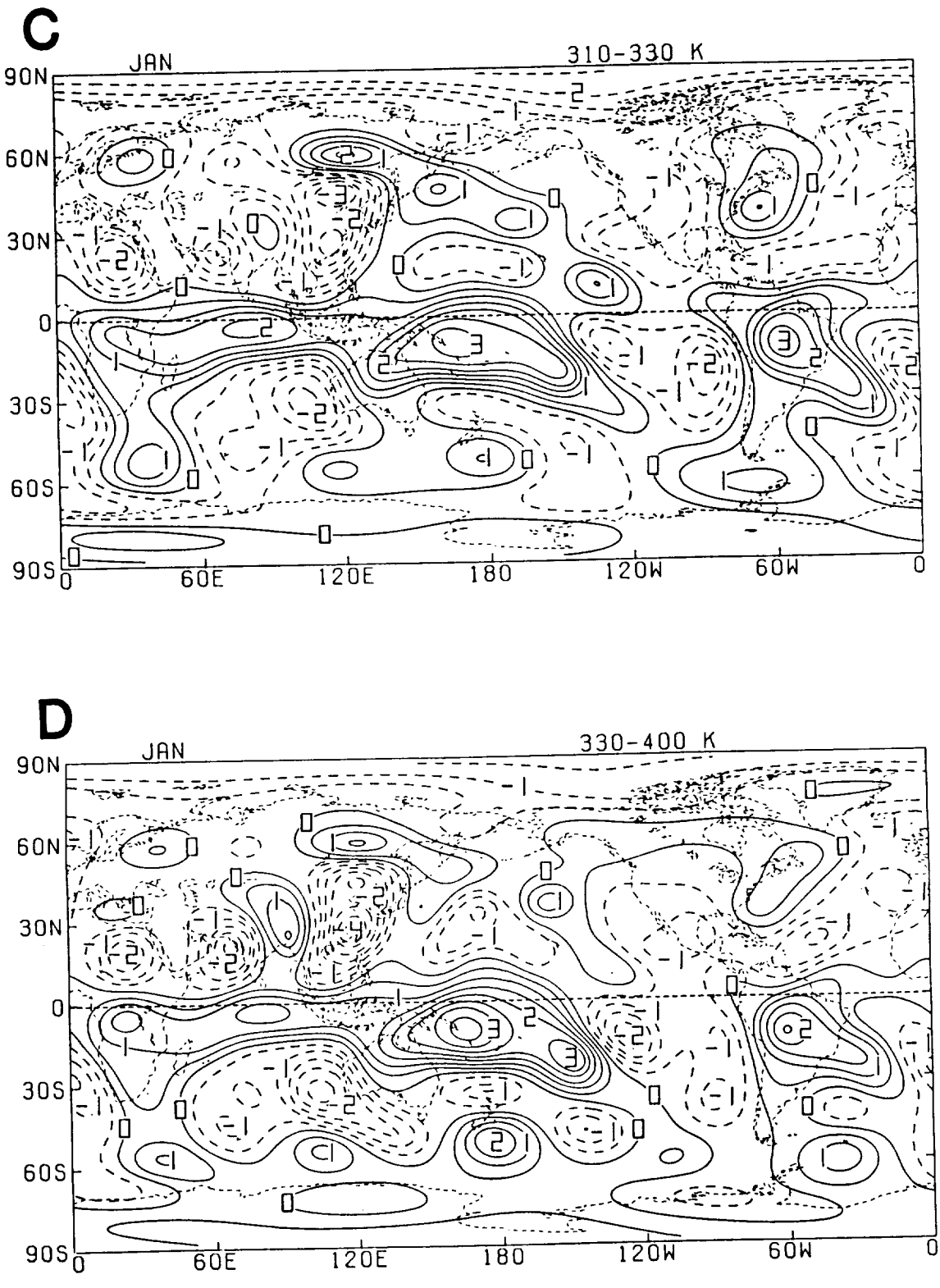

Fig. 39: (Continued).

January

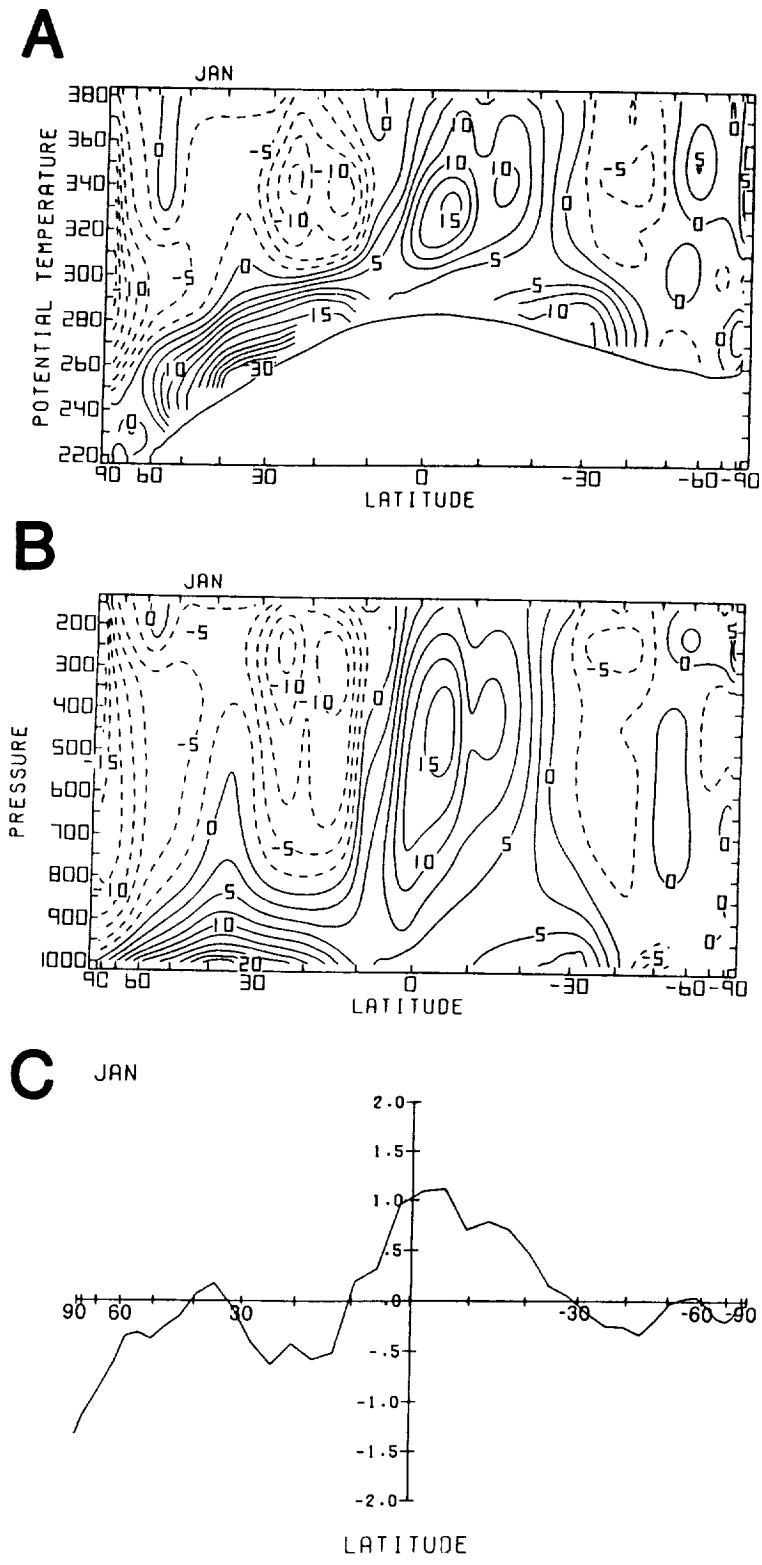

Fig. 40: Meridional cross sections of monthly (A) isentropically and (B) isobarically zonally averaged heating (10^{-1} K day^{-1}), and (C) meridional profile of zonally-vertically averaged heating for January 1979 (K day^{-1}). Contour interval in (A) and (B) is 0.25 K day^{-1}.

January

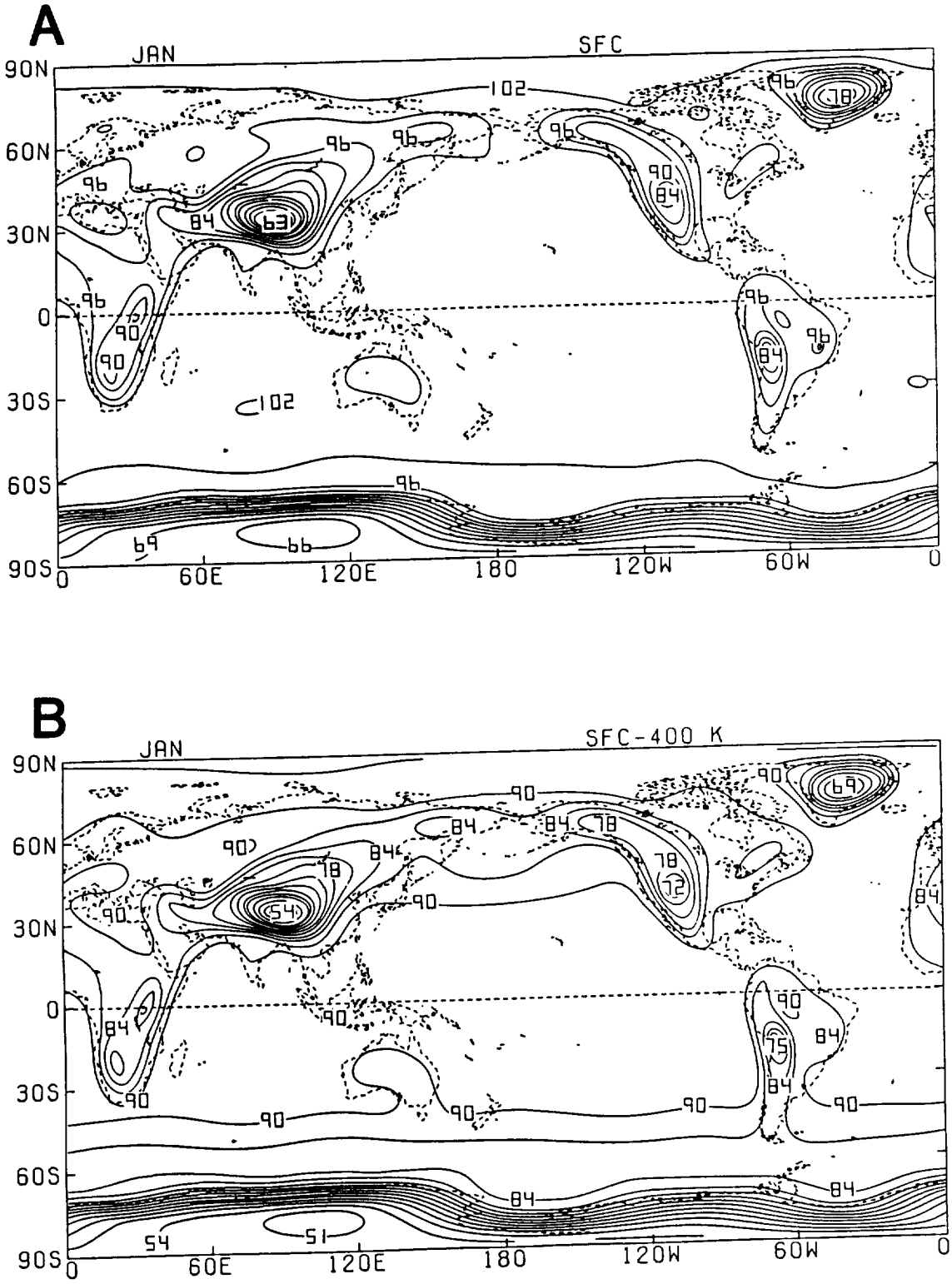

Fig. 41: Global distributions of monthly averaged (A) surface pressure (10^1 mb) and (B) pressure difference (10^1 mb) between the surface and the 400 K isentropic level for January 1979. Contour interval is 30 mb.

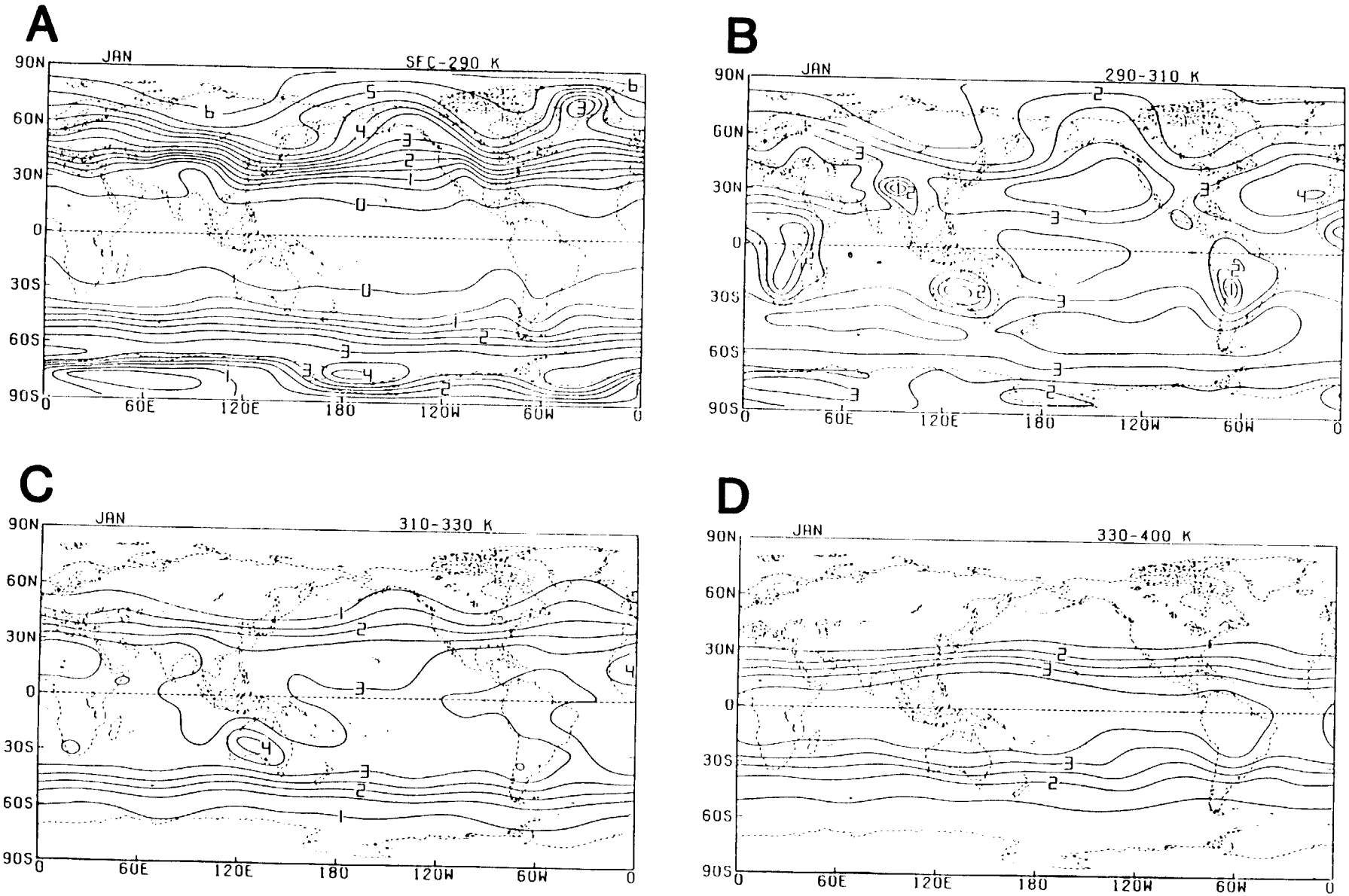

Fig. 42: Monthly averaged pressure difference (10^2 mb) between the upper and lower isentropic levels of the (A) surface-290 K, (B) 290-310 K, (C) 310-330 K and (D) 330-400 K isentropic layers for January 1979. Contour interval is 50 mb.

February

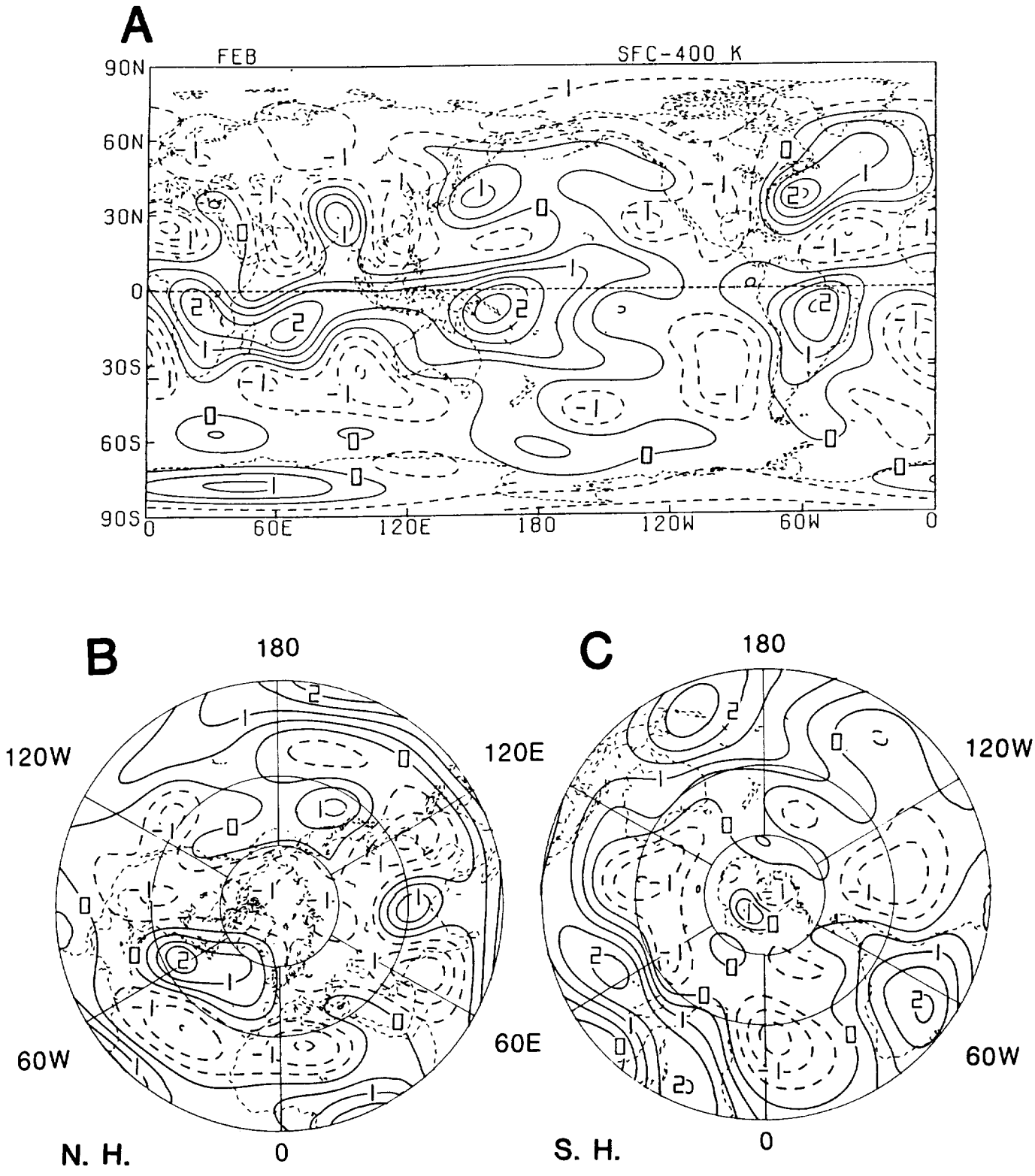

Fig. 43: Monthly vertical-averaged heating (K day^{-1}) for Feburary 1979; (A) global, (B) Northern and (C) Southern Hemisphere. Contour interval is 0.5 K day^{-1}.

February

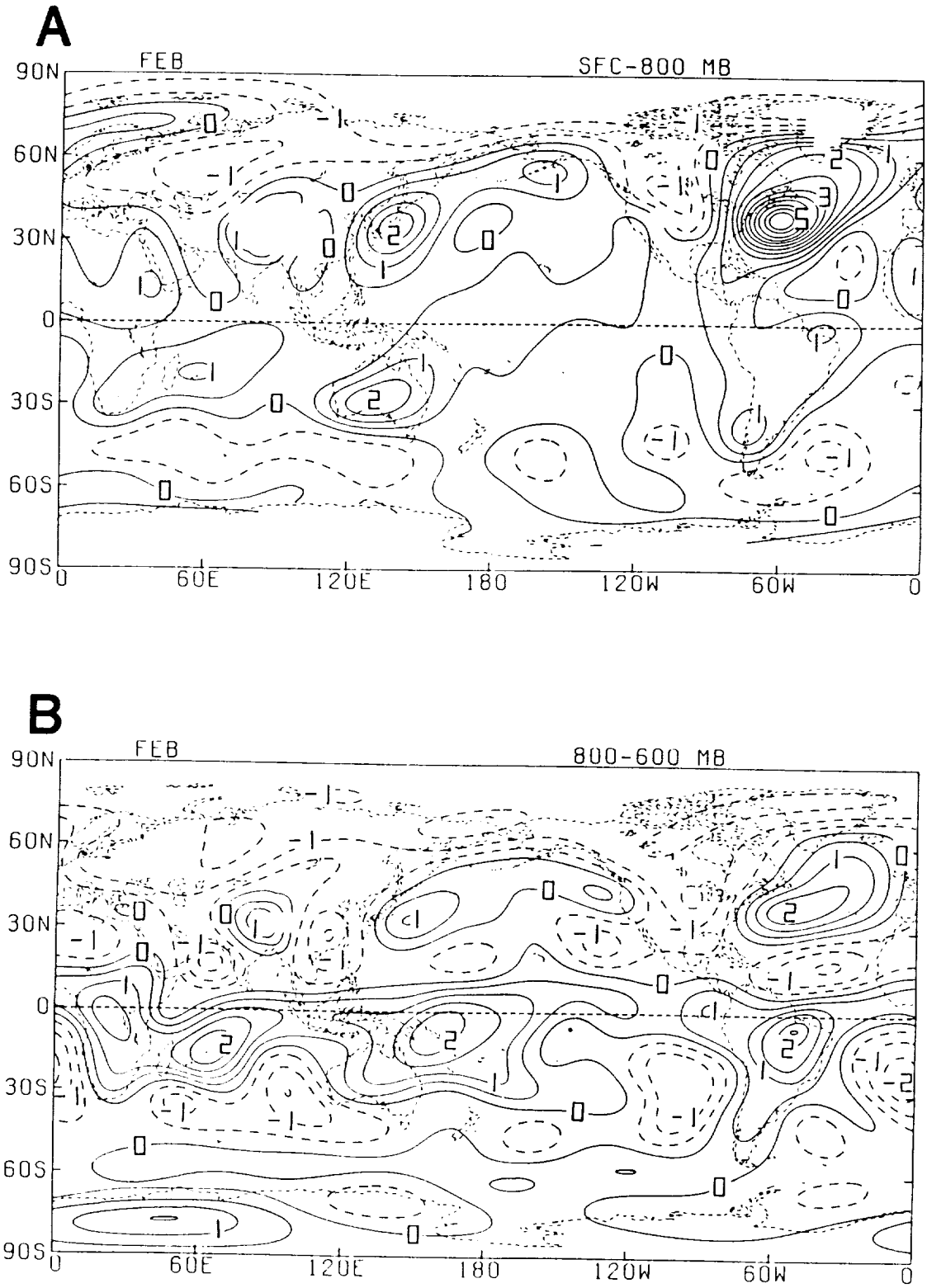

Fig. 44: Monthly layer-averaged heating (K day^{-1}) for the (A) surface-800 mb, (B) 800-600 mb, (C) 600-400 mb and (D) 400-200 mb isobaric layers for February 1979. Contour interval is 0.5 K day^{-1}.

February

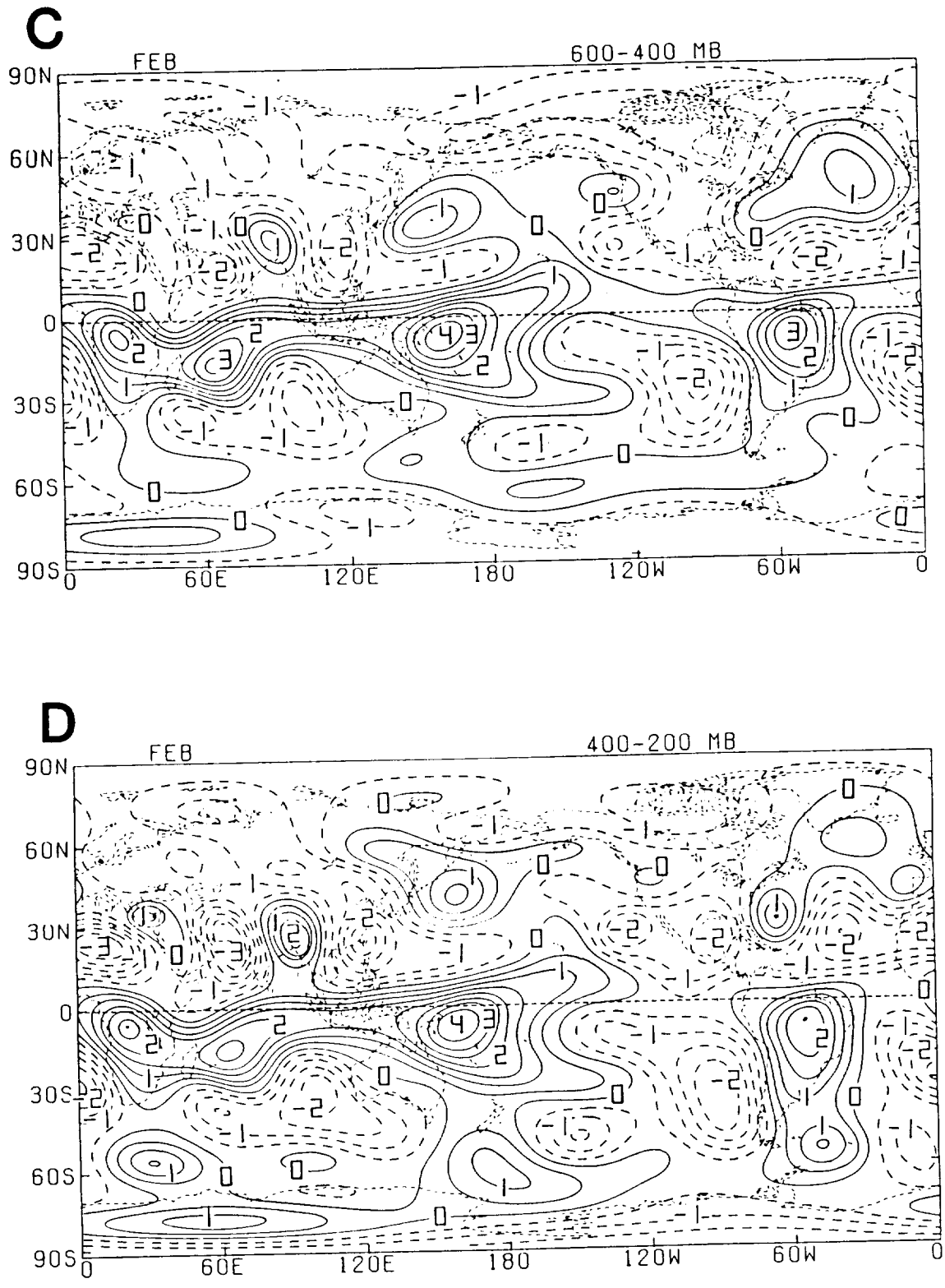

Fig. 44: (Continued).

February

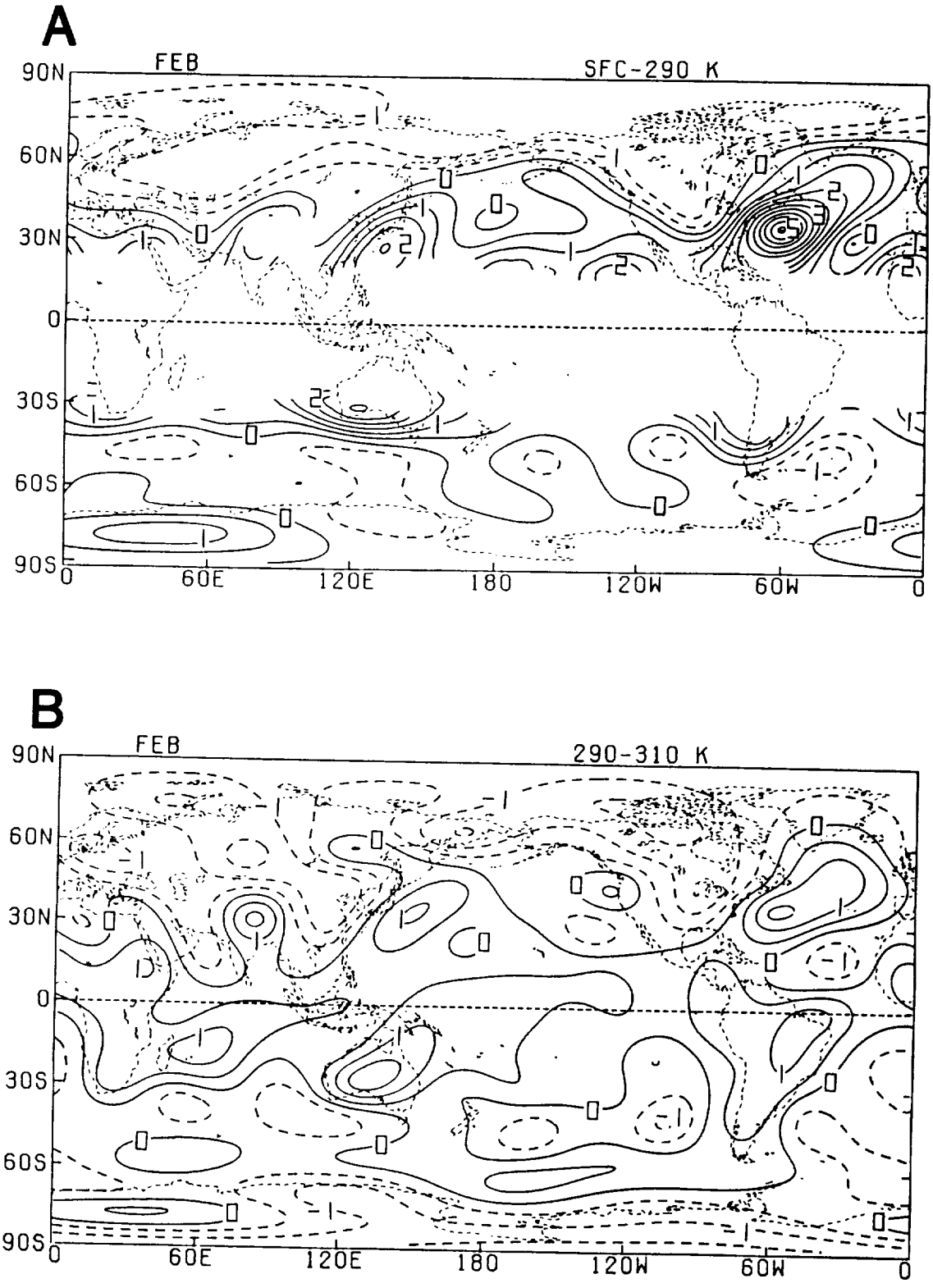

Fig. 45: Monthly layer-averaged heating (K day^{-1}) for the (A) surface-290 K, (B) 290-310 K, (C) 310-330 K and (D) 330-400 K isentropic layers for February 1979. Contour interval is 0.5 K day^{-1}.

February

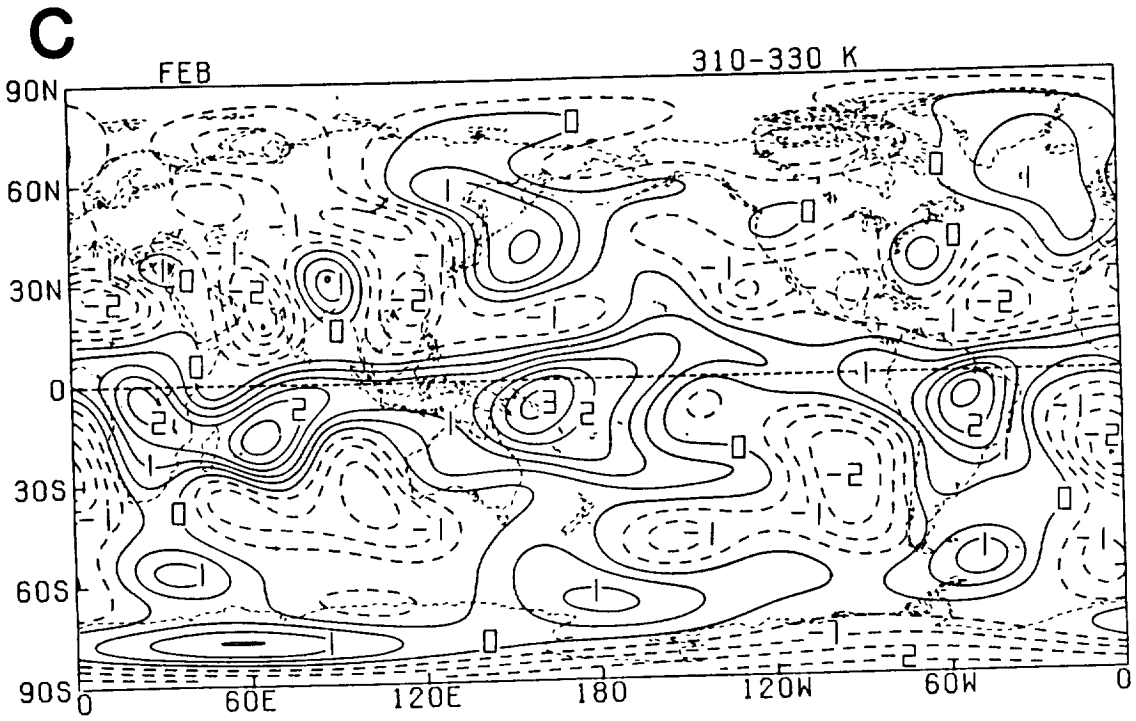

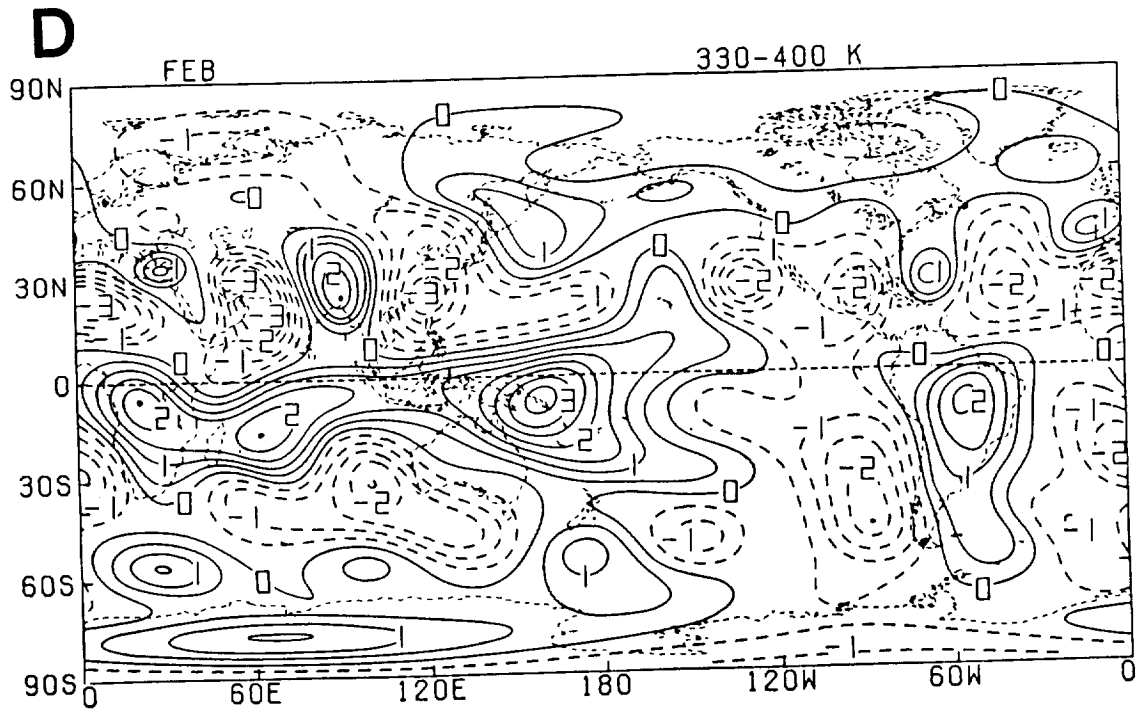

Fig. 45: (Continued).

February

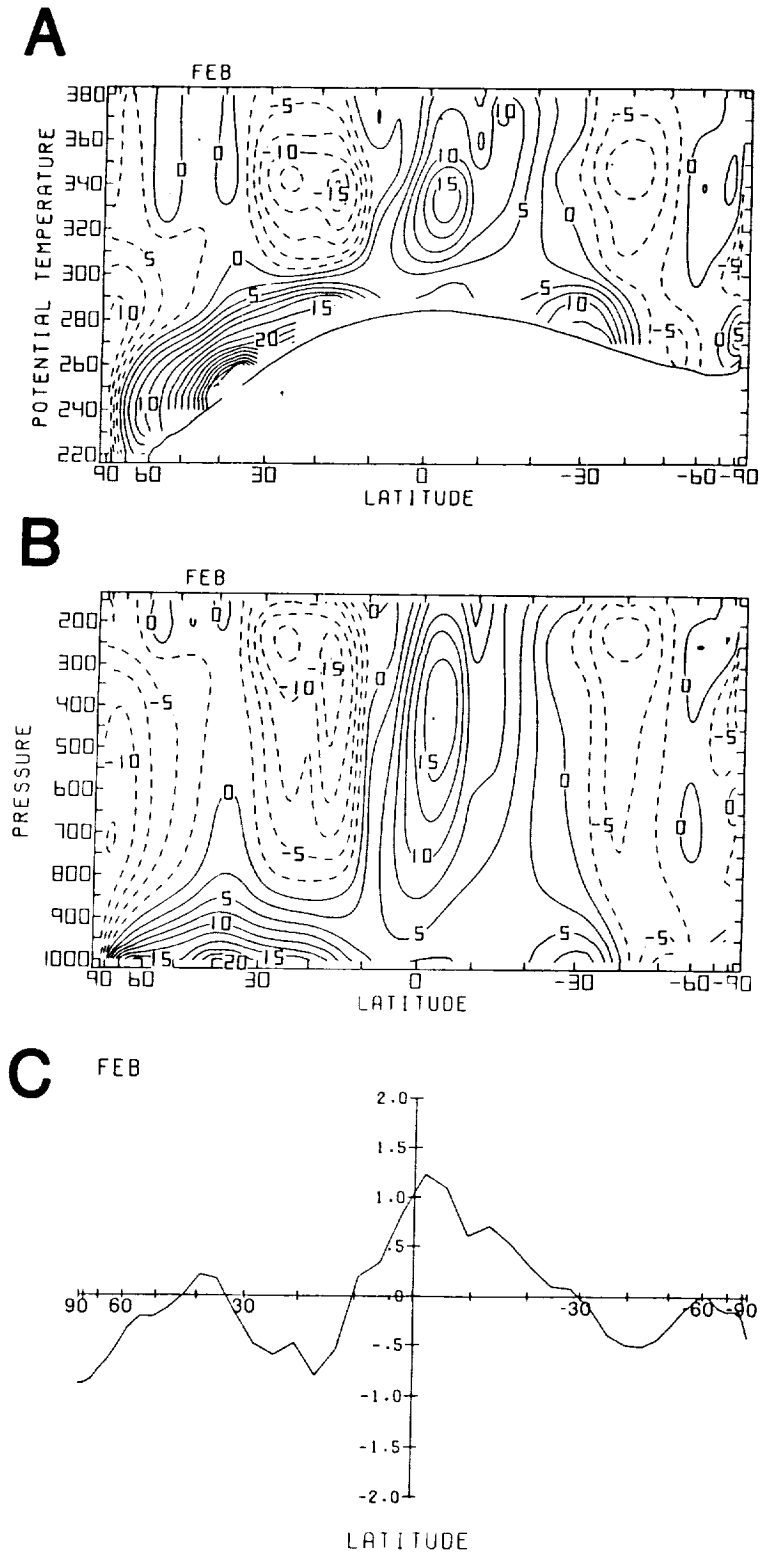

Fig. 46: Meridional cross sections of monthly (A) isentropically and (B) isobarically zonally averaged heating (10^{-1} K day^{-1}), and (C) meridional profile of zonally-vertically averaged heating for February 1979 (K day^{-1}). Contour interval in (A) and (B) is 0.25 K day^{-1}.

February

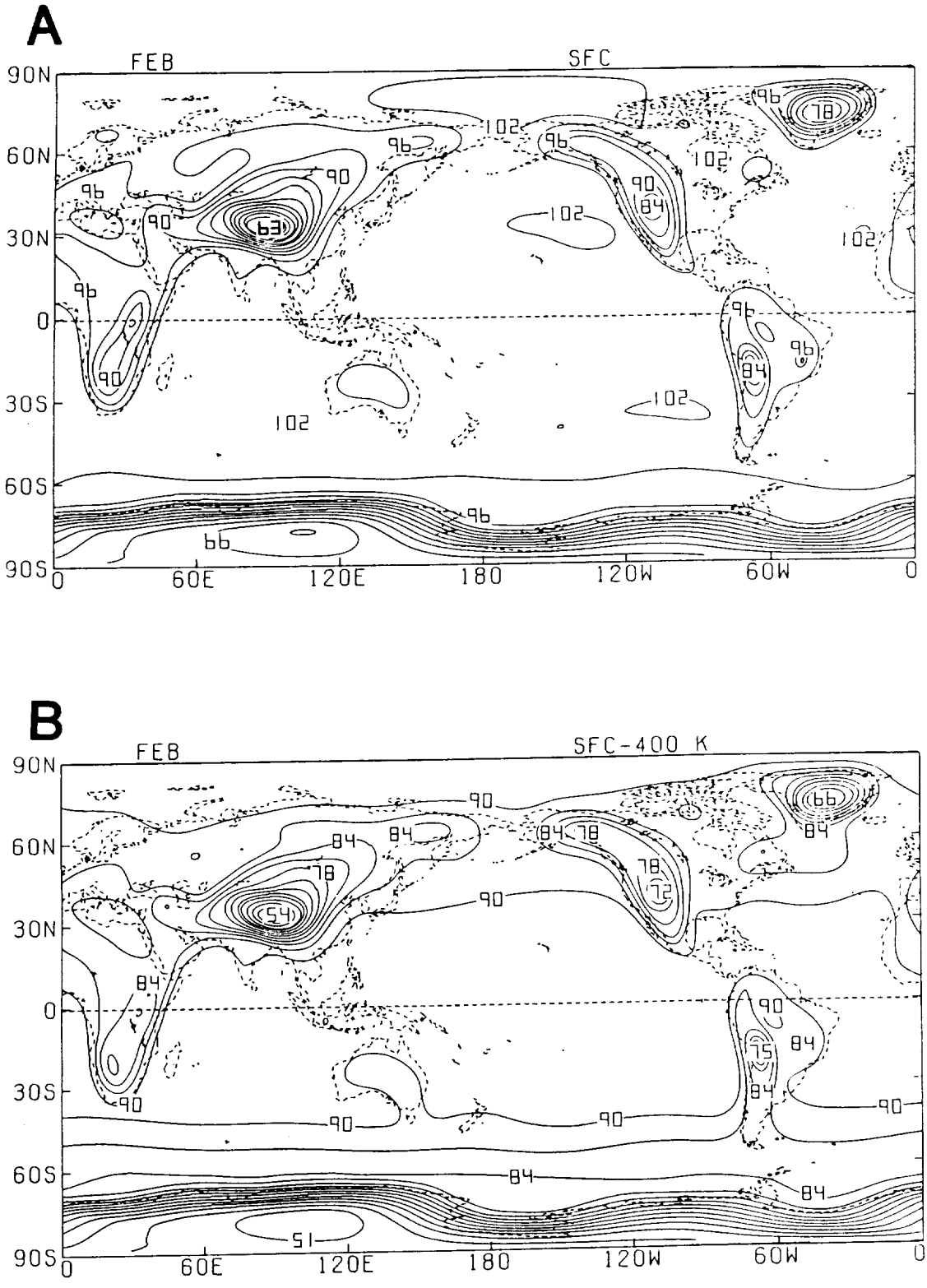

Fig. 47: Global distributions of monthly averaged (A) surface pressure (10^1 mb) and (B) pressure difference (10^1 mb) between the surface and the 400 K isentropic level for February 1979. Contour interval is 30 mb.

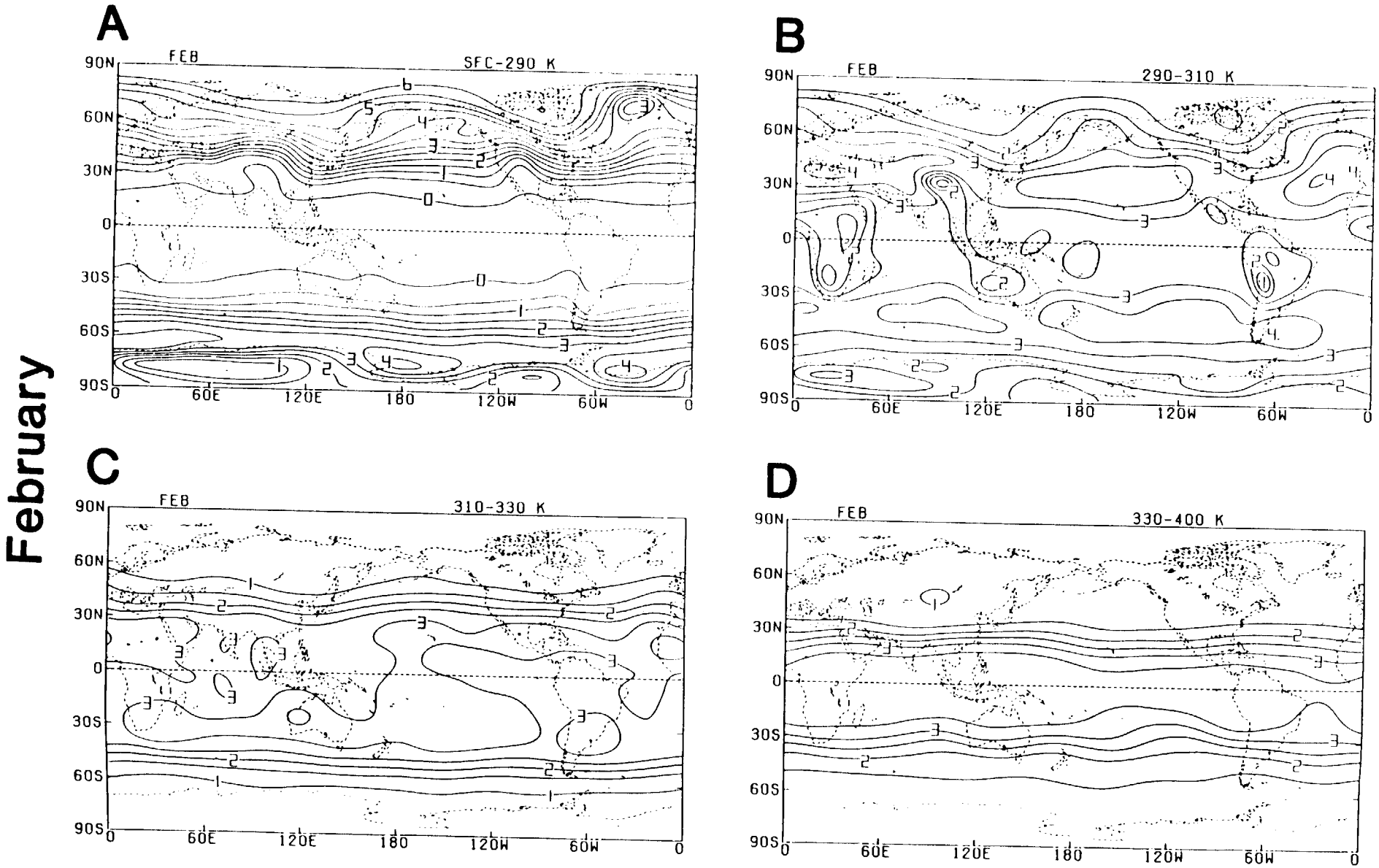

Fig. 48: Monthly averaged pressure difference (10^2 mb) between the upper and lower isentropic levels of the (A) surface-290 K, (B) 290-310 K, (C) 310-330 K and (D) 330-400 K isentropic layers for February 1979. Contour interval is 50 mb.

March

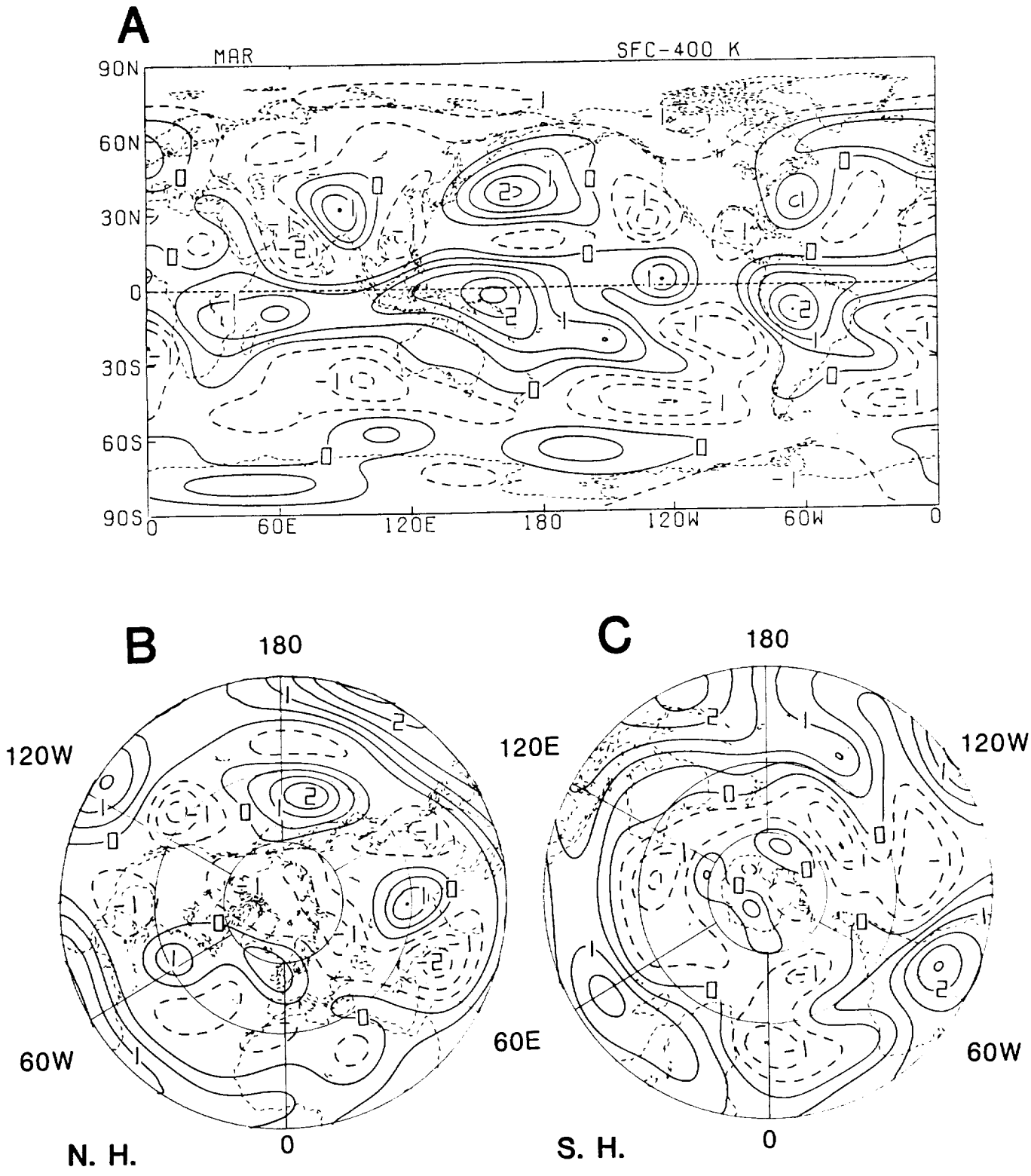

Fig. 49: Monthly vertical-averaged heating (K day^{-1}) for March 1979; (A) global, (B) Northern and (C) Southern Hemisphere. Contour interval is 0.5 K day^{-1}.

March

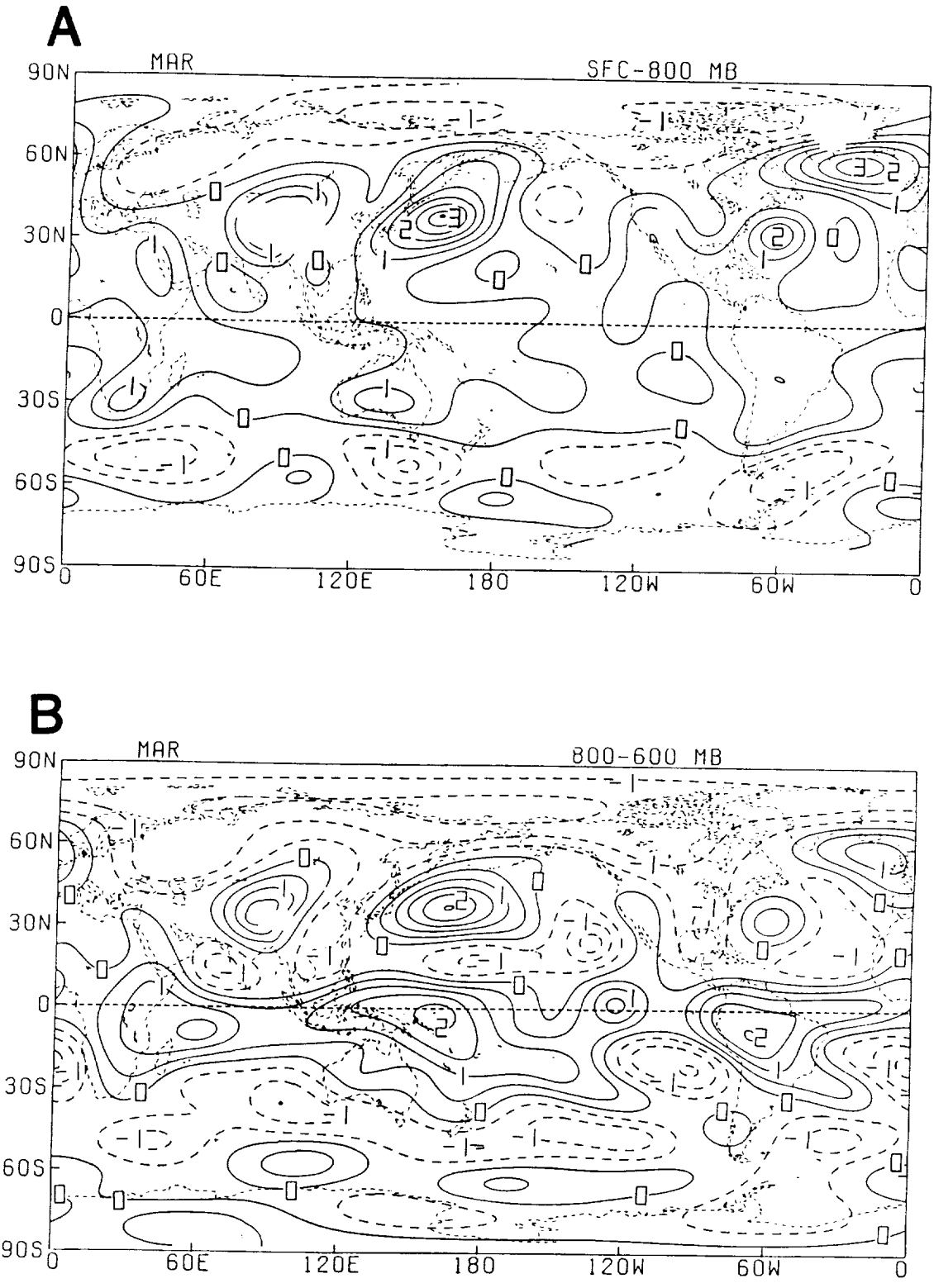

Fig. 50: Monthly layer-averaged heating (K day^{-1}) for the (A) surface-800 mb, (B) 800-600 mb, (C) 600-400 mb and (D) 400-200 mb isobaric layers for March 1979. Contour interval is 0.5 K day^{-1}.

March

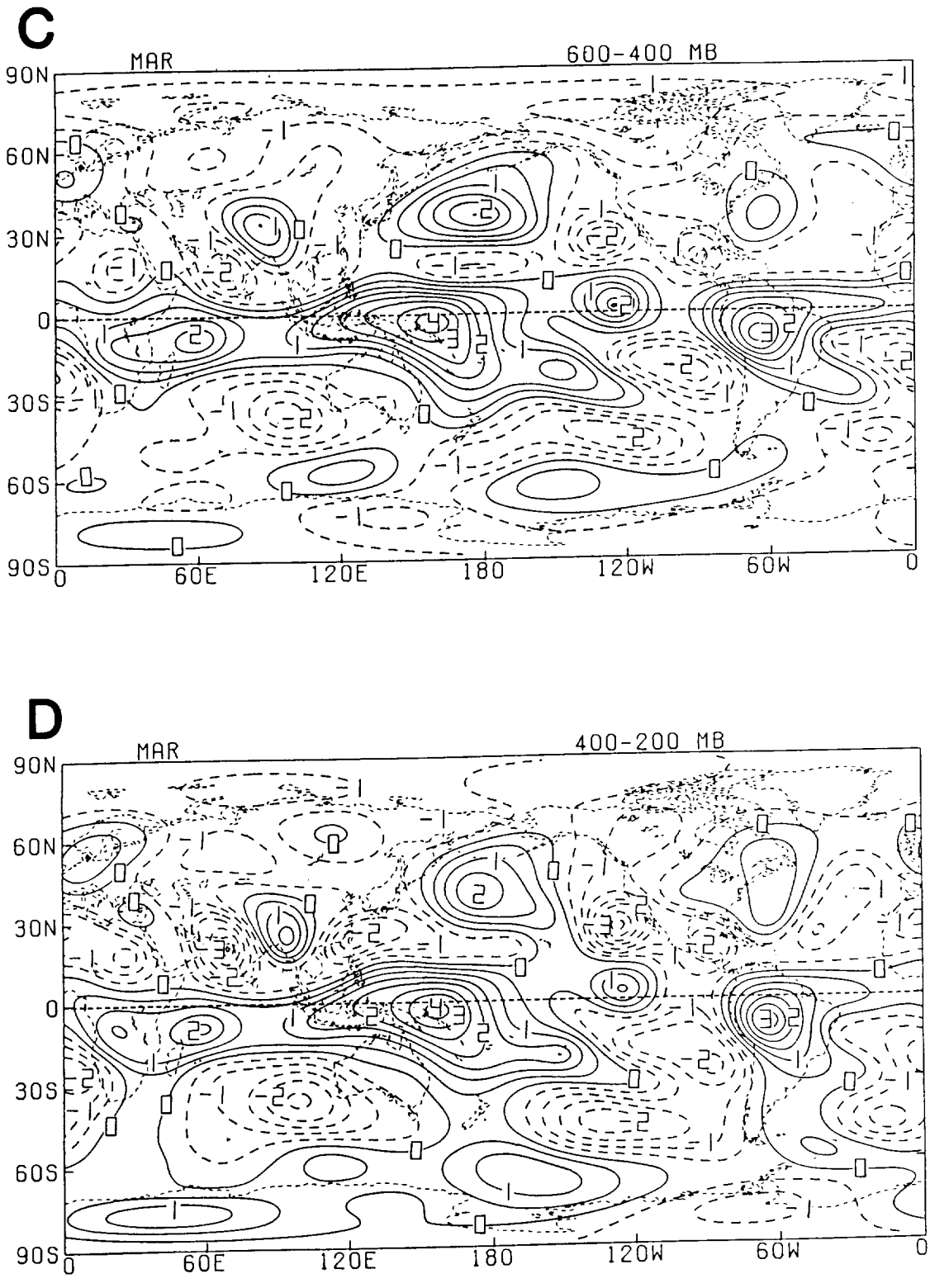

Fig. 50: (Continued).

March

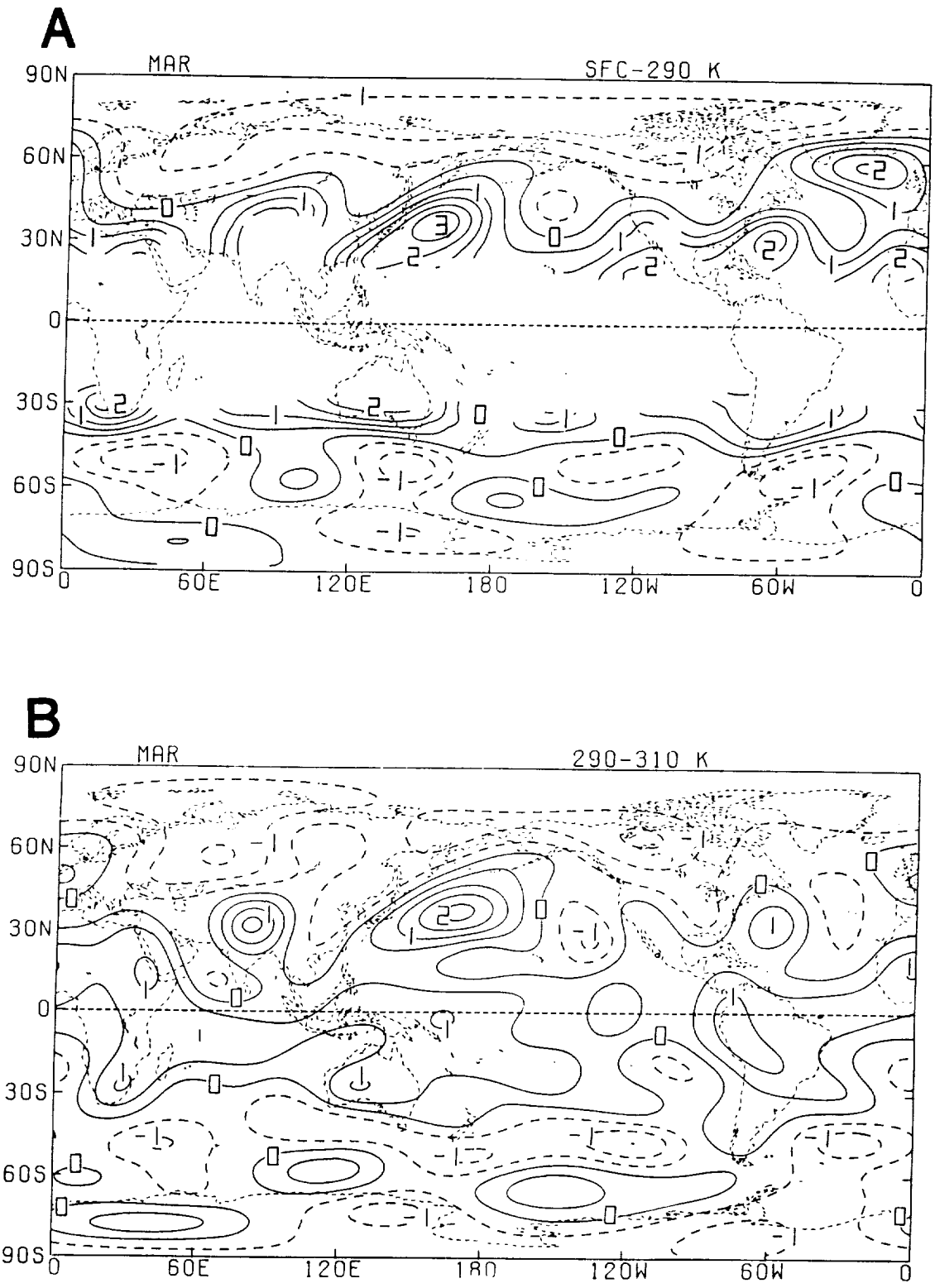

Fig. 51: Monthly layer-averaged heating (K day^{-1}) for the (A) surface-290 K, (B) 290-310 K, (C) 310-330 K and (D) 330-400 K isentropic layers for March 1979. Contour interval is 0.5 K day^{-1}.

March

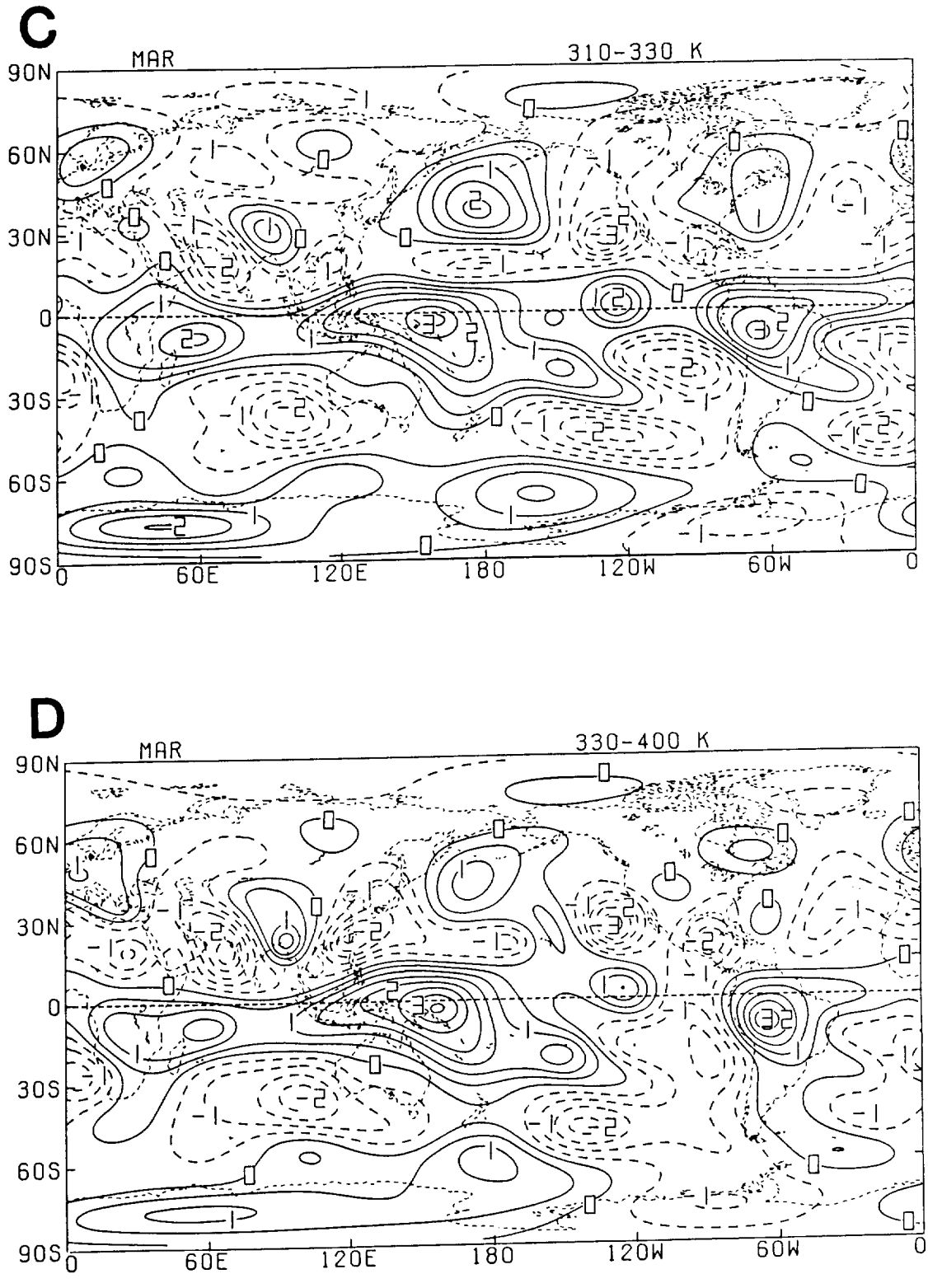

Fig. 51: (Continued).

March

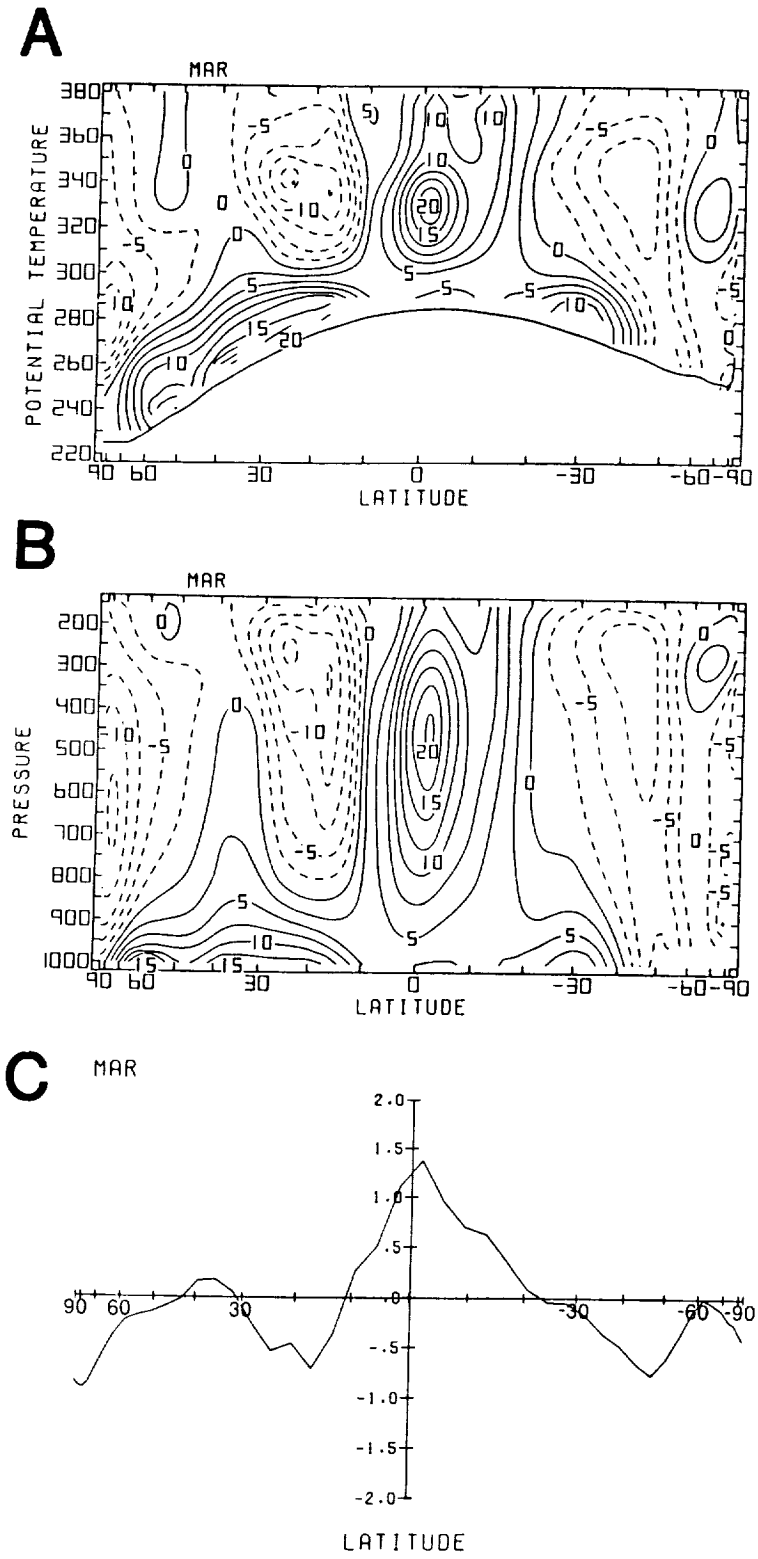

Fig. 52: Meridional cross sections of monthly (A) isentropically and (B) isobarically zonally averaged heating (10^{-1} K day^{-1}), and (C) meridional profile of zonally-vertically averaged heating for March 1979 (K day^{-1}). Contour interval in (A) and (B) is 0.25 K day^{-1}.

March

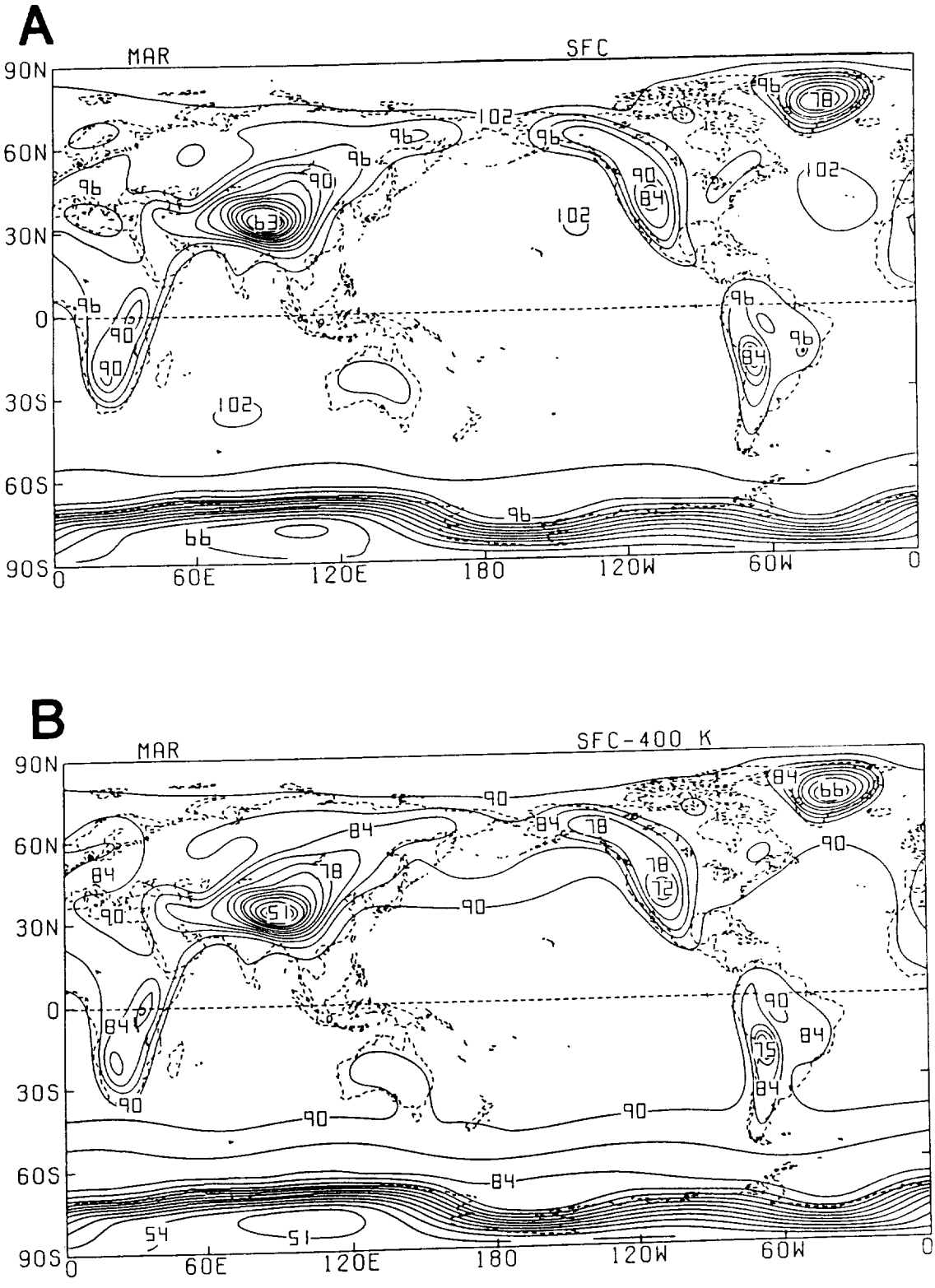

Fig. 53: Global distributions of monthly averaged (A) surface pressure (10^1 mb) and (B) pressure difference (10^1 mb) between the surface and the 400 K isentropic level for March 1979. Contour interval is 30 mb.

March

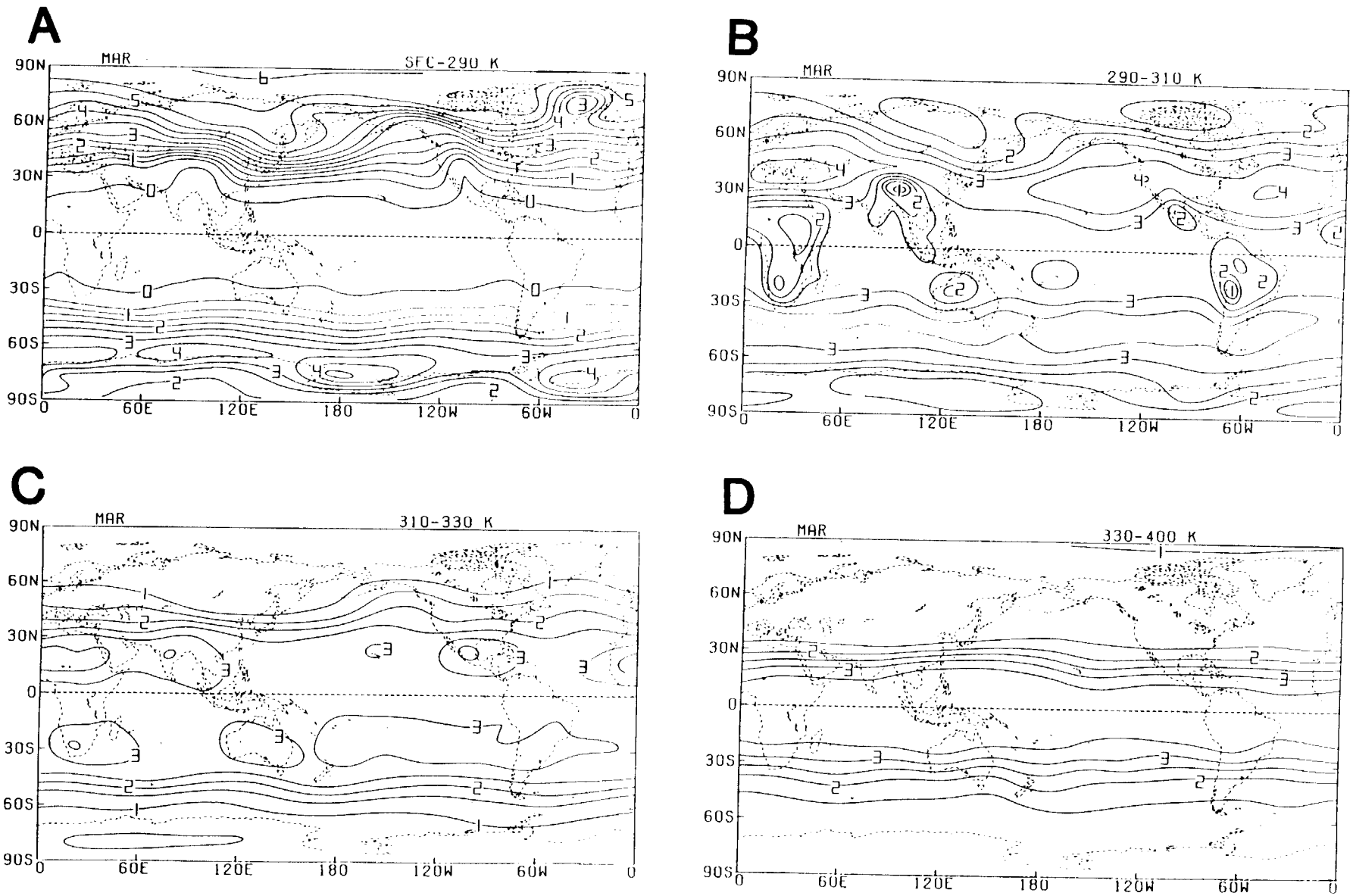

Fig. 54: Monthly averaged pressure difference (10^2 mb) between the upper and lower isentropic levels of the (A) surface-290 K, (B) 290-310 K, (C) 310-330 K and (D) 330-400 K isentropic layers for March 1979. Contour interval is 50 mb.

April

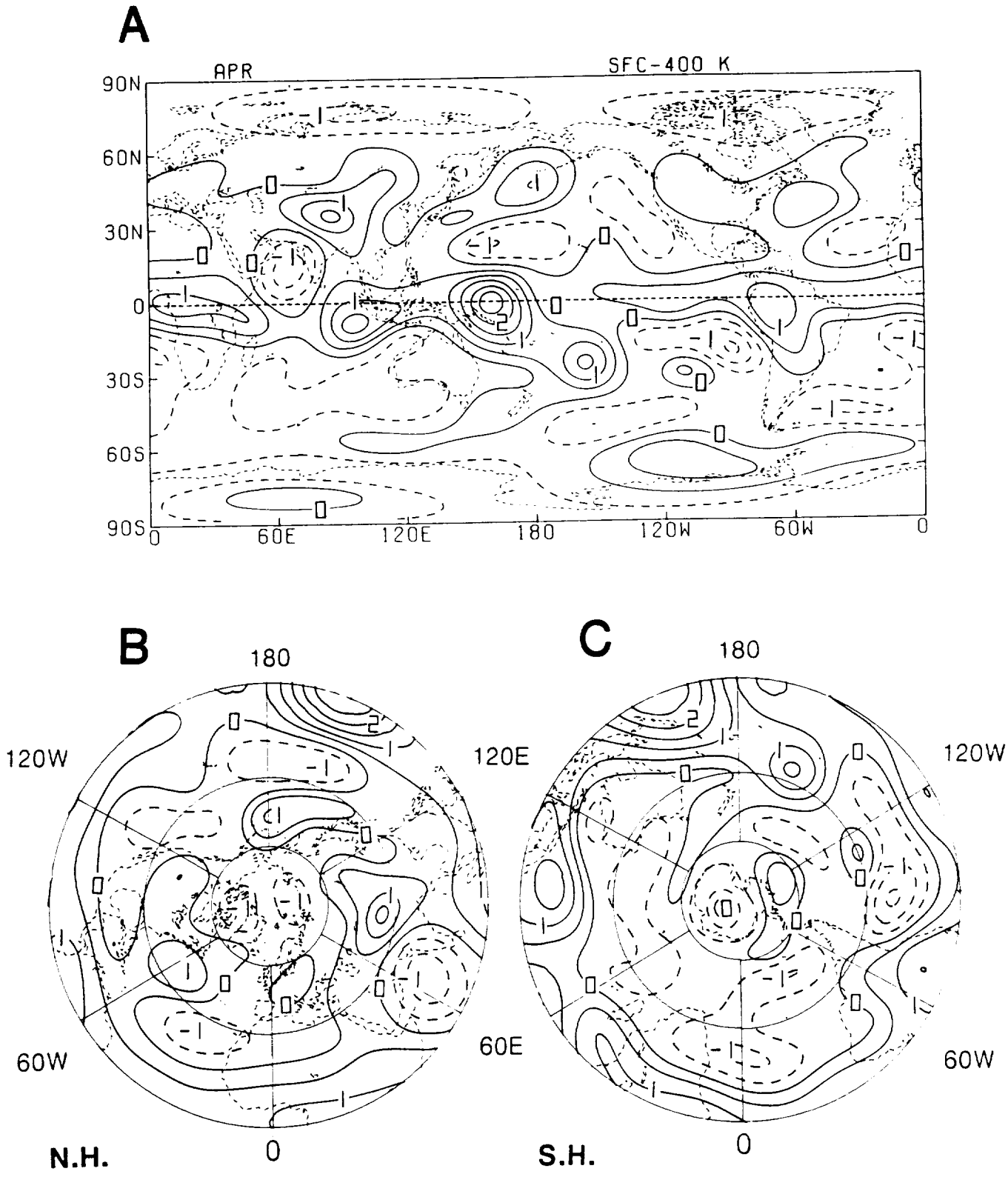

Fig. 55: Monthly vertical-averaged heating (K day^{-1}) for April 1979; (A) global, (B) Northern and (C) Southern Hemisphere. Contour interval is 0.5 K day^{-1}.

April

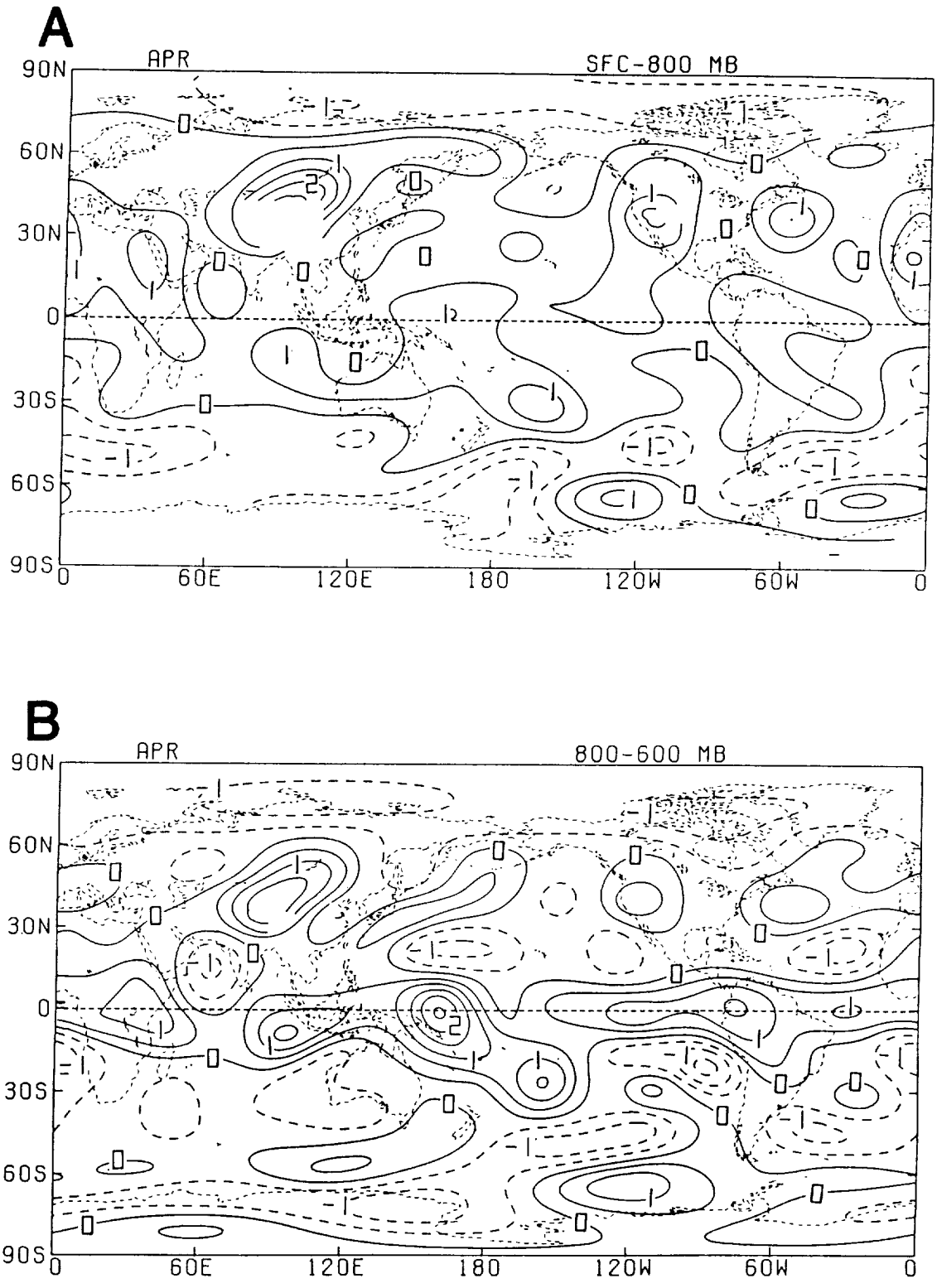

Fig. 56: Monthly layer-averaged heating (K day^{-1}) for the (A) surface-800 mb, (B) 800-600 mb, (C) 600-400 mb and (D) 400-200 mb isobaric layers for April 1979. Contour interval is 0.5 K day^{-1}.

April

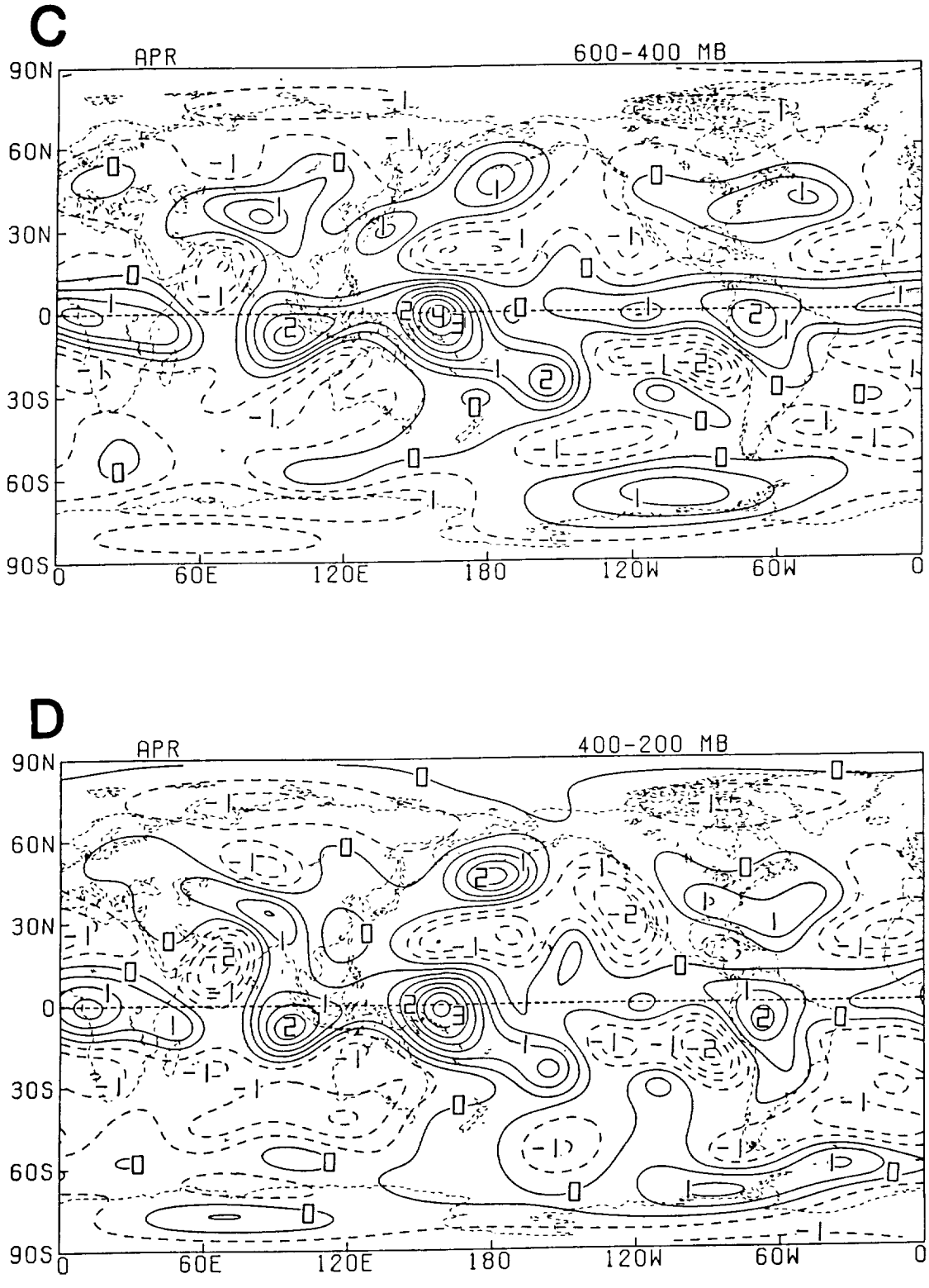

Fig. 56: (Continued).

April

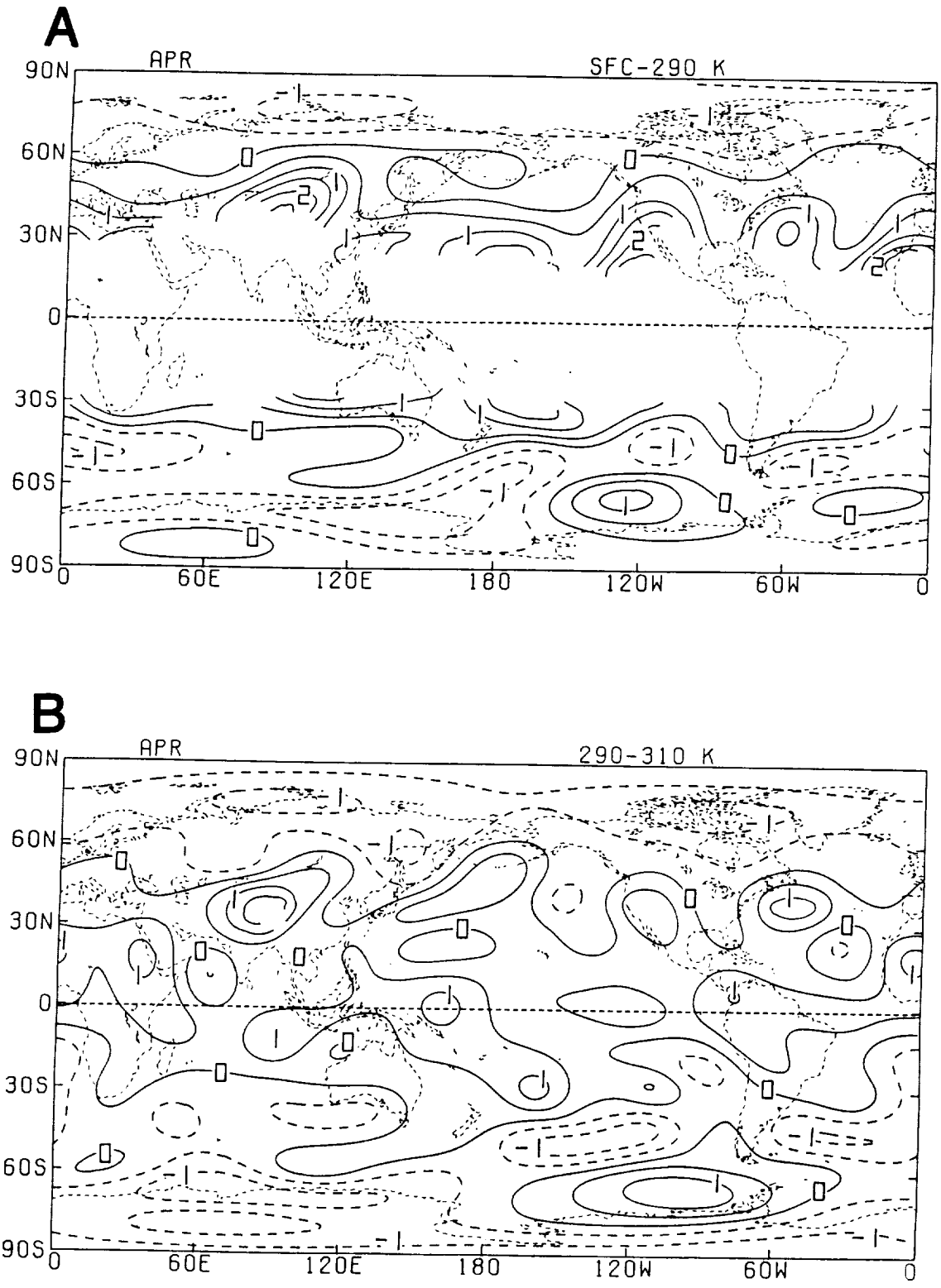

Fig. 57: Monthly layer-averaged heating (K day^{-1}) for the (A) surface-290 K, (B) 290-310 K, (C) 310-330 K and (D) 330-400 K isentropic layers for April 1979. Contour interval is 0.5 K day^{-1}.

April

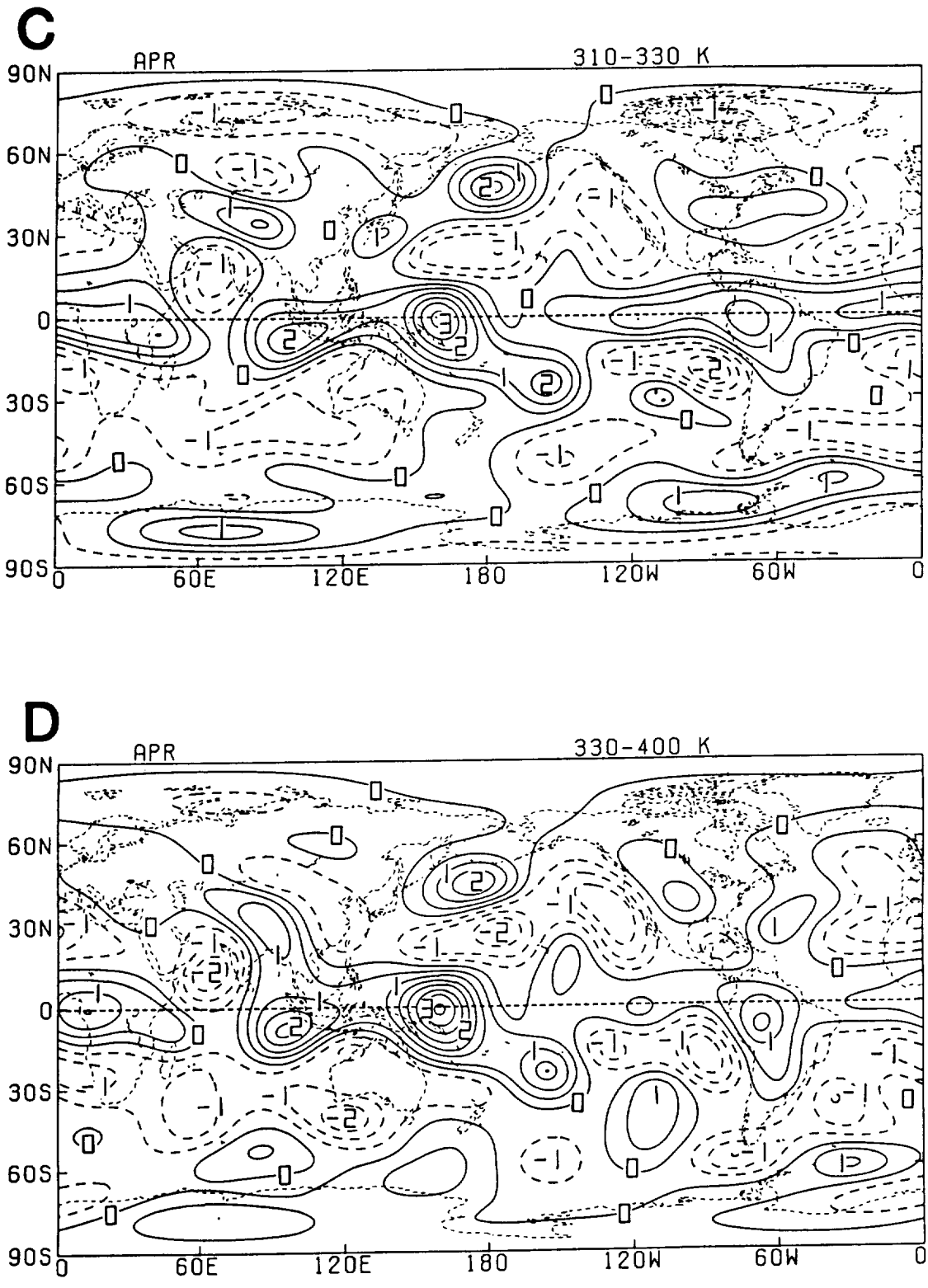

Fig. 57: (Continued).

April

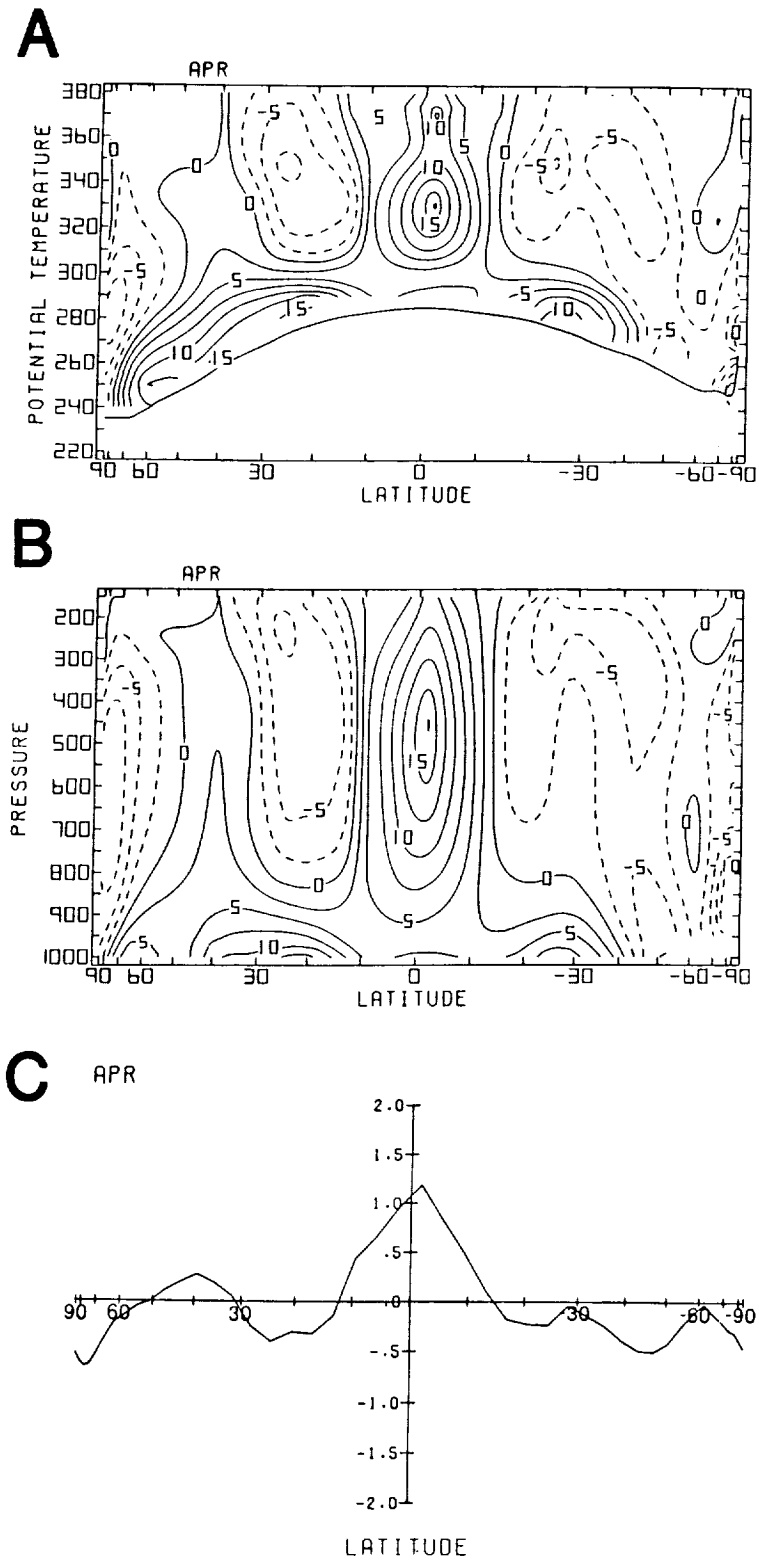

Fig. 58: Meridional cross sections of monthly (A) isentropically and (B) isobarically zonally averaged heating (10^{-1} K day^{-1}), and (C) meridional profile of zonally-vertically averaged heating for April 1979 (K day^{-1}). Contour interval in (A) and (B) is 0.25 K day^{-1}.

April

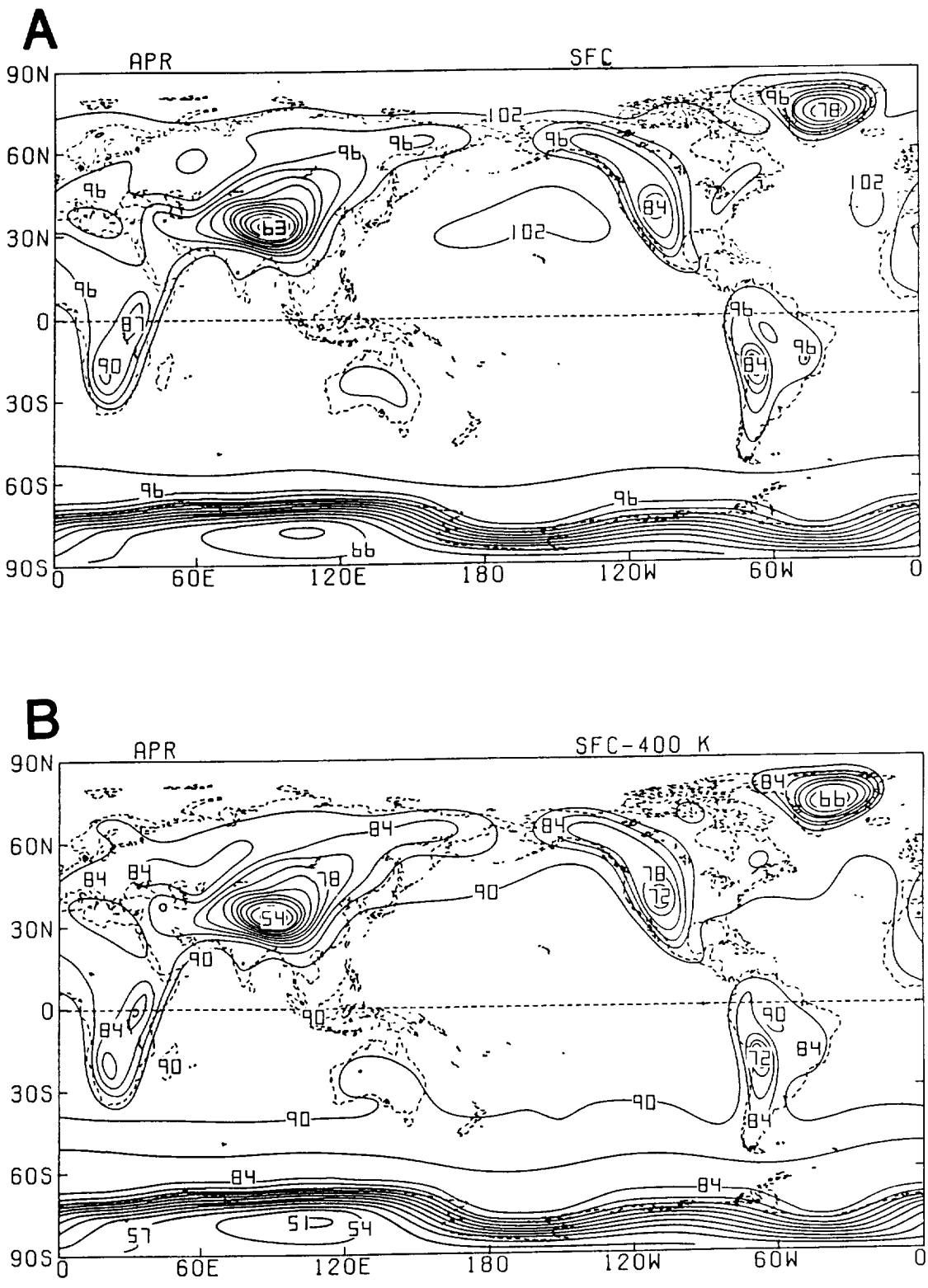

Fig. 59: Global distributions of monthly averaged (A) surface pressure (10^1 mb) and (B) pressure difference (10^1 mb) between the surface and the 400 K isentropic level for April 1979. Contour interval is 30 mb.

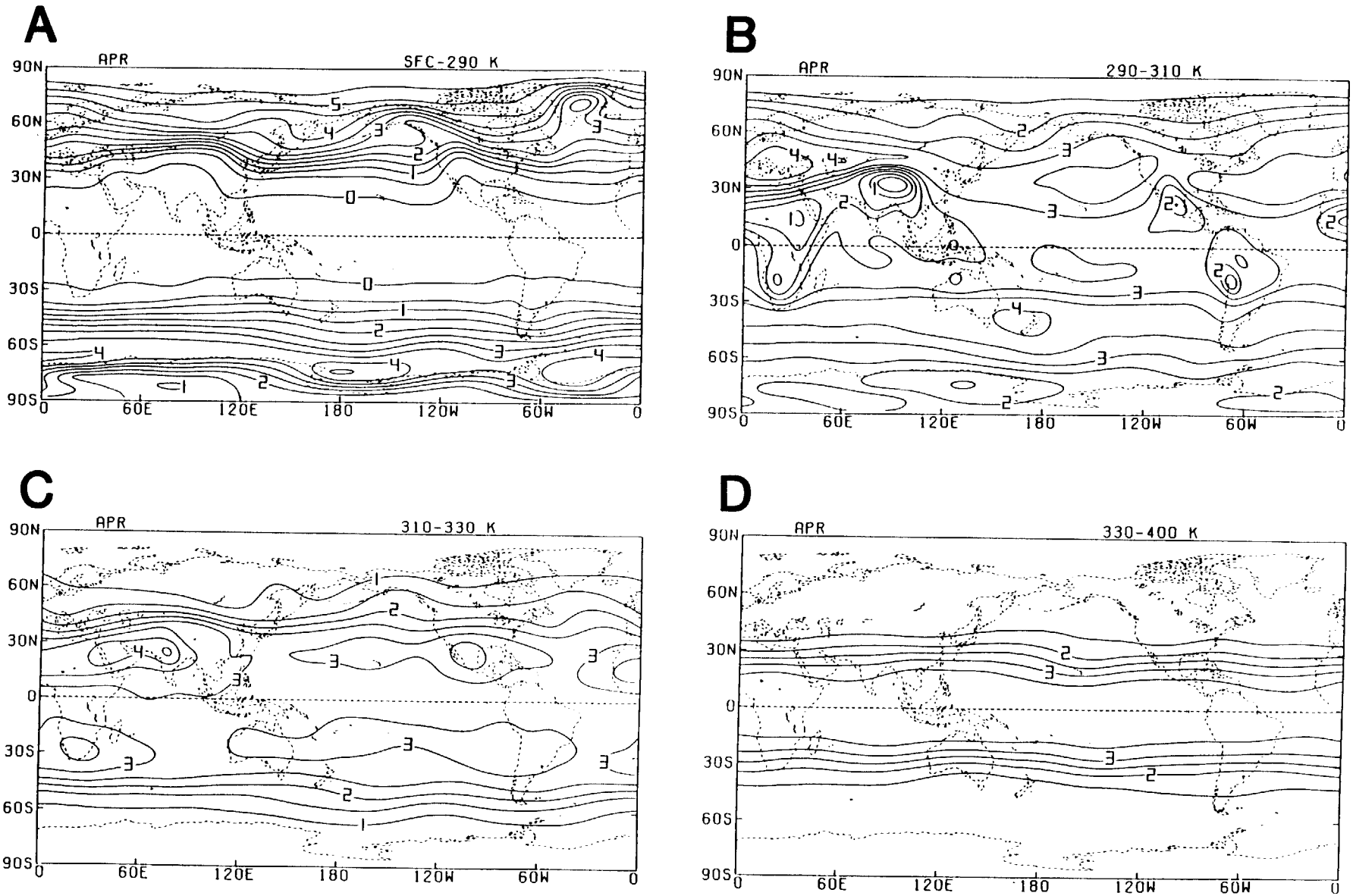

Fig. 60: Monthly averaged pressure difference (10^2 mb) between the upper and lower isentropic levels of the (A) surface-290 K, (B) 290-310 K, (C) 310-330 K and (D) 330-400 K isentropic layers for April 1979. Contour interval is 50 mb.

May

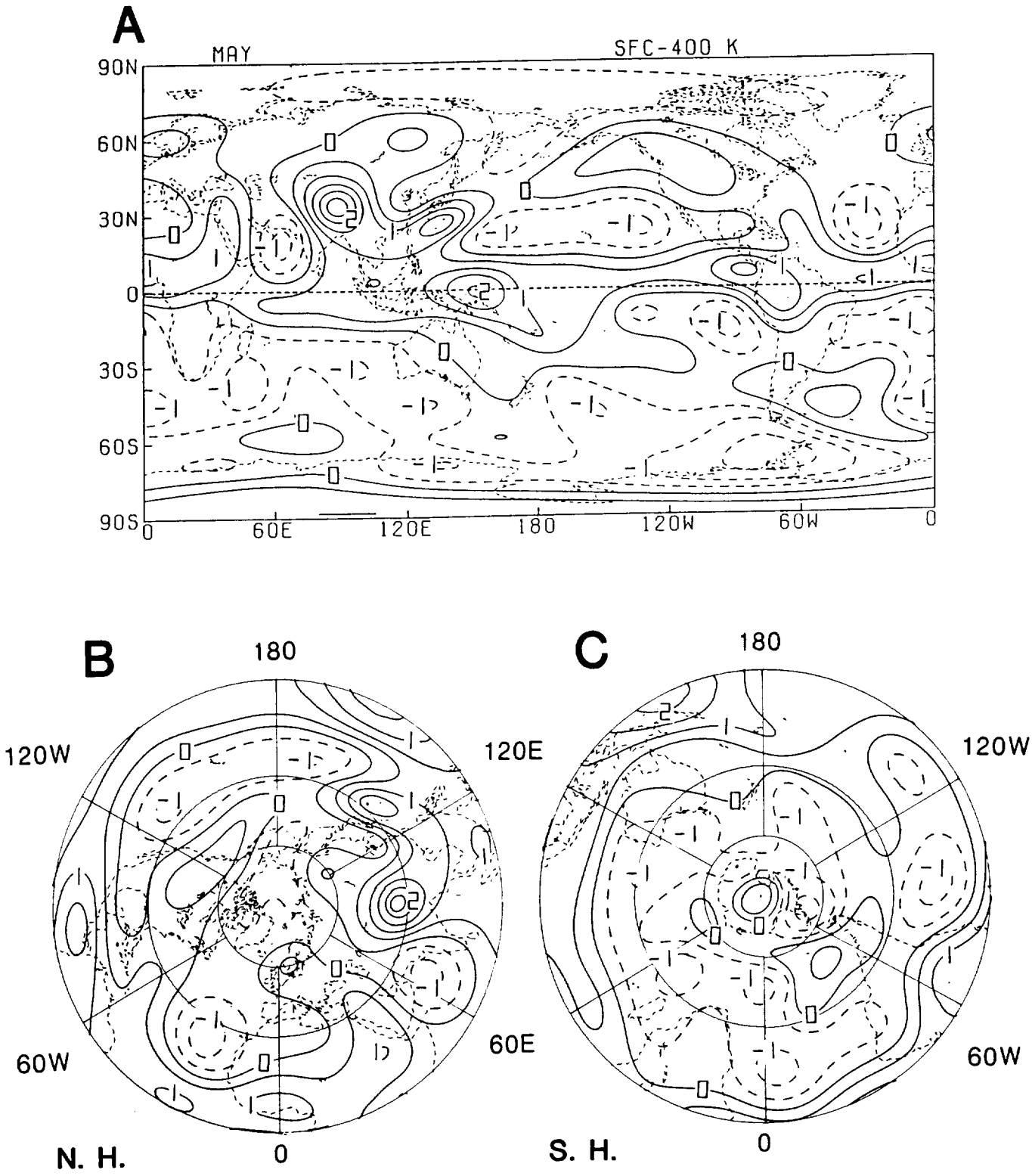

Fig. 61: Monthly vertical-averaged heating (K day^{-1}) for May 1979; (A) global, (B) Northern and (C) Southern Hemisphere. Contour interval is 0.5 K day^{-1}.

May

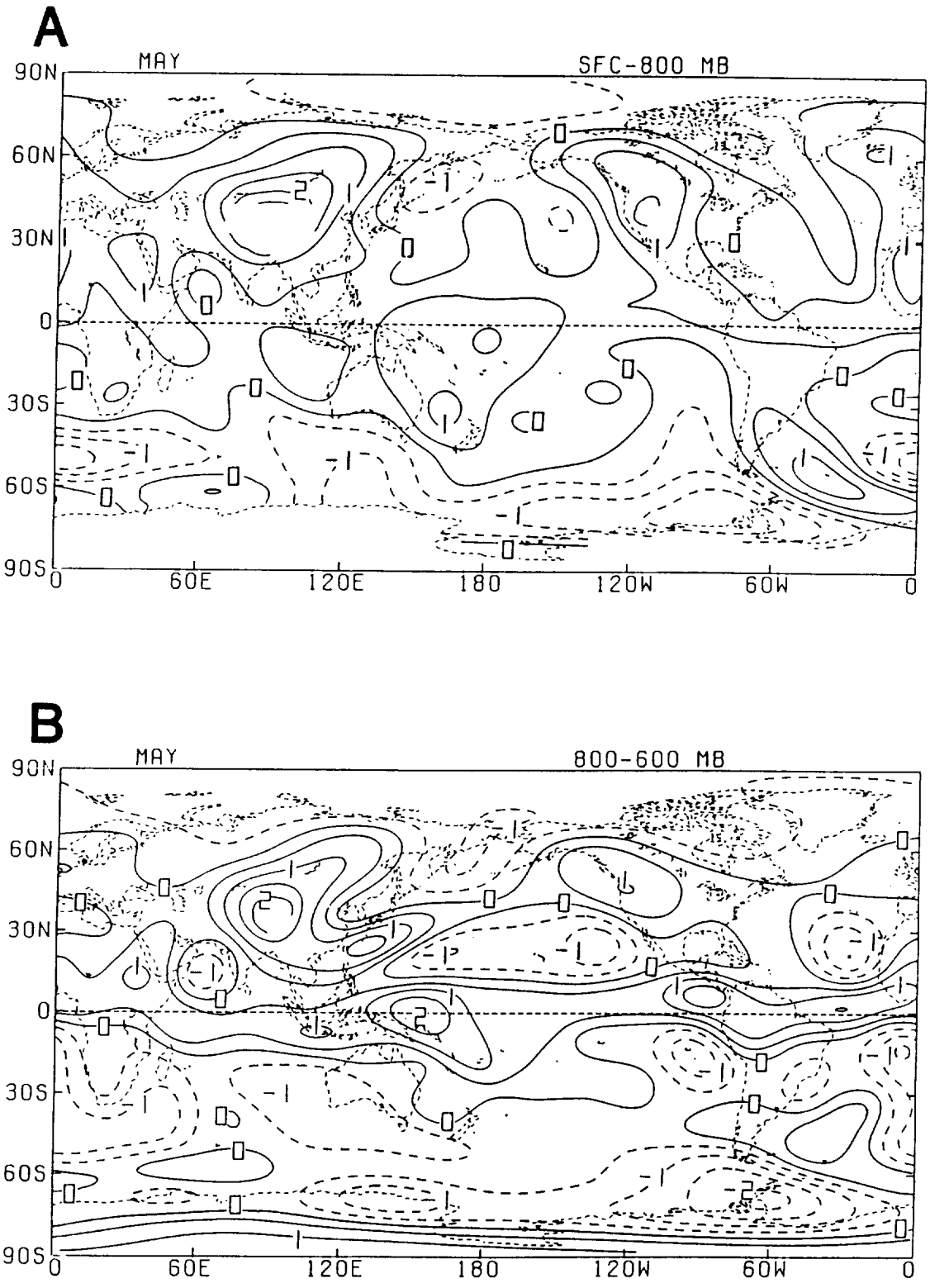

Fig. 62: Monthly layer-averaged heating (K day^{-1}) for the (A) surface-800 mb, (B) 800-600 mb, (C) 600-400 mb and (D) 400-200 mb isobaric layers for May 1979. Contour interval is 0.5 K day^{-1}.

May

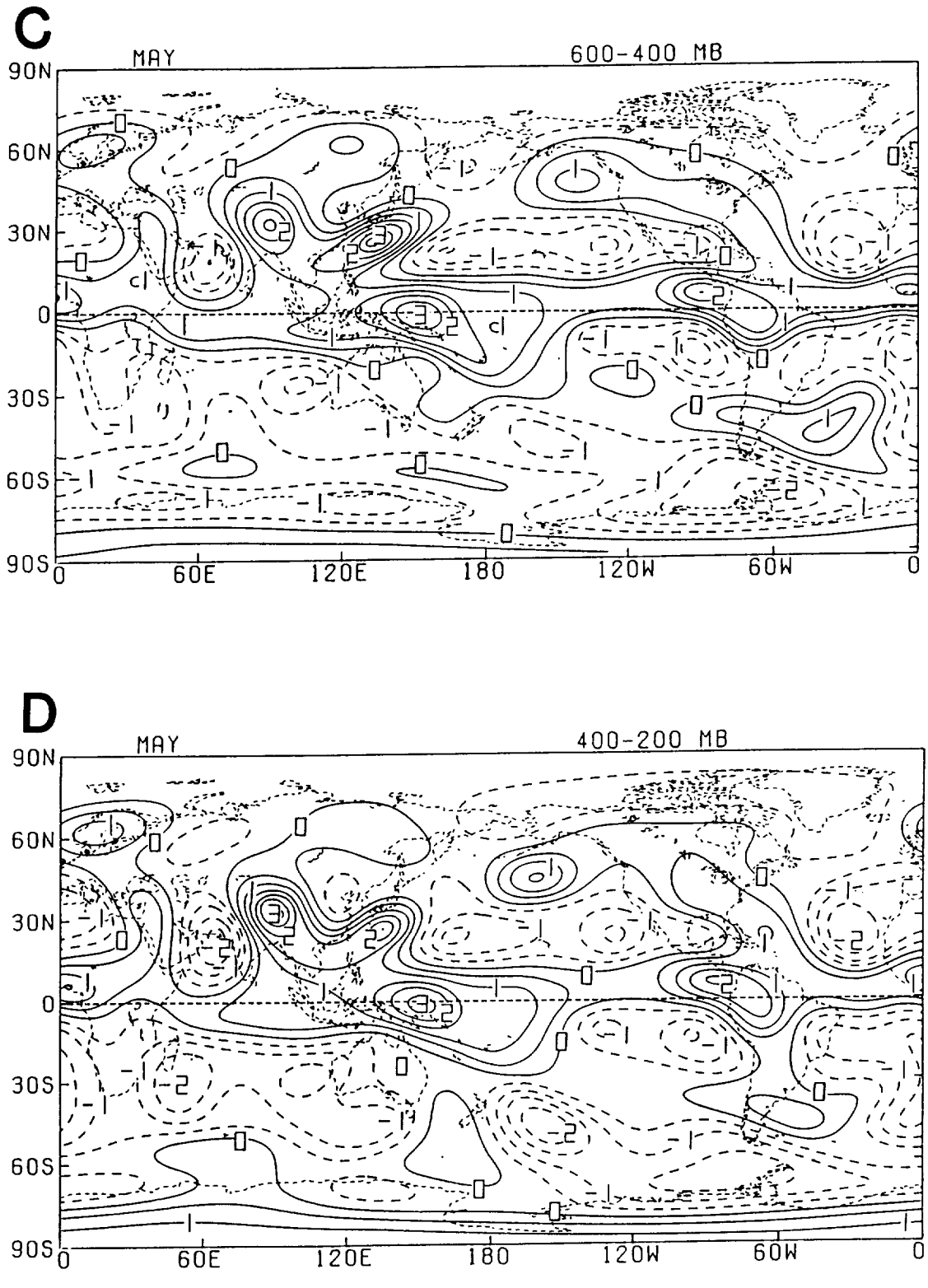

Fig. 62: (Continued).

May

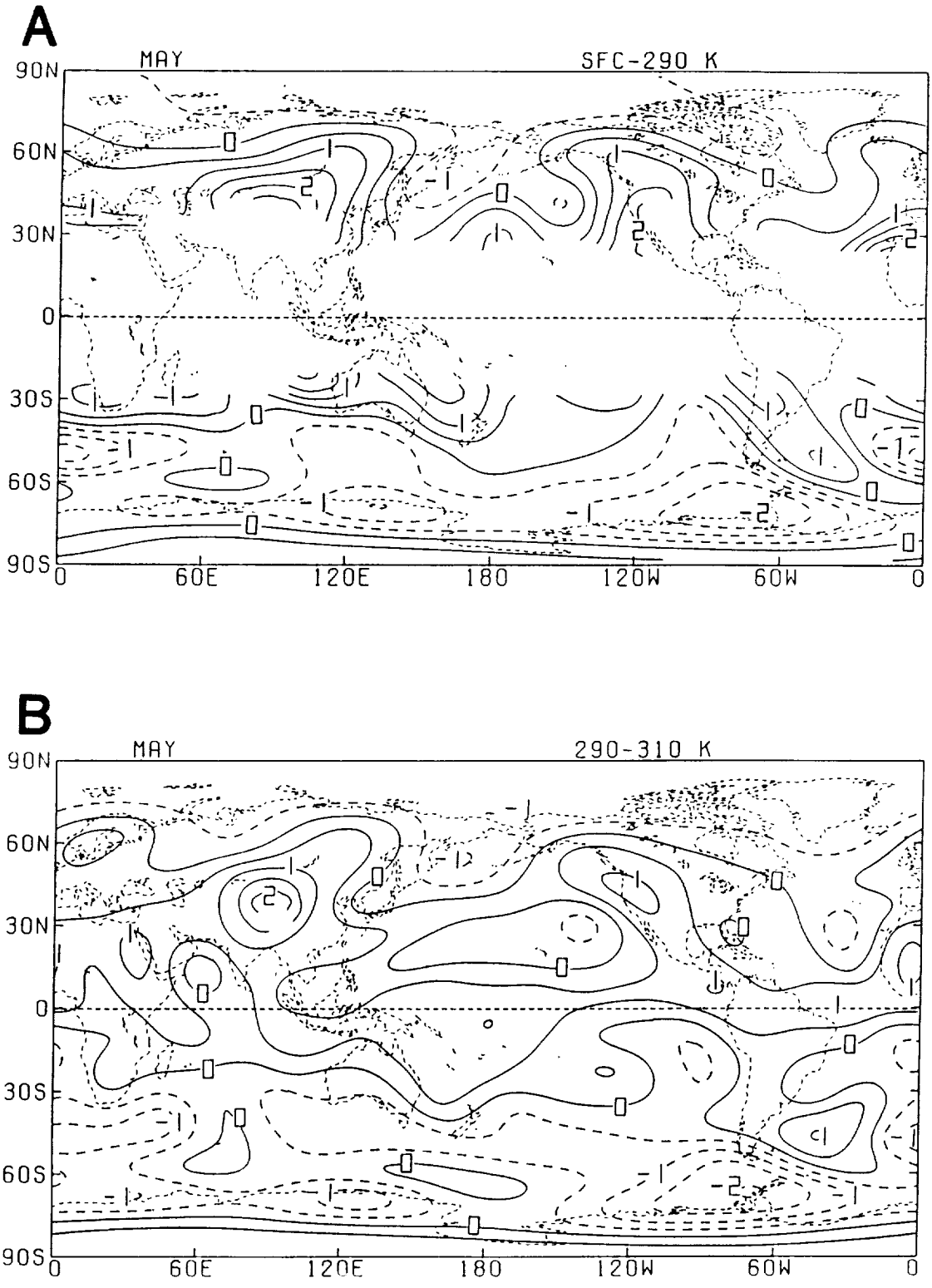

Fig. 63: Monthly layer-averaged heating (K day^{-1}) for the (A) surface-290 K, (B) 290-310 K, (C) 310-330 K and (D) 330-400 K isentropic layers for May 1979. Contour interval is 0.5 K day^{-1}.

May

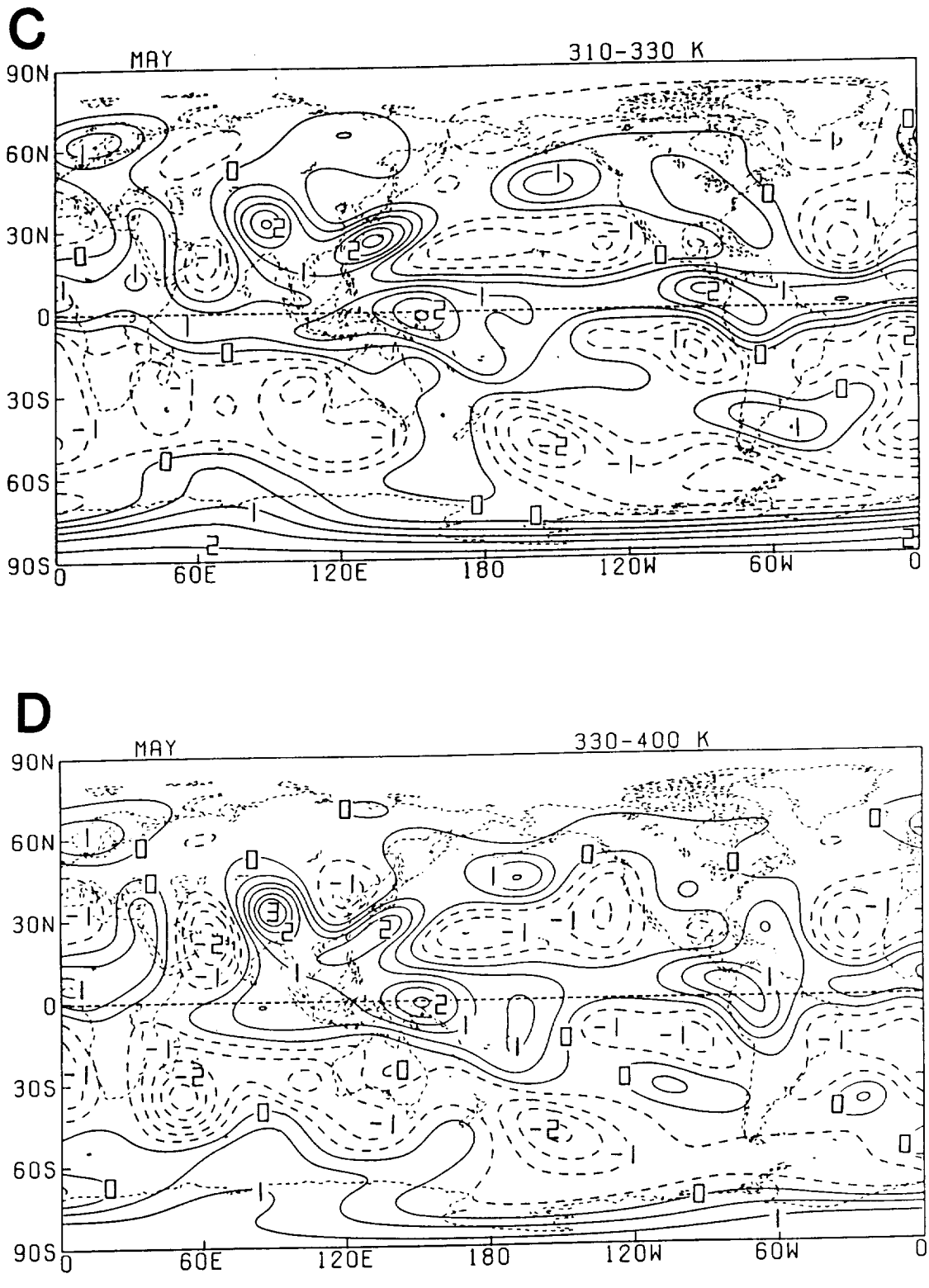

Fig. 63: (Continued).

May

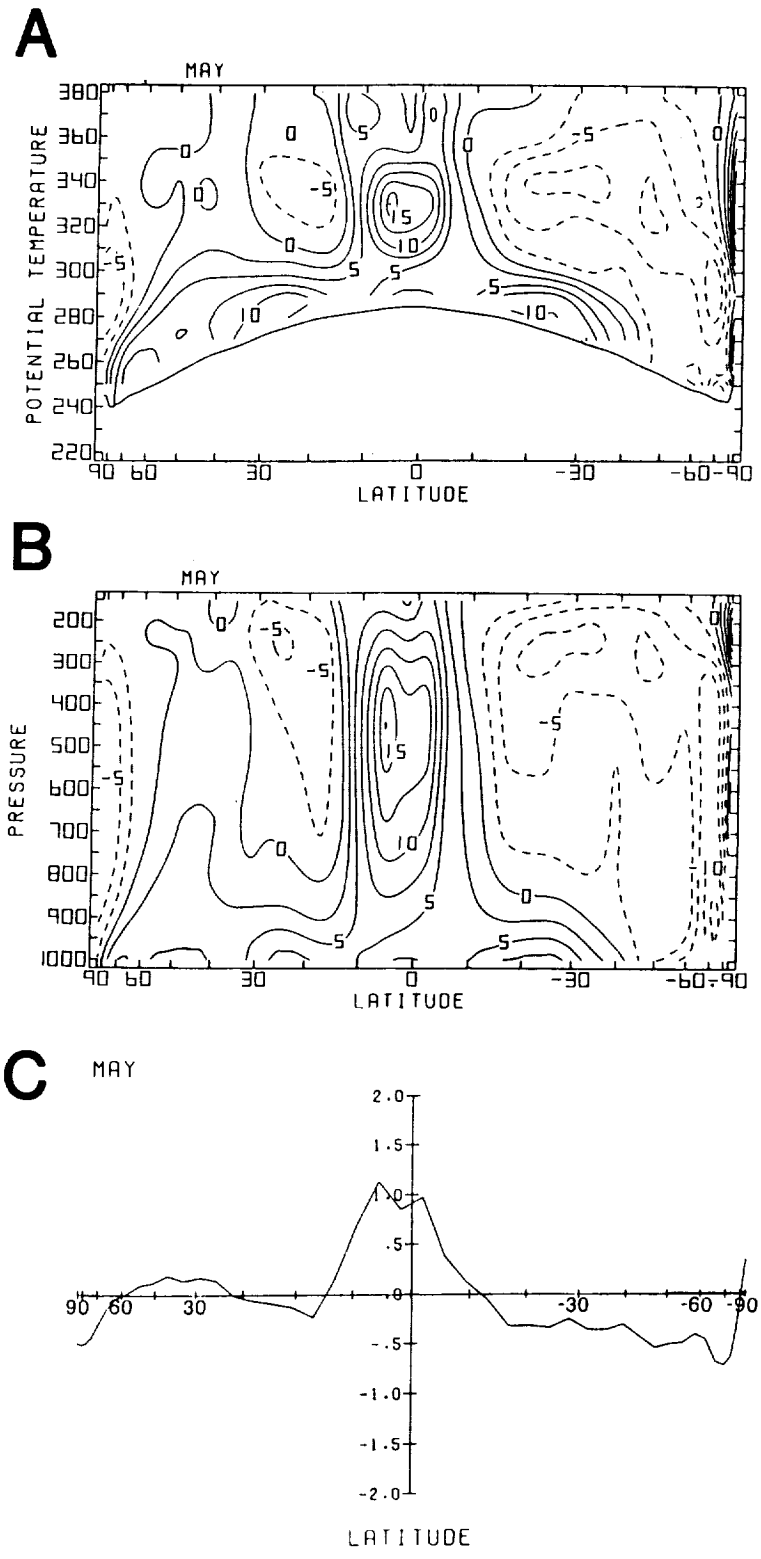

Fig. 64: Meridional cross sections of monthly (A) isentropically and (B) isobarically zonally averaged heating (10^{-1} K day^{-1}), and (C) meridional profile of zonally-vertically averaged heating for May 1979 (K day^{-1}). Contour interval in (A) and (B) is 0.25 K day^{-1}.

May

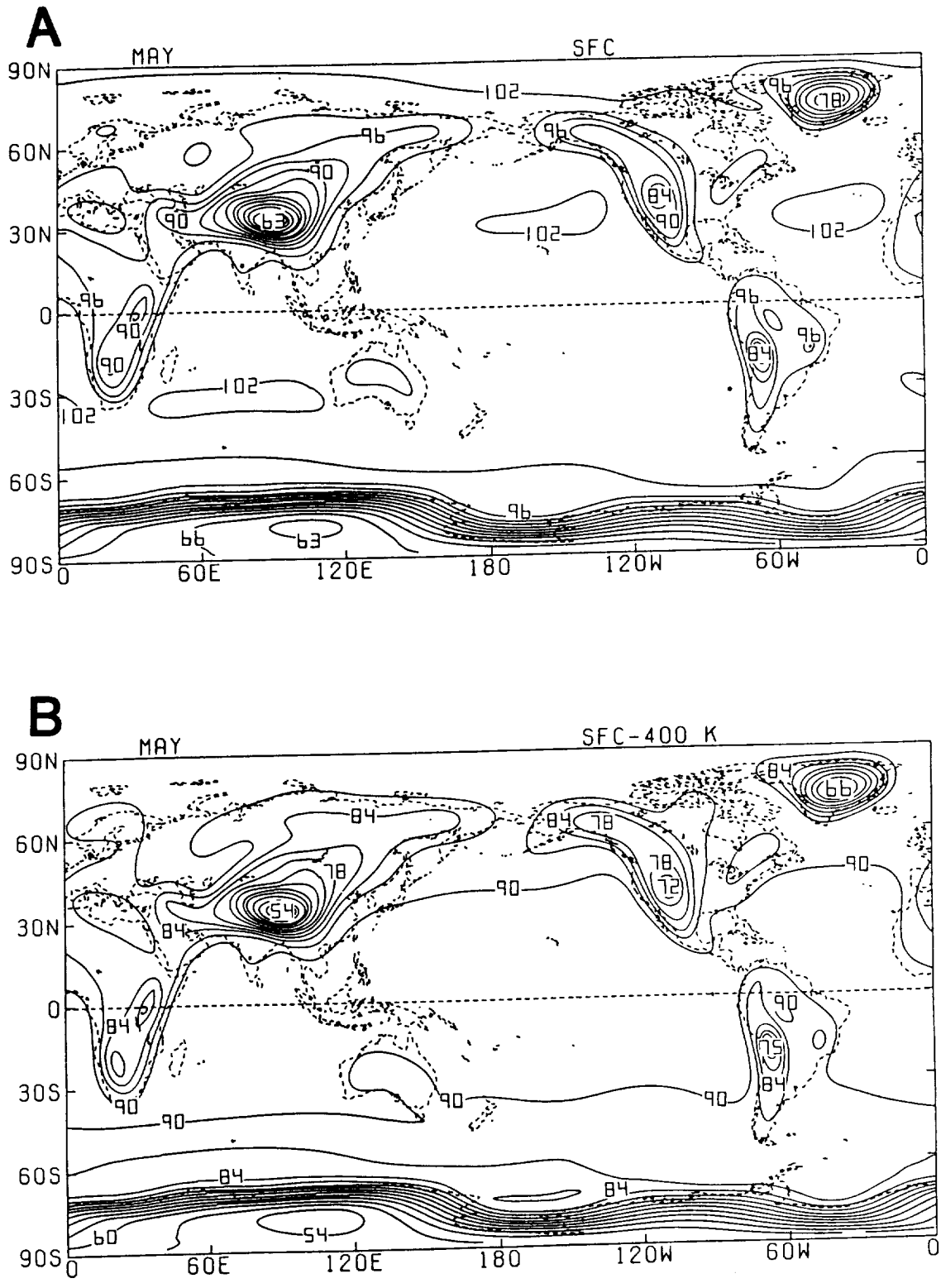

Fig. 65: Global distributions of monthly averaged (A) surface pressure (10^1 mb) and (B) pressure difference (10^1 mb) between the surface and the 400 K isentropic level for May 1979. Contour interval is 30 mb.

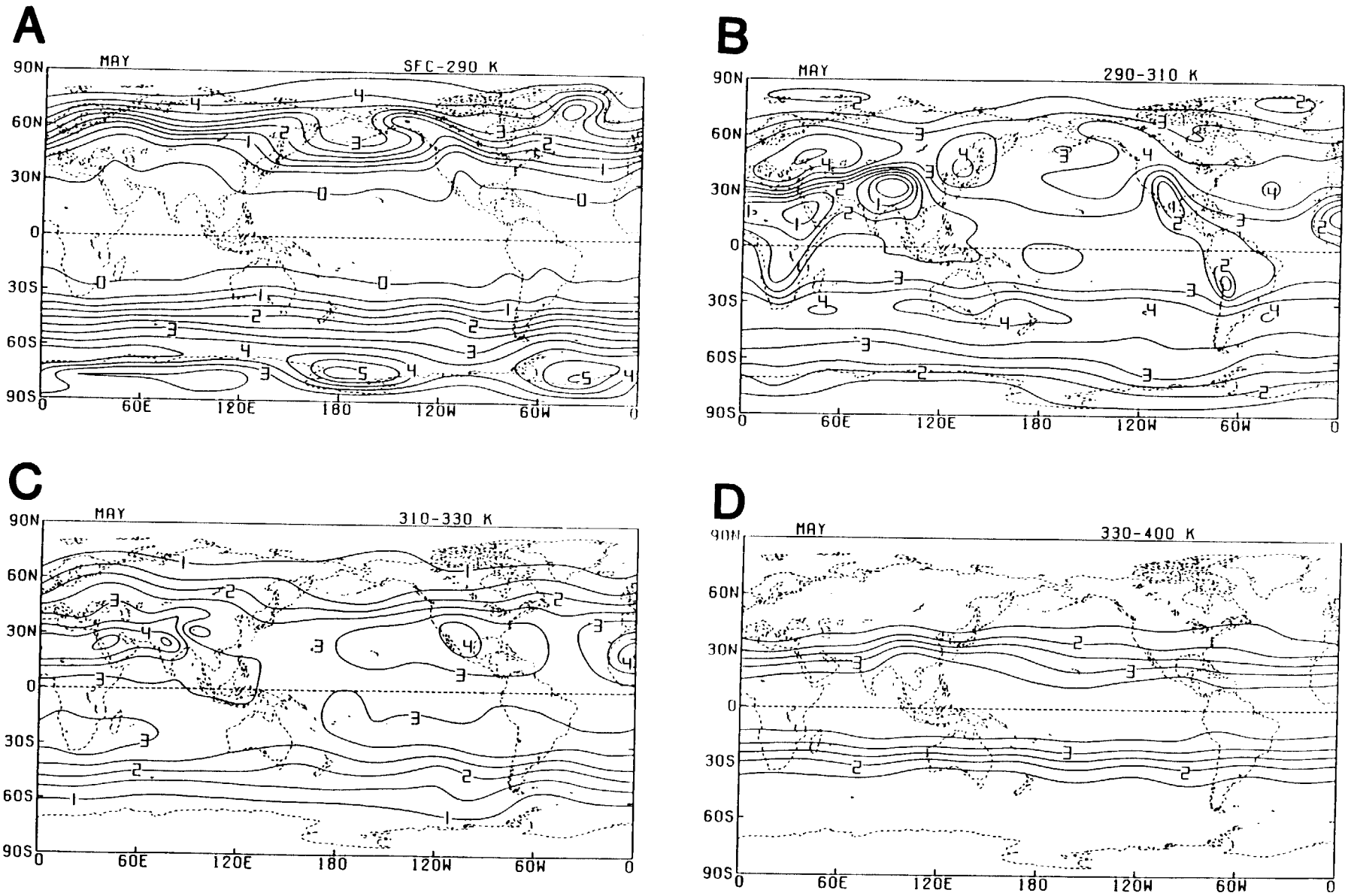

Fig. 66: Monthly averaged pressure difference (10^2 mb) between the upper and lower isentropic levels of the (A) surface-290 K, (B) 290-310 K, (C) 310-330 K and (D) 330-400 K isentropic layers for May 1979. Contour interval is 50 mb.

June

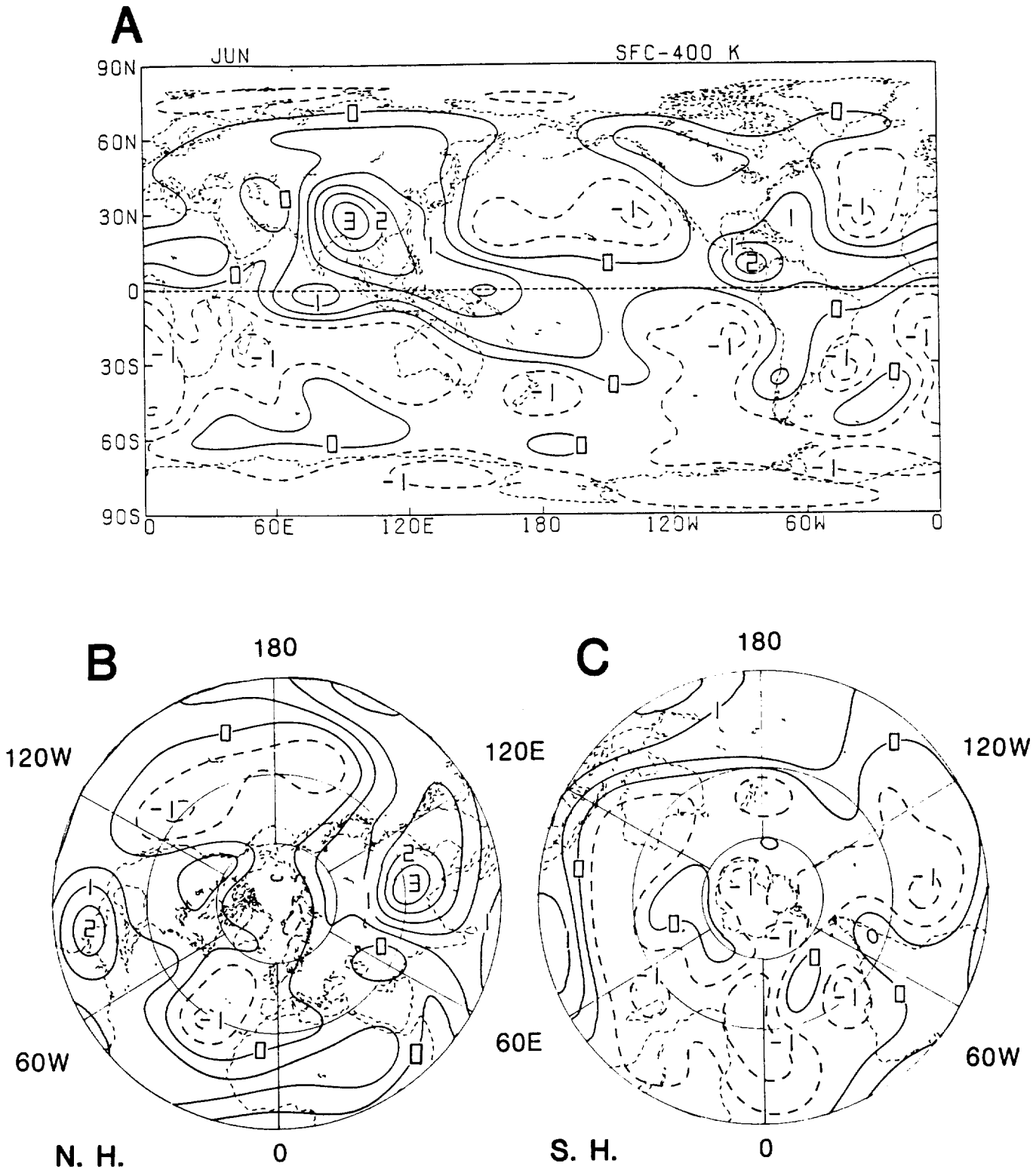

Fig. 67: Monthly vertical-averaged heating (K day^{-1}) for June 1979; (A) global, (B) Northern and (C) Southern Hemisphere. Contour interval is 0.5 K day^{-1}.

June

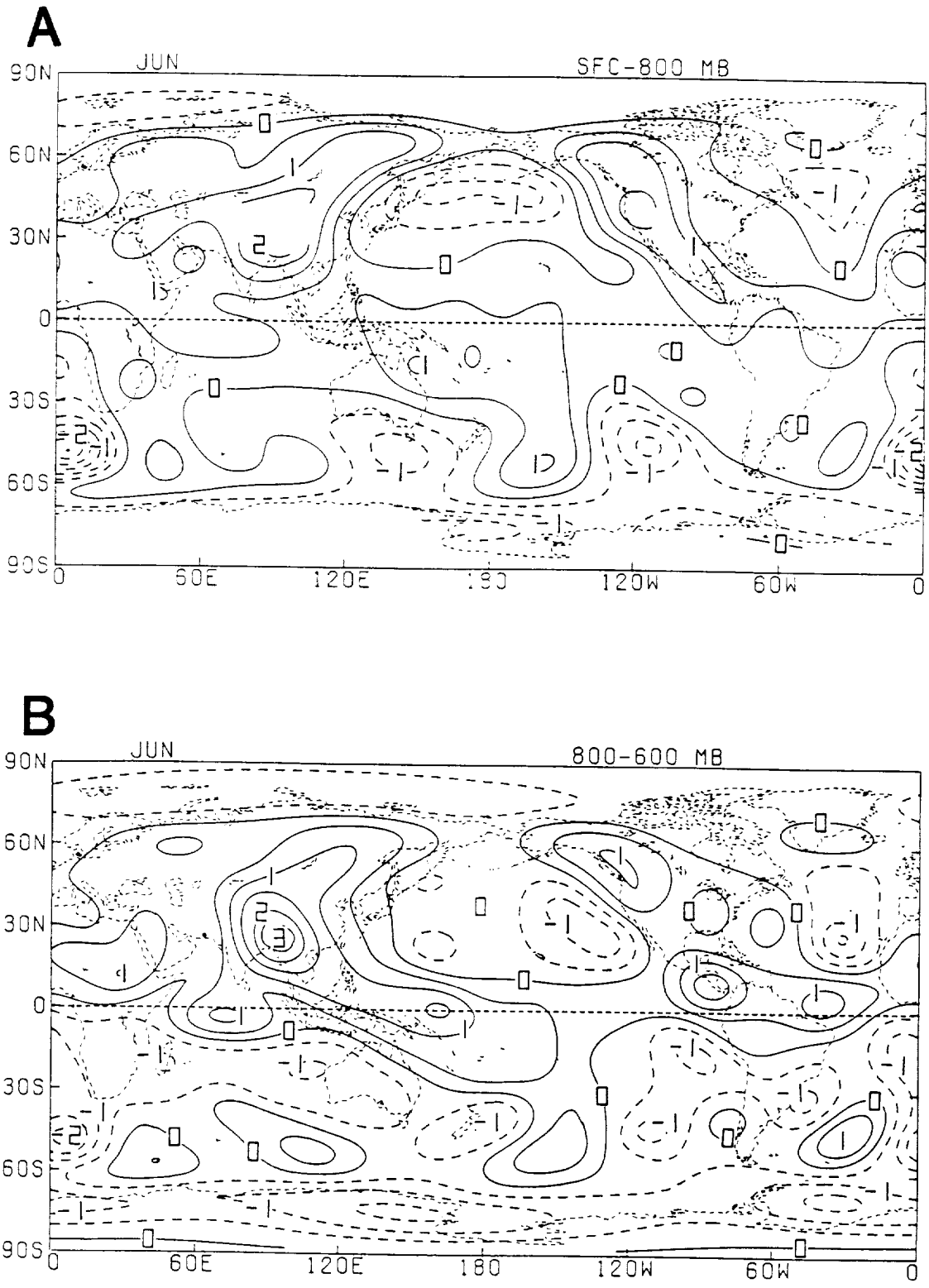

Fig. 68: Monthly layer-averaged heating (K day^{-1}) for the (A) surface-800 mb, (B) 800-600 mb, (C) 600-400 mb and (D) 400-200 mb isobaric layers for June 1979. Contour interval is 0.5 K day^{-1}.

June

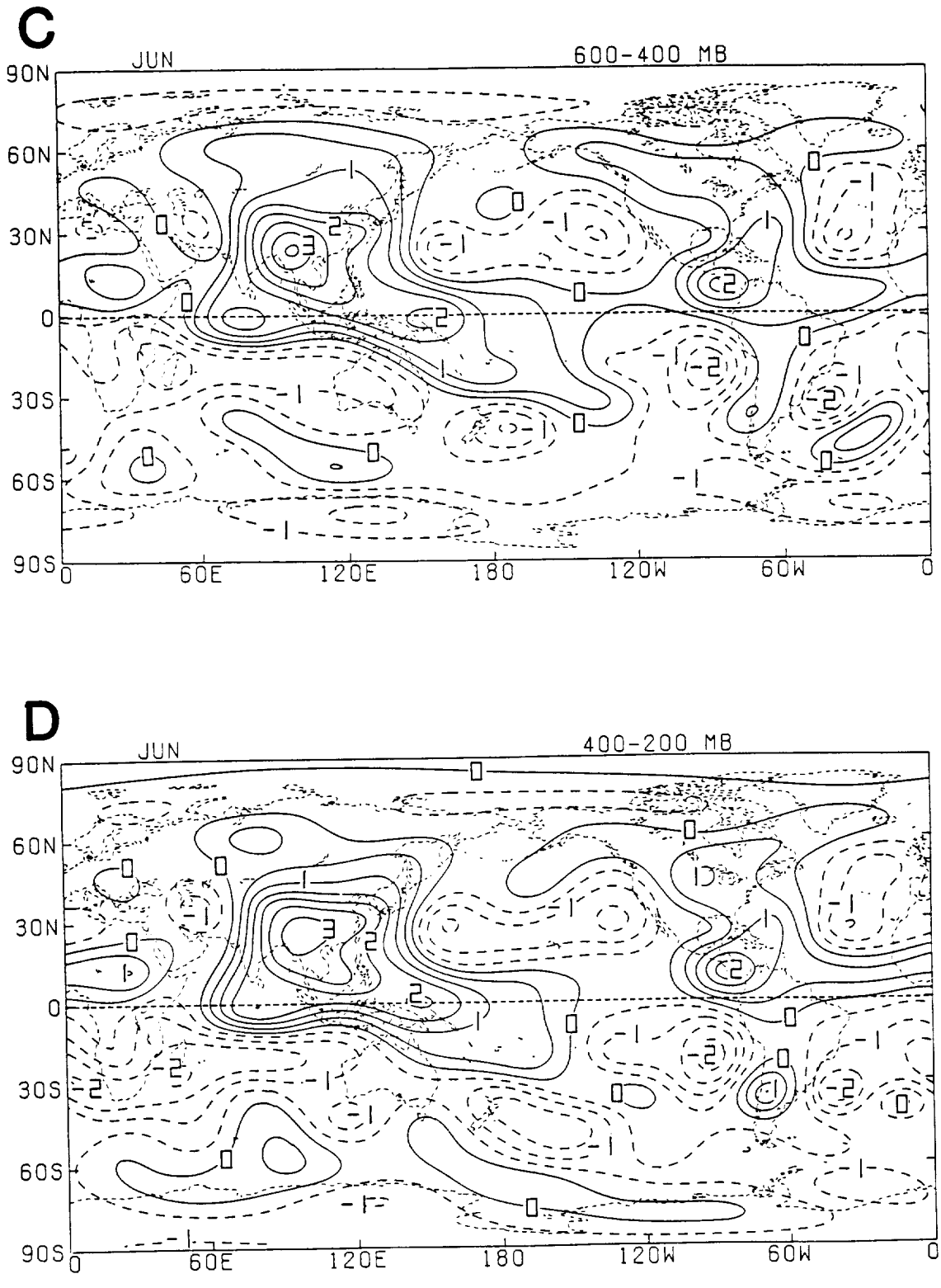

Fig. 68: (Continued).

June

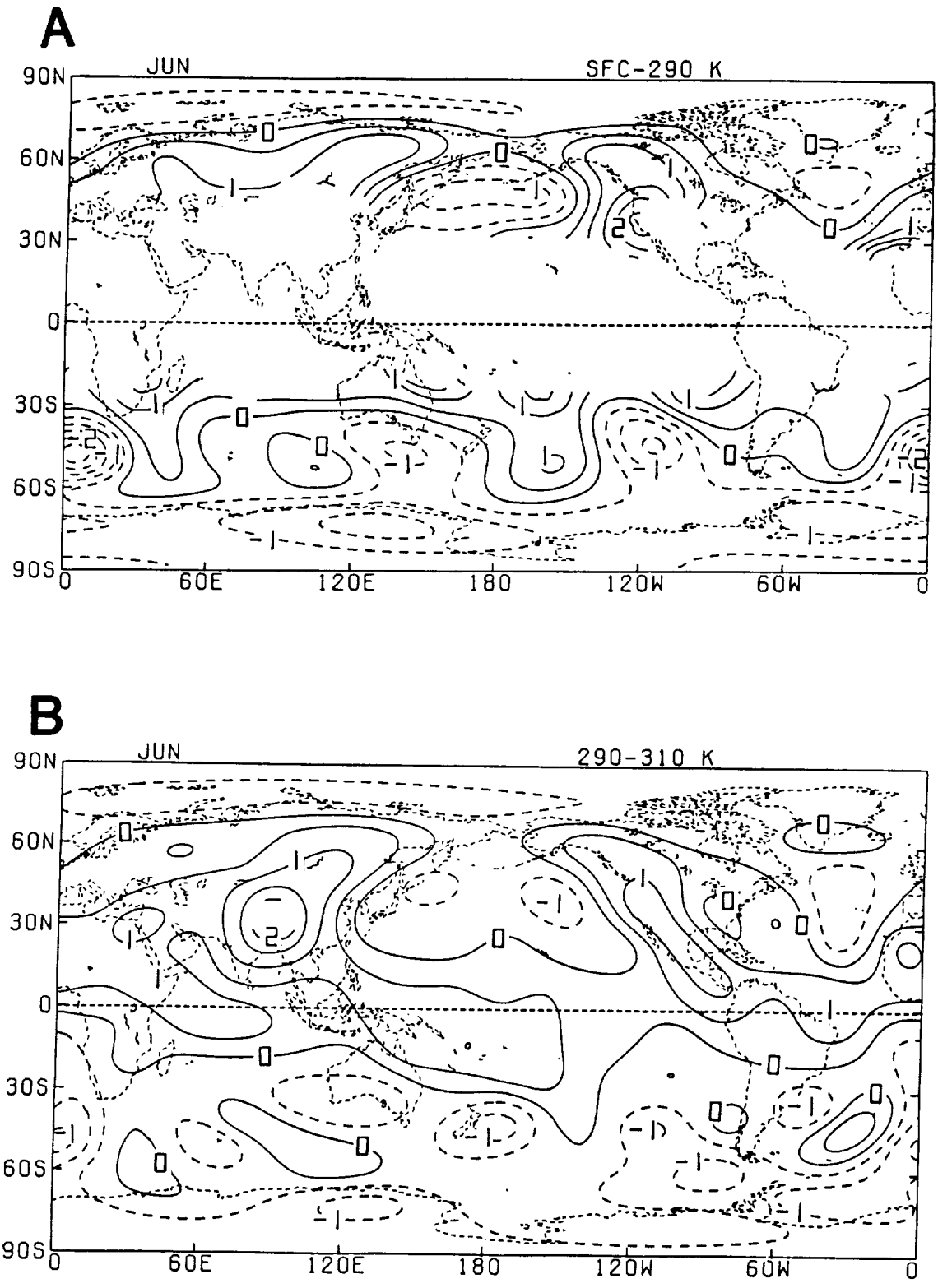

Fig. 69: Monthly layer-averaged heating (K day^{-1}) for the (A) surface-290 K, (B) 290-310 K, (C) 310-330 K and (D) 330-400 K isentropic layers for June 1979. Contour interval is 0.5 K day^{-1}.

June

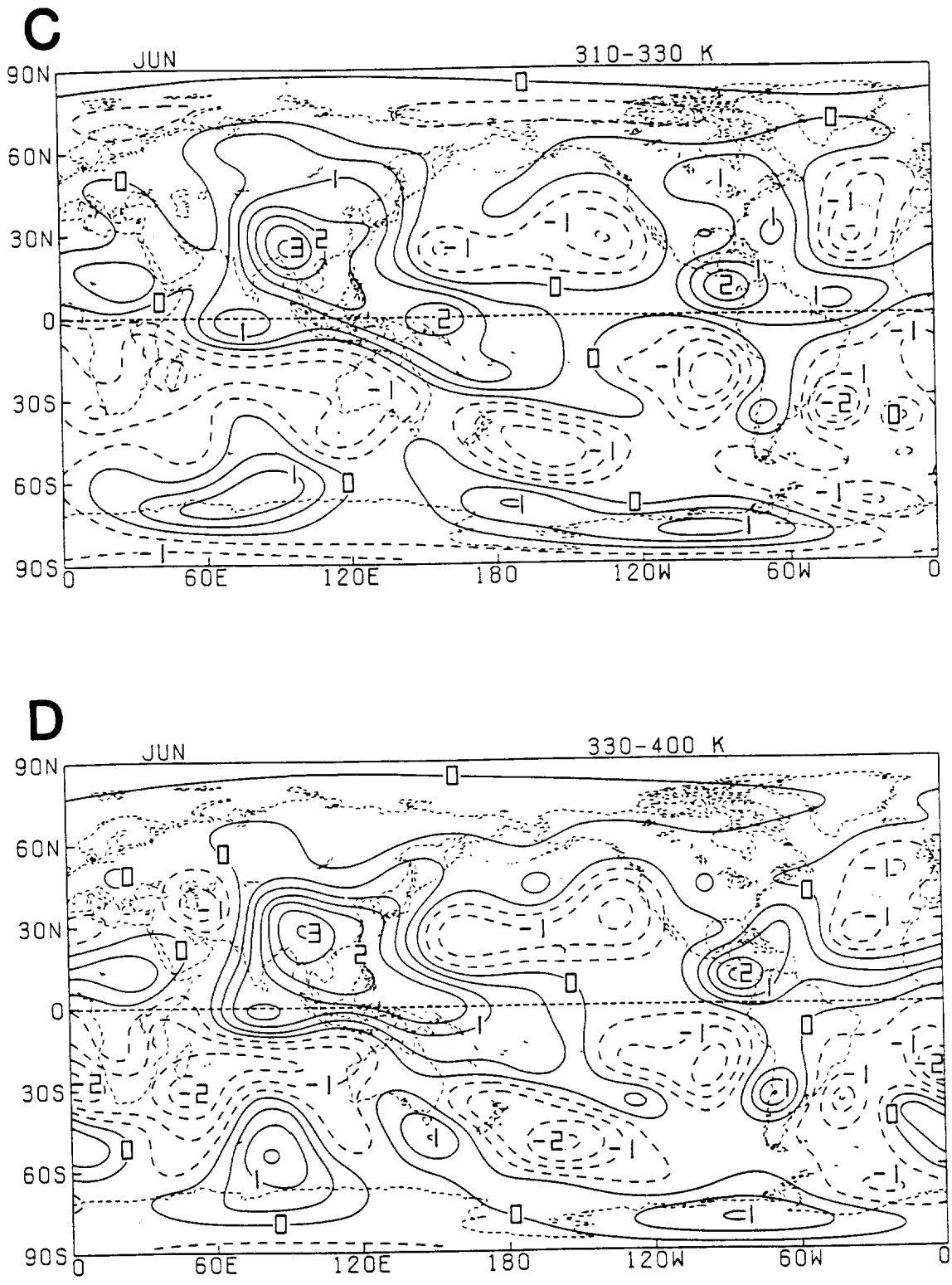

Fig. 69: (Continued).

June

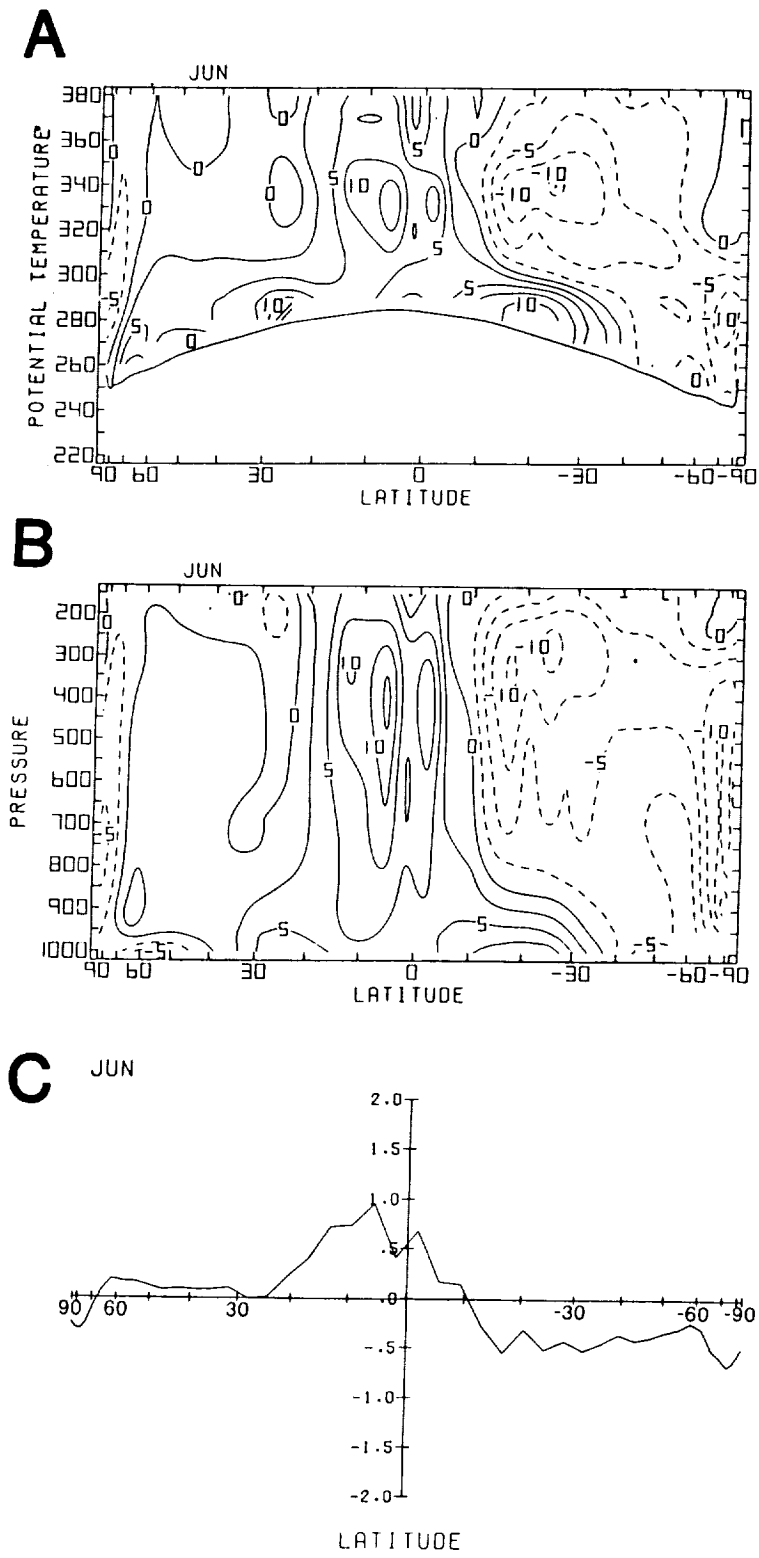

Fig. 70: Meridional cross sections of monthly (A) isentropically and (B) isobarically zonally averaged heating (10^{-1} K day^{-1}), and (C) meridional profile of zonally-vertically averaged heating for June 1979 (K day^{-1}). Contour interval in (A) and (B) is 0.25 K day^{-1}.

June

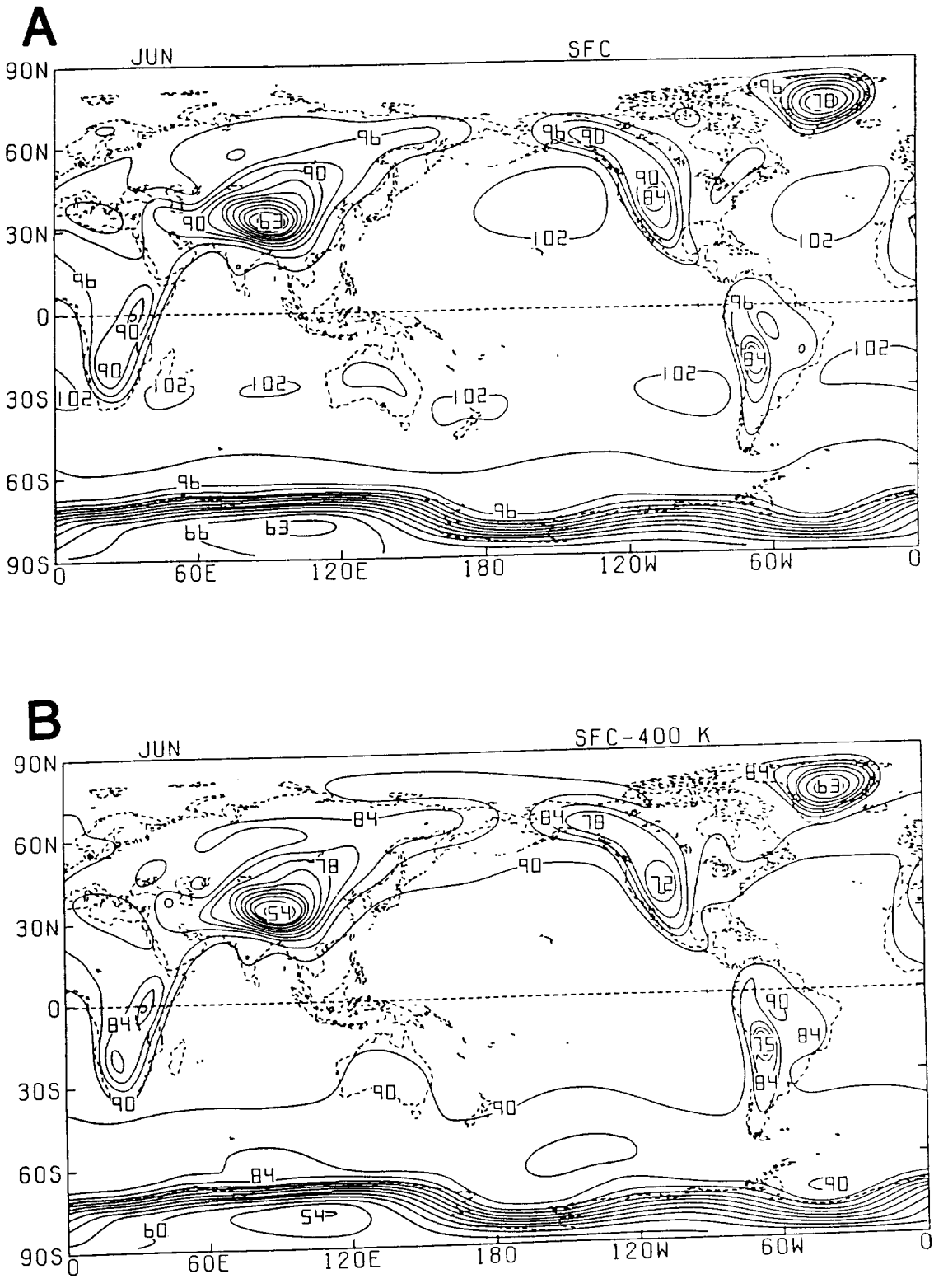

Fig. 71: Global distributions of monthly averaged (A) surface pressure (10^1 mb) and (B) pressure difference (10^1 mb) between the surface and the 400 K isentropic level for June 1979. Contour interval is 30 mb.

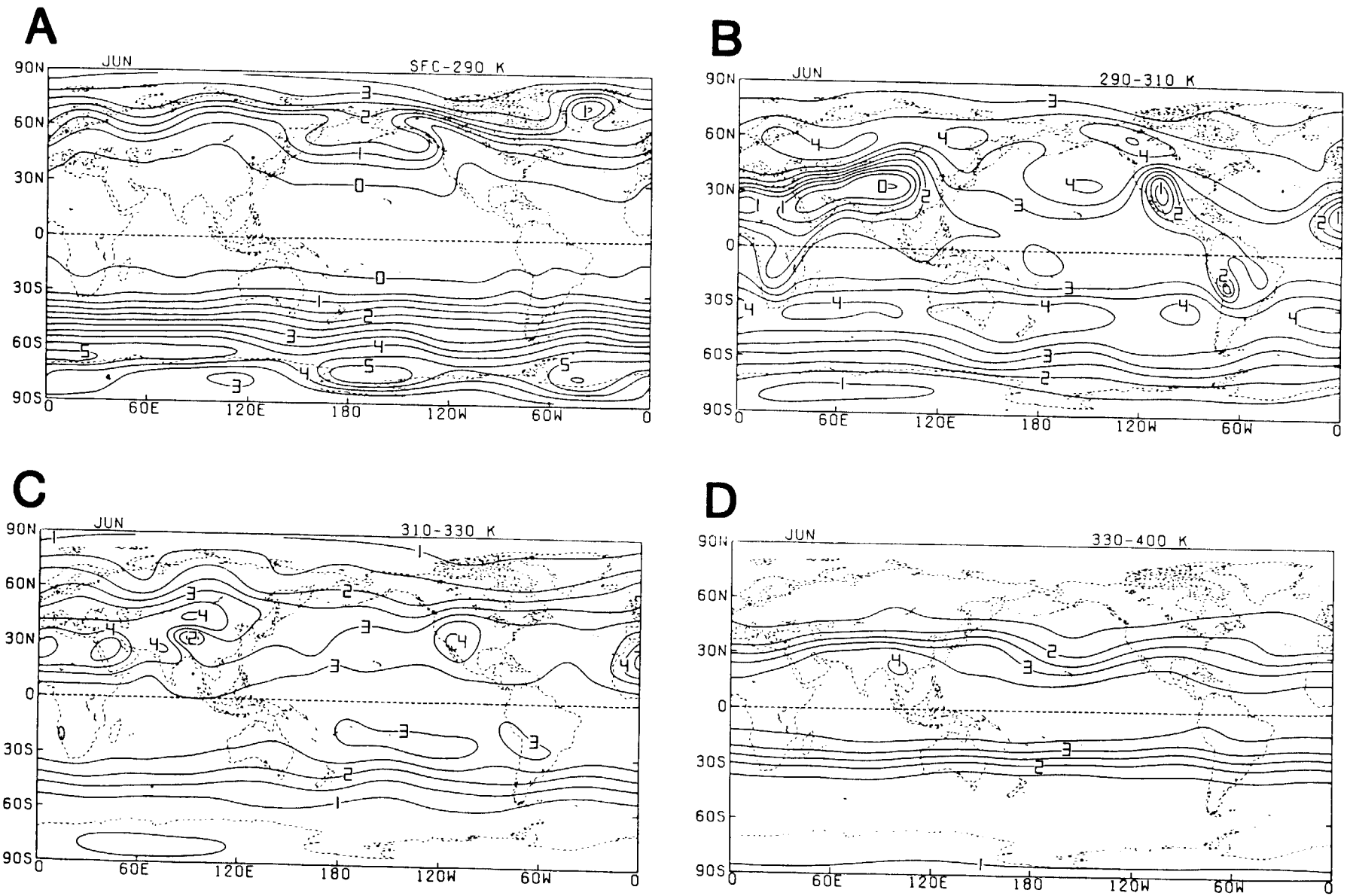

Fig. 72: Monthly averaged pressure difference (10^2 mb) between the upper and lower isentropic levels of the (A) surface-290 K, (B) 290-310 K, (C) 310-330 K and (D) 330-400 K isentropic layers for June 1979. Contour interval is 50 mb.

July

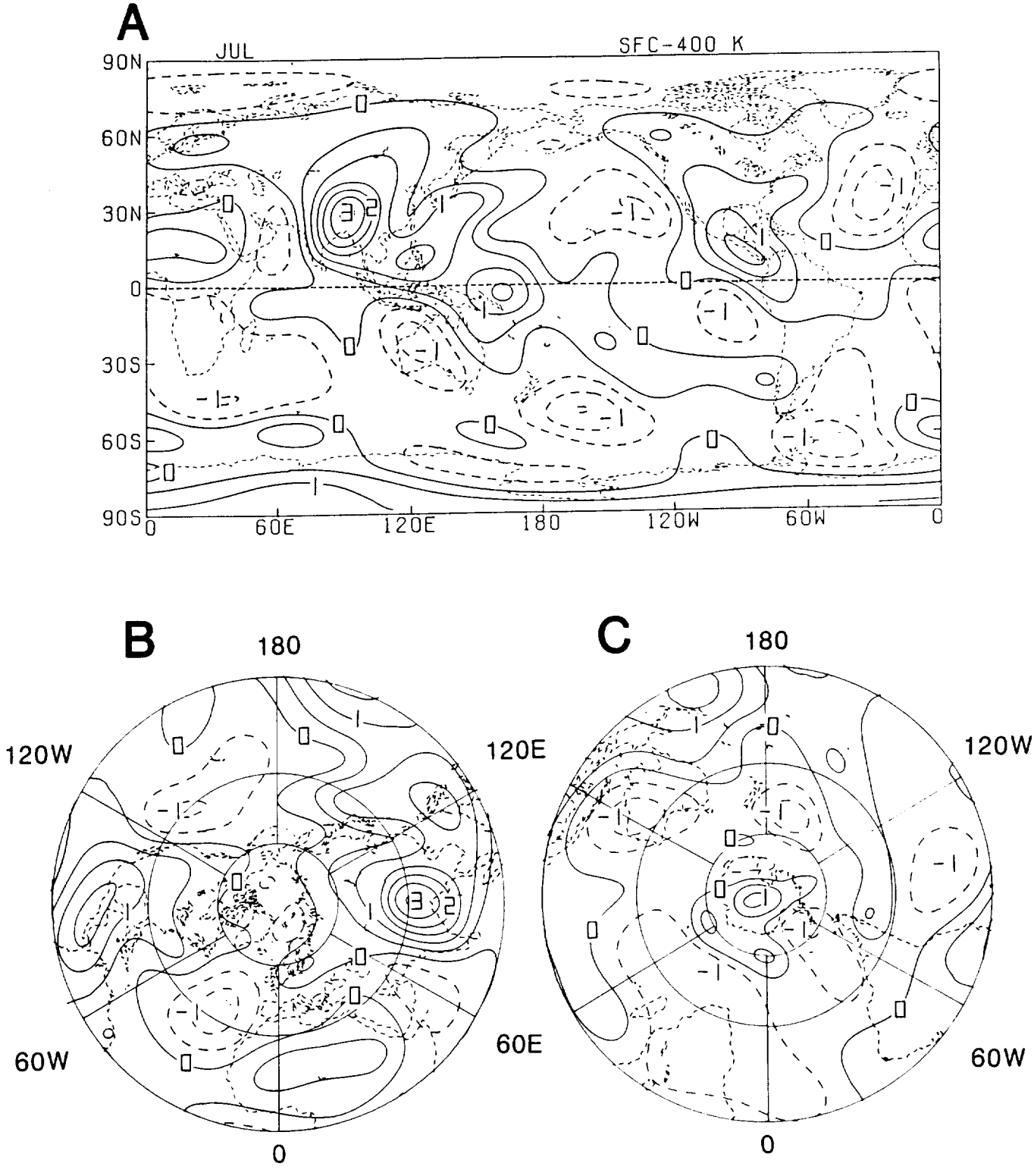

Fig. 73: Monthly vertical-averaged heating (K day^{-1}) for July 1979; (A) global, (B) Northern and (C) Southern Hemisphere. Contour interval is 0.5 K day^{-1}.

July

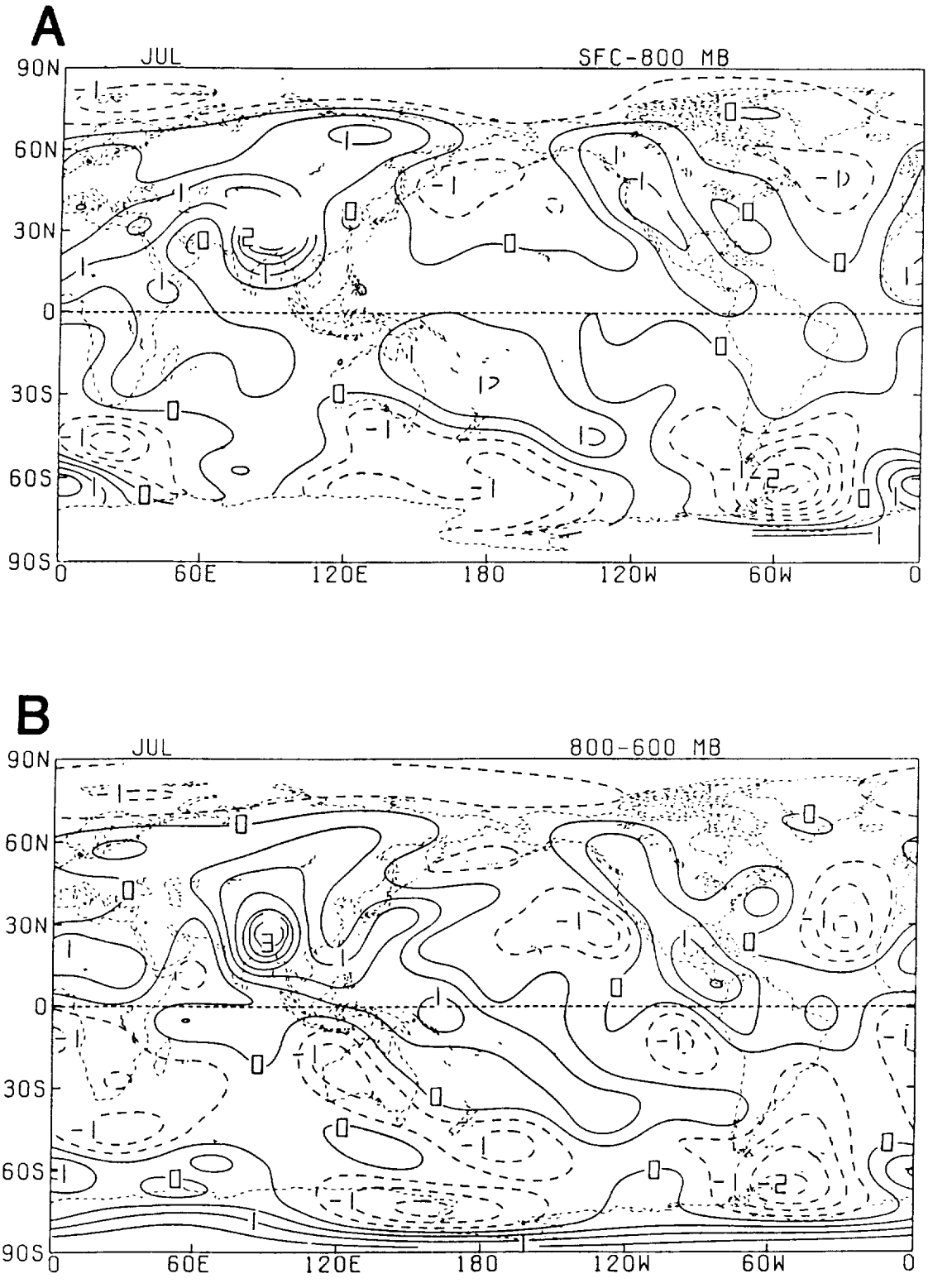

Fig. 74: Monthly layer-averaged heating (K day^{-1}) for the (A) surface-800 mb, (B) 800-600 mb, (C) 600-400 mb and (D) 400-200 mb isobaric layers for July 1979. Contour interval is 0.5 K day^{-1}.

July

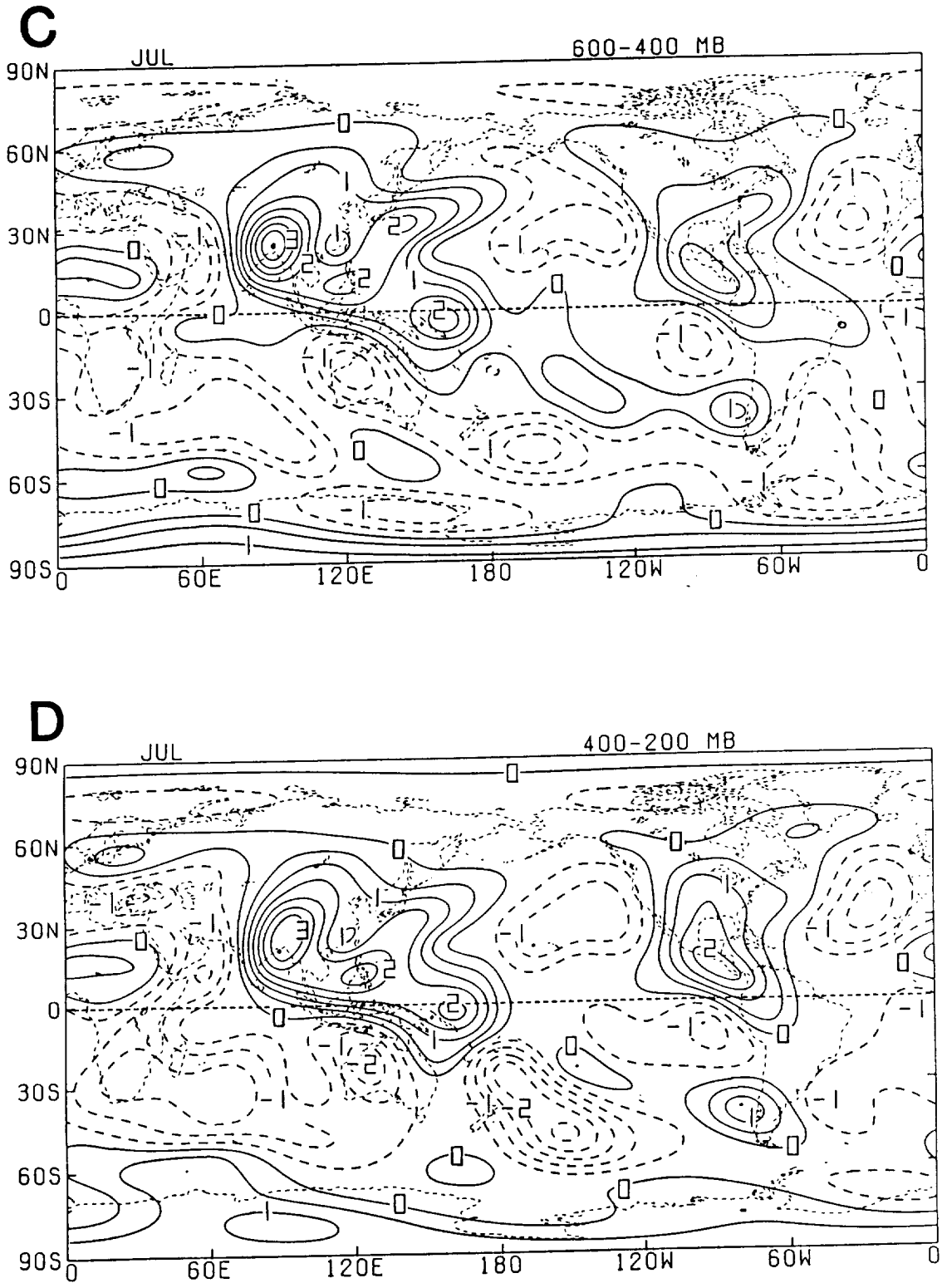

Fig. 74: (Continued).

July

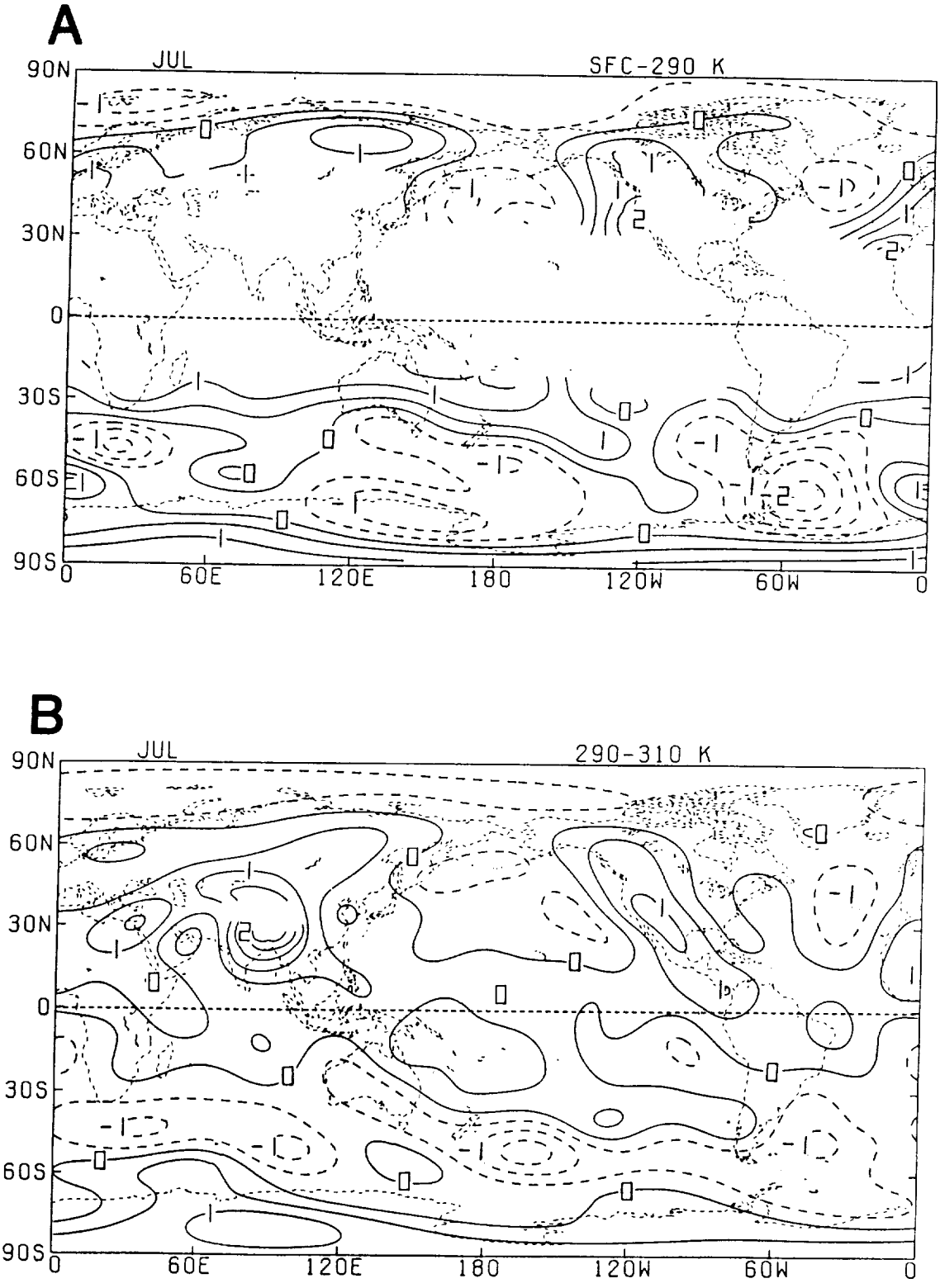

Fig. 75: Monthly layer-averaged heating (K day^{-1}) for the (A) surface-290 K, (B) 290-310 K, (C) 310-330 K and (D) 330-400 K isentropic layers for July 1979. Contour interval is 0.5 K day^{-1}.

July

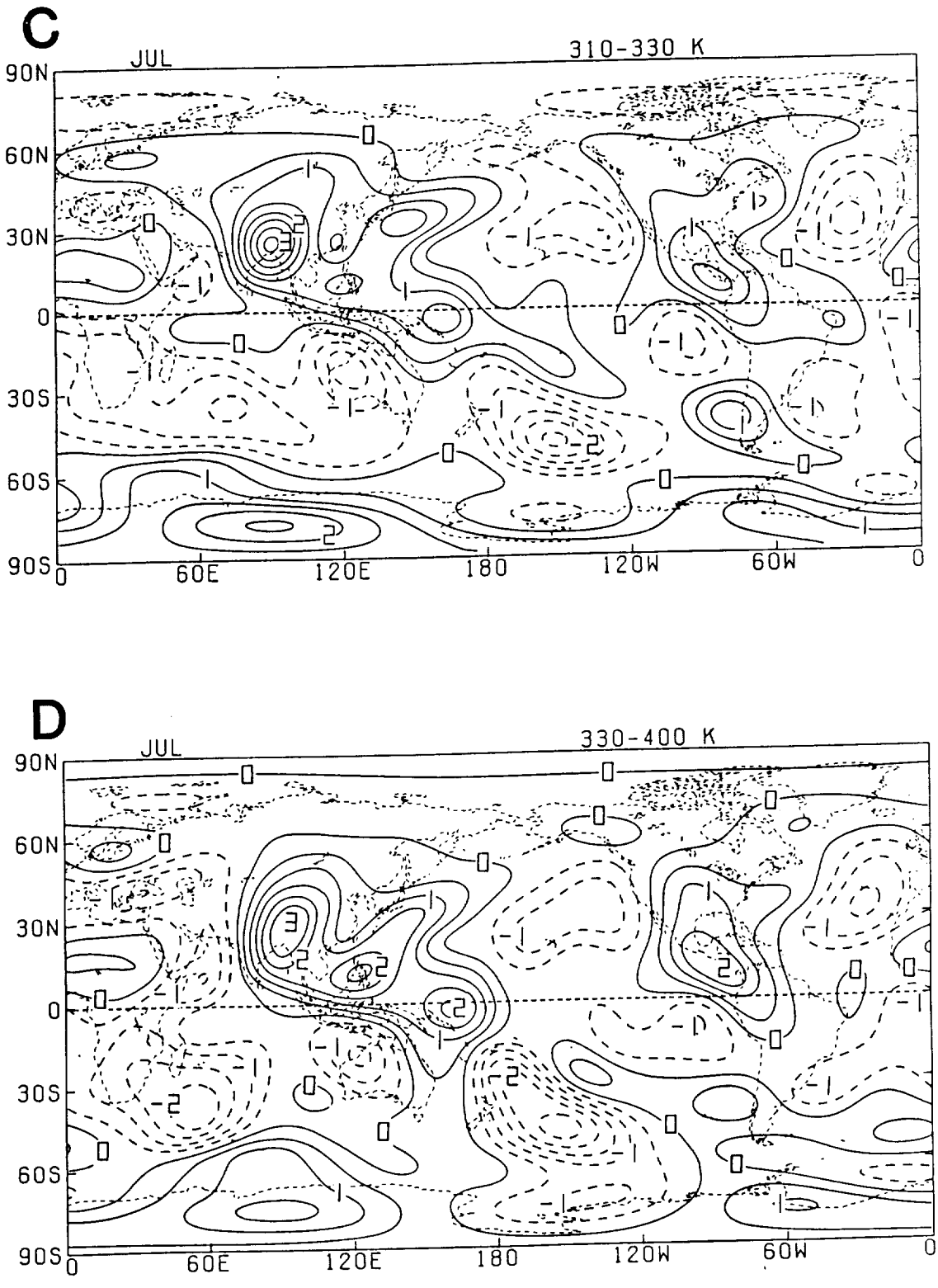

Fig. 75: (Continued).

July

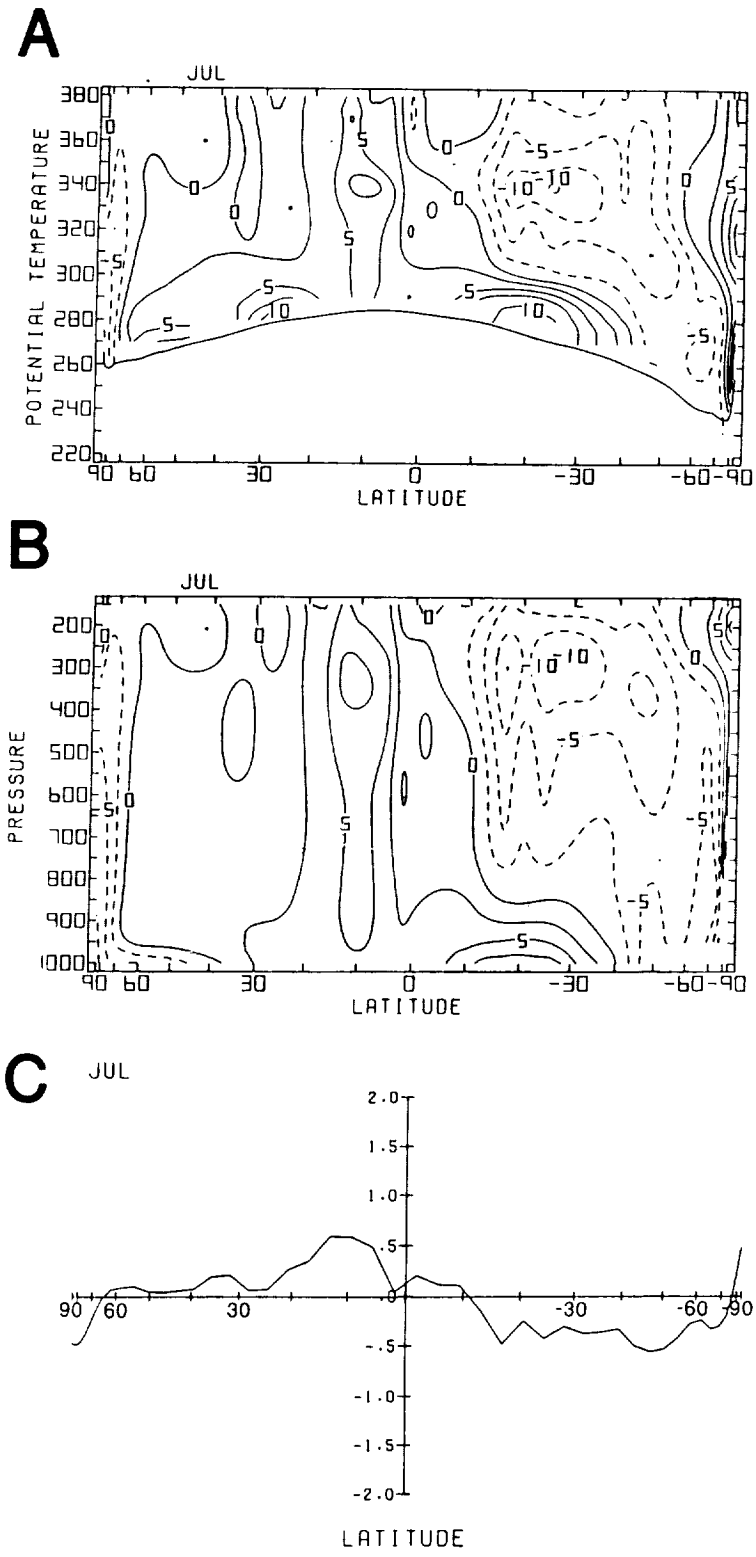

Fig. 76: Meridional cross sections of monthly (A) isentropically and (B) isobarically zonally averaged heating (10^{-1} K day^{-1}), and (C) meridional profile of zonally-vertically averaged heating for July 1979 (K day^{-1}). Contour interval in (A) and (B) is 0.25 K day^{-1}.

July

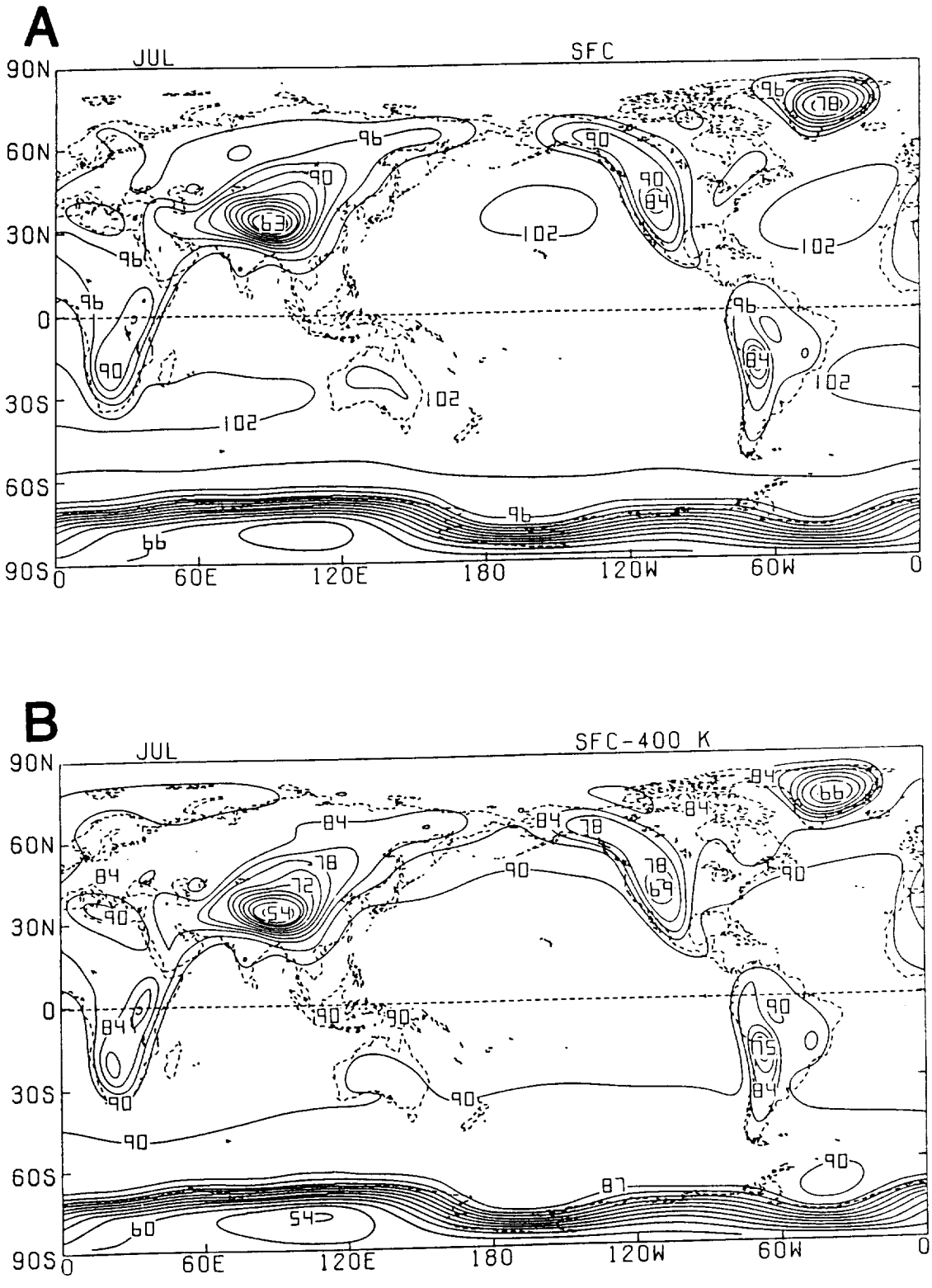

Fig. 77: Global distributions of monthly averaged (A) surface pressure (10^1 mb) and (B) pressure difference (10^1 mb) between the surface and the 400 K isentropic level for July 1979. Contour interval is 30 mb.

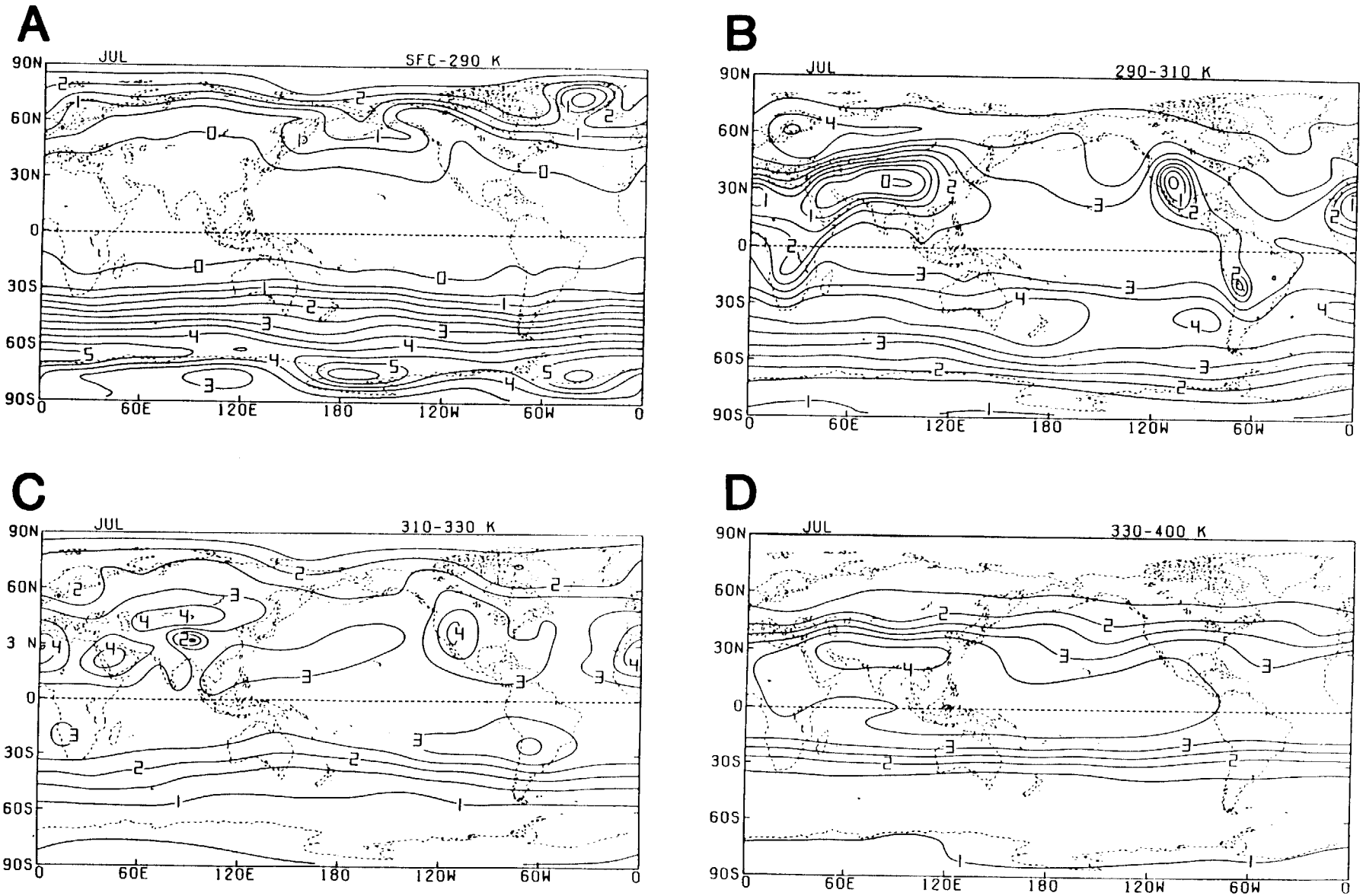

Fig. 78: Monthly averaged pressure difference (10^2 mb) between the upper and lower isentropic levels of the (A) surface-290 K, (B) 290-310 K, (C) 310-330 K and (D) 330-400 K isentropic layers for July 1979. Contour interval is 50 mb.

August

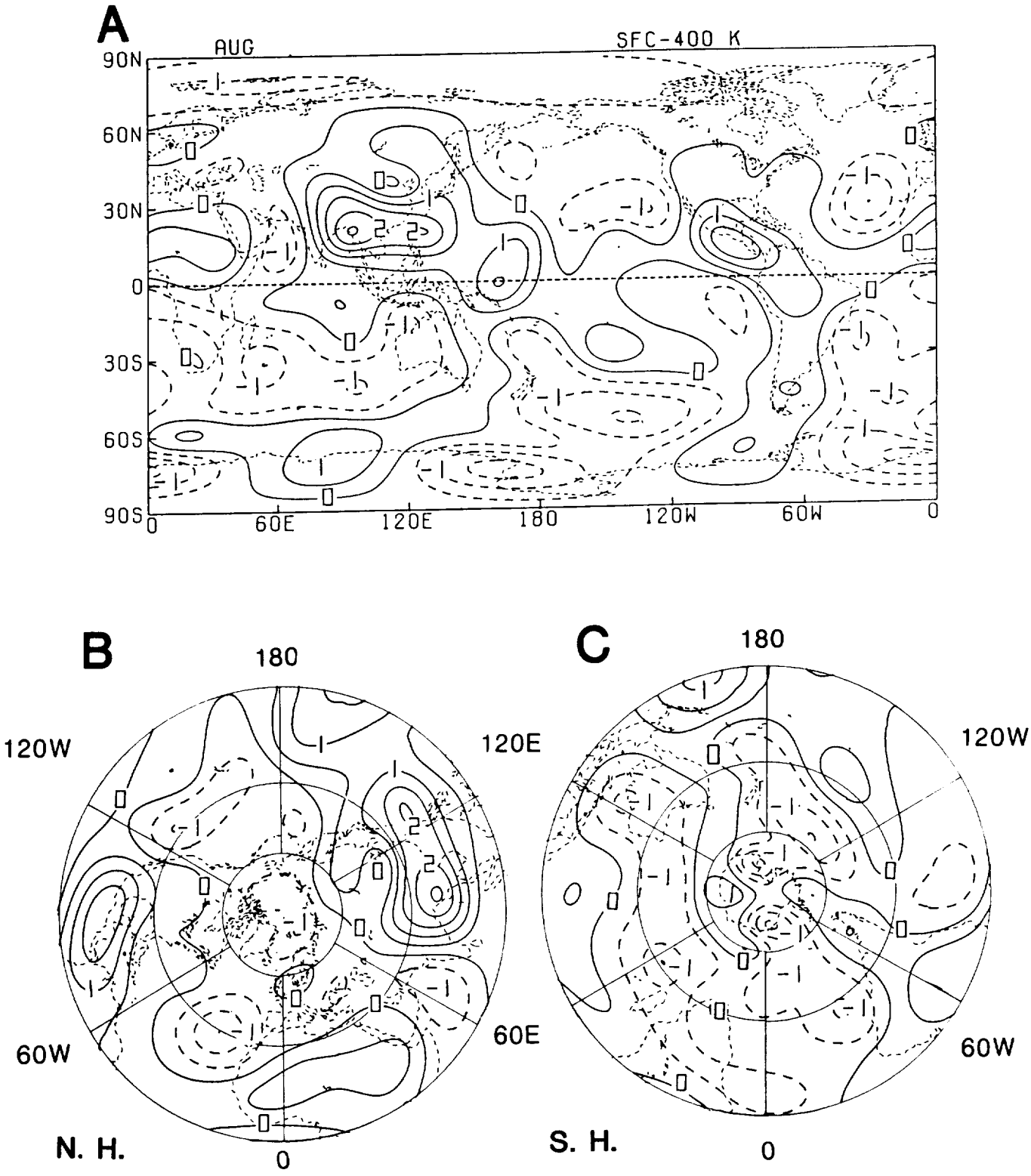

Fig. 79: Monthly vertical-averaged heating (K day^{-1}) for August 1979; (A) global, (B) Northern and (C) Southern Hemisphere. Contour interval is 0.5 K day^{-1}.

August

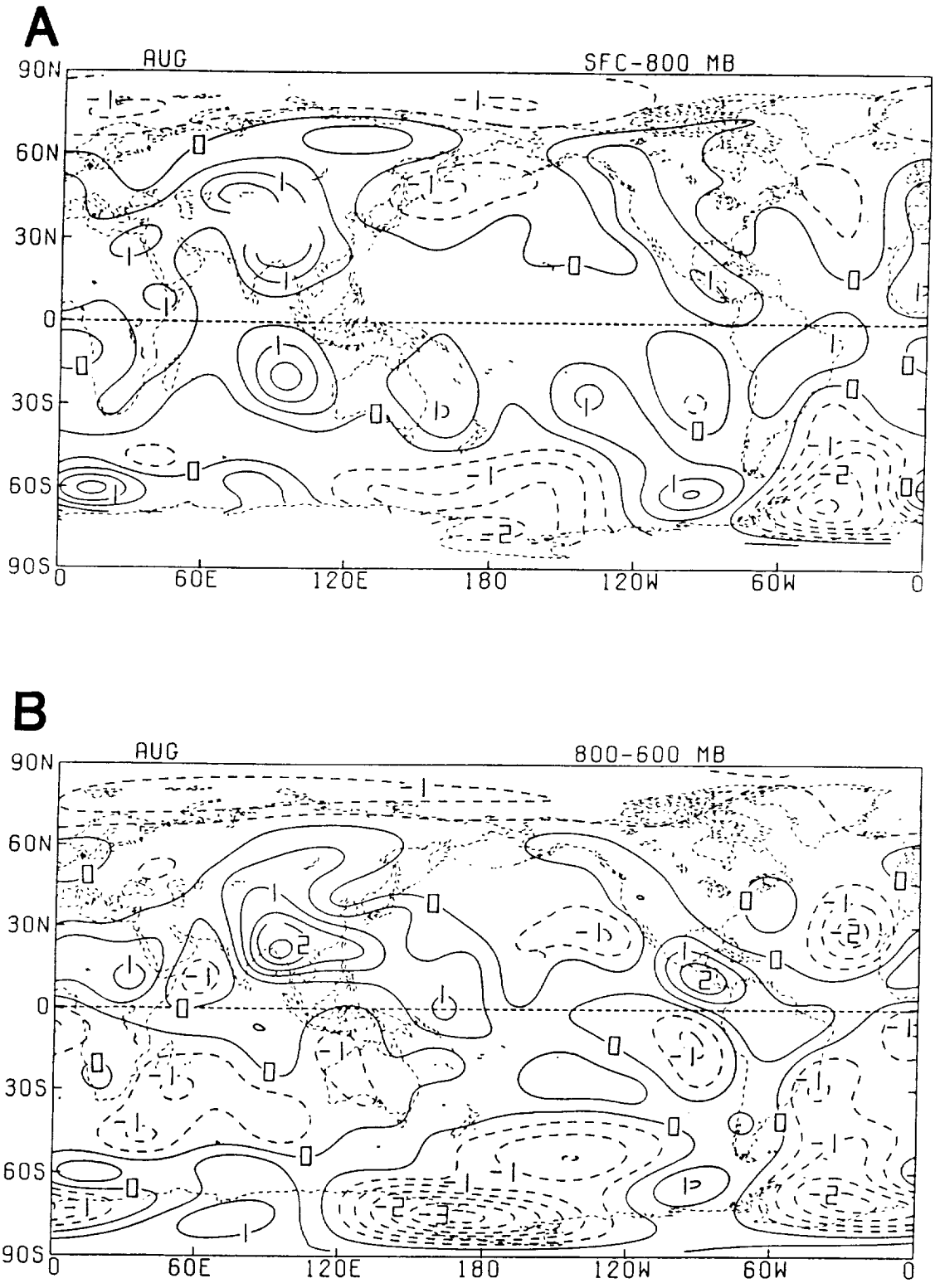

Fig. 80: Monthly layer-averaged heating (K day^{-1}) for the (A) surface-800 mb, (B) 800-600 mb, (C) 600-400 mb and (D) 400-200 mb isobaric layers for August 1979. Contour interval is 0.5 K day^{-1}.

August

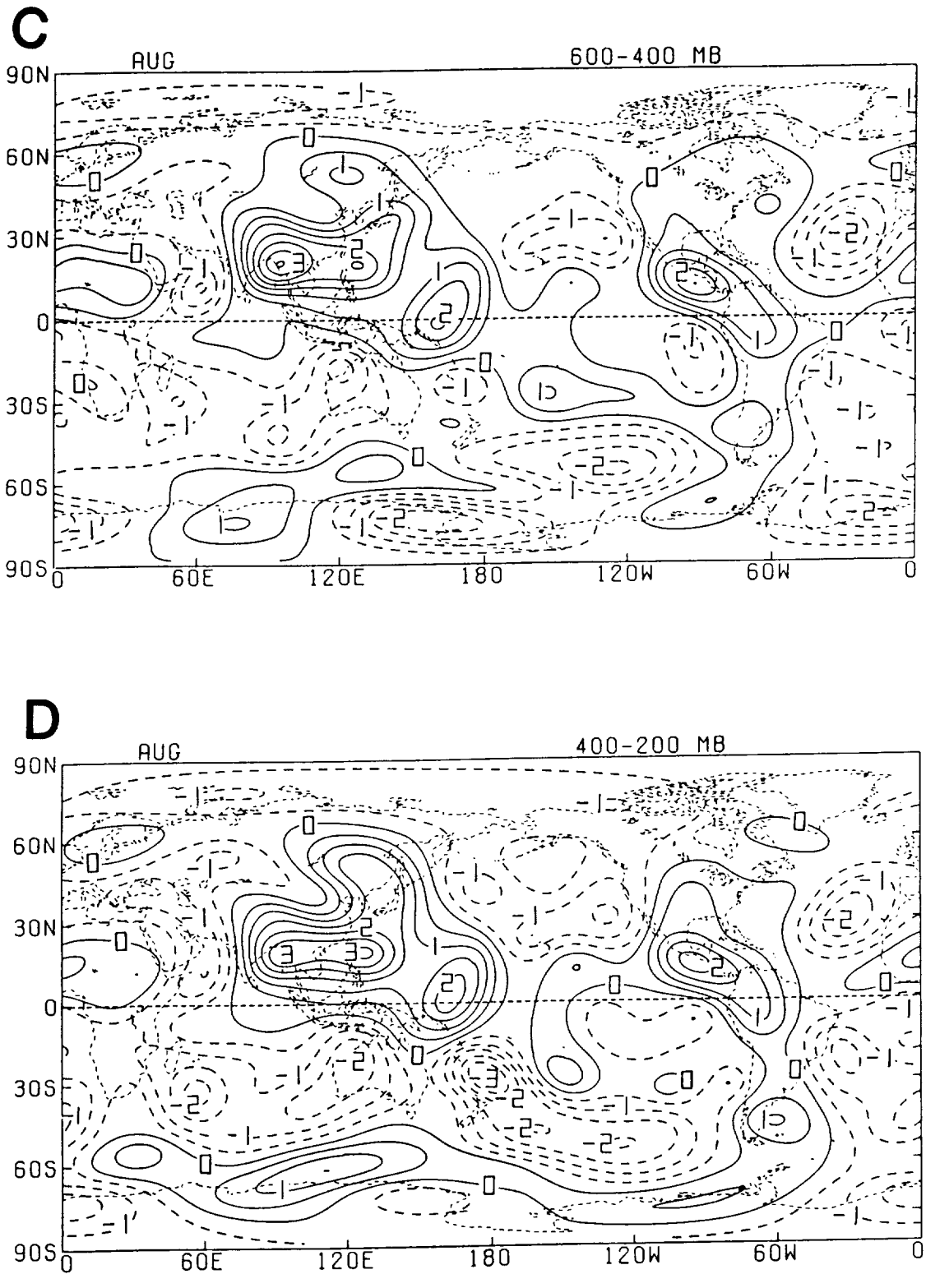

Fig. 80: (Continued).

August

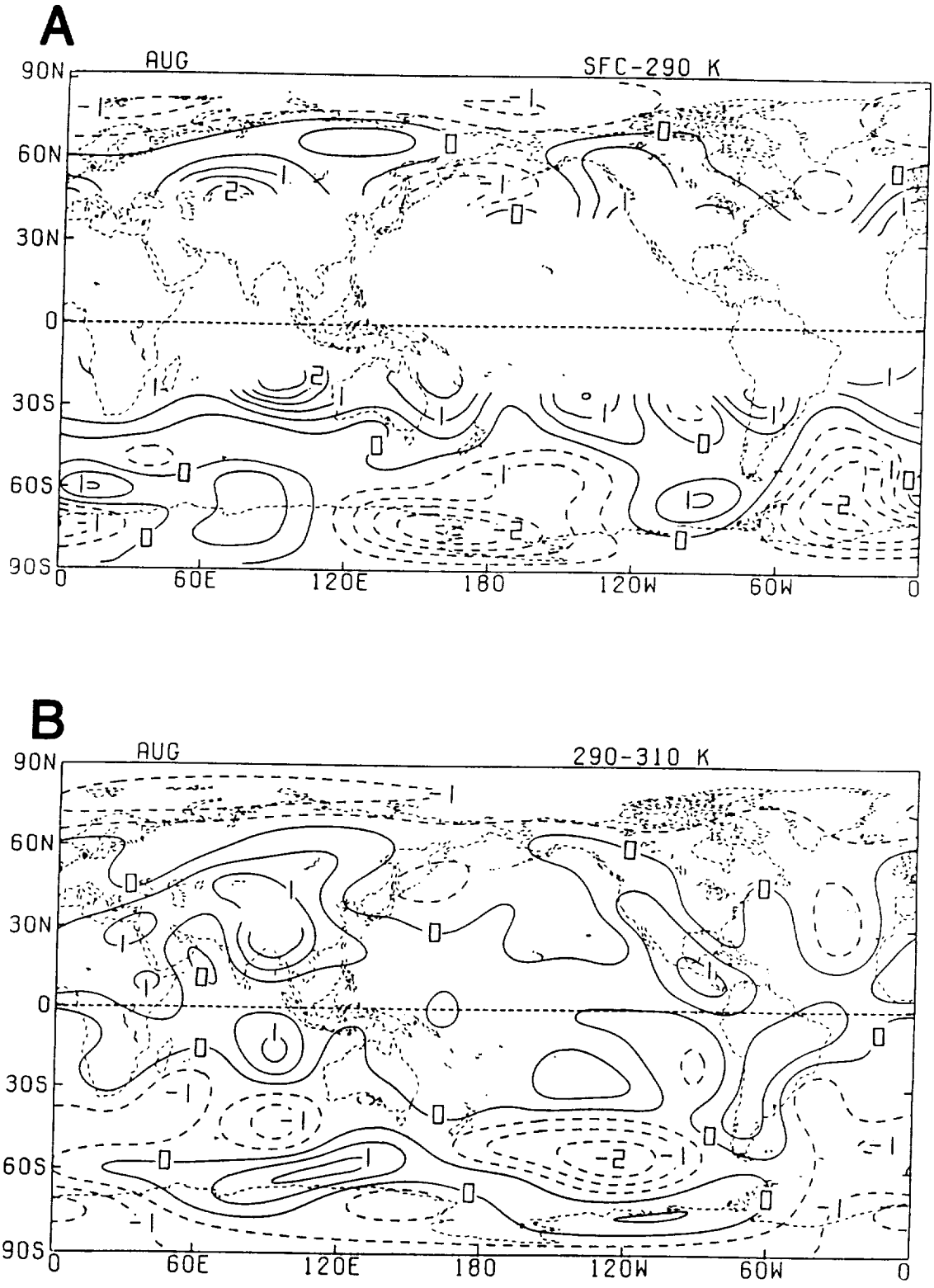

Fig. 81: Monthly layer-averaged heating (K day^{-1}) for the (A) surface-290 K, (B) 290-310 K, (C) 310-330 K and (D) 330-400 K isentropic layers for August 1979. Contour interval is 0.5 K day^{-1}.

August

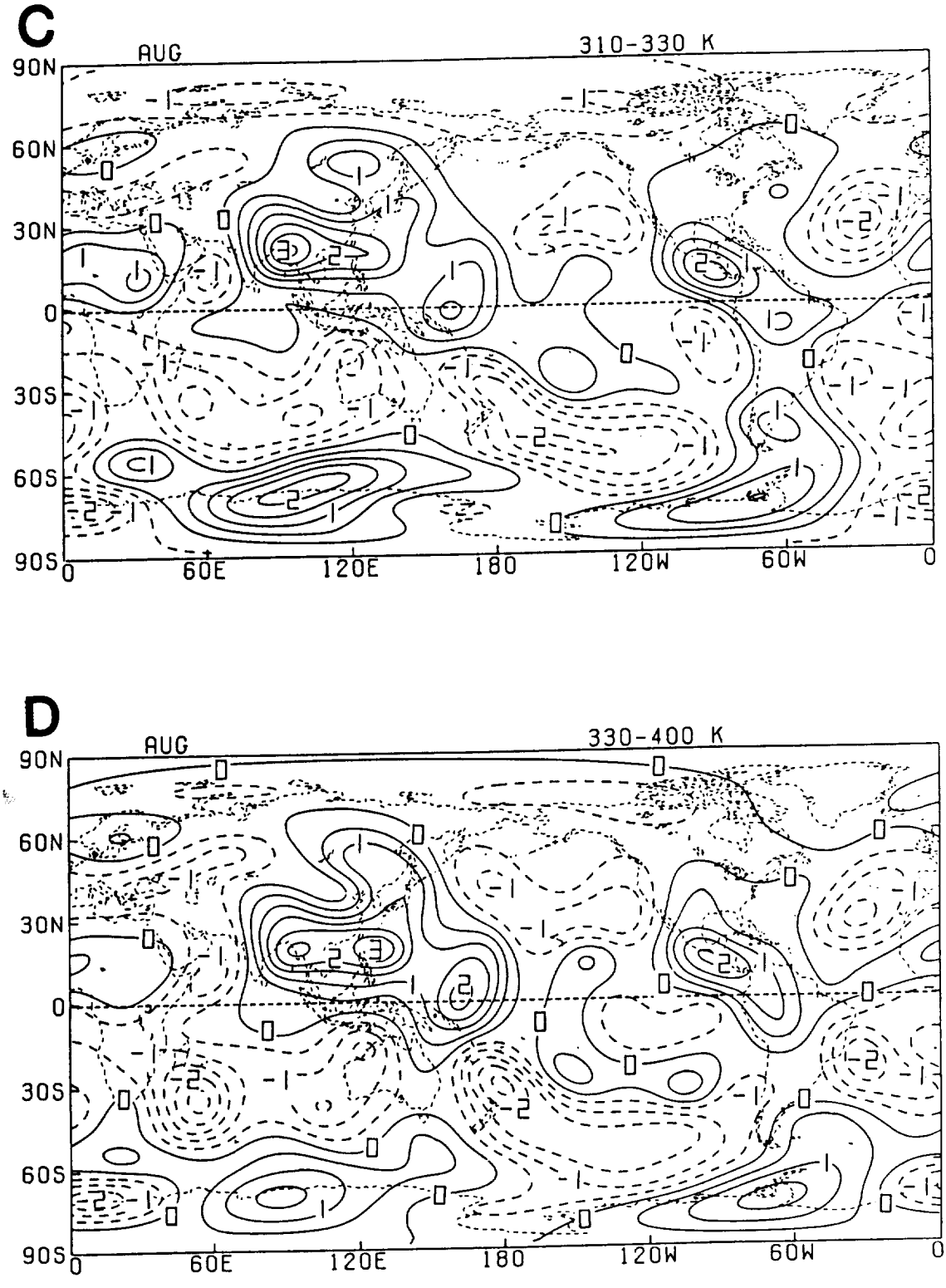

Fig. 81: (Continued).

August

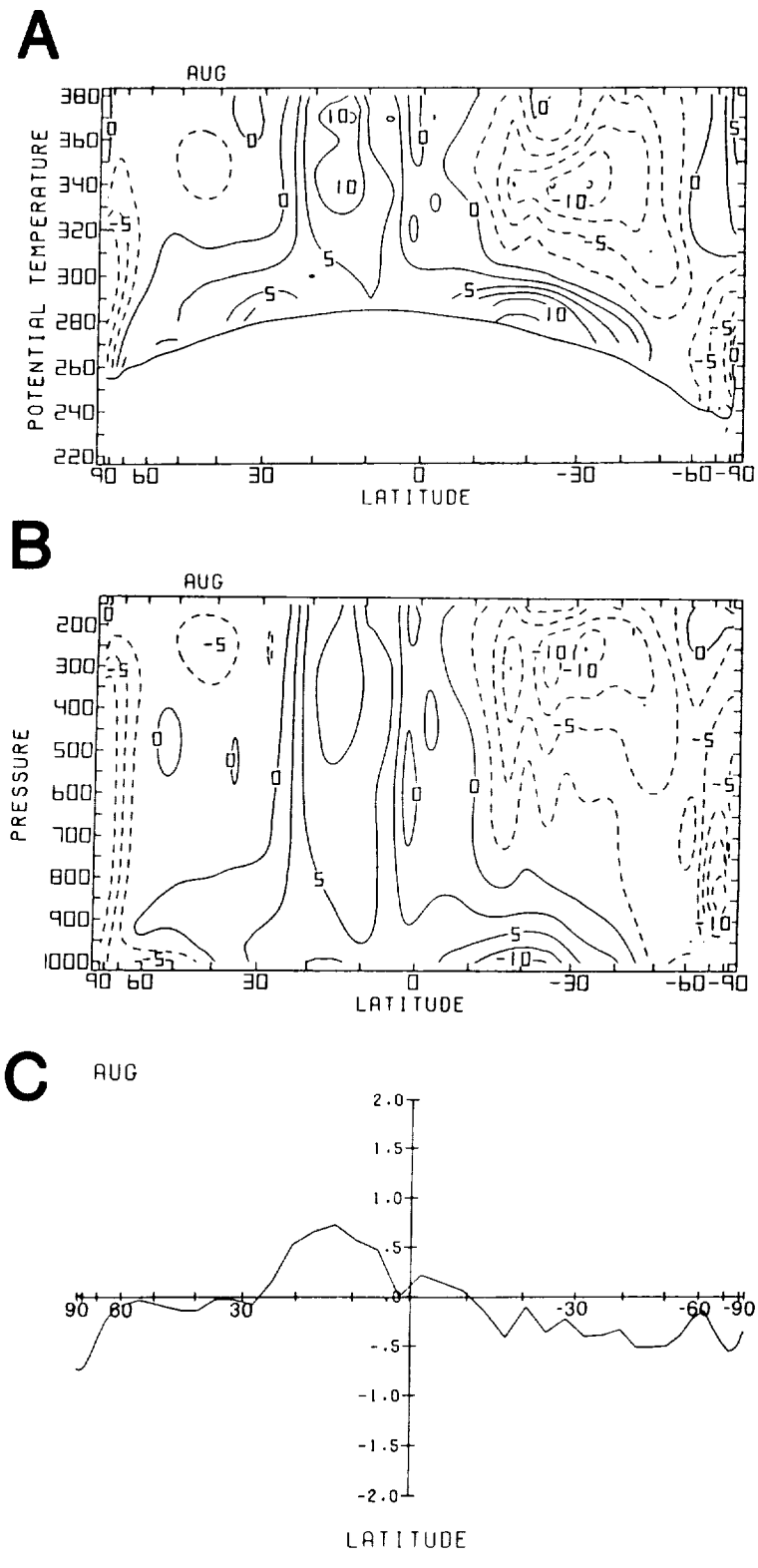

Fig. 82: Meridional cross sections of monthly (A) isentropically and (B) isobarically zonally averaged heating (10^{-1} K day^{-1}), and (C) meridional profile of zonally-vertically averaged heating for August 1979 (K day^{-1}). Contour interval in (A) and (B) is 0.25 K day^{-1}.

August

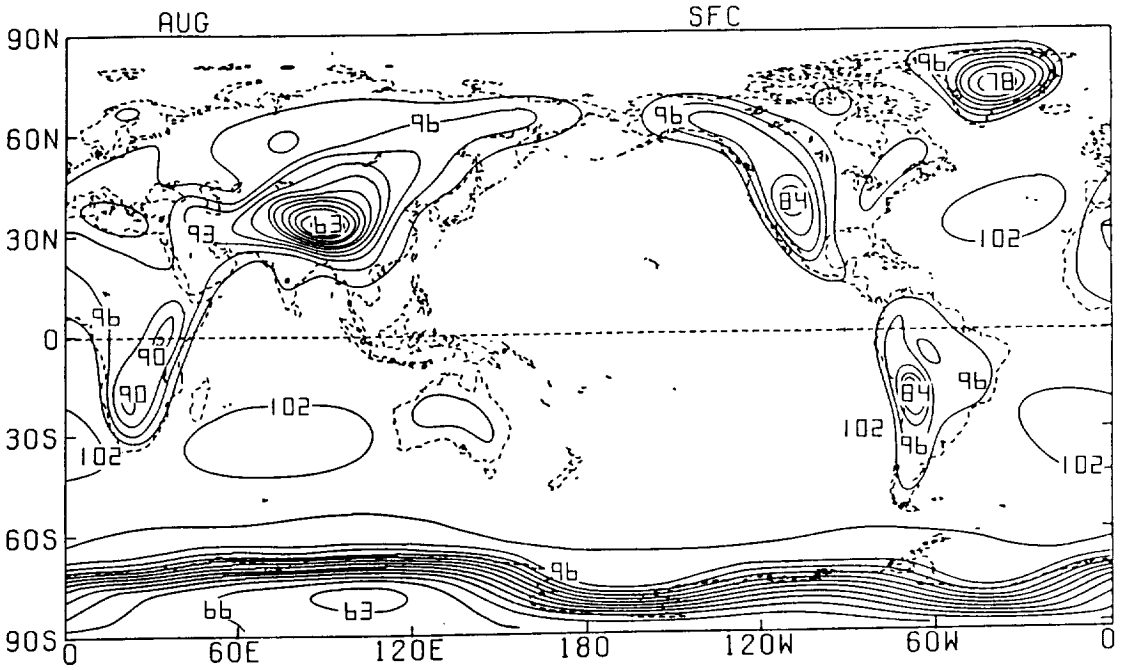

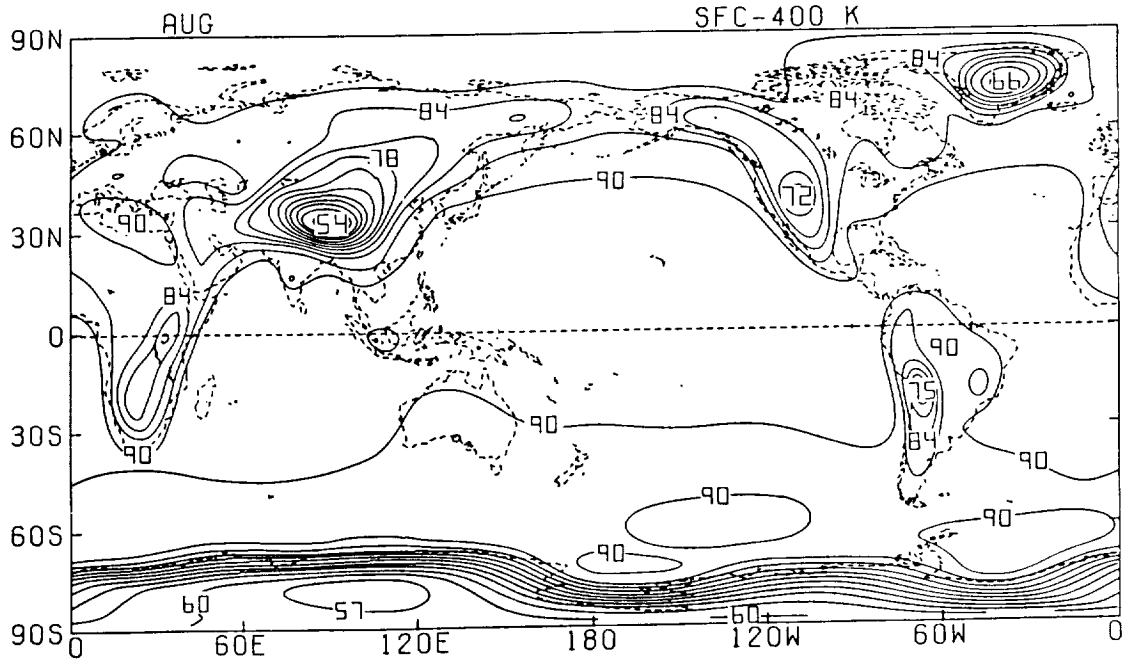

Fig. 83: Global distributions of monthly averaged (A) surface pressure (10^1 mb) and (B) pressure difference (10^1 mb) between the surface and the 400 K isentropic level for August 1979. Contour interval is 30 mb.

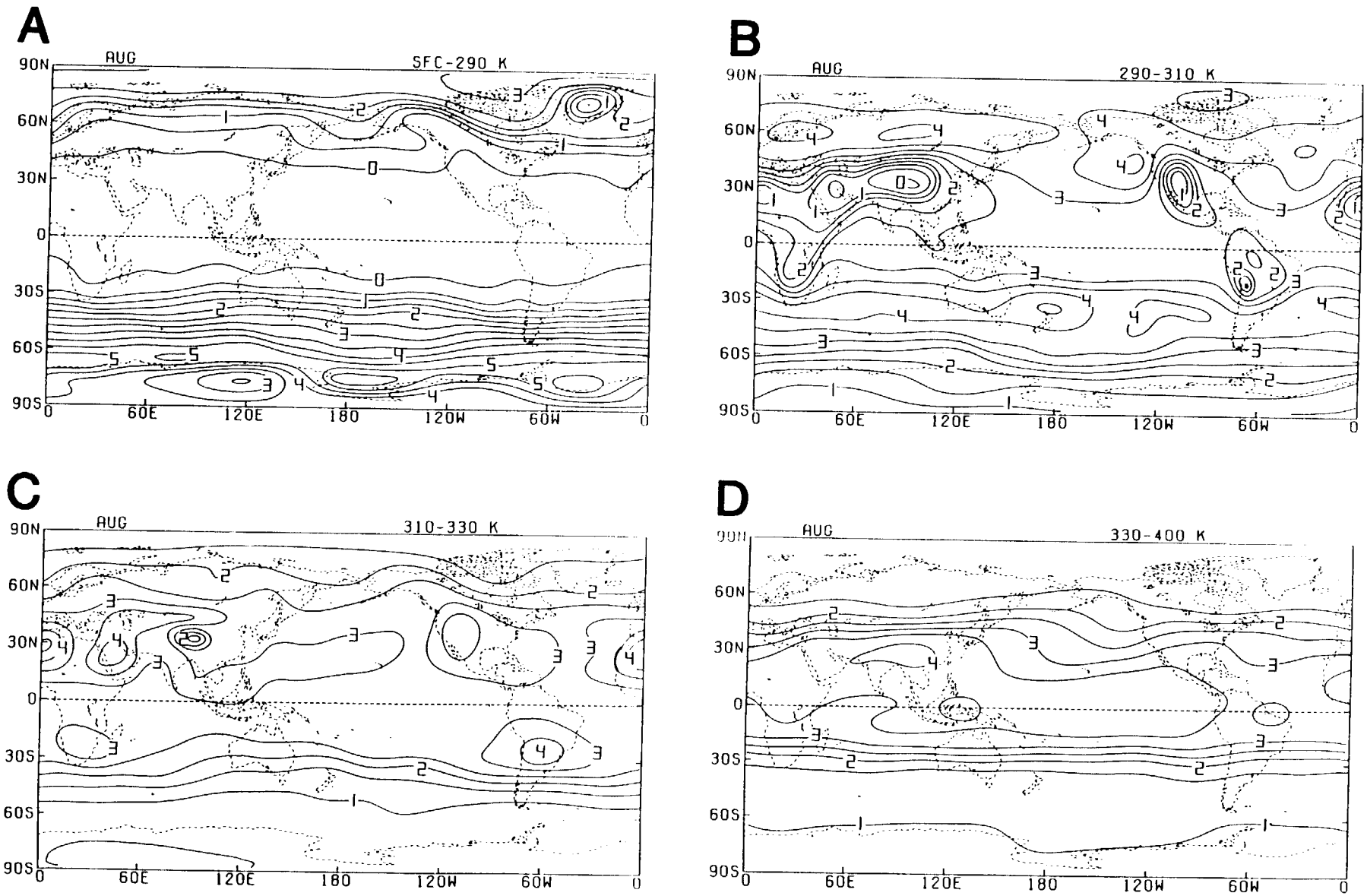

Fig. 84: Monthly averaged pressure difference (10^2 mb) between the upper and lower isentropic levels of the (A) surface-290 K, (B) 290-310 K, (C) 310-330 K and (D) 330-400 K isentropic layers for August 1979. Contour interval is 50 mb.

September

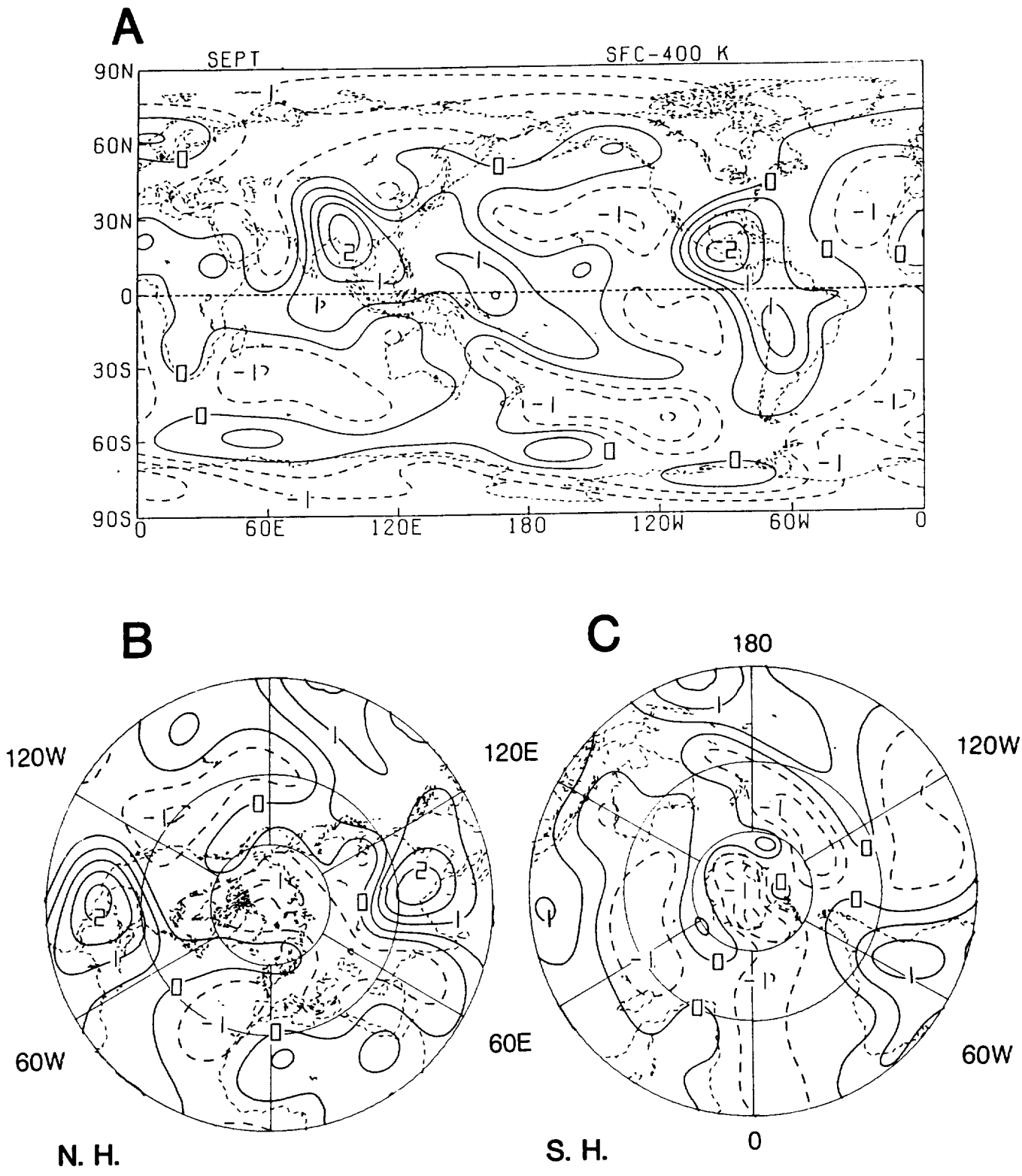

Fig. 85: Monthly vertical-averaged heating (K day^{-1}) for September 1979; (A) global, (B) Northern and (C) Southern Hemisphere. Contour interval is 0.5 K day^{-1}.

September

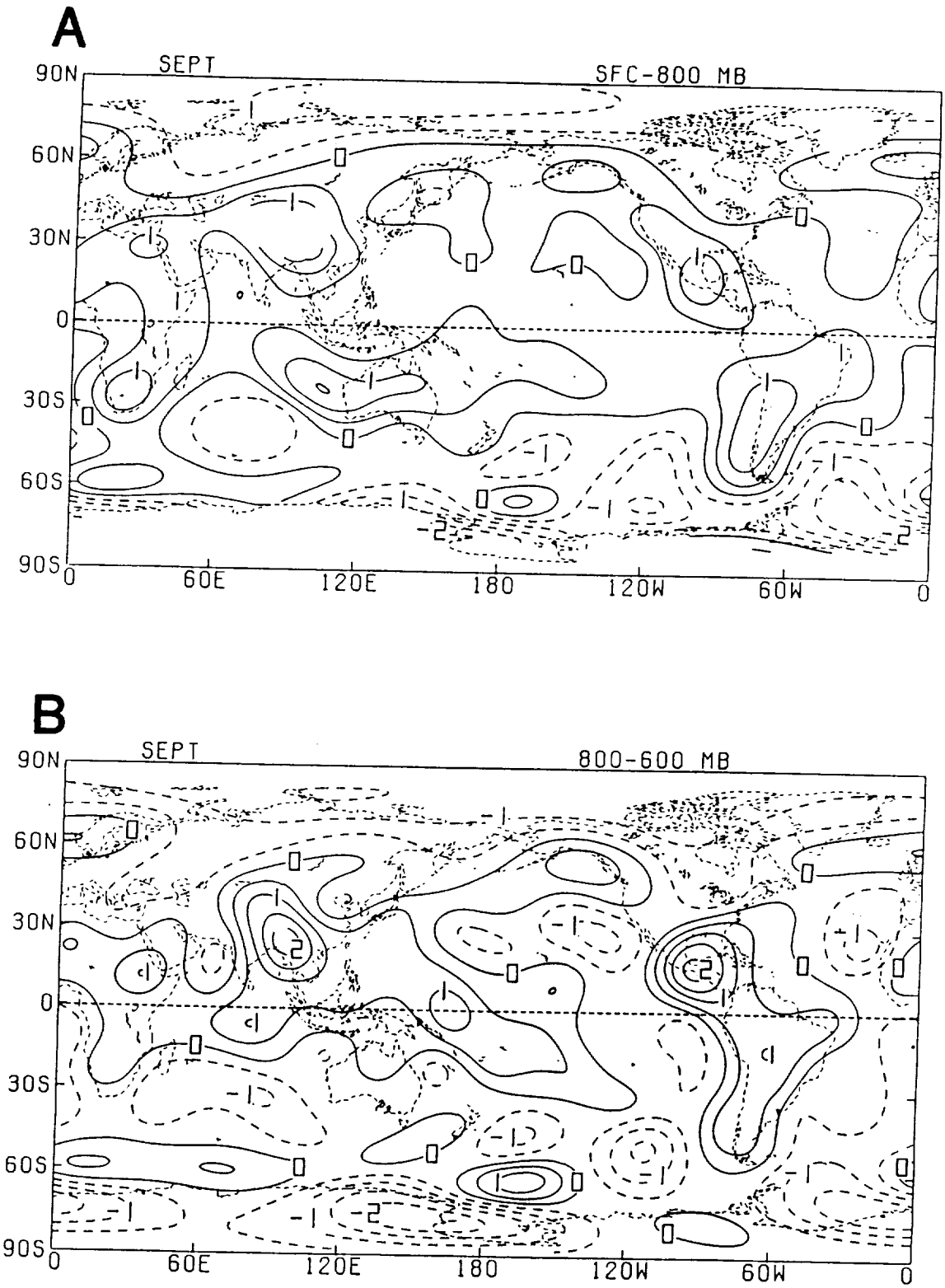

Fig. 86: Monthly layer-averaged heating (K day^{-1}) for the (A) surface-800 mb, (B) 800-600 mb, (C) 600-400 mb and (D) 400-200 mb isobaric layers for September 1979. Contour interval is 0.5 K day^{-1}.

September

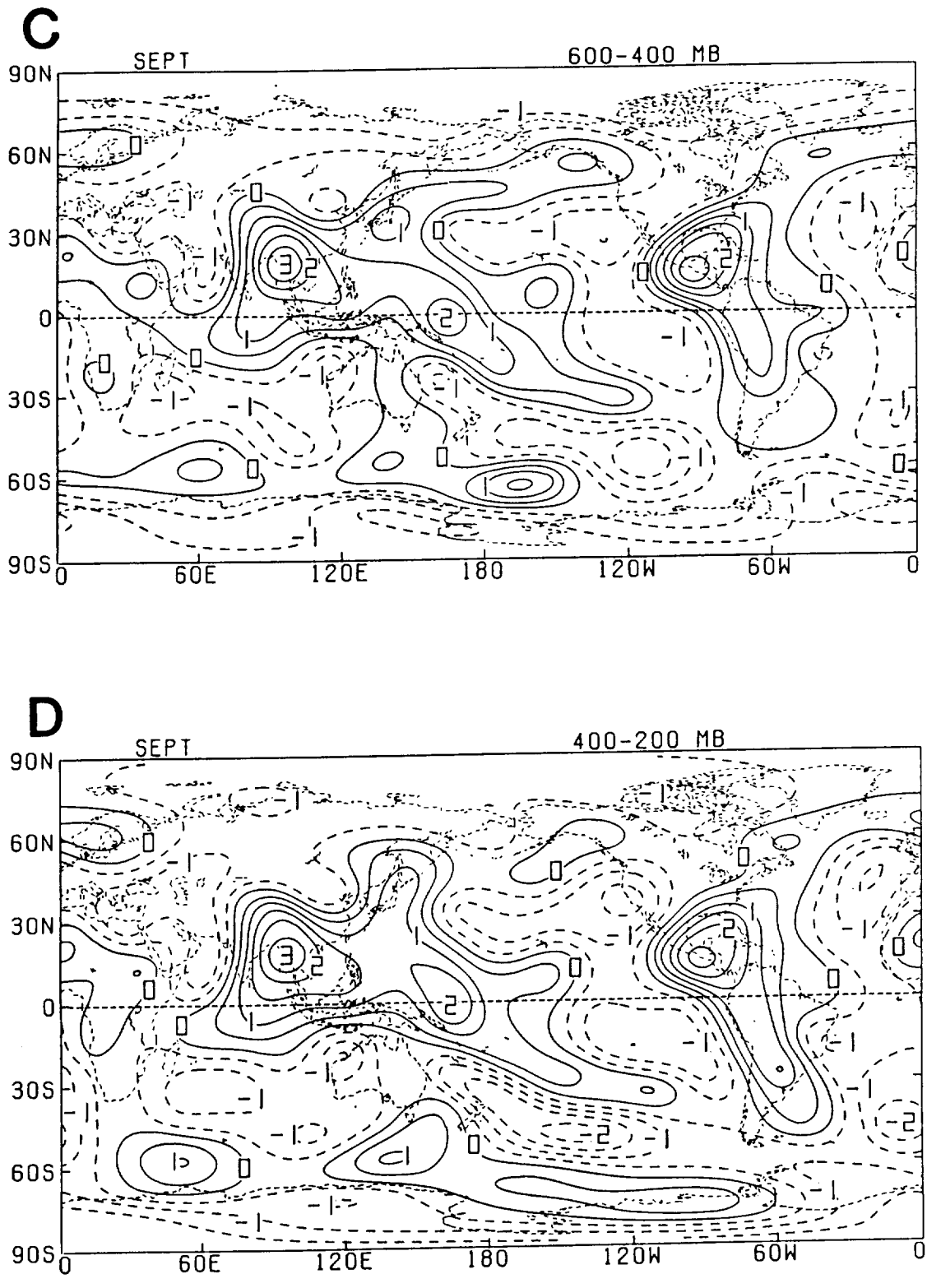

Fig. 86: (Continued).

September

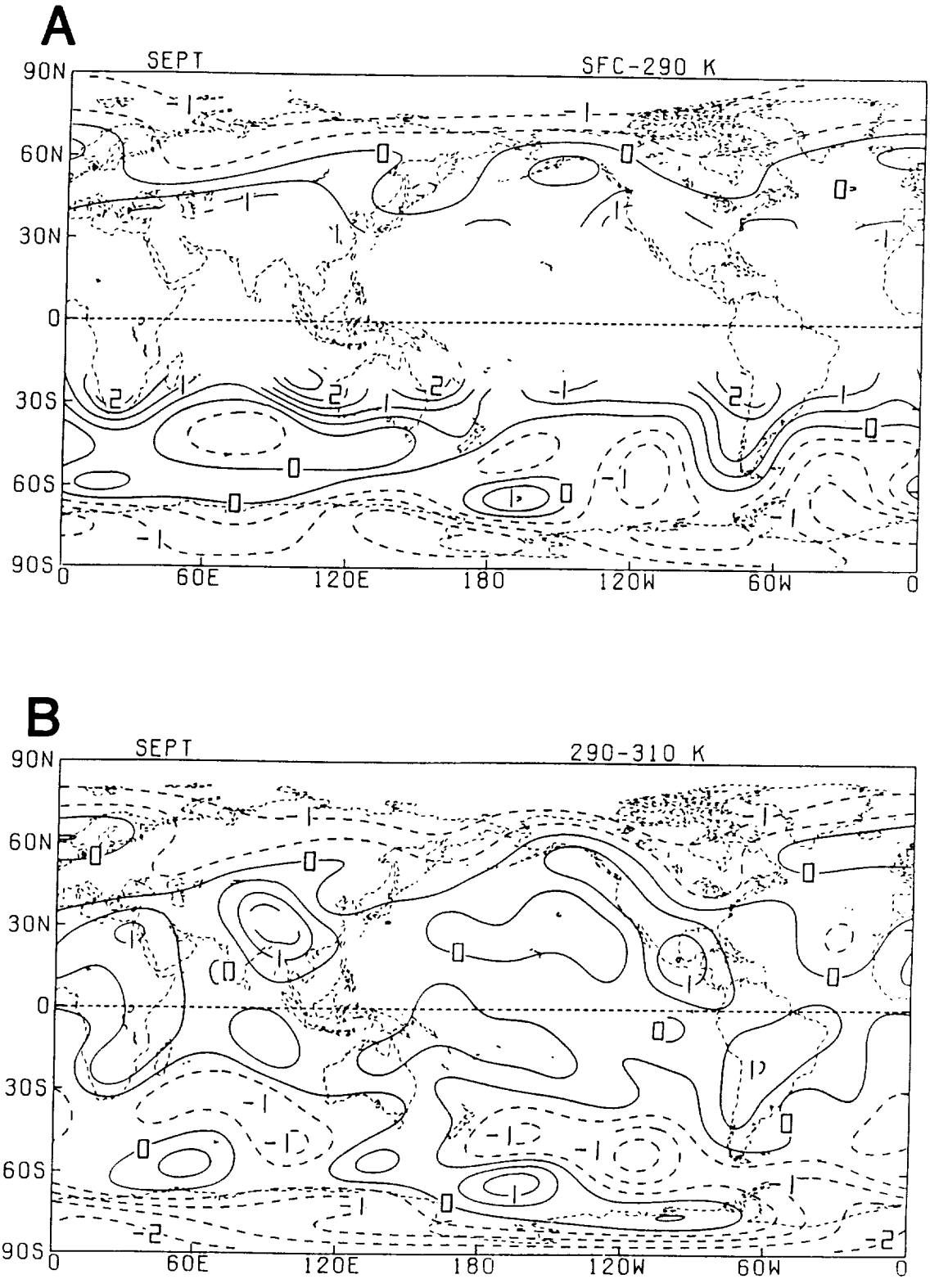

Fig. 87: Monthly layer-averaged heating (K day^{-1}) for the (A) surface-290 K, (B) 290-310 K, (C) 310-330 K and (D) 330-400 K isentropic layers for September 1979. Contour interval is 0.5 K day^{-1}.

September

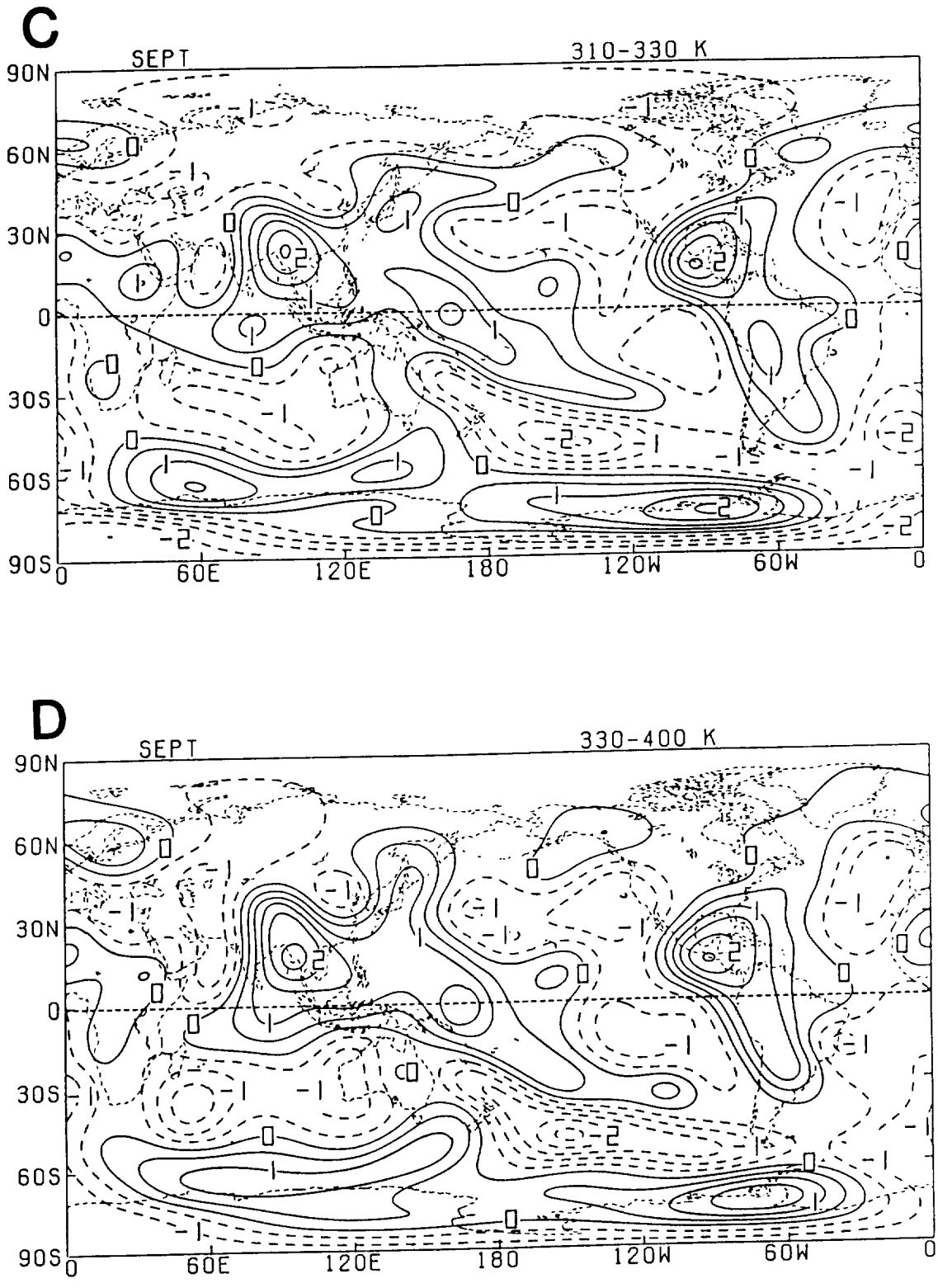

Fig. 87: (Continued).

September

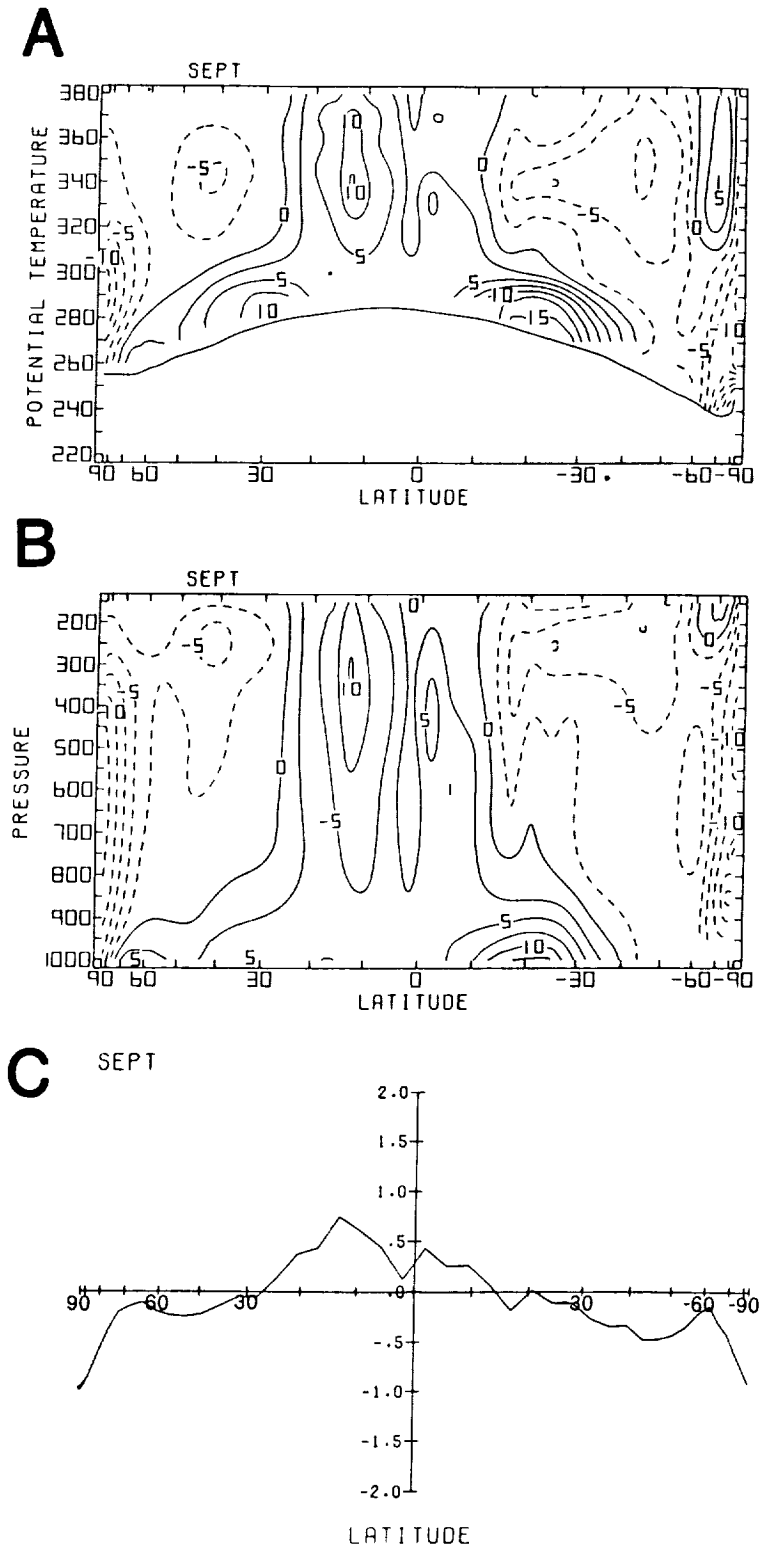

Fig. 88: Meridional cross sections of monthly (A) isentropically and (B) isobarically zonally averaged heating (10^{-1} K day^{-1}), and (C) meridional profile of zonally-vertically averaged heating for September 1979 (K day^{-1}). Contour interval in (A) and (B) is 0.25 K day^{-1}.

September

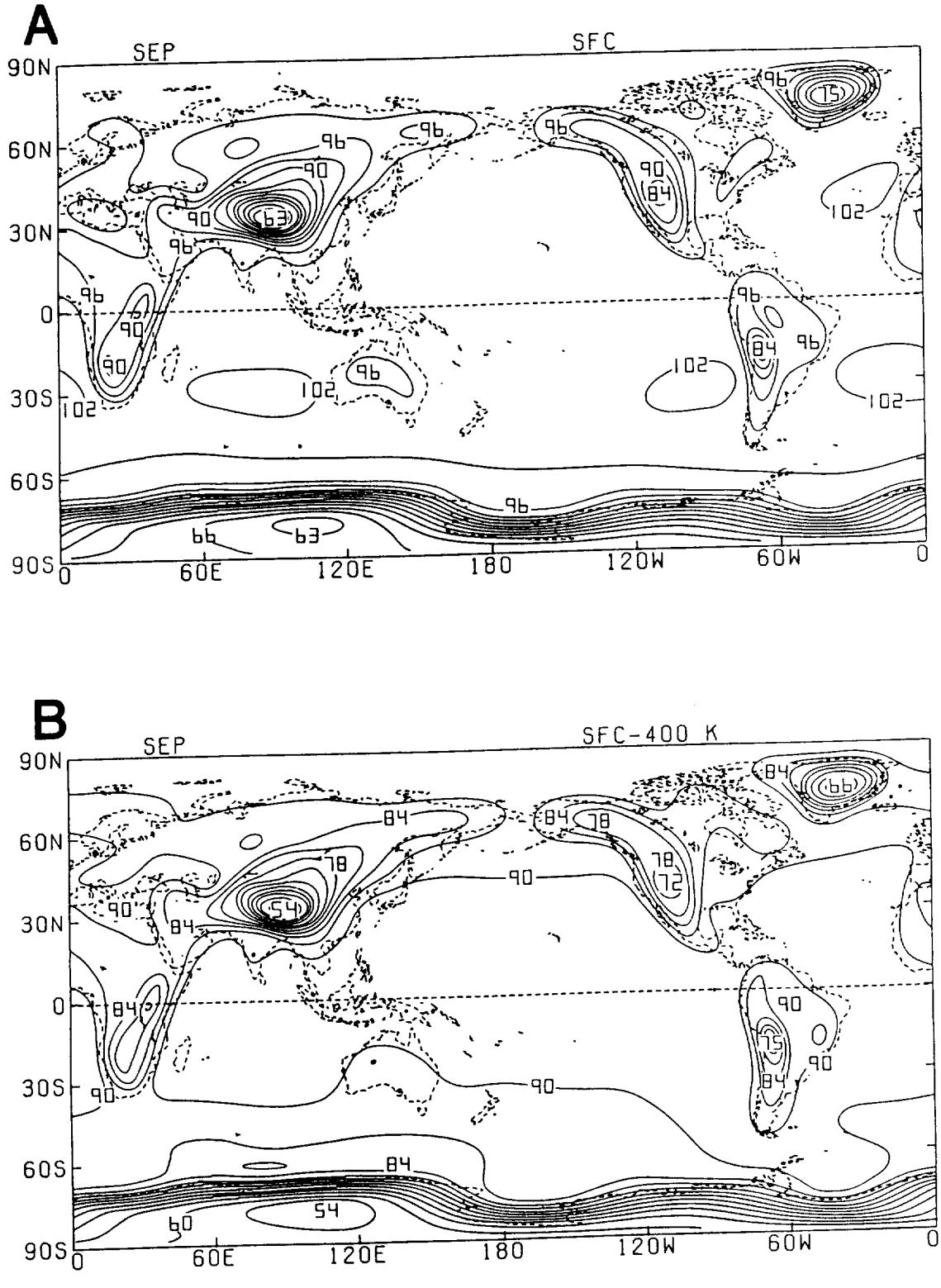

Fig. 89: Global distributions of monthly averaged (A) surface pressure (10^1 mb) and (B) pressure difference (10^1 mb) between the surface and the 400 K isentropic level for September 1979. Contour interval is 30 mb.

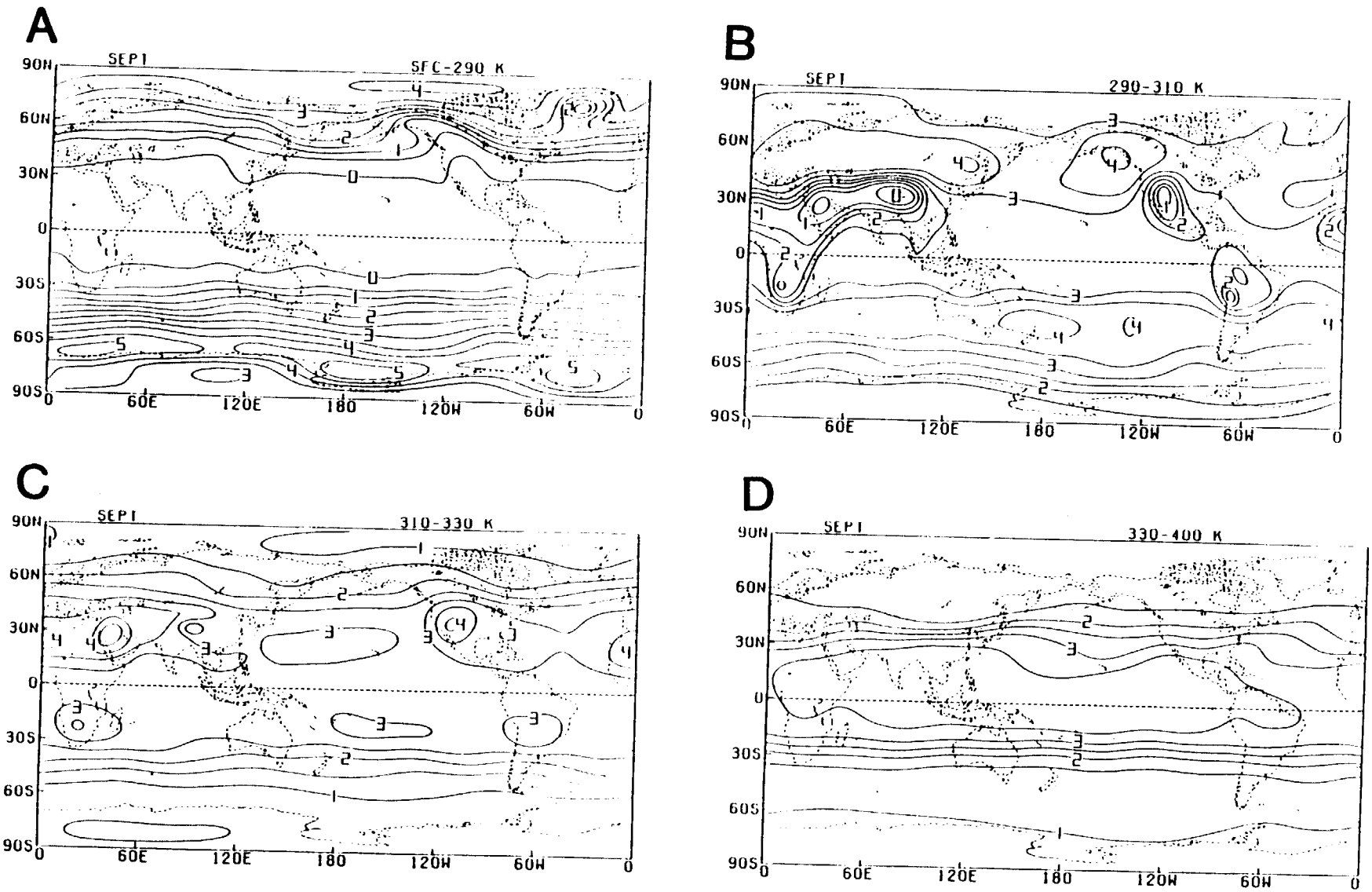

Fig. 90: Monthly averaged pressure difference (10^2 mb) between the upper and lower isentropic levels of the (A) surface-290 K, (B) 290-310 K, (C) 310-330 K and (D) 330-400 K isentropic layers for September 1979. Contour interval is 50 mb.

October

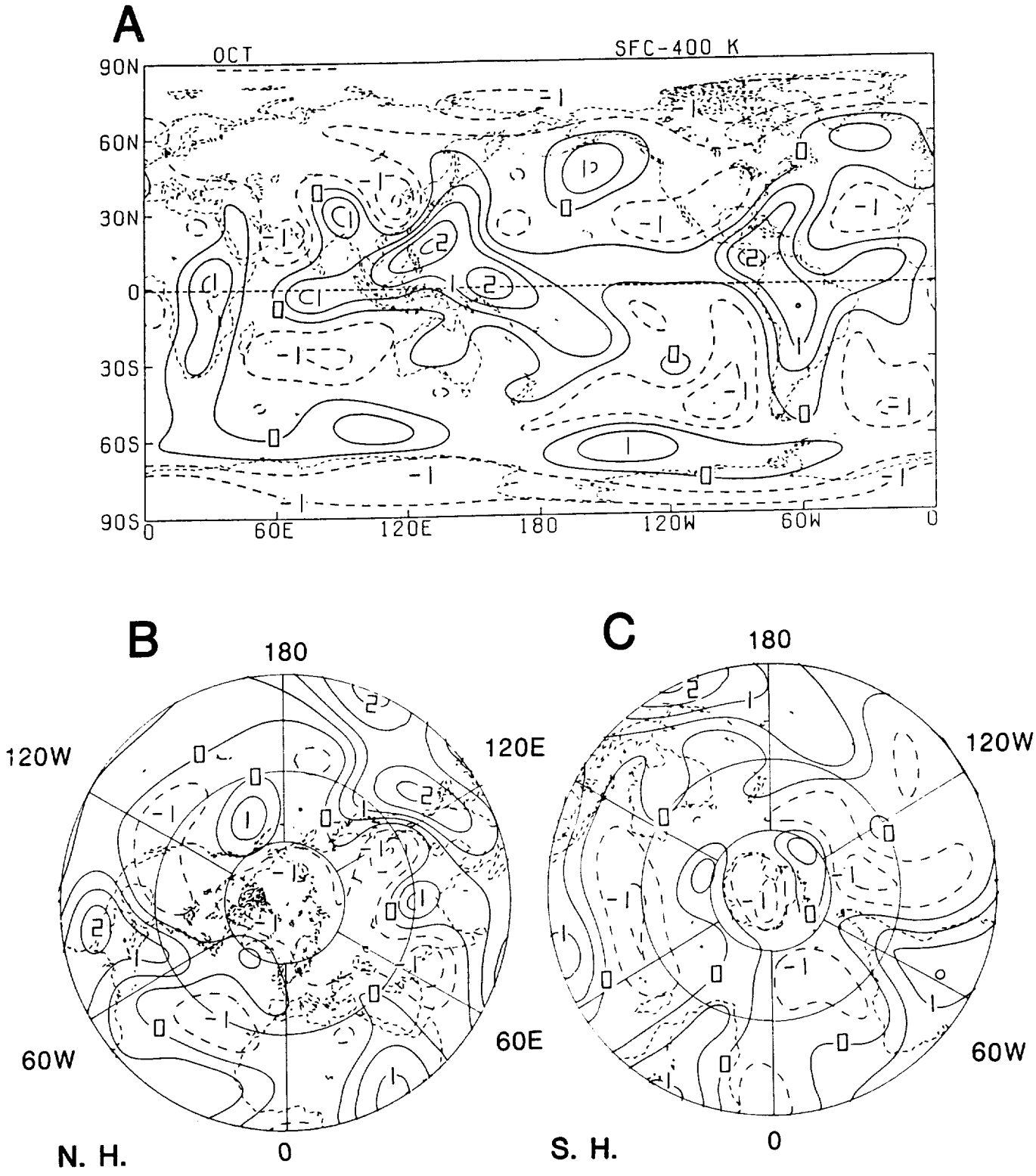

Fig. 91: Monthly vertical-averaged heating (K day^{-1}) for October 1979; (A) global, (B) Northern and (C) Southern Hemisphere. Contour interval is 0.5 K day^{-1}.

October

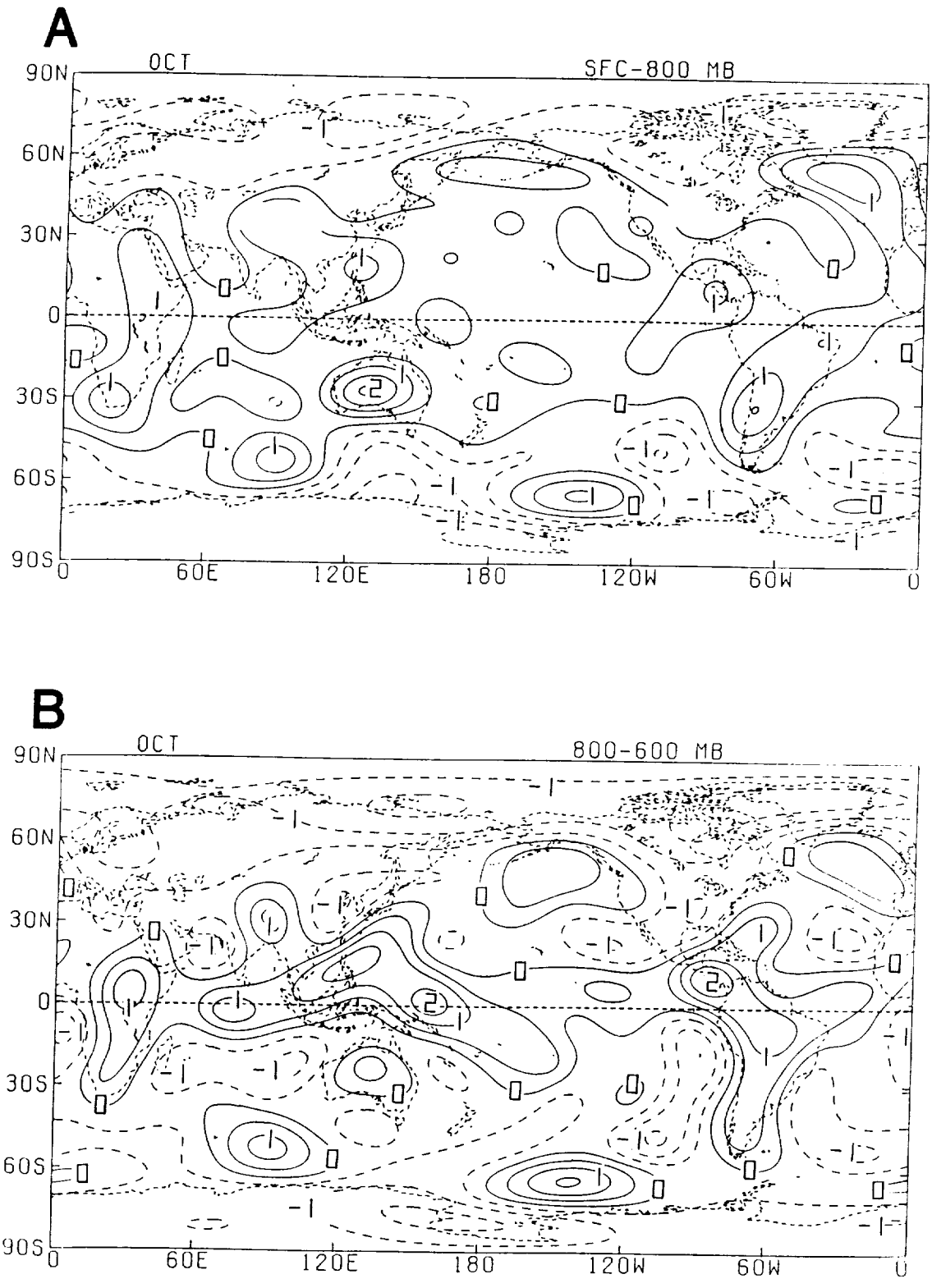

Fig. 92: Monthly layer-averaged heating (K day^{-1}) for the (A) surface-800 mb, (B) 800-600 mb, (C) 600-400 mb and (D) 400-200 mb isobaric layers for October 1979. Contour interval is 0.5 K day^{-1}.

October

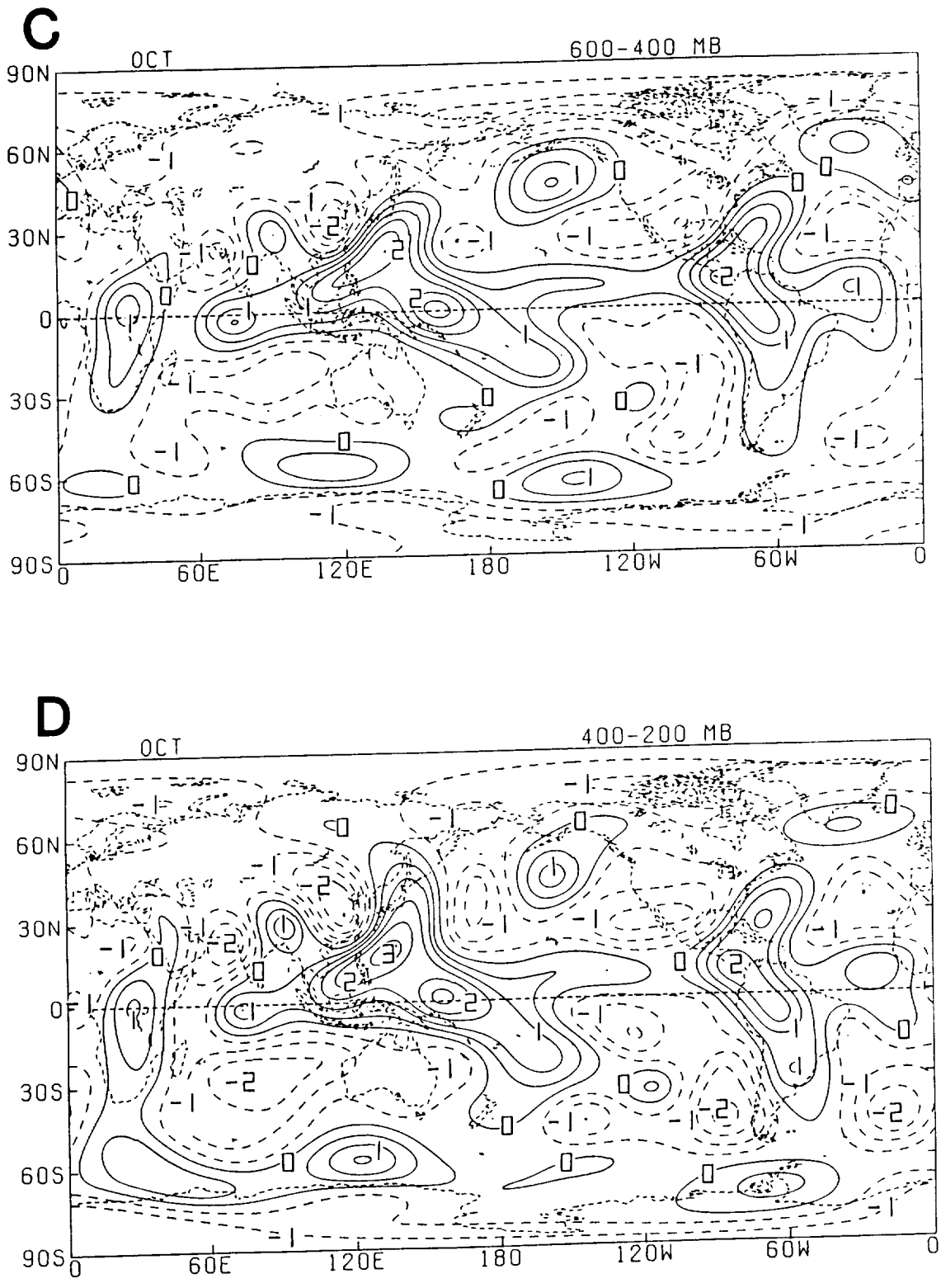

Fig. 92: (Continued).

October

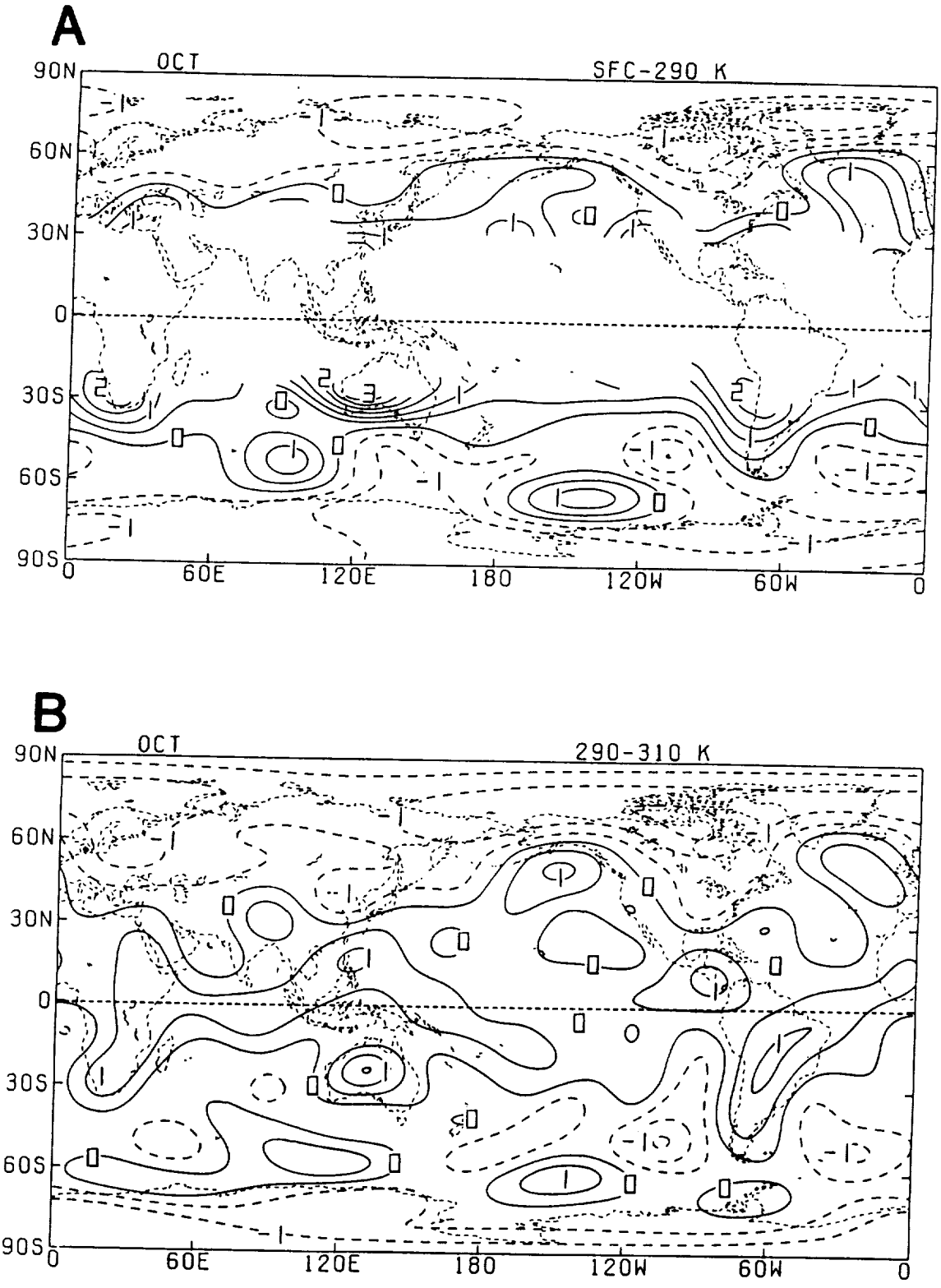

Fig. 93: Monthly layer-averaged heating (K day^{-1}) for the (A) surface-290 K, (B) 290-310 K, (C) 310-330 K and (D) 330-400 K isentropic layers for October 1979. Contour interval is 0.5 K day^{-1}.

October

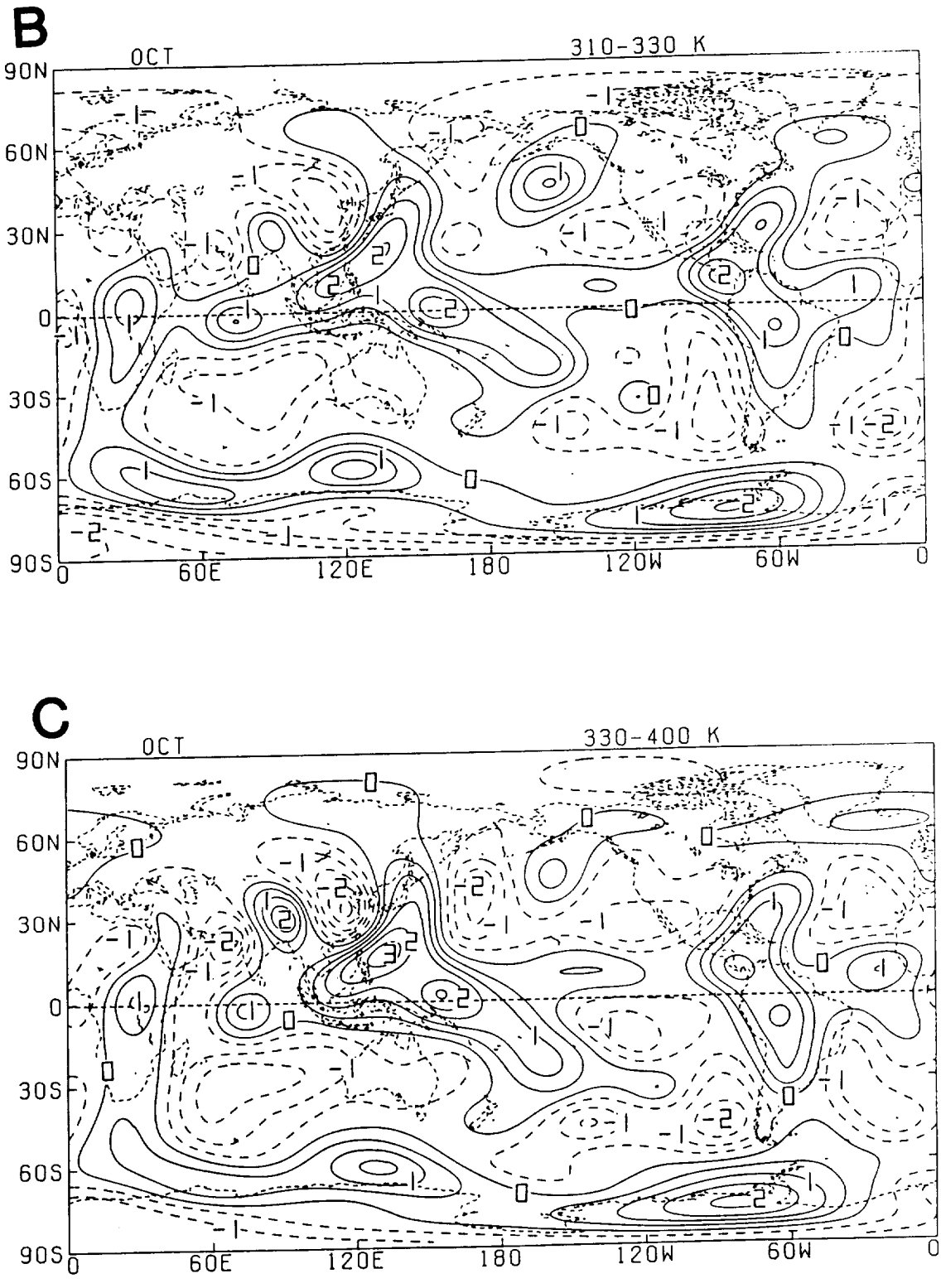

Fig. 93: (Continued).

October

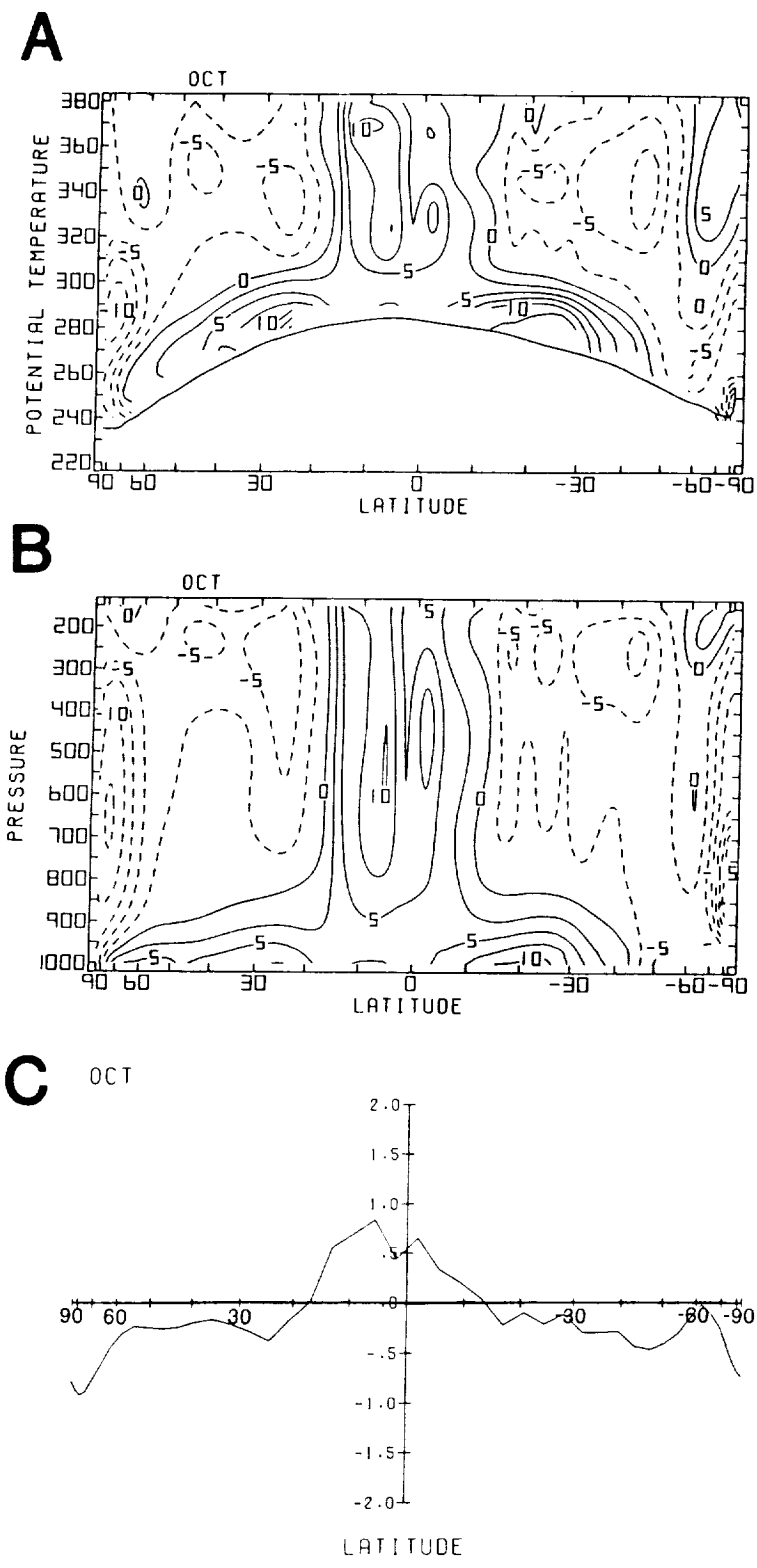

Fig. 94: Meridional cross sections of monthly (A) isentropically and (B) isobarically zonally averaged heating (10^{-1} K day^{-1}), and (C) meridional profile of zonally-vertically averaged heating for October 1979 (K day^{-1}). Contour interval in (A) and (B) is 0.25 K day^{-1}.

October

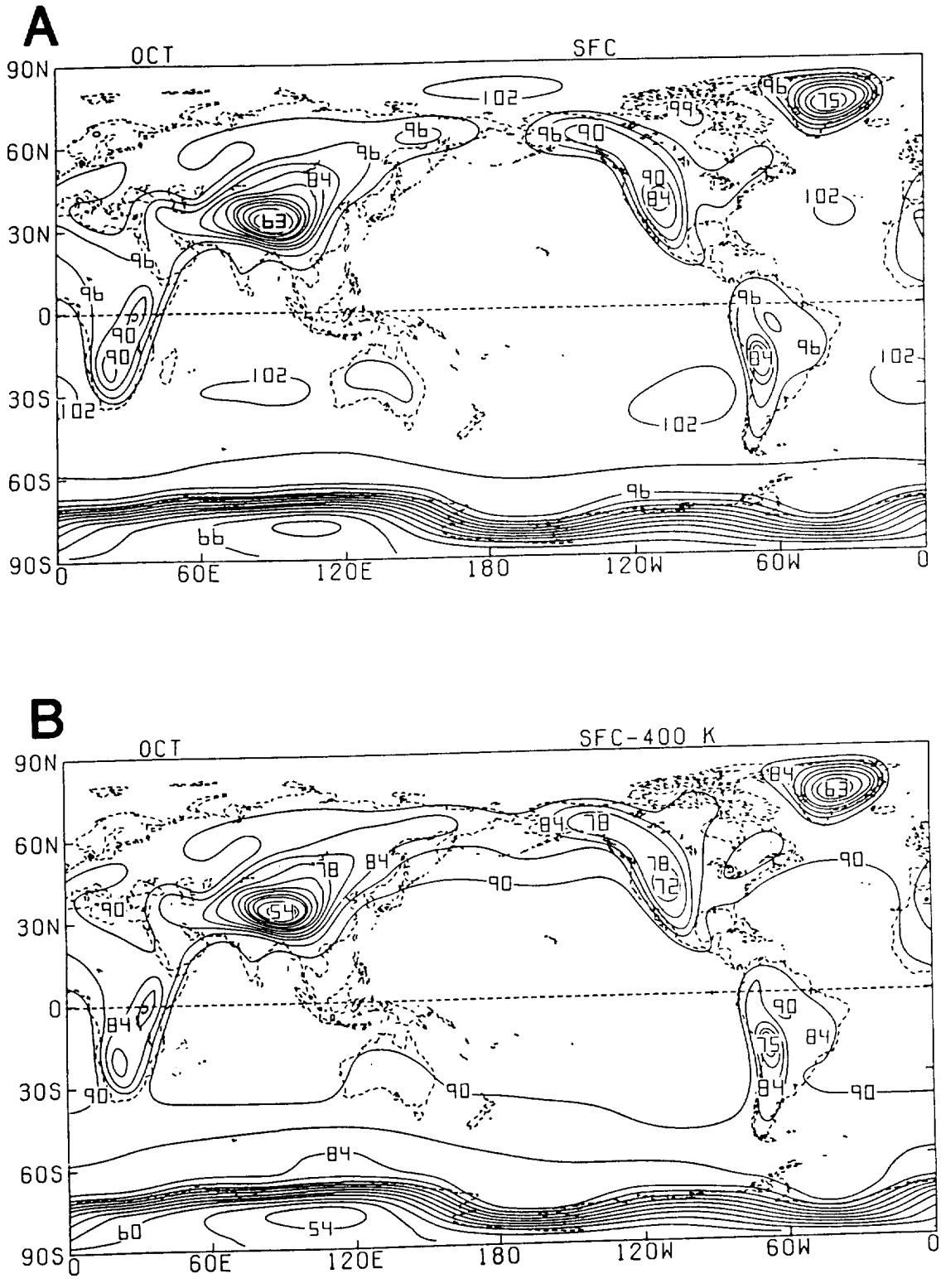

Fig. 95: Global distributions of monthly averaged (A) surface pressure (10^1 mb) and (B) pressure difference (10^1 mb) between the surface and the 400 K isentropic level for October 1979. Contour interval is 30 mb.

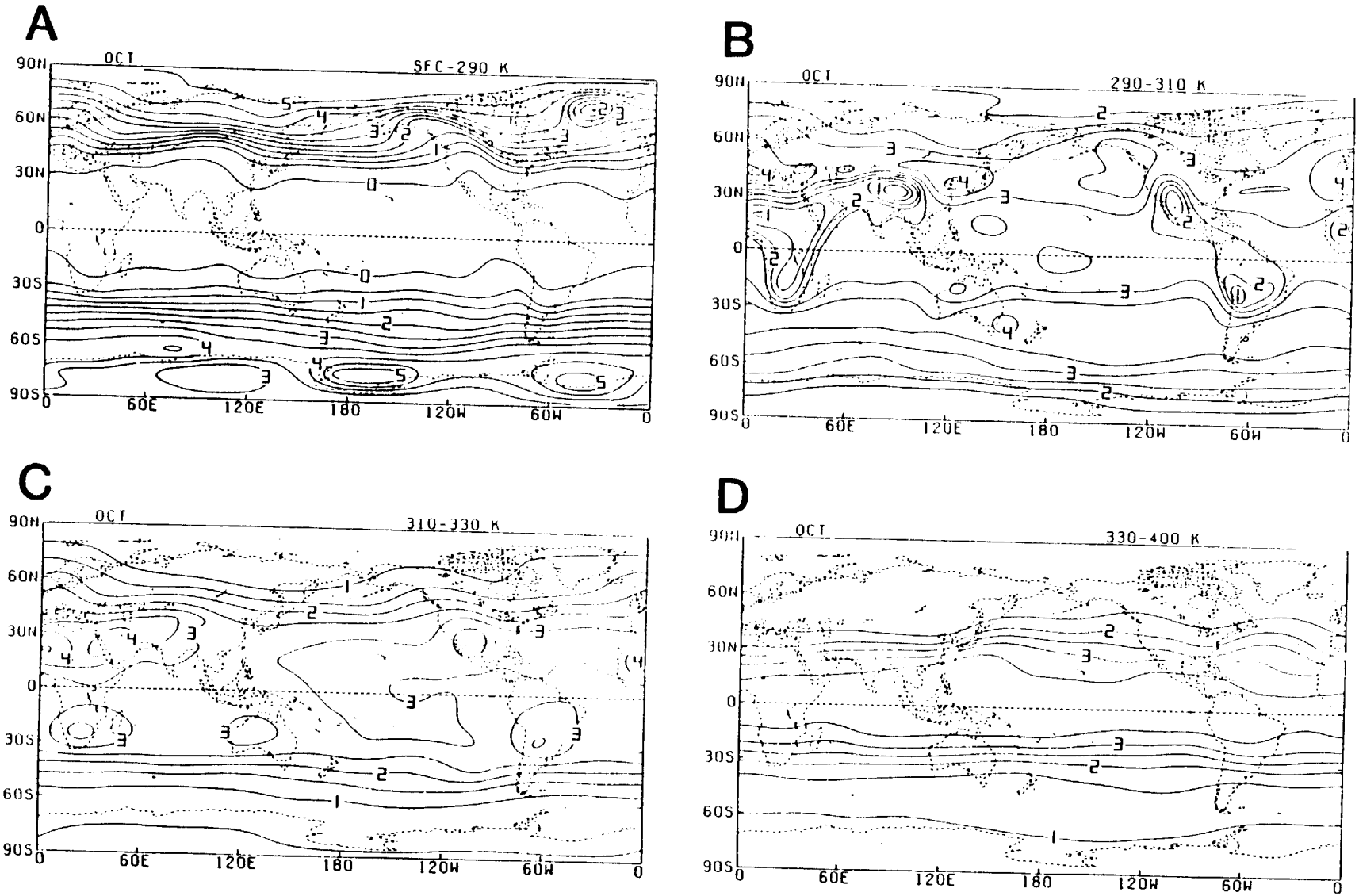

Fig. 96: Monthly averaged pressure difference (10^2 mb) between the upper and lower isentropic levels of the (A) surface-290 K, (B) 290-310 K, (C) 310-330 K and (D) 330-400 K isentropic layers for October 1979. Contour interval is 50 mb.

November

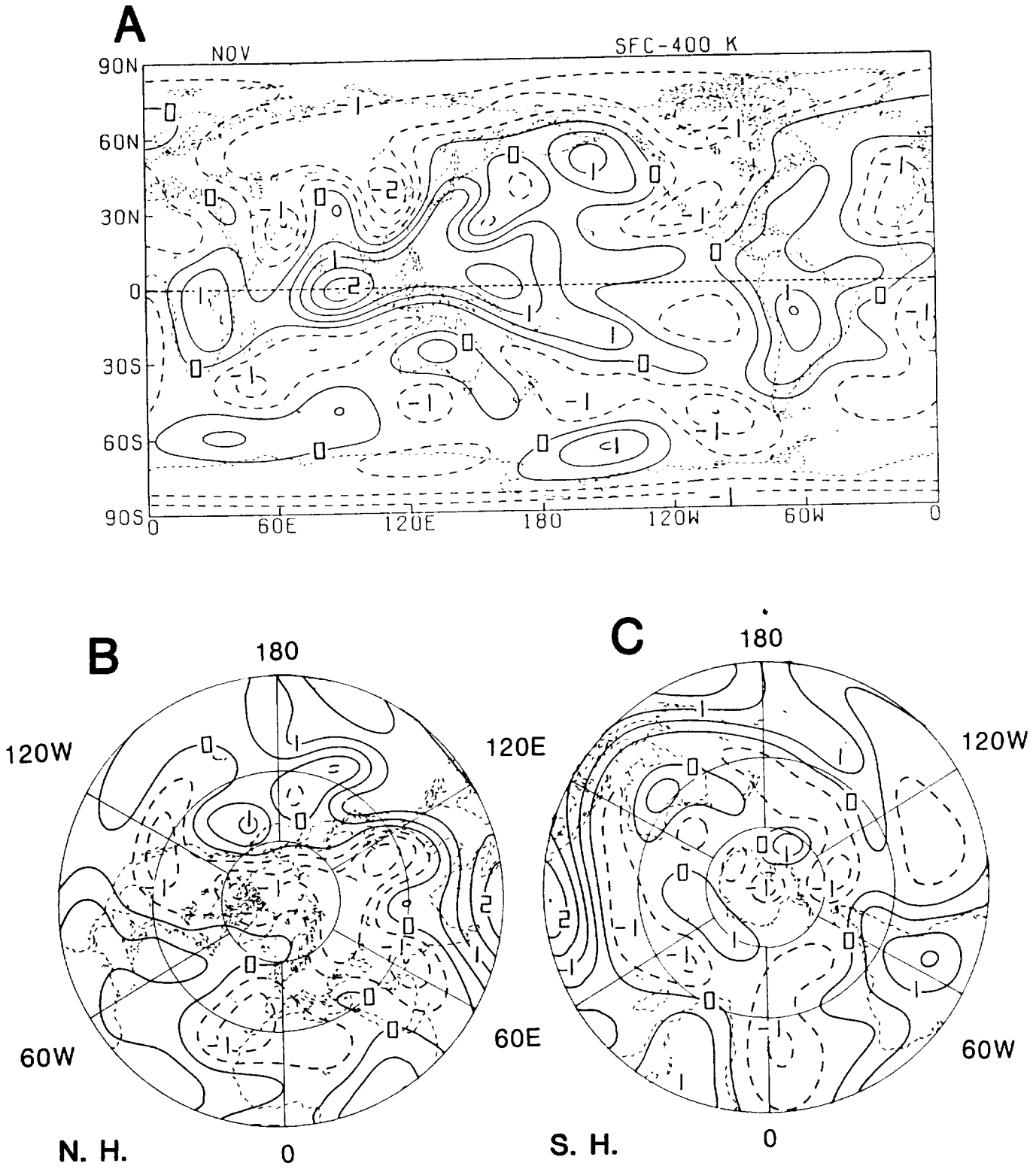

Fig. 97: Monthly vertical-averaged heating (K day^{-1}) for November 1979; (A) global, (B) Northern and (C) Southern Hemisphere. Contour interval is 0.5 K day^{-1}.

November

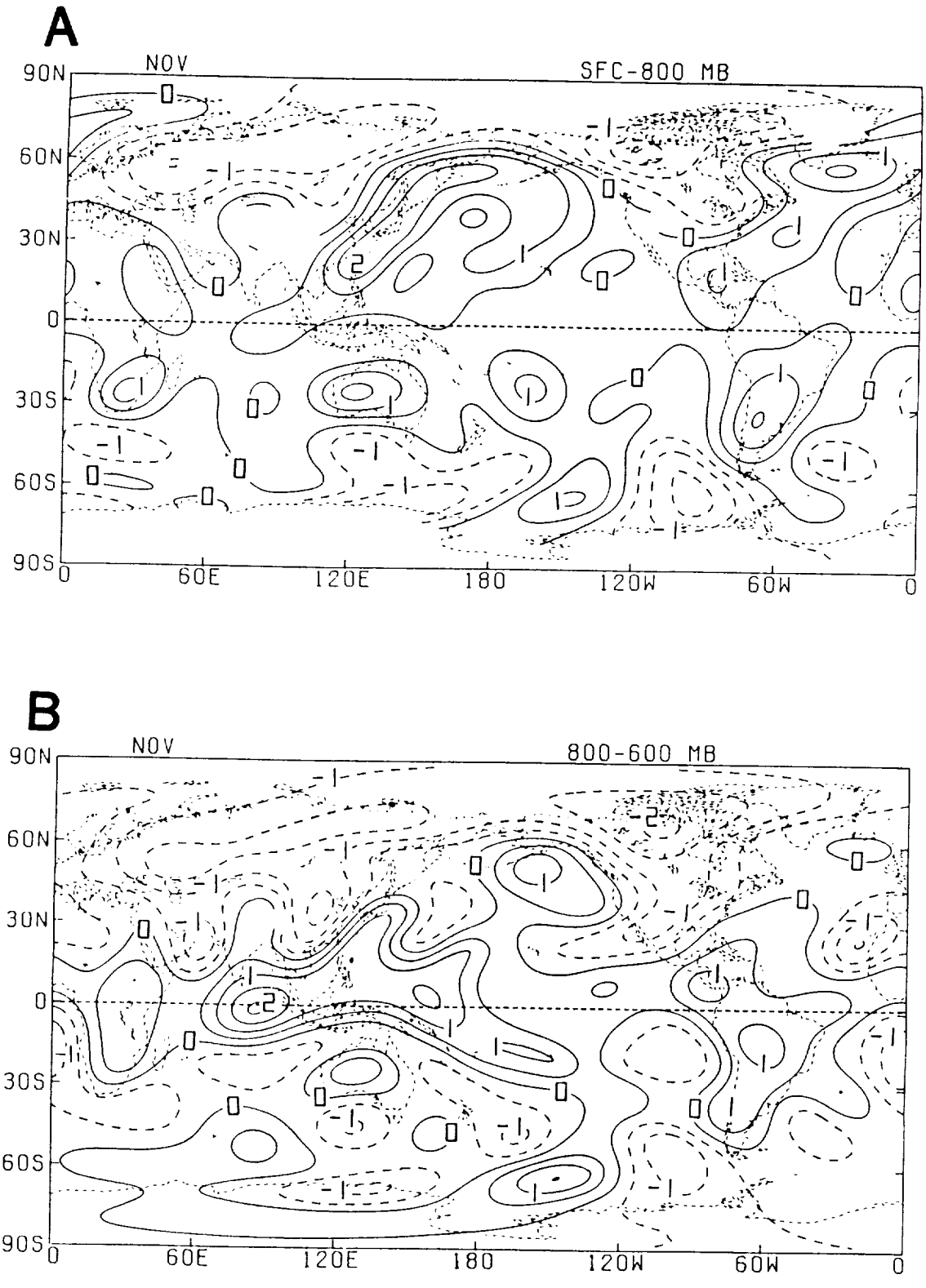

Fig. 98: Monthly layer-averaged heating (K day^{-1}) for the (A) surface-800 mb, (B) 800-600 mb, (C) 600-400 mb and (D) 400-200 mb isobaric layers for November 1979. Contour interval is 0.5 K day^{-1}.

November

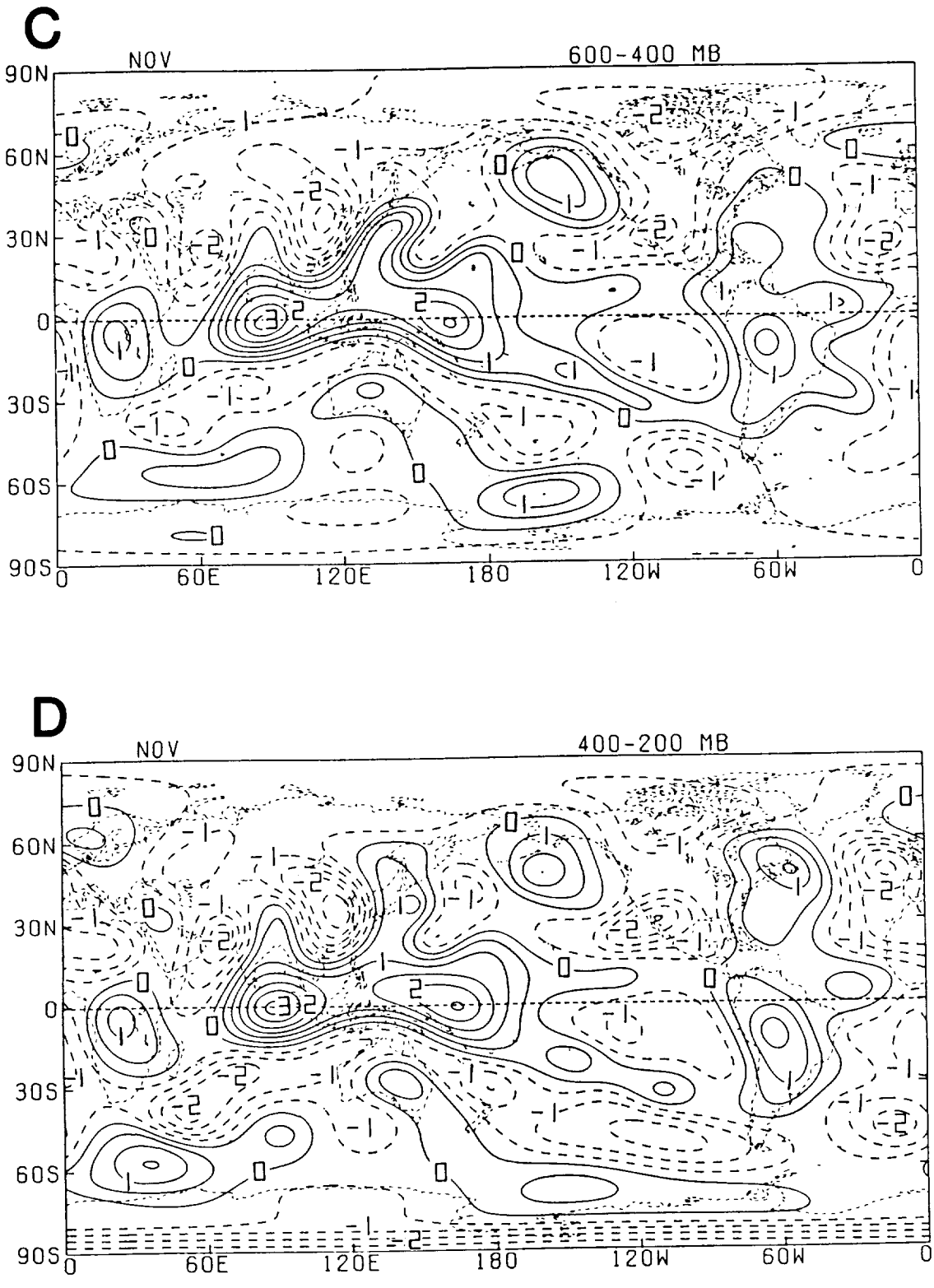

Fig. 98: (Continued).

November

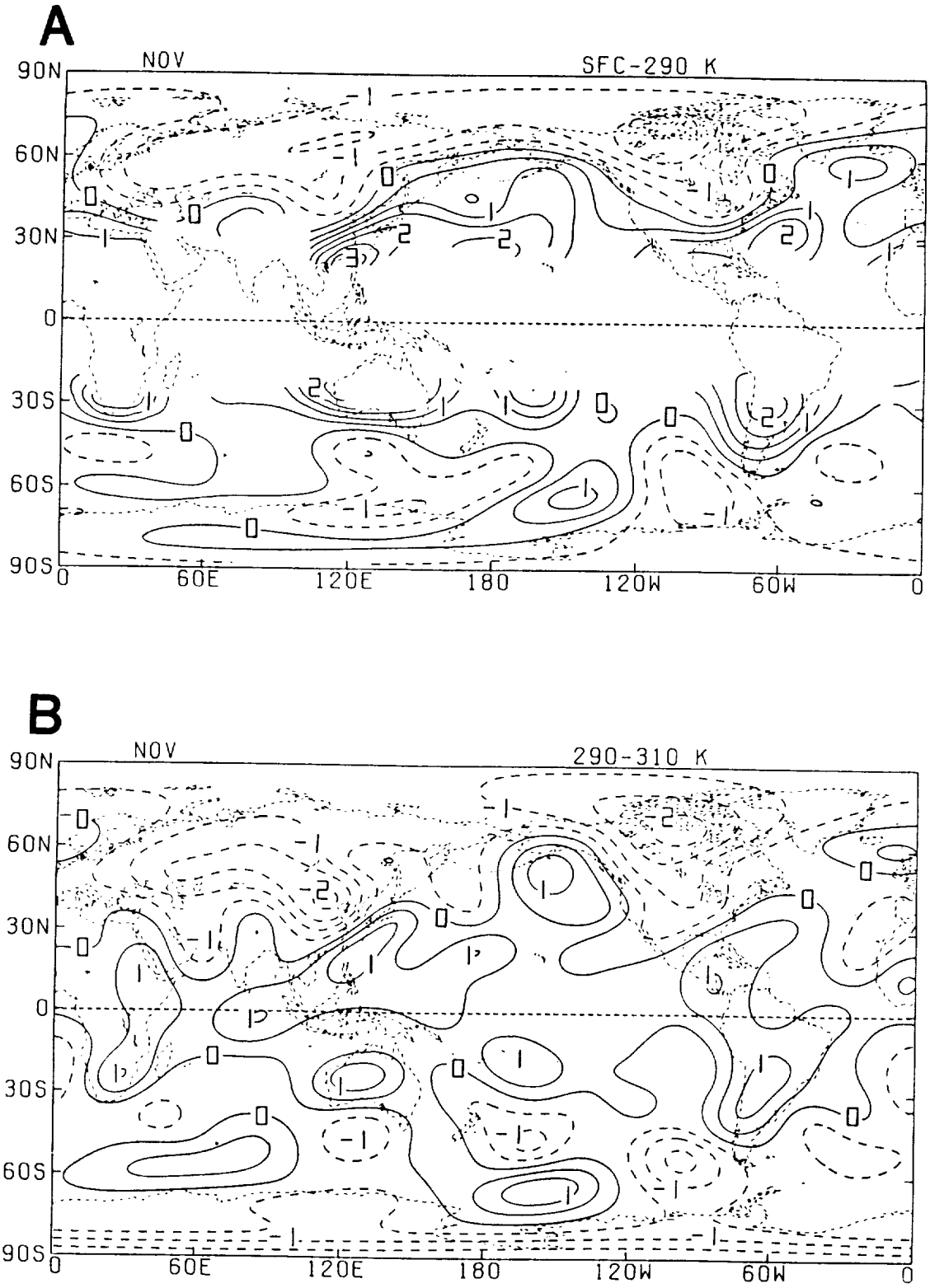

Fig. 99: Monthly layer-averaged heating (K day^{-1}) for the (A) surface-290 K, (B) 290-310 K, (C) 310-330 K and (D) 330-400 K isentropic layers for November 1979. Contour interval is 0.5 K day^{-1}.

November

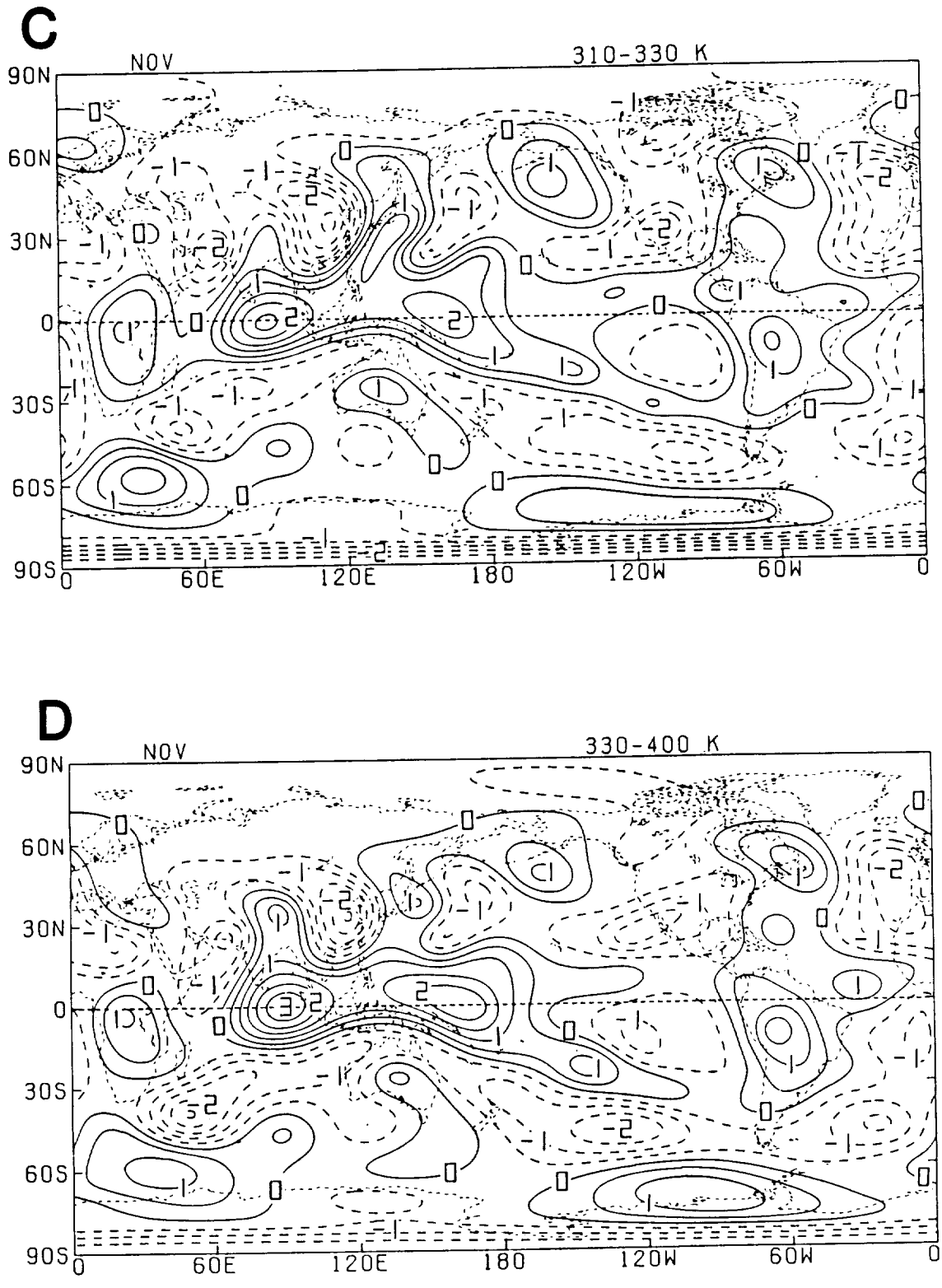

Fig. 99: (Continued).

November

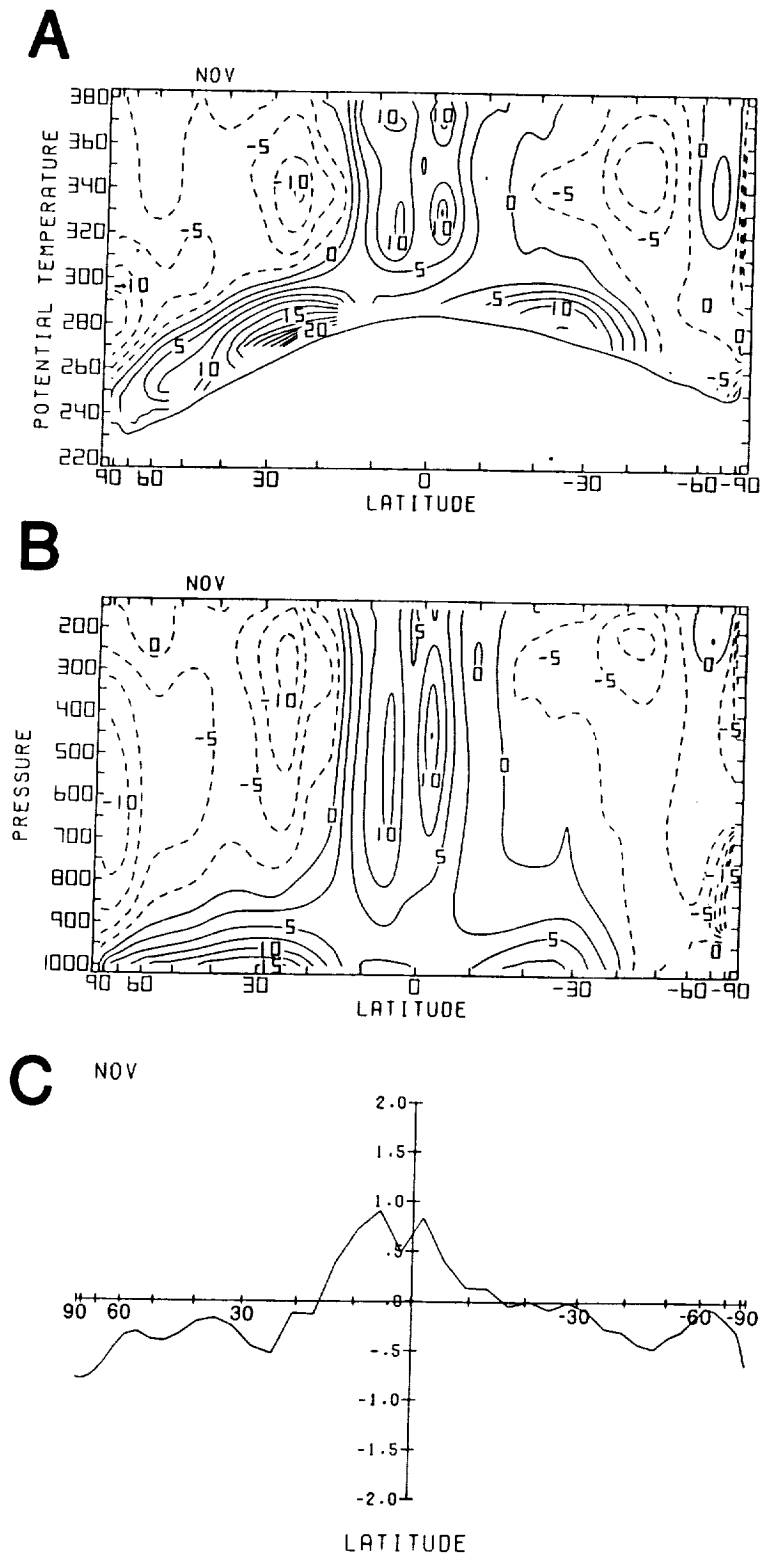

Fig. 100: Meridional cross sections of monthly (A) isentropically and (B) isobarically zonally averaged heating (10^{-1} K day^{-1}), and (C) meridional profile of zonally-vertically averaged heating for November 1979 (K day^{-1}). Contour interval in (A) and (B) is 0.25 K day^{-1}.

November

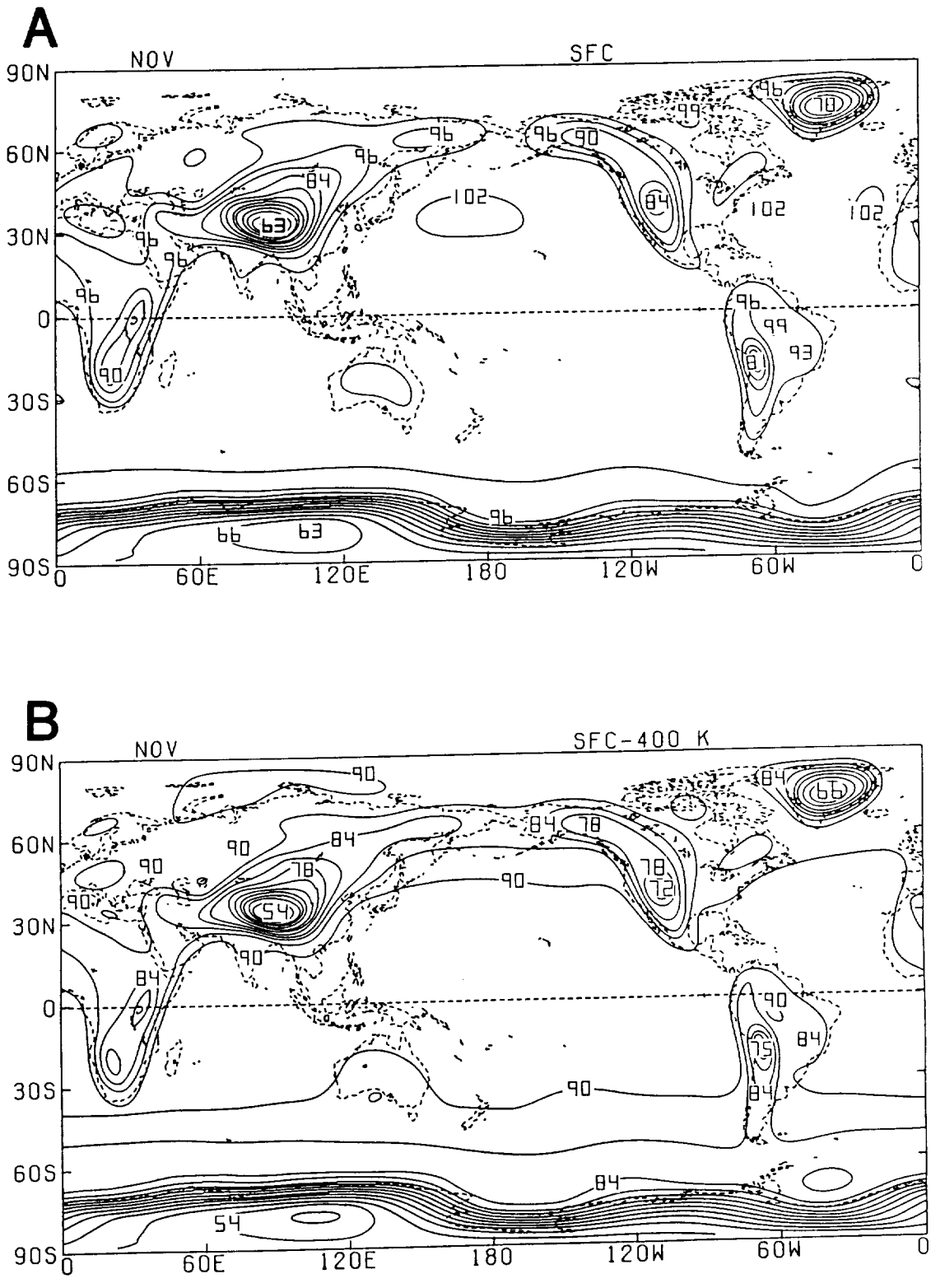

Fig. 101: Global distributions of monthly averaged (A) surface pressure (10^1 mb) and (B) pressure difference (10^1 mb) between the surface and the 400 K isentropic level for November 1979. Contour interval is 30 mb.

★U.S. GOVERNMENT PRINTING OFFICE: 1991 527-054/60004

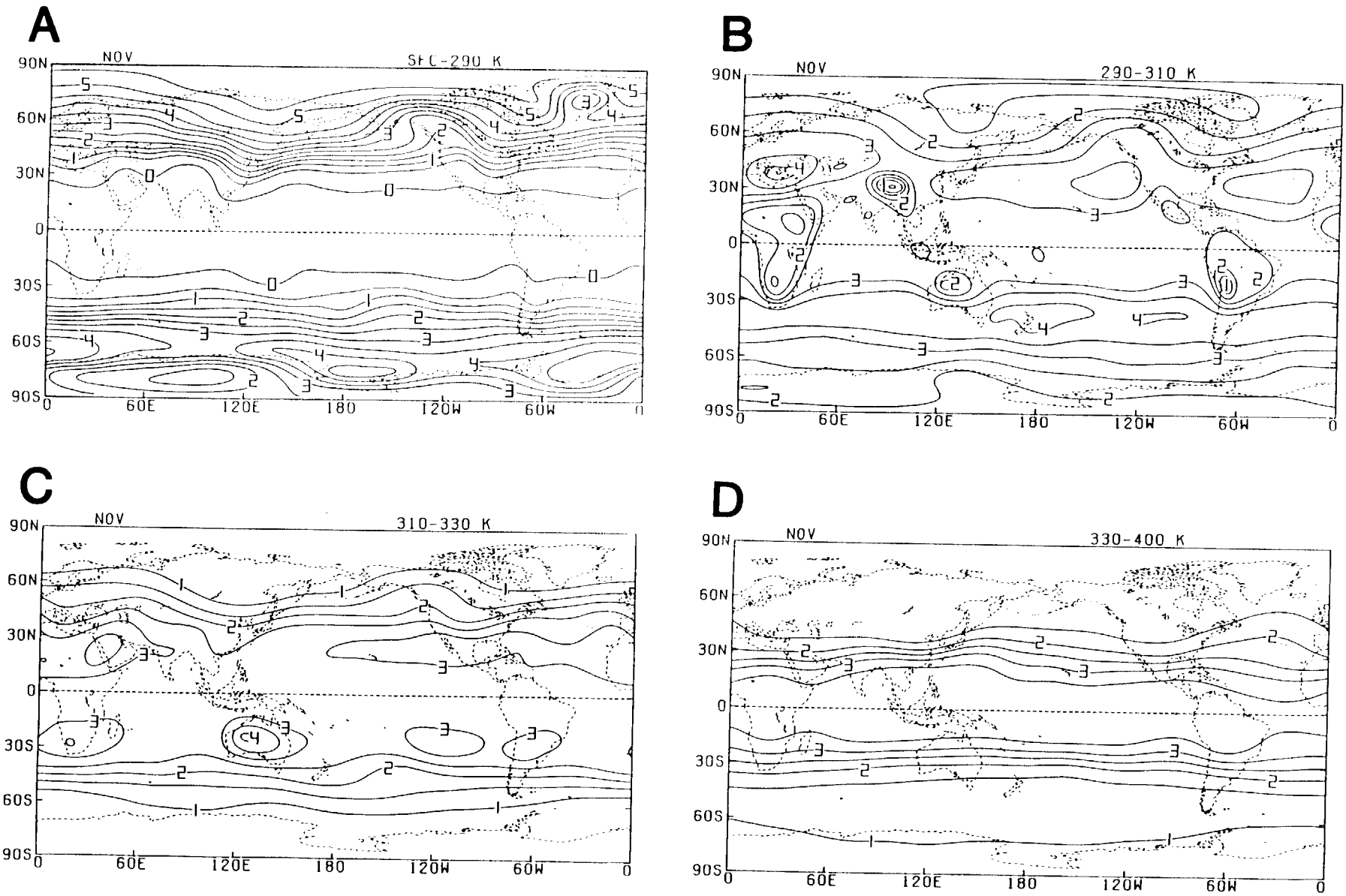

Fig. 102: Monthly averaged pressure difference (10^2 mb) between the upper and lower isentropic levels of the (A) surface-290 K, (B) 290-310 K, (C) 310-330 K and (D) 330-400 K isentropic layers for November 1979. Contour interval is 50 mb.

NASA
National Aeronautics and Space Administration

Report Documentation Page

1. Report No.	2. Government Accession No.	3. Recipient's Catalog No.
NASA CR-4370		

4. Title and Subtitle

Atlas of the Global Distribution of Atmospheric Heating During the Global Weather Experiment
December 1978 - November 1979

5. Report Date
May 1991

6. Performing Organization Code
911

7. Author(s)
Todd K. Schaack and Donald R. Johnson

8. Performing Organization Report No.
91A01339

10. Work Unit No.

9. Performing Organization Name and Address
University of Wisconsin
Space Science and Engineering Center
1225 West Dayton Street
Madison, Wisconsin 53706

11. Contract or Grant No.
NAG5-81

13. Type of Report and Period Covered
Contractor Report

12. Sponsoring Agency Name and Address
Goddard Space Flight Center
National Aeronautics and Space Administration
Washington, D.C. 20546-0001

14. Sponsoring Agency Code

15. Supplementary Notes

Todd K. Schaack and Donald R. Johnson: University of Wisconsin, Madison, WI.

16. Abstract

Global distributions of atmospheric heating for the annual cycle of the Global Weather Experiment are estimated from the European Centre for Medium-Range Weather Forecasts (ECMWF) Level IIIb data set. Distributions of monthly, seasonally and annually averaged heating are presented for isentropic and isobaric layers within the troposphere and for the troposphere as a whole. The distributions depict a large-scale structure of atmospheric heating that appears spatially and temporally consistent with known features of the global circulation and the seasonal evolution.

17. Key Words (Suggested by Author(s))	18. Distribution Statement
Atmospheric heating, Heat sources and sinks, Global Weather Experiment, European Center for Medium-Range Weather Forecasts (ECMWF) Level III Data	Unclassified - Unlimited Subject Category 47

19. Security Classif. (of this report)	20. Security Classif. (of this page)	21. No. of pages	22. Price
Unclassified	Unclassified	151	A08

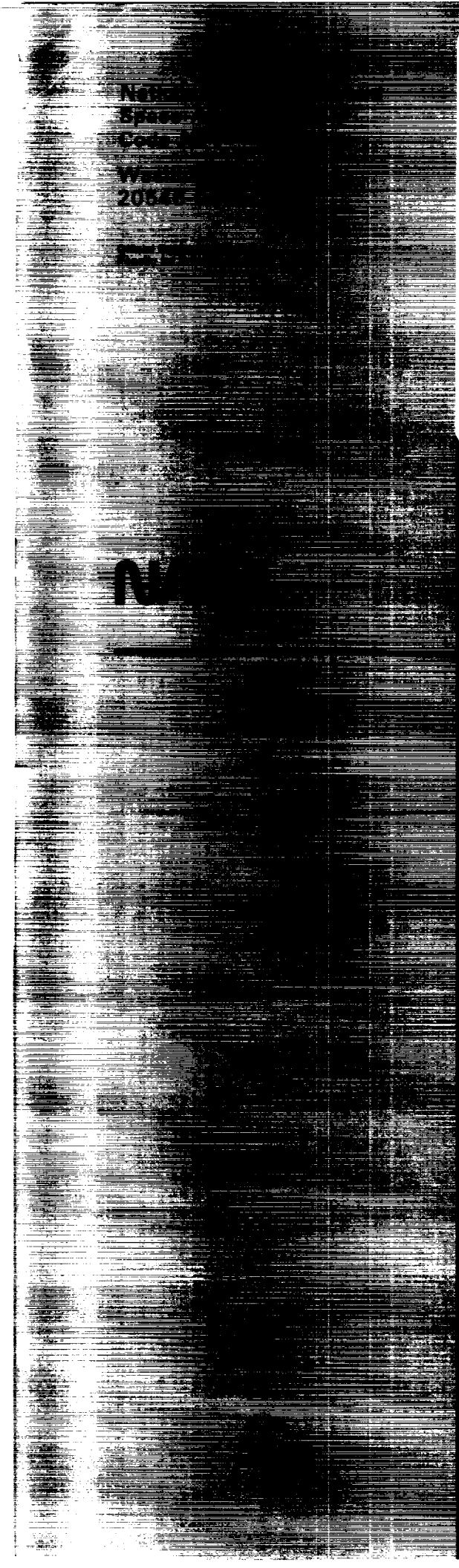

NASA

National Aeronautics and
Space Administration

Washington, D.C.
20546

Postage an Fees Paid
National Aeronautics and
Space Administration
NASA-451

Official Business
Penalty for Private Use $300

**SPECIAL FOURTH CLASS MAIL
BOOK**

L1 001 CR-4370 91071BS090569A
NASA
CENTER FOR AEROSPACE INFORMATION
ACCESSIONING DEPT
P O BOX 8757 BWI ARPRT
BALTIMORE MD 21240